APPLYING THE COMPLEX REPRESENTATION OF POLARIZED LIGHT FOR THREE DIMENSIONAL SCATTERED LIGHT PHOTOELASTIC STRESS ANALYSIS

A THESIS

Presented to

The Faculty of the Division of Graduate

Studies and Research

By

John Phillip Buban

In Partial Fulfillment

of the Requirements for the Degree

Doctor of Philosophy in the

School of Engineering Science and Mechanics

Georgia Institute of Technology

June, 1974

APPLYING THE COMPLEX REPRESENTATION OF

POLARIZED LIGHT FOR THREE DIMENSIONAL SCATTERED

LIGHT PHOTOELASTIC STRESS ANALYSIS

Approved:

Donald G. Berghaus, Chairman

George Cain, Jr.

Wilfred Horton

Date approved by Chairman:

ACKNOWLEDGMENTS

I am most grateful to Professors Donald Berghaus, George Cain, Jr. and Wilfred Horton for their time and guidance towards the completion of this dissertation.

I would also like to express my appreciation to my family for their constant encouragement.

TABLE OF CONTENTS

TABLE OF CONTENTS (Continued)

LIST OF TABLES

LIST OF ILLUSTRATIONS

LIST OF ILLUSTRATIONS (Continued)

LIST OF ILLUSTRATIONS (Continued)

LIST OF ILLUSTRATIONS (Continued)

LIST OF ILLUSTRATIONS (Continued)

SUMMARY

A new technique has been developed for determining relevant parameters in scattered light photoelasticity. The pertinent mathematical equations are established using the Jones' Calculus. It is shown from these that the photoelastic parameters can be determined at virtually any point along the path of a propagating light beam within the model. This ability makes the developed technique more versatile than previous methods.

The process also has the advantage that it can be completely automated. A scattered light polariscope in which this is partially accomplished was constructed. With this system the capabilities of remotely controlling the polarization of the input light and that of positioning and recording the observations has been attained. The polariscope is unique, simple in construction, and is such that the operator has considerable access, both manual and visual, to the model.

The method was used to determine the stress distribution in a point loaded cube. Boussinesq' solution for the corresponding half space problem could thus be used as a guide. The model was stress frozen and the results obtained by the new method were compared with those obtained from the standard technique of slicing and using transmitted light photoelasticity. The comparison was excellent.

The solution of the equation, from which the relevant photoelastic parameters are obtained, is accomplished by the Newton-Raphson's Method. A method of obtaining the stress tensor from the photoelastic

parameters is described. Cubic smoothed-spline functions are used to determine derivatives for the solution of the shear stresses from the photoelastic parameters with excellent results. A least squares technique is used to demonstrate the ability to find the normal stresses. Computer programs were written and used for these computations.

NOTATIONS

The following list of notations summarizes the uses of symbols throughout this dissertation.

A_x, A_y	maximum values of x,y scalar component of polarized light beam intensity respectively.
α	angle through which polarization rotator is turned counter clockwise about the z-axis w.r.t. x-axis.
$\alpha_i, \alpha_j, \alpha_a, \alpha_b$	fixed values of α.
C	constant, representing the stress-optic sensitivity.
E	Jones' vector representation of polarized light beam.
E_o	Jones' vector representation of initially plane polarized light beam.
E_1, E_2, E_3	Jones' vector representation of polarized light as it emerges from various optical elements.
E_{2x}, E_{3x}	x component of Jones' vectors (E_2, E_3) representation of polarized light.
$f(x_i)$	general function evaluated at point x_i.
γ	x scalar component of relative retardation induced by an elliptical retarder.
γ_i, γ_j	fixed values of γ.
M	matrix representation of general optical element.
m_1, m_2, m_3, m_4	elements of general optical matrix.
N	retardation in wave-length.
n	number of points.

ν	wave length of light beam.
η_x, η_y	phase components of polarized light at time t = 0
$\eta_{x'}$	relative phase change along axis x′ rotated counter-clockwise from the x-axis.
ω	direction of the effective principal stress axis.
P,Q	effective principal stresses.
RMS	standard deviation.
S	standard error of estimate.
s	light path length.
$\sigma_x, \sigma_y, \sigma_z$	normal stresses.
σ_1, σ_2	effective principal stresses.
t	time.
$\perp$	denotes planes perpendicular to the propagating light beam.
$\tau_\perp$	shear stress on plane normal to propagating light.
$\tau_{xy}, \tau_{xz}, \tau_{yz}$	shear stresses.
$x_1, x_2, \ldots$	set of points.
x,y,z	cartesian coordinate directions.

CHAPTER I

INTRODUCTION

The basis of photoelasticity is the observation that suitably transparent materials which are optically isotropic when unstressed become birefringent when loaded by a system of forces. The birefringence obeys the following relationships which are called the stress-optic laws (Ref. Weller [1]):

1) Light passing through the stressed material is separated into two components polarized at right angles to each other. These vibrate along the directions of the "effective principal stresses." (If the stress ellipsoid at a point is centrally intersected by a plane of the wave front, the section cut out will be an ellipse. The principal semi-axes of the ellipse are called the "effective principal stresses" in the plane of the wave front).

2) The relative velocity of the two light components as the light passes through such a point is proportional to the difference between the effective principal stresses.

The relative velocity is a measure of the rate at which the phases of the two light components differs along the light path. If this shift is expressed as a function of wave-length, then

$$(P-Q) = C \frac{dN}{dS}$$

where

$\frac{dN}{ds}$ is the rate of change of retardation

in wave-length N per unit path length S

P and Q are the effective principal stresses, and

C is a constant representing the stress-optical sensitivity of the model material.

Weller [2] proposed the technique of scattered light photoelasticity. Subsequently he [1] built the first scattered light polariscope and applied the technique. However, the method found few adherents until the introduction of the laser. The laser provided the high intensity monochromatic collimated light source essential to the practical application of the technique [3].

An introduction to the technique of scattered light photoelasticity can be found in Dally and Riley [4]. The method is based upon the scattering characteristics of a transparent medium. Most transparent materials are not optically homogeneous. It is the optical inhomogeneity which gives rise to the scattering. To develop a simple description of the mechanism involved, consider the inhomogeneity to be caused by discrete particles embedded in an otherwise homogeneous matrix. When a wave of monochromatic light propagating in the z direction and vibrating in the x-y plane strikes one of these particles a secondary set of vibrations, which propagates radially outward from the particle, is emitted (Figure 1). These secondary light "beams" are plane polarized and their intensity is directly proportional to that of the incident light beam. Two distinct photoelastic possibilities arise from this phenomenon. In one case an unpolarized incident beam is directed through the model. The state of polarization of the radially scattered light is determined as it emerges from the model. The incident beam is now moved parallel to its initial position. The change in polarization of the emerging scattered light, with

respect to translation of the incident light, can be used to determine the effective principal stresses on planes parallel to the incident beam (for a complete description of this technique, see Dally and Riley [4]). Robert and Guillemet [5] also use this technique. However, most work to date uses the model to determine the state of polarization of the incident light beam, as does the method presented herein.

In this case polarized light enters the stressed model along the z-axis (Figure 2) and is resolved into two components along the effective principal stress axes (principal stress axes in planes normal to the z-axis). These two components along the effective principal stress axes travel with different velocities, and in transversing a distance M to O, they acquire a relative phase difference. As the beam travels an incremental distance ds from O to O′; the relative phase difference varies depending upon the additional retardation acquired over the incremental distance O to O′. This change in relative retardation, dN, over the incremental distance, ds, is the space rate of change of retardation in successive planes normal to the incident light beam. The ratio $\frac{dN}{ds}$ is proportional to the difference in effective principal stresses on planes normal to the incident light. Thus the difference in the effective principal stresses can be found. Also from the description of the light as it travels through the model, the directions of the effective principal stress axes can be found, as will be shown later.

Drucker and Mindlin [6] suggested a technique to employ this method to determine states of stress in two and three dimensional

models. They also pointed out the difficulties in studying problems where the effective principal stress axes rotated along the path of the light beam. This problem has been treated by Jessop [7], Mindlin and Goodman [8], Aben [9], and Srinath [10]. Although refinements to the basic stress-optic laws have come from these studies, they all point out that in the limiting case, where rotation of effective principal stress axes is small (which is the case in most problems), the basic stress-optic laws produce accurate results.

Recent work in scattered light photoelasticity has been concentrated on techniques for obtaining the maximum information from a minimum amount of data. Cheng [11] and Frocht and Srinath [12] have derived techniques for using the varying intensity of the light as it passes through a photoelastic model to accomplish this. This method also is in keeping with this trend, and at the same time gives a more general approach to find the necessary data to obtain the stress state throughout a photoelastic model.

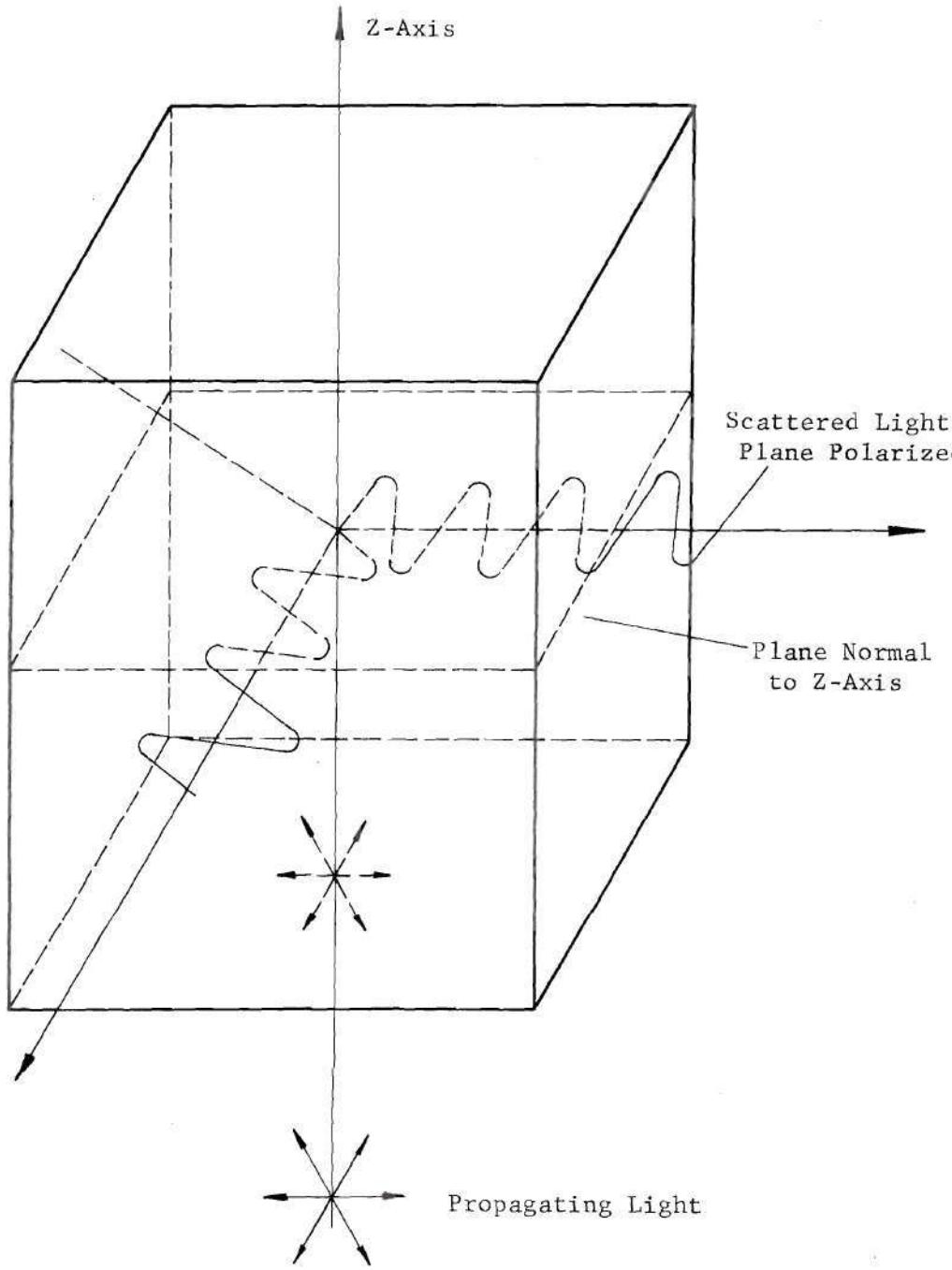

Figure 1. Light Scattering Phenomenon

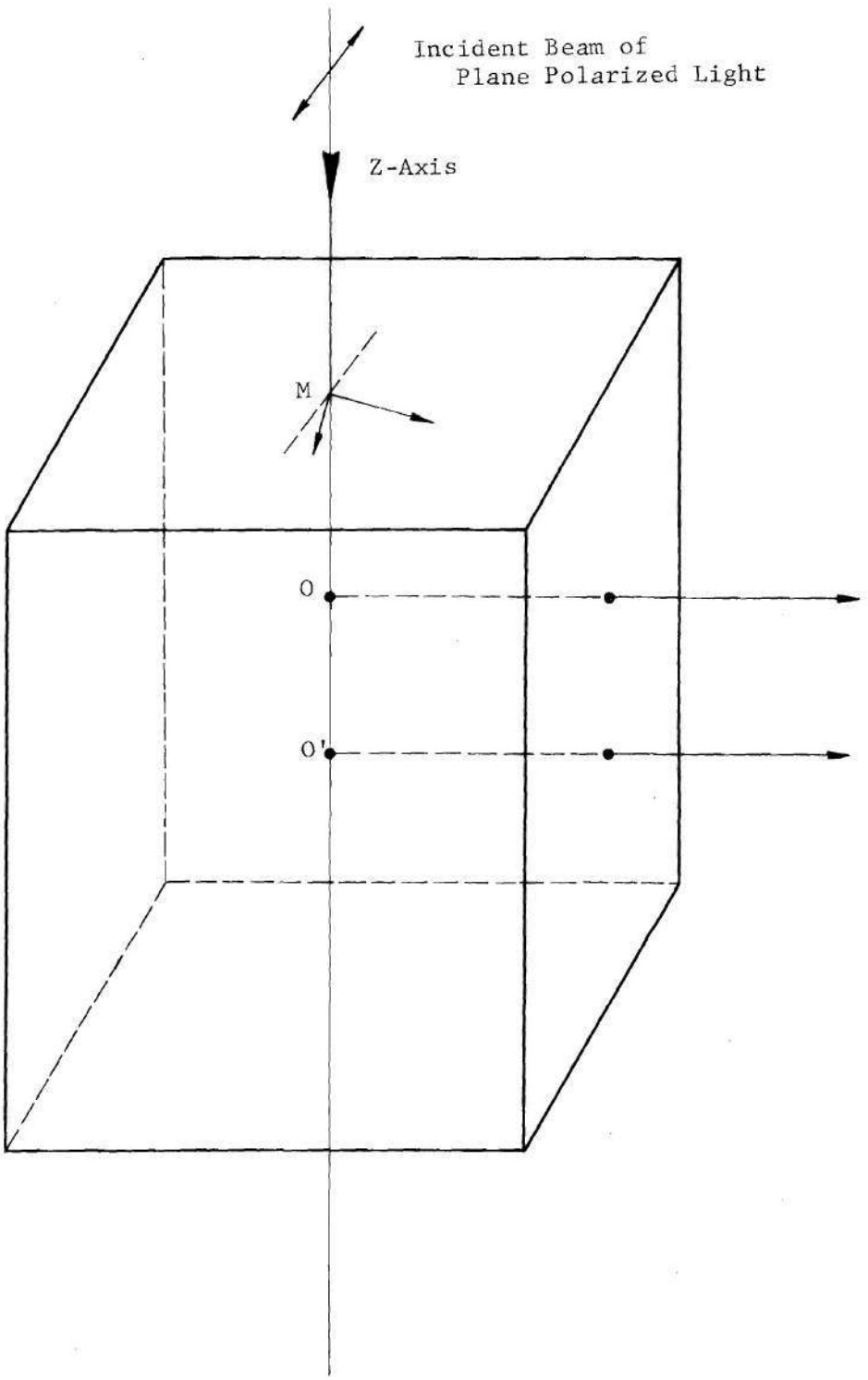

Figure 2. Scattered Light Photoelasticity- Model Used as an Analyzer.

CHAPTER II

ESTABLISHMENT OF THE PERTINENT MATHEMATICAL EQUATIONS TO DESCRIBE POLARIZED LIGHT

In scattered light photoelasticity the light beam encounters various polarizers and retarders including the stressed model itself. The information which can be obtained at each point in the stressed model by this method consists of the directions of the effective principal stresses, and the relative phase difference of the light components. The directions of the effective principal stresses are, of course, the directions of the principal axes of the light ellipse in each plane normal to the direction of light propagation. The relative phase difference is proportional to the difference of the effective principal stresses.

To obtain the information, an appropriate mathematical description is essential. In most classical cases this is based upon the concepts of wave theory. The pertinent data is determined from the variation of intensity of the light as it passes through the body. This is the basis of the method given by Frocht and Srinath [12], Cheng [11], and Weller [1].

There are other mathematical methods for dealing with the variables. These include two closely related techniques which bring some measure of computational simplification. These are the so termed Poincaré Sphere and the Stoke's Vector methods. The former is a graphical interpretation of analytically derivable conditions;

while the latter depends primarily upon empericism.

Robert and Guillemet [4] use the Poincaré Sphere in their analysis to find the photoelastic information; however, they also use the method of scattered light photoelasticity where the model is used as the initial polarizer. The Stoke's Vector is closely related to the Poincaré Sphere. The method employs a four element column matrix, called the Stoke's Vector. A 4 x 4 matrix called the Mueller Matrix describes the operation of polarized light transformation. Multiplication of the Stoke's Vector by the Mueller Matrix gives the light state as it leaves an optical element (Shurcliff [13]). This matrix calculus is described by Walker [14], Priebe [15] and Schneider [16]. A. J. Michael [17] uses this description of light with good results in transmitted light photoelasticity. However, the experimental parameters necessary to determine the four elements of the Stoke's Vector limits its use primarily to transmitted light photoelasticity.

The variables which constitute the Stoke's Vector are determined by observing intensity changes in transmitted polarized light when this light is passed through filters which determine various polarization preferences of the light. Robert and Guillemet [5] could use this type of light representation because they determined changes produced in the scattered light between the incident light beam and the surface of the model through which they viewed the light. It is not possible to determine these variables when observing a light beam normal to its path of propagation.

More recently Mylonas and Brown [18] suggested that the Jones' Calculus had great potential in determining the state of polarization

of light in photoelastic applications. He verified this suggestion by applying the concepts to transmitted light photoelasticity. This dissertation is concerned with the extension to scattered light photoelasticity. R. Clark Jones described a matrix calculus using electromagnetic wave theory as its basis. This matrix calculus is eminently suited to the study of polarization changes in light beams. The polarized light beam is described with algebraic brevity.

The Jones' Vector is represented by a two-element column matrix which describes a light beam's polarization form and amplitude components at some given position along the beam.* If the beam is traveling along the z-direction, the vector has the form

$$E = \begin{bmatrix} A_x \, e^{i(\eta_x + 2\pi\nu t)} \\ \\ A_y \, e^{i(\eta_y + 2\pi\nu t)} \end{bmatrix}$$

where

$A_x e^{i(\eta_x + 2\pi\nu t)}$, and $A_y e^{i(\eta_y + 2\pi\nu t)}$ are the scalar components along the x and y directions;

A_x is the maximum value of the x scalar component, and

A_y is the maximum value of the y scalar component.

The quantities η_x and η_y are the phase components at time $t = 0$ at the given location of the x and y scalar components.

ν is the wave length of the light beam.

*A description of Jones's Calculus can be found in Shurcliff [13] and Jones [19].

The optical elements that the light beam travels through are represented by 2 x 2 matrices. For the purpose of scattered light photoelasticity, optical elements simply rotate the semi-axes of the light ellipse, and retard, that is, cause a relative phase change between the light components along the semi-axes of the light ellipse of the propagating light.

A method will now be described whereby the directions of the light's principal axes and the relative retardation at each point in the model can be determined with the aid of this matrix calculus. This description is divided into two parts for clarity. First the light beam will be described as it travels through various optical elements including a general optical element, which represents the model; and then a comparison of this description with the actual experimental procedure will be made.

Consider a fixed coordinate system (Figure 3). The light is directed along the z-axis and vibrates in the x-y plane. The incoming monochromatic light is plane polarized with its vibration along the x-axis and can be described as

$$E_o = e^{i2\pi\nu t}\begin{bmatrix}1\\0\end{bmatrix} .$$

The light passes through a polarization rotator. A polarization rotator is described by a 2 x 2 matrix of the form

$$\begin{pmatrix}-\cos 2\alpha & -\sin 2\alpha\\ -\sin 2\alpha & \cos 2\alpha\end{pmatrix},$$

where 2α is the angle that the plane polarized light is rotated counterclockwise about the z-axis. The angle is measured from the x-axis. The output light is simple

$$E_1 = \begin{pmatrix} -\cos 2\alpha & -\sin 2\alpha \\ -\sin 2\alpha & \cos 2\alpha \end{pmatrix} \begin{pmatrix} 1 \\ 0 \end{pmatrix} e^{<2\pi\nu t}$$

$$= \begin{pmatrix} -\cos 2\alpha \\ -\sin 2\alpha \end{pmatrix} e^{i2\pi\nu t} \quad .$$

Light now enters an optical element which has unknown properties. Its principal axes are rotated through an angle ω measured counterclockwise w.r.t the x-axis. In addition the retardation or phase relationship of the light component along one axis with respect to that along the other is changed.* The optical element can be represented by the general 2 x 2 matrix.

$$M = \begin{pmatrix} m_1 & m_4 \\ m_3 & m_2 \end{pmatrix},$$

where

$$m_1 = e^{-i\eta_{x'}} \cos^2\omega + \sin^2\omega ,$$

$$m_2 = e^{-i\eta_{x'}} \sin^2\omega + \cos^2\omega ,$$

*Only relative retardation is measured in scattered light photoelasticity; so that the light component along the other principal axis may be considered to always be in phase with the input light. No generality in the description of the light vector is lost by this assumption, although, in fact, both components are retarded with respect to the initial state of the incident beam.

$$m_3 = m_4 = (e^{-i\eta_{x'}} - 1)\cos\omega \sin\omega ,$$

where $\eta_{x'}$ is the relative retardation along the x'-axis rotated counterclockwise from the

Thus, the light vector is

$$E_2 = M\begin{pmatrix} -\cos 2\alpha \\ -\sin 2\alpha \end{pmatrix} e^{i2\pi\nu t} ,$$

$$E_2 = \begin{pmatrix} \cos 2\alpha(e^{-i\eta_{x'}}\cos^2\omega + \sin^2\omega) + \sin 2\alpha(e^{-i\eta_{x'}} 1)\cos\omega \sin\omega \\ \cos 2\alpha(e^{-i\eta_{x'}} -1)\cos\omega \sin\omega + \sin 2\alpha(e^{-i\eta_{x'}}\sin^2\omega + \cos^2\omega) \end{pmatrix} e^{i2\pi\nu t}$$

Jones [20] proved that this representation was not only valid for the light following transmission through an optical element, but it also described the light at any point along the path of the beam through the optical element. In fact, the retardation and rotation of the output beam are line integrals of the retardation and rotation along the beam path.

Consideration is now given to a point along the light beam's path in the optical element. E_2 describes the light beam at this point. Again consider that an observer is positioned along the y-axis and views the beam normal to the z-axis through that point. The observer sees an intensity proportional to the intensity of the x component of the beam, which is

$$E_{2x} = (\cos 2\alpha(e^{-i\eta_{x'}}\cos^2\omega + \sin^2\omega) + \sin 2\alpha(e^{-i\eta_{x'}} -1)\cos\omega \sin\omega).$$

This intensity can be minimized w.r.t. the rotation of the polarization

rotator. At a minimum intensity

$$\frac{\partial(E_{2x})^2}{\partial\alpha} = 0 \ ,$$

or

$$\cos^2 2\omega \sin 4\alpha - \sin 2\omega \cos 2\omega \cos 4\alpha[1-\cos \eta_{x'}] + \sin^2 2\omega \sin 4\alpha \cos \eta_{x'} = 0 \qquad (1)$$

This gives one equation with the two unknowns of the optical element, ω and $\eta_{x'}$, at that point.

Consideration is again given to the same fixed coordinate system (Figure 4) with monochromatic plane polarized light propagating along the z-axis and vibrating in the x-y plane.

The light is again passed through a polarization rotator with its principal axes rotated through an angle, 2α, measured counter-clockwise w.r.t. the x-axis about the z-axis. The output light vector is described as

$$E_1 = - \begin{pmatrix} \cos 2\alpha \\ \sin 2\alpha \end{pmatrix} e^{i2\pi\nu t} \ .$$

Now an optical retarder with its principal axis aligned with the fixed coordinate axes is placed in the path of the light beam. The matrix for an elliptical retarder is

$$\begin{pmatrix} e^{-i\gamma} & 0 \\ 0 & 1 \end{pmatrix} ,$$

where γ is the relative retardation of the x scalar component of the light vector. The light coming from the optical element is simply

$$E_2 = \begin{pmatrix} e^{-i\gamma} & 0 \\ 0 & 1 \end{pmatrix} E_1 ,$$

$$= - \begin{pmatrix} (\cos 2\alpha) e^{-i\gamma} \\ \sin 2\alpha \end{pmatrix} e^{i2\pi\nu t} .$$

The light is now elliptically polarized and the x scalar component is out of phase by an amount γ with the y component.

The light is now passed through a general optical element; and, as before, this element is represented by the matrix

$$M = \begin{pmatrix} m_1 & m_4 \\ m_3 & m_2 \end{pmatrix}$$

At a specific point of interest along the beam's path through the optical element, the light vector will be of the form

$$E_3 = ME_2 ,$$

$$E_3 = - \begin{pmatrix} \cos 2\alpha\ m_1 e^{-i\gamma} + \sin 2\alpha\ m_4 \\ \cos 2\alpha\ m_3 e^{-i\gamma} + \sin 2\alpha\ m_2 \end{pmatrix} e^{i2\pi\nu t} .$$

Again suppose that an observer is positioned normal to the z-axis, and views the beam along the y-axis through the specified

point. He will see an intensity proportional to the x component of the light beam, which is

$$E_{3_x} = [\cos 2\alpha\, e^{-i\gamma}(e^{-i\eta_{x'}}\cos^2\omega + \sin^2\omega) + \sin 2\alpha(e^{-i\eta_{x'}}-1)\sin\omega\cos\omega]$$

This intensity can be minimized w.r.t. the retardation, γ, of the optical retarder with a fixed rotation α_i, of the rotator. At a minimum intensity

$$\left.\frac{\partial(E_{3_x})^2}{\partial\gamma}\right|_{\alpha_i} = 0$$

or

$$\cos^2\omega[-\sin\gamma_i + \sin(\gamma_i+\eta_{x'})] + \sin^2\omega[\sin(\eta_{x'}-\gamma_i) + \sin\gamma_i] = 0 \quad (2)$$

providing

$$\omega \neq 0, \frac{\pi}{2}$$

$$\alpha_i \neq 0, \frac{\pi}{4}, \frac{\pi}{2}$$

Also the amplitude of the light vector component can be minimized w.r.t. the rotation, α, with a fixed retardation of the optical retarder γ_j. At a minimum intensity

$$\left.\frac{\partial(E_{3_x})^2}{\partial\alpha}\right|_{\gamma_j} = 0 \ ,$$

or

$$\sin 4\alpha_j \cos^2 2\omega + \sin 4\alpha_j \sin^2 2\omega \cos \eta_{x'}$$

$$+ \cos 4\alpha_j \sin 2\omega \cos^2 \omega[\cos(\gamma_j + \eta_{x'}) - \cos \gamma_j]$$

$$+ \cos 4\alpha_j \sin 2\omega[\cos \gamma_j - \cos(\gamma_j - \eta_{x'})]$$

$$\sin^2 \omega = 0 \qquad (3)$$

This gives two families (2), (3) of equations for the determination of $\eta_{x'}$, and ω.

The relationship between the above and scattered light photoelasticity will now be shown. In scattered light photoelasticity, as in the preceding problem, an optical element with unknown properties is studied, in this case, a stressed model. Through the stress optic laws, if the direction of the principal axes of the light ellipse were known at each point in the model, then the direction of the effective principal stresses on planes normal to the light path would be known at each point; and if the relative retardation could be plotted along the light beam's path as it passes through the model, then the rate of change in this retardation relative to the distance along the path could be used to determine the effective principal stress difference at each point on planes normal to the light path. In scattered light photoelasticity the following optical property is known. As the light beam passes through the model the light which is scattered normal to the direction of the propagation of the beam is

plane polarized and its intensity is proportioned to the square of the apparent amplitude, i.e., the square of the component of the amplitude normal to the line of sight. Thus an observer positioned along the y-axis looking normal to the propagating beam through a specific point should see an intensity proportional to the x component of the light beam at that point.

The rotator and retarder in the above problem are the optical elements of the scattered light polariscope which is described in the chapter titled "Design of the Basic Equipment". Briefly, the light is plane polarized as it exits a laser light source. It is passed through a half wave plate or a polarization rotator. Then the light is passed through a Soliel-Babinet compensator, i.e., an elliptical retarder. The light now enters the model. An observer is positioned along the y-axis and views the light beam. The relative retardation and the rotation are found at points along the light path through the model with the aid of the preceding result.

The ability to obtain rotation and retardation information at each point along the light path is an important feature of this method. In most methods, the data obtained is at specific points where known values of retardation and rotation can be determined. In other words, only certain points can be used to plot the retardation of the light beam, and these same points must be used in determining the rotation (Ref. [21]). A method was proposed by Cheng [22] in which data is collected at general points. However, it varies from the preceding method in that four intensity measurements must be made to determine the retardation and rotation; and two of these

measurements are in the unstressed model.

The proposed method was checked mathematically for retardation of wave length $\frac{1}{4}$, $\frac{1}{2}$, and 1, and a comparison with Berghaus [21] showed complete agreement. This demonstrates that previous methods are special cases of a now more general method. The method was demonstrated experimentally with a disk loaded in diametral compression. The light beam was directed along the diameter of the disk normal to the load. In this manner, the principal stress directions in planes normal to the light beam were known and could be used as a check upon the results*. Good agreement was produced between known directions of effective principal stresses and calculated values.

*This same technique was used to determine the accuracy of the scattered light polariscope (Ref. [23]).

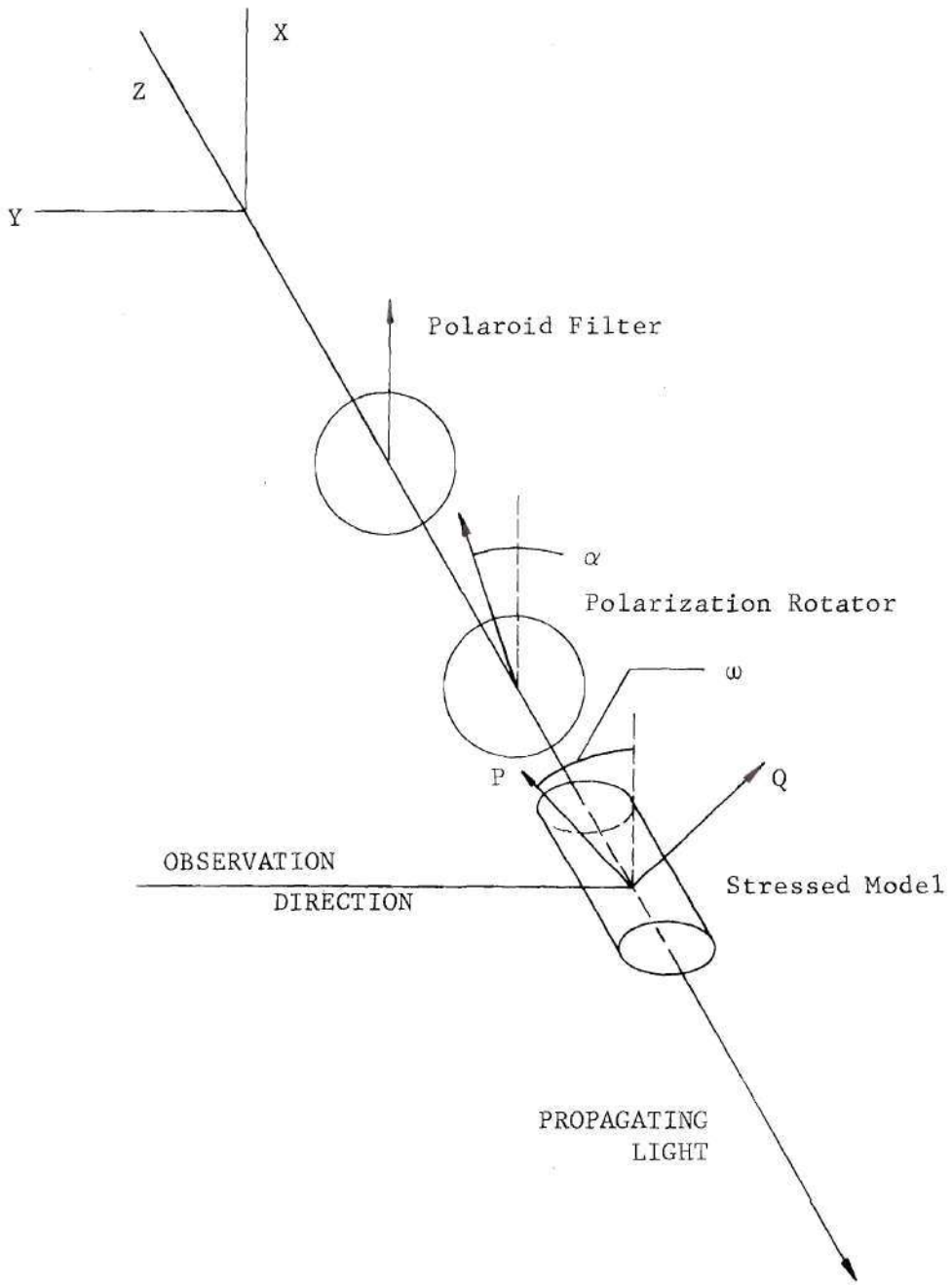

Figure 3. Plane Polarized Light Enters Stressed Model.

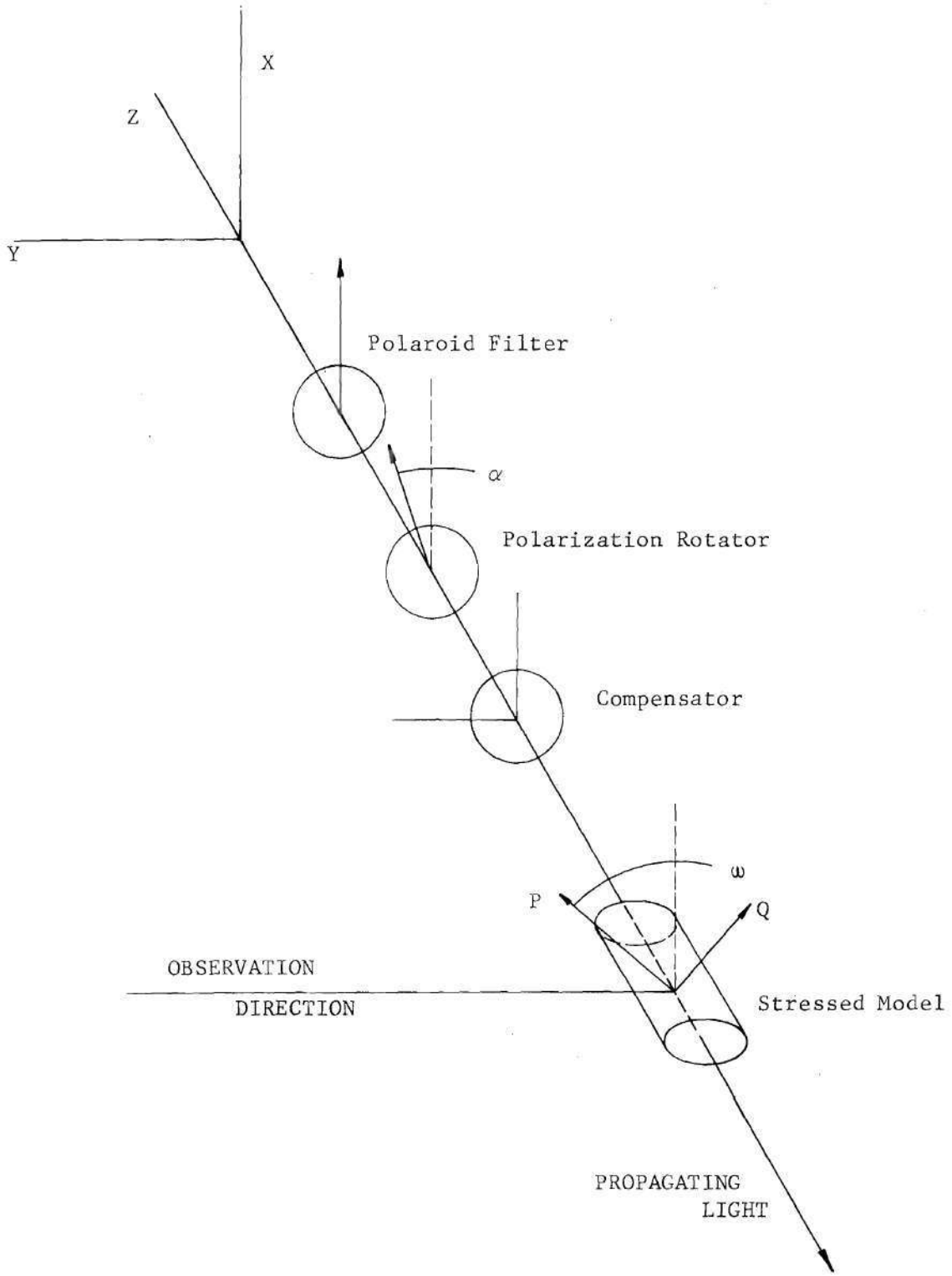

Figure 4. Elliptically Polarized Light Enters Stressed Model.

CHAPTER III

DESIGN OF THE BASIC EQUIPMENT

Polariscope

A scattered light polariscope was designed and built (Ref. [23]). The arrangement of the various components follows that of Berghaus [21]. Schematically the necessary features are arranged as shown in Figure 5. The basic polariscope is depicted in Figures 6 and 7 where the components are identified.

The polariscope frame consists of a vertical column supporting a single overarm. The entire input optical system (Figure 8) is contained in the overarm. The model and loading fixture stage is mounted above the input optical system on the overarm, and has horizontal plane motion capabilities only. The immersion tank is located directly below the overarm. The tank is octagonal with plate glass sides (a contribution credited to Swinson at Auburn University) and is placed upon a rotary table which may be raised or lowered by a hydraulic lift table. The observation system is normal to one side of the immersion tank and sits upon an optical rail fixed to the base of the tank.

The configuration of this polariscope allows considerable access, both manual and visual, to the model. The experimental variables that can be controlled are the polarization of the input light, the location of the light beam in the model, and the position of the observation. In order to discuss the control of these variables and to make obvious the reasons for the considerable access to the model

the rest of this section is divided into three parts which describe the features of the basic polariscope.

Input Optical System

The input optical system (Figure 8) consists of a light source, a polarization rotator and a Soliel-Babinet compensator. The light source is a continuous wave helium-neon laser, Spectra-Physics Model 124A. It has a power output greater than 15 milliwatts at 632.8 nm. The light beam's diameter is 1.1 mm. with a divergence of 1.0 milliradians. This size laser has an adequate intensity and a sufficiently small beam diameter to permit very good scattered light results (Ref. Swinson [13]). The laser is mounted horizontally within the overarm of the polariscope frame. The light is directed vertically downward by reflecting it 90 degrees through a pentaprism placed immediately in front of the laser.

After being directed downward the light beam is passed through a polarizing filter. This filter references the polarization of the beam to a fixed X-Y-Z coordinate system and removes any small ellipticity in the light source due to the Brewster angle windows of the laser. On emerging from the filter, the light beam passes through a polarization rotator and then a Soliel-Babinet compensator.

These components are contained in the overarm. Thus the light path through these optical elements is at a minimum, and the elements do not obstruct access to the model.

From the input optical system, the light enters the immersion tank and model. By this arrangement the distance that the light

must travel to the model has been so adjusted that its final size is optimal in relation to its initial size and divergence. In most polariscopes using lasers as a light source this is not so. Generally the laser is placed at a considerable distance from the model, and due to the divergence a large beam is obtained at the entrance of the model. To alleviate this problem the beam is converged by means of a lense arrangement placed close to the model.

The light beam polarization is controlled by the polarization rotator and the compensator. These two elements are controlled electromechanically. Both elements are driven through antibacklash gears by synchronous/stepping motors*. Movement of the motors is controlled remotely through the use of rotary dials calibrated in degrees (Figure 9). The use of stepping motors provides a positive method of positioning the optical elements from a remote data recording location. The antibacklash gears ensure a repeatability of position of the optical elements when rotated in either direction. The stepping motors have a non-accumulative error from step to step. This is, of course, essential for good repeatability. Including the inaccuracy of the stepping motors and the gear tolerances, the location can be repeated to within $\pm$ .1 degree. Each step of the stepping motor rotates the polarization rotator one half of a degree and the compensator one degree.

In addition to these controls the ability to remotely control the retardation of the compensator would have been useful in the

*Slo-Syn stepping motors manufactured by Superior Electric Company, Bristol, Connecticut.

scattered light photoelastic method introduced by this dissertation. Only the rotational position is now controlled remotely. This would have allowed the use of Equation (2), which is dependent upon the change in retardation $'\gamma$, for the determination of the polarization of the light beam.

Mechanical Systems

The mechanical system consists of the model stage and the immersion tank. The model stage is a set of cross-slides. The model is suspended in the path of the light beam by a suitable frame mounted to the stage (Figure 6 and 7). The location of the light beam as it passes through the model can be accomplished by moving the model in the horizontal plane. Dial indicators have been incorporated along both directions of the cross-slides. Thus change in location is easily determined without attention being directed to the effect of backlash when reversing directions.

The immersion tank is raised around the model (Figure 7) from its initial rest position (Figure 6) with the aid of the hydraulic lift table. The tank contains an immersion fluid with the same index of refraction as the model, so that the light beam will traverse vertically through the model without refraction. Due to the large surface area of the fluid in the tank, it was susceptible to outside disturbances which caused it to be in continual motion. This motion kept the fluid surface from being normal to the light beam; thus the beam was continually moving in the fluid due to refraction. Various methods were tried to alleviate this problem such as a flat

glass plate half immersed in the fluid for the beam to traverse through and baffles in the tank. The best solution was to determine data at times when outside disturbances were at a minimum. With the technique described herein this became a serious problem.

Observation System

The intensity of the scattered light from the propagating light beam as it travels through the model may be recorded photographically or plotted directly, using the observation system on the optical rail. The direction of observation can be changed by rotating the rotary table (Figure 7) which rotates the optical rail relative to the model. Rotational viewing directional freedom is greater than 270° with the use of the simple column supporting structure of the polariscope.

The observation system consists of a 4" x 5" view camera and a photometric scanner. The camera may be used either to photograph the fringe pattern or as a lens system to magnify and focus this pattern for direct plotting of the light intensity using the scanner. The scanner is of the synchronous detection type as opposed to the photon counting type (Ref. Cheng [24]). It consists of a photomultiplier tube* which is exposed to the focused image of the scattered light profile through a pin hole aperture, plus a vertical traversing mechanism which transports the photomultiplier tube vertically along the image. The synchronous detection type scanner is as accurate as the photon counting type with the high light level present in this polariscope. The

*The photomultiplier tube is the RCA-7265. It employs a multialkali photocathode providing high quantum efficiency into the red spectrum, low dark current and good time resolution characteristics.

photomultiplier tube output is used to drive the vertical axis of an x-y chart recorder via a Kiethly Model 150B microvolt-ammeter.

The traversing mechanism is driven by a stepping motor attached to a lead screw. This allows positive positioning of the photomultiplier tube. A linear potentiometer was attached to the traversing mechanism to measure the vertical travel of the traversing mechanism. The output from the potentiometer drives the horizontal axis of the x-y chart recorder.

The output from the scanner versus the output from the potentiometer gives a direct plot of light intensity versus displacement.

This scattered light polariscope is considered to be more versatile and more accurate than similar systems using the same components. It is considered more versatile because of its construction. It is considered more accurate for its intended use because it was possible to determine effective principal stress directions in a plane model when the observation direction was only two degrees from the effective principal stress directions*. It was felt this is very good accuracy for scattered light photoelasticity.

*For a discussion of this test of accuracy see (Ref. [23]).

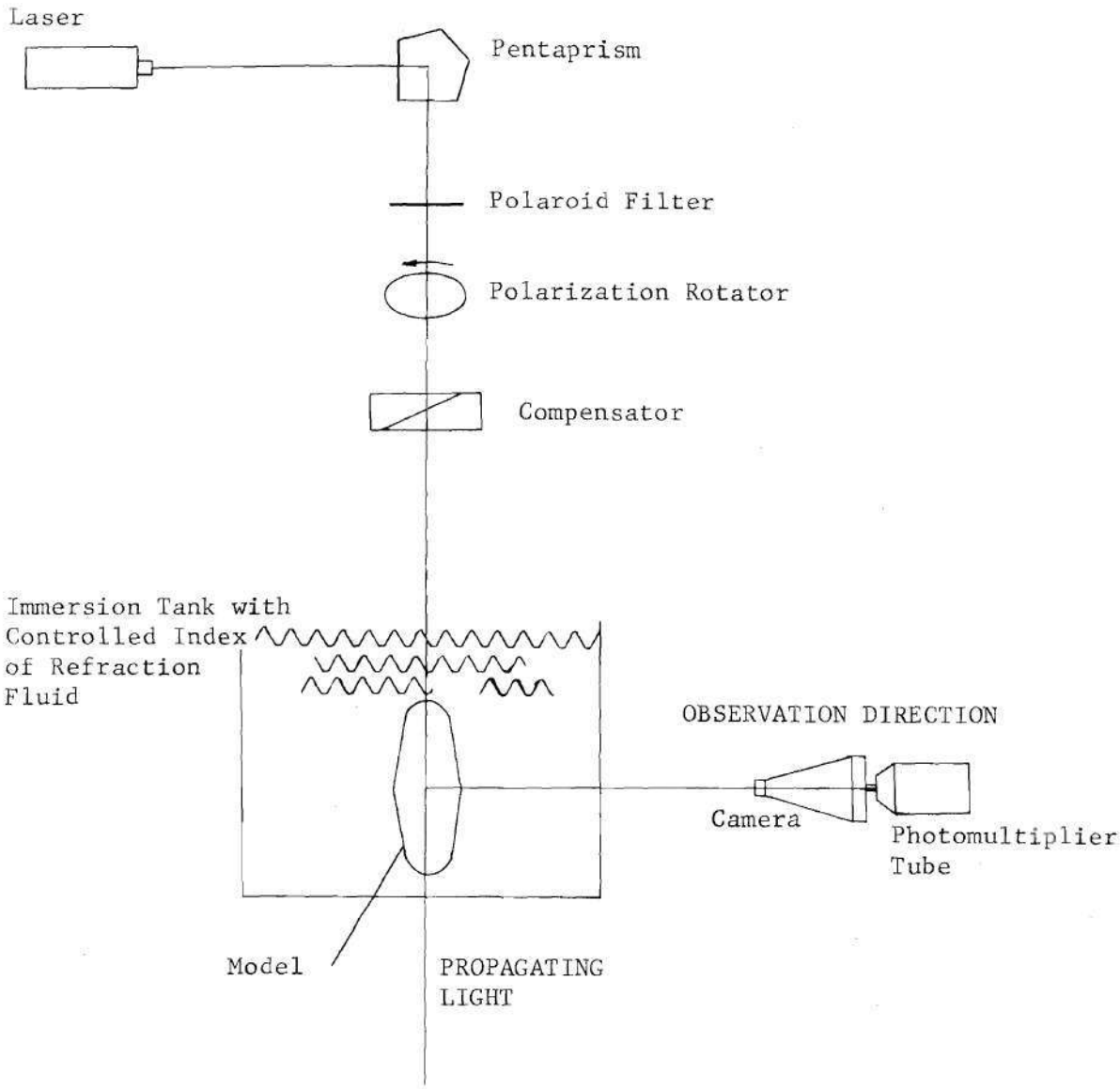

Figure 5. Schematic of Scattered Light Polariscope.

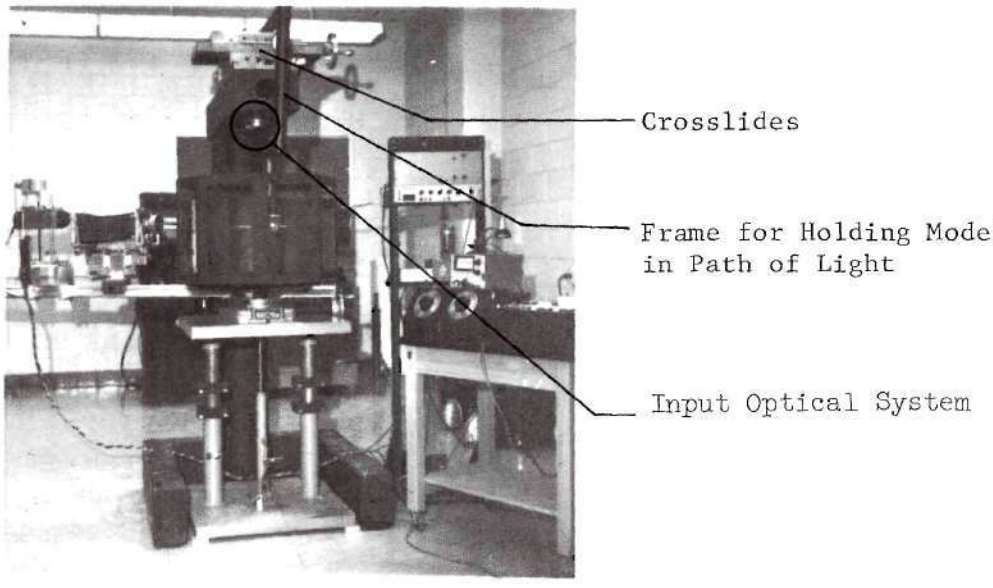

Figure 6. Scattered Light Polariscope with Immersion Tank in Up position.

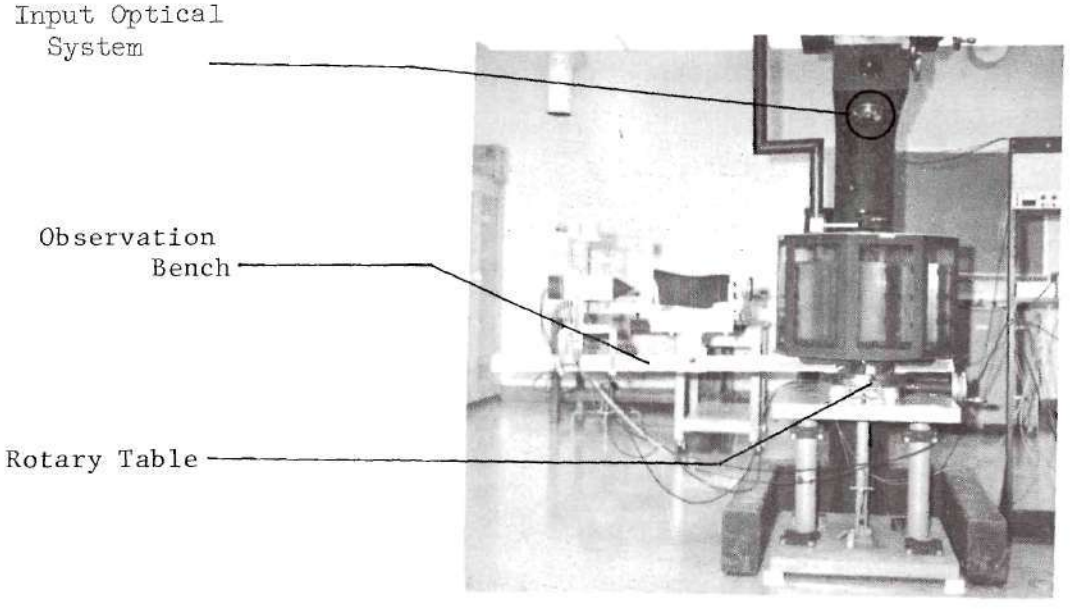

Figure 7. Scattered Light Polariscope with Immersion Tank in Down Position.

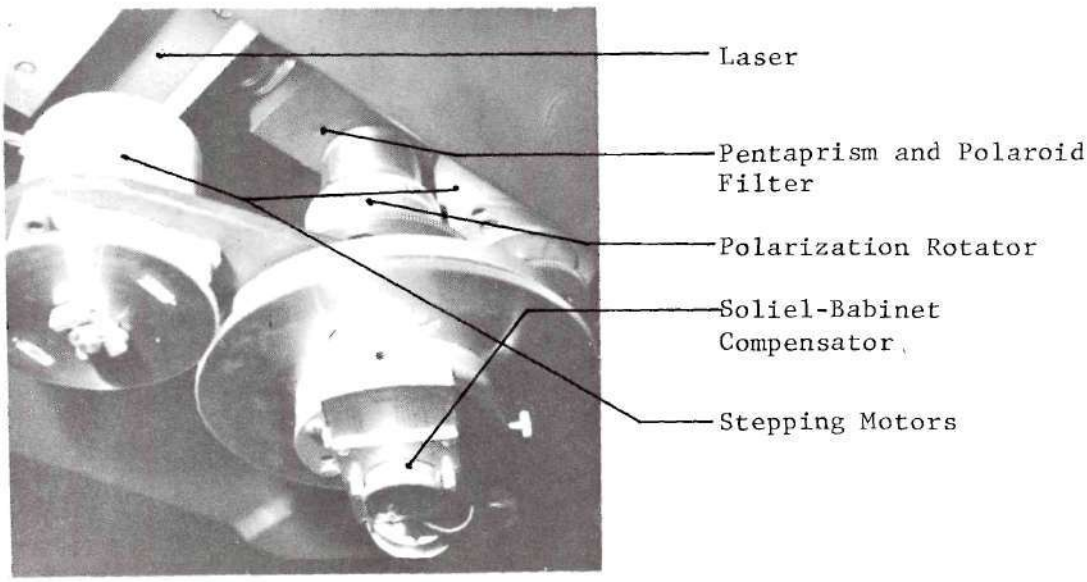

Figure 8. Input Optical System.

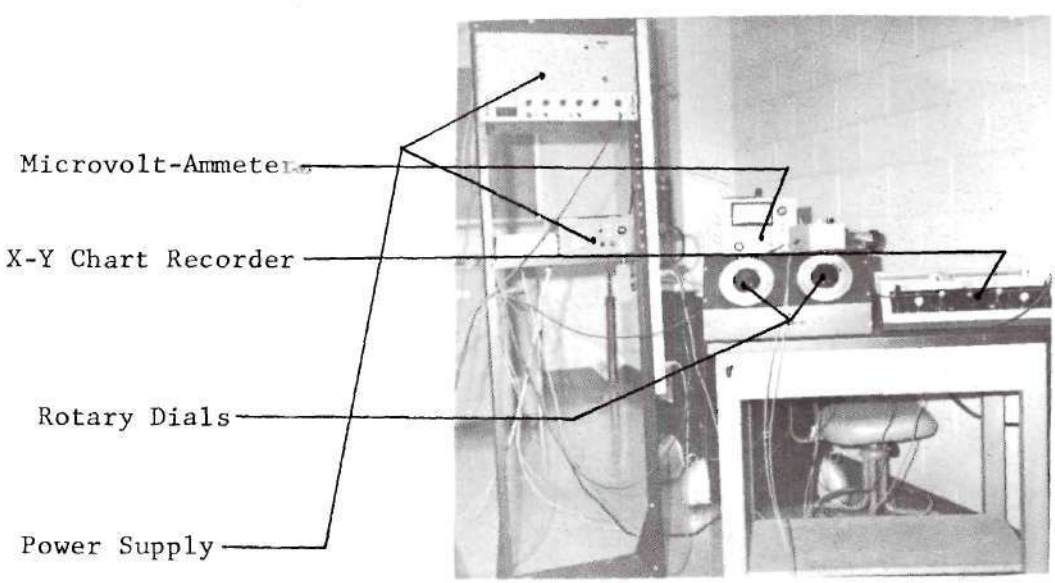

Figure 9. Remote Data recording Location.

CHAPTER IV

DEVELOPMENT OF A SOLUTION METHOD

Photoelasticity is, as the name implies, the art and science concerned with one inter-relationship between elasticity, material behavior and optics. The state of stress in a transparent body is studied by observing changes of polarization of a ray of light passing through the body. This change is related to the stress at points along the light path by the stress optic laws. In this section, methods to determine the polarization of the propagating light beam as it travels through the body will be explained using the previously described scattered light polariscope. The stress optic laws will then be used to obtain the shear stresses and the effective principal stress directions. The total stress tensor at each point can then be found using these shear stresses and effective principal stress directions in conjunction with the stress equilibrium equations. A method for so doing is outlined.

Obtaining Scattered Light Photoelastic Data

Experimentally, the following procedure was used to determine the retardation, $\eta x'$, and the direction of the semi-axes of the light ellipse, ω, along the propagating light beam as it traveled through the model. The incident light beam was plane polarized with its direction of vibration along the x-axis (Figure 4). The camera and photomultiplier tube were aligned with the y-axis of the polariscope.

The coordinate system of the model was aligned with the fixed coordinate system of the polariscope. Then the model was immersed in the tank of fluid and the incident light beam was passed through it. The scatter component was then focused on the camera's view screen. The light intensity along the path of the light beam as it travels through the model was recorded using the observation system of the polariscope.* This intensity plot was recorded for two reasons:

1) To provide a calibrated reference guide for subsequent relocation of the scanner; and

2) To determine locations of maximum and minimum intensity.

These maximum and minimum intensity points are locations of 0° and 180° of retardation of the propagating light beam, respectively.

Points corresponding to .1 inch intervals in the model were noted on the intensity plot. The aperture of the photomultiplier tube transport was positioned at each of these points. The retardation of the Soliel-Babinet compensation was set at a predetermined γ_i; and the direction of the polarization rotator, α_i, which made the intensity of the scatter component a maximum was determined. This procedure was repeated for two more values of γ. The three values of γ which were used were $\gamma_1 = 0^{\circ}$, $\gamma_2 = 38.1^{\circ}$ and $\gamma_3 = 142^{\circ}$. The retardation of 0° was chosen for convenience. The other two values were chosen because it was observed that, generally, α_2 was distinctly different from α_3 if γ_2 and γ_3 lay in different quadrants. This was necessary in order to have a stable solution for η_x, and ω.

*A typical intensity plot can be seen in Figure 10.

The mathematical techniques were given previously. It was shown that by setting the retardation, γ, of the compensator and varying the direction of the polarization rotator, α, the retardation and the direction of the semi-axes of the light ellipse at maximum intensity could be obtained from the following family of equations,

$$\cos \eta_{x'} \left[\sin 4\alpha_i \sin^2 2\omega + \frac{\cos \gamma_i \sin 4\omega \cos \alpha_i}{2}\right]$$

$$- \sin \eta_{x'} \sin \gamma_i \sin 2\omega \cos 4\alpha_i$$

$$+ \sin 4\alpha_i \cos^2 2\omega - \frac{\cos \gamma_i \sin 4\omega \cos 4\alpha_i}{2} = 0. \quad (4)$$

Two families of equations are actually developed. The other family (equation 2) presented a procedure in which the direction of the polarization rotator, α, was set and the retardation, γ, of the compensator was determined to correspond to a position of maximum intensity. The first technique was chosen because it could be more readily adapted to the arrangement of variables and their adjustments as provided by the polariscope.

Solution of the Pertinent Mathematical Equations

Given the three items of data (α_1, α_2, α_3) at each investigation point, the family of equations (4) is solved for the relative retardation, $\eta_{x'}$, and the directions of the semi-axes of the light ellipse, ω, using the Newton-Raphson method. This program and its flowchart are shown in Appendix C. The three equations corresponding to the three items of data were solved two at a time yielding three

sets of answers for the two unknowns, $\eta_{x'}$ and ω, and the arithmetic mean of these answers was computed.

Due to the cyclic nature of the trigonometric functions, the equations yield no unique solution. This difficulty was partially removed by restricting the search for a solution to the region $0 < \eta_{x'} < 2\pi$ and $-\pi/2 < \omega < \pi/2$ (Figure 11). Although this solution region was established to restrict the range of unknown variables, there was no apparent method of selecting a first approximation to the solution within this region which insured convergence of the Newton-Raphson method. It was discovered that if the first approximation was not chosen properly, the incremental changes of the unknowns would not converge to a solution within the region. Therefore a solution was forces by repeated trials of new first approximations. The region of search was divided into four rectangles (Figure 12) by joining the midpoints of opposite sides of the region. The midpoints of each of these four rectangles were then used in turn as a first approximation to the solution. If the iterative process did not converge to a solution using one of these points, then each rectangle was again divided into four rectangles by joining the midpoints of the opposite sides of the rectangles (Figure 13) and the midpoints of these rectangles were used as first approximations. Continuing in this manner a first approximation was found which would be sufficiently close to the solution for the Newton-Raphson method to converge to that solution.

This was not the only difficulty in determining the solution to these equations. If α is determined at the rotation which yields

a maximum intensity and is then denoted $\alpha = \alpha_a$, then $\alpha = \alpha_a \pm 45^\circ = \alpha_b$ gave a minimum intensity at that point. Therefore both, α_a and α_b, satisfied equation (4). However it was, in general, a possibility that $\alpha = \alpha_b$ was the value of α which produced a maximum intensity. It was necessary to determine to which solution the Newton-Raphson method had converged. The point solution for η_x, and ω was used with γ_i to solve both of the equations (equation 4) for α. If the solution obtained corresponded to the problem when α gave a maximum intensity (α_a), then this check of α gave $\alpha = \alpha_a$; if the solution corresponded to the problem when α gave a maximum intensity (α_b) then $\alpha = \alpha_b$ in this check. Thus a simple technique was established to determine the correct solution.

Experimentally the knowledge that $\alpha \pm 45^\circ$ yields a minimum intensity when α yields a maximum intensity is useful. If α was not a distinct value, that is, the neighboring values of α caused approximately the same value of intensity, the minimum intensity at $\alpha \pm 45^\circ$ can be used to check the α determined previously.

At each point of interest along the light beam the direction of the semi-axes of the light ellipse and the relative retardation of the corresponding point of the incident beam in the model were determined as described. However, all the values of retardation that were determined by the solution of the family of equations (4) lay between 0° and 360°. To obtain a table of data for the retardation with respect to the distance along the light beam, it was necessary to use the intensity plot and add the appropriate number of complete cycles of retardation, 2π, to the determined value of retardation at each

point of interest. For this problem, the derivative of the function was required and not the function explicitly, thus it was not necessary to use an entire plot if interest was only in a small length of the light path.

Determination of Shear Stresses

To this point a method to determine the state of the polarized light as it propagates through the model has been presented. This information will now be related to stress through the stress optic laws.

In planes normal to the incident light beam, the directions of the effective principal stresses were given by the angles ω and $\omega + 90^{\circ}$ (Figure 4). The difference in the effective principal stresses is proportional to the rate of phase change between the two light components along the light path. This rate of phase change was found by numerically differentiating the tabulated values of retardation along the path of the incident light.

In order to differentiate this function of discrete points, it was necessary to know values of retardation at all intermediate points. Since this information was not available, assumptions concerning these intermediate points were essential. Southwell [25] states it is reasonable to identify the function necessary for differentiation with a continuously differentiable function which is consistent with the data. He constructs a polynomial of degree n which assumes the specified values at n + 1 points, thus satisfying the requirements.

Southwell points out that undue reliance on derived polynomials,

especially in the case of differentiation, should be avoided. He states that imposing complete continuity necessitates the use of increasingly complex formulas for the derivative as more and more points are taken into account since the previously constructed polynomial are of higher order. These formulas do not necessarily yield results of increasing accuracy (Ref. Bickeley [26]).

To attempt to avoid some of the above disadvantages it was decided a smoothed cubic spline function would be used to fit the tabular data for this derivative determination. A cubic spline is a piecewise interpolation polynomial define over a set of points (x_i), $i = 0, 1, \ldots, n$, and that continuity of derivative is preserved to order two (Ref. Reinsch [27]). In addition the smoothed-spline is so constructed that is not constrained to pass through all the data points, but replaces this constraint with a smoothing constraint (Ref. Berghaus and Cannon [28] and Reinsch [27]. It provides a fit similar to a least squares fit. Reinsch presents an algorithm to determine the smooth cubic spline function.

Berghaus and Cannon [28] took this technique and used it for computation of derivatives in scattered light photoelasticity. It was this application which was used herein. The smoothed-spline gave good first derivative results for the discrete data. It had the advantage of continuity of the derivative without the use of large order polynomials; and it allowed for smoothing as would be accomplished in a least squares polynomial fit.

Using this technique, the effective principal stress differences at each point of interest along the propagating light path was

determined. This is

$$(\sigma_1-\sigma_2)_{\perp} = C \frac{dN}{ds}$$

where

$\frac{dN}{ds}$ = rate change of retardation,

C is the stress-optical constant,

the symbol $\perp$ denotes planes perpendicular to the propagating light beam, and

$(\sigma_1-\sigma_2)$ is the effective principal stress difference.

By transformation equations the shear stresses are obtained directly from these results. The shear stress $\tau_{\perp}$ is related as follows:

$$\tau_{\perp} = -\frac{1}{2}(\sigma_1-\sigma_2)_{\perp} \sin 2\omega \qquad (5)$$

Determination of the Total Stress Tensor

The shear stress can be determined at points on planes normal to the incident light beam. The model was rotated so that the beam propagated through the model in a direction normal to the initial direction; and the shear stress at points on the planes normal to the light beam were determined. This procedure was repeated once more with the final direction of the propagating light beam normal to the plane formed by the previous two propagation directions. These three orthonormal directions were the cartesian coordinate directions assigned to our model. Thus, the effective principal stress differences at each point of interest are:

$$(\sigma_{1_z} - \sigma_{2_z}) = C \frac{dN_z}{ds} \tag{6}$$

$$(\sigma_{1_x} - \sigma_{2_x}) = C \frac{dN_x}{ds} \tag{7}$$

and

$$(\sigma_{1_y} - \sigma_{2_y}) = C \frac{dN_y}{ds} \tag{8}$$

where the subscripts (x,y,z) signify the directions of the propagating light. By coordinate transformation the shear stresses were determined.

$$\tau_{xy} = -\frac{1}{2}(\sigma_{1_z} - \sigma_{2_z}) \sin 2\omega_z \tag{9}$$

$$\tau_{xz} = -\frac{1}{2}(\sigma_{1_y} - \sigma_{2_y}) \sin 2\omega_y \tag{10}$$

$$\tau_{yz} = -\frac{1}{2}(\sigma_{1_x} - \sigma_{2_x}) \sin 2\omega_x \tag{11}$$

The normal stresses are also related to the effective principal stress differences by the following equations.

$$(\sigma_x - \sigma_y) = (\sigma_{1_z} - \sigma_{2_z}) \cos 2\omega_z \tag{12}$$

$$(\sigma_y - \sigma_z) = (\sigma_{1_x} - \sigma_{2_x}) \cos 2\omega_x \tag{13}$$

$$(\sigma_x - \sigma_z) = (\sigma_{1_y} - \sigma_{2_y}) \cos 2\omega_y \tag{14}$$

However, these equations are not independent. Therefore, it is

necessary to employ numerical methods to find the normal stresses. It is possible to integrate one of the stress equilibrium equations by finite difference techniques and obtain one of the normal stresses.

The stress equilibrium equation

$$\frac{\partial \sigma_z}{\partial z} + \frac{\partial \tau_{xz}}{\partial x} + \frac{\partial \tau_{yz}}{\partial y} = 0 \tag{15}$$

can be numerically integrated starting at the boundary, $z = 0$, and progressing inward parallel to the z-axis. The well known first approximation to the derivative

$$f'(x_i) = \frac{f(x_{i+1}) - f(x_{i-1})}{x_{i+1} - x_{i-1}}$$

is used to construct the finite difference equations

$$\sigma_z\Big|_{z_i} = \sigma_z\Big|_{z_{i-1}} - \frac{\Delta \tau_{xz}}{\Delta x}\,\Delta z\Big|_{z_{i-1}}^{z_i} - \frac{\Delta \tau_{yz}}{\Delta y}\,\Delta z\Big|_{z_{i-1}}^{z_i} \tag{16}$$

or

$$\frac{\sigma_z(i,j,k+1) - \sigma_z(i,j,k)}{z(i,j,k+1) - z(i,j,k)} = \frac{\tau_{xz}(i-1,j,k) - \tau_{xz}(i+1,j,k)}{2[x(i+1,j,k) - x(i-1,j,k)]}$$

$$+ \frac{\tau_{xz}(i-1,j,k+1) - \tau_{xz}(i+1,j,k+1)}{2[x(i+1,j,k+1) - x(i-1,j,k+1)]}$$

$$+ \frac{\tau_{yz}(i,j-1,k) - \tau_{yz}(i,j+1,k)}{2[y(i,j+1,k) - y(i,j-1,k)]}$$

$$+ \frac{\tau_{yz}(i,j-1,k+1) - \tau_{yz}(i,j+1,k+1)}{2[y(i,j+1,k+1) - y(i,j-1,k+1)]} \qquad (17)$$

where (i,j,k) denotes the finite difference mesh points.

This incremental integration is known as the "shear difference" method. It was developed by Frocht [29] for two dimensional photoelastic problems and by Frocht and Guernsey [30] for three dimensional problems. Cumulative error and no means of assessing error are inherent problems with this technique.

Berghaus [31] has devised a technique which clearly alleviates these problems. Finite difference approximations of all the stress equilibrium equations plus the photoelastic relationships (12, 13, 14) present an overdetermined system of equations for the solution of the normal stresses. Thus, Berghaus used a least squares solution to this system of equations. This type of a solution takes all the information and gives a means of being sure that this solution is a good match to this information.

For the present problem, this system of equations included the boundary conditions (at each boundary mesh point),

$$\sigma_z = 0 \quad \text{on} \quad z = 0 \qquad (18)$$

(except at the point of application of load) the photoelastic relationships (12-14) and the difference equations for the two stress equilibrium equations (15) and

$$\frac{\partial \sigma_x}{\partial x} + \frac{\partial \tau_{xy}}{\partial y} + \frac{\partial \tau_{xz}}{\partial z} = 0 \qquad (19)$$

A computer program for this technique is in Appendix C. This system of equations is written in matrix form. The algorithm for the solution of this matrix equation is given by Businger and Golub [32] and adapted to photoelastic stress analysis by Berghaus [31].

Although Berghaus' adaption alleviates some short comings of the "shear difference" technique, it does not help in the determination of stress information in the neighborhood of a concentrated load. Hence, it was not possible to determine the total stress tensor for this problem. This is discussed fully in Appendix A.

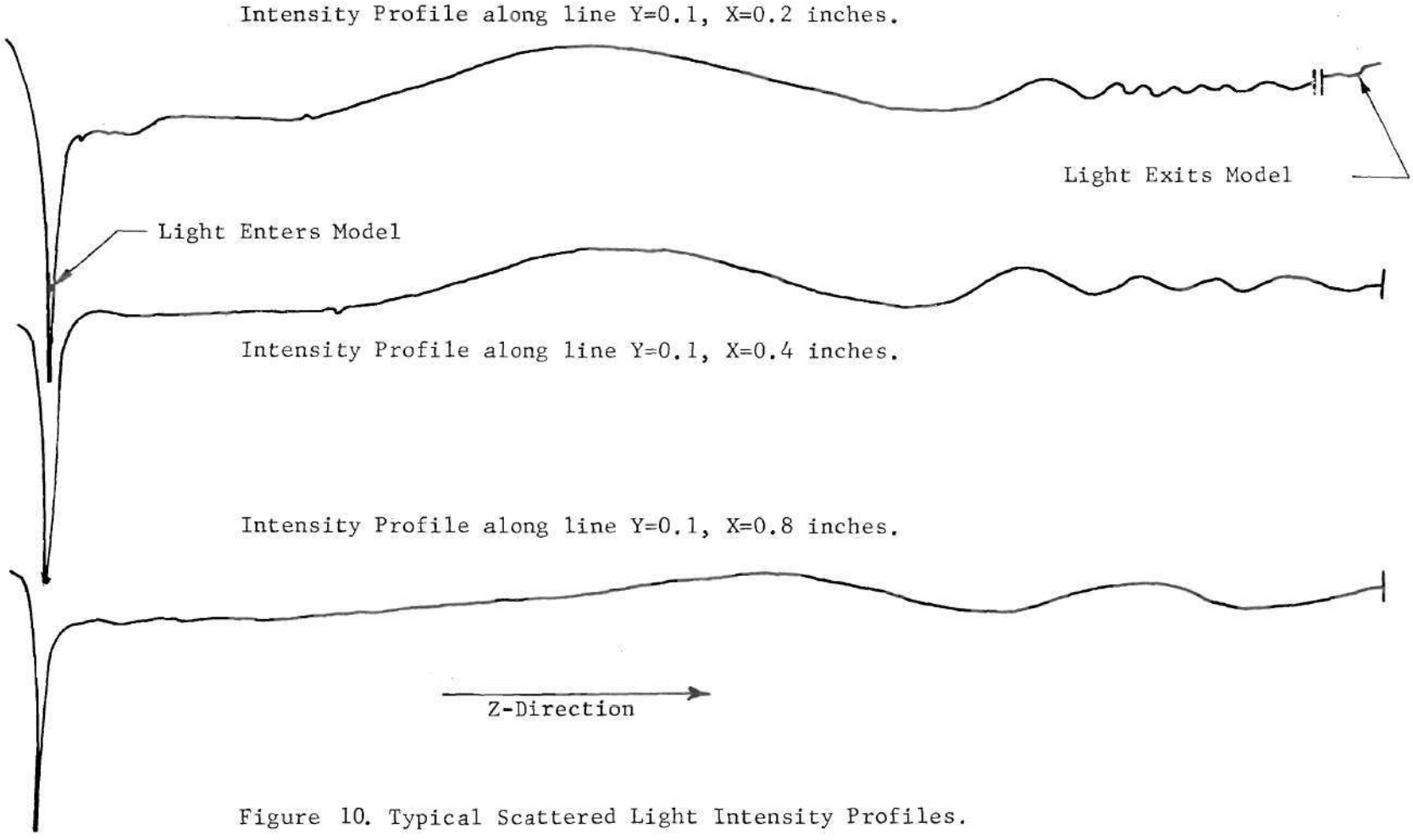

Figure 10. Typical Scattered Light Intensity Profiles.

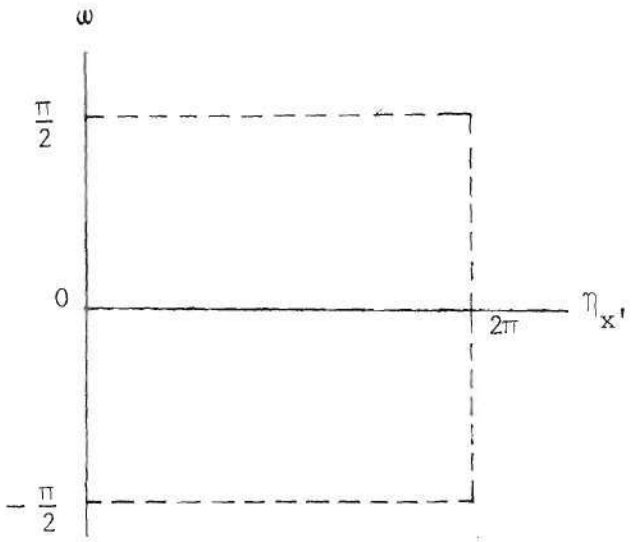

Figure 11. Region of Search for Solution $(\omega, \eta_{x'})$.

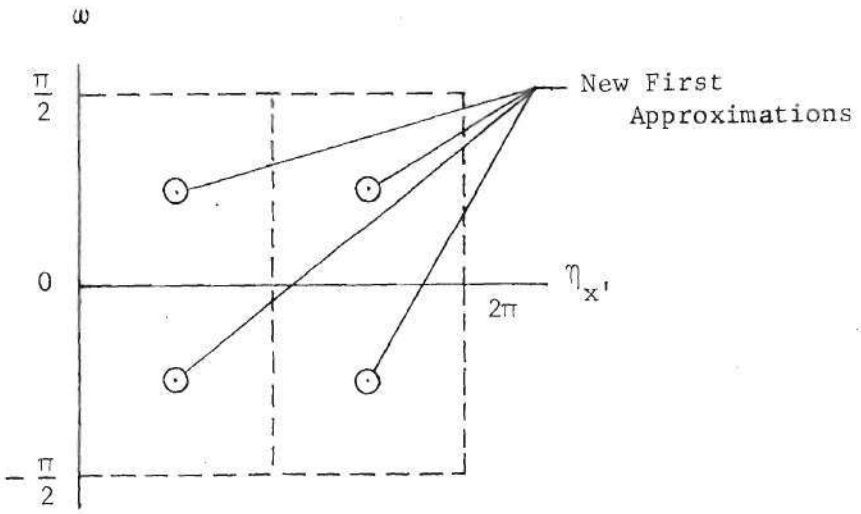

Figure 12. First Division of Region of Search.

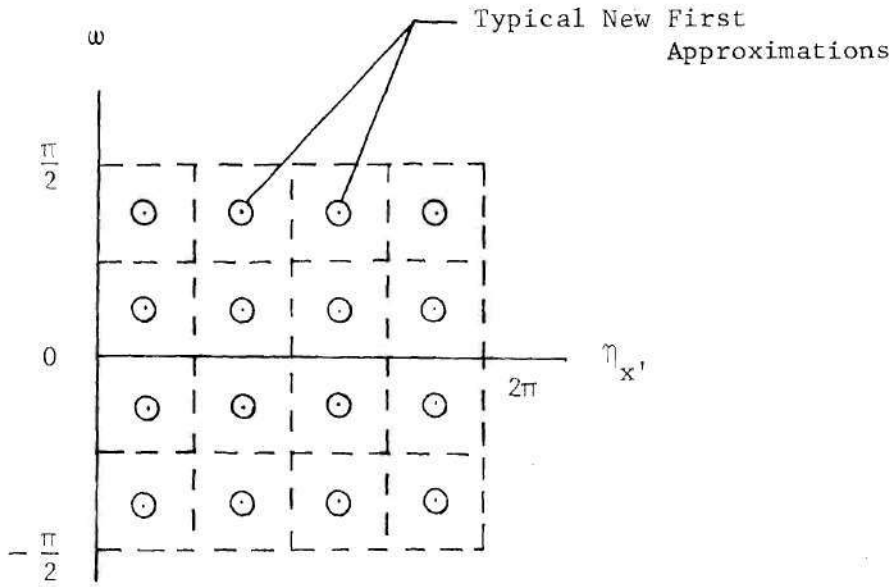

Figure 13. Second Division of Region of Search.

CHAPTER V

APPLICATION OF THE NEW TECHNIQUE TO DETERMINE THE STRESS DISTRIBUTION IN A POINT LOADED CUBE

This technique of scattered light photoelasticity was applied to a three dimensional problem. The problem was to find the state of stress in an epoxy resin cube with a concentrated load directed normal to the center of one of its faces. The opposite face was supported by a lubricated flat surface which retained the cube in equilibrium.

The problem was chosen because it resembled the classical elasticity problem known as the Boussinesq problem. The Boussinesq results could therefore be used as valid indicators of the results expected in the solution of this problem. The Boussinesq problem has a closed form solution; there are regions of comparatively high and low stress gradients; and on successive planes parallel to the load the effective principal stress axes rotate. A scattered light photoelastic technique should be able to deal with all of these stress field properties; and therefore it was felt that this problem was sufficiently general to demonstrate the capabilities of the techniques herein presented.

The Boussinesq solution, is at best, merely an approximation to the solution of the problem adopted; therefore, the results were verified by using an accepted photoelastic technique. The model was stress frozen and then sliced (Ref. Heywood [33]). The standard transmitted light technique was used on the slices (Ref. Frocht and

Guernsey [30]).

Designing the Model with the Aid of the Boussinesq Model

Consider an elastic solid body to which forces are applied in the neighborhood of a single point on the surface. If all of the linear dimensions of the body are large compared with those of the area subjected to the load, then the body can be regarded as bounded by an infinite plane. The load is applied at a point which is called the origin, the plane $Z = 0$ is the bounding surface of the body, and the positive direction of the Z-axis is that which goes into the interior of the body (Figure 14). Since the local effect of the force applied at the origin is very great, the origin is excluded by a hemispherical surface.

The above constitutes a description of the mathematical model to the Boussinesq problem. The problem herein was to resemble Boussinesq's; therefore the physical model had to resemble his mathematical model. Not only were the size of the neighborhood of the point to which the resultant force was applied and the dimensions of the solid body to fit the above description; but the model was also to be of convenient size to use with existing facilities. With this in mind, those factors which influenced the decisions in the construction of the model are now described. These decisions are divided into two broad areas, the size of the model and the neighborhood of the load. The latter is discussed first.

Love [34] shows that in particular instances strain due to equilibrating forces in a small portion of a body are unimportant at a distance from that portion. In particular, the displacement due to

a distribution of forces having a finite resultant for a small volume varies inversely as the distance from the resultant. It can be concluded that strain produced at a distance, by a force applied locally, depends upon the resultant force, and it is practically independent of the type of distribution of the forces which are statically equivalent to this resultant. The effect of the type of distribution of the forces is practically confined to a comparatively small portion of the body near to the place of application of the forces. These local effects are called by Boussinesq "perturbations locales" [34]. This result has been credited to Saint Venant and is often termed Saint Venant's Principal. However, Saint Venant was actually talking of self-equilibriating systems, i.e., those systems in which the distribution of forces over a small volume has a resultant of zero (Ref. von Mises [35]). Regardless of who first discussed this result, it does allow some freedom in choosing the type of distribution of a resultant concentrated load.

Frocht [36] also discussed the problem of a point load. In his discussion of Flammant's problem (the two dimensional analogue of the Boussinesq problem Figure 15), he shows that a distributed force acting on a semi-circular groove very nearly approximates a concentrated load. Frocht states that plastic deformation will always occur, no matter how small the applied force, around a concentrated load. In view of the above factors it was decided to apply the concentrated load through a steel ball. Such a body has a satisfactory shape and gives a confined distribution for the resultant force. Moreover as plastic deformation occurs, more surface area between the

ball and the model come into contact thus distributing the load over a greater area.

Having derived the type of neighborhood and established the force distribution for the resultant load, it remained to determine the size of the neighborhood. Here again Frocht's observations on the Flammant problem were used as a guide.

Dowel pins were used to produce the resultant load on the edge of a square of Columbia resin CR-39. A comparison of the isochromatic fringe pattern was made using various size dowel pins. It could be seen that away from the point of load the location of the fringes was the same (Figure 16). However, close to the load point there was a difference. This difference showed itself in the point of intersection of the isochromatic fringes and the loaded boundary of the plate. When the dowel pin was larger than $\frac{1}{2}$ inch in diameter, the fringes contacted the boundary over a greater distance. Pins below 1/8 inch in diameter tended to leave deep deformed notches (Figure 17) in the boundary after loading. Since the model was stress frozen its figure of merit was decreased (Ref. Frocht [37]). Therefore, it was felt a ball well over the 1/8 inch diameter suggested from the above should be used. A 3/8 inch diameter ball bearing was used to exert the resultant load upon the model.

A four inch cube was selected as the body which would support the concentrated load. The characteristic dimensions indicate a ratio of approximately 100 times more surface area on the loading surface of the body as compared to the cross-sectional area of the loading element.

The σ_{zz} normal stress at a distance of one diameter of the steel ball below the application of the point load was compared with σ_{zz} at approximately four inches below the point of application load; and it was determined by using the Boussinesq solution that the former normal stress was 100 times less than the latter. These observations influenced the final size model. However existing facilities were the deciding factors. It was felt that a larger cube would have made it extremely difficult to control the casting process without producing extreme exothermic reactions in solidification. Moreover, the evacuation chamber would not hold much more volume conveniently. A larger model would have meant increased machine shop time to finish the cast cube and slice the frozen stressed model for the transmitted light photoelastic study.

The shape of the model was chosen for convenience. The determination of coordinate position in the model was greatly simplified with this shaped body. Not only could alignment of the model be accomplished with respect to the fixed coordinate system of the scattered light polariscope, but the surfaces through which the propagating light beam enters the model were always normal to the beam. This eliminated the experimental problems associated with curved boundaries (Ref. Berghaus [21]).

The model was supported by a lubricated plate opposite to the load (Figure 18). It was decided that a check should be made to see whether this distributed load induced by the lubricated plate greatly changed the predicted results to the problem. The question was answered by looking at the Flammant problem. The model of the Flammant

problem was approximated by a finite element technique. A concentrated load was applied to the central mesh point on one side of a square net. The opposite side was loaded with a uniformly distributed load along the mesh points opposite in direction to the concentrated load. The remaining boundaries were free (Figure 19). The problem was solved by a finite element routine by Desai and Abel [38] and presently being modified for use in a Ph.D. thesis in crack propagation by Ronald H. Hardy in the School of Engineering Science and Mechanics at Georgia Institute of Technology. A comparison between the solution of the Flammant problem and the solution to the finite element problem showed that the distributed load in the finite element problem did not alter the results which would have been predicted by the Flammant results (Figures 20-22).*

The Constructed Model

The final model was constructed from a four inch cube of room temperature cure epoxy. (A description of the model manufacture is in Appendix B.) The concentrated load was directed vertically downward through the steel ball located in the center of one side of the cube (Figure 18). The opposite side was supported by the lubricated surface. The lubrication tended to keep frictional forces to a minimum when the model was stress frozen. The model was stress frozen with 5.375 lb. of applied load upon the steel ball.

*More reference to the approximation is found in the discussion of the results.

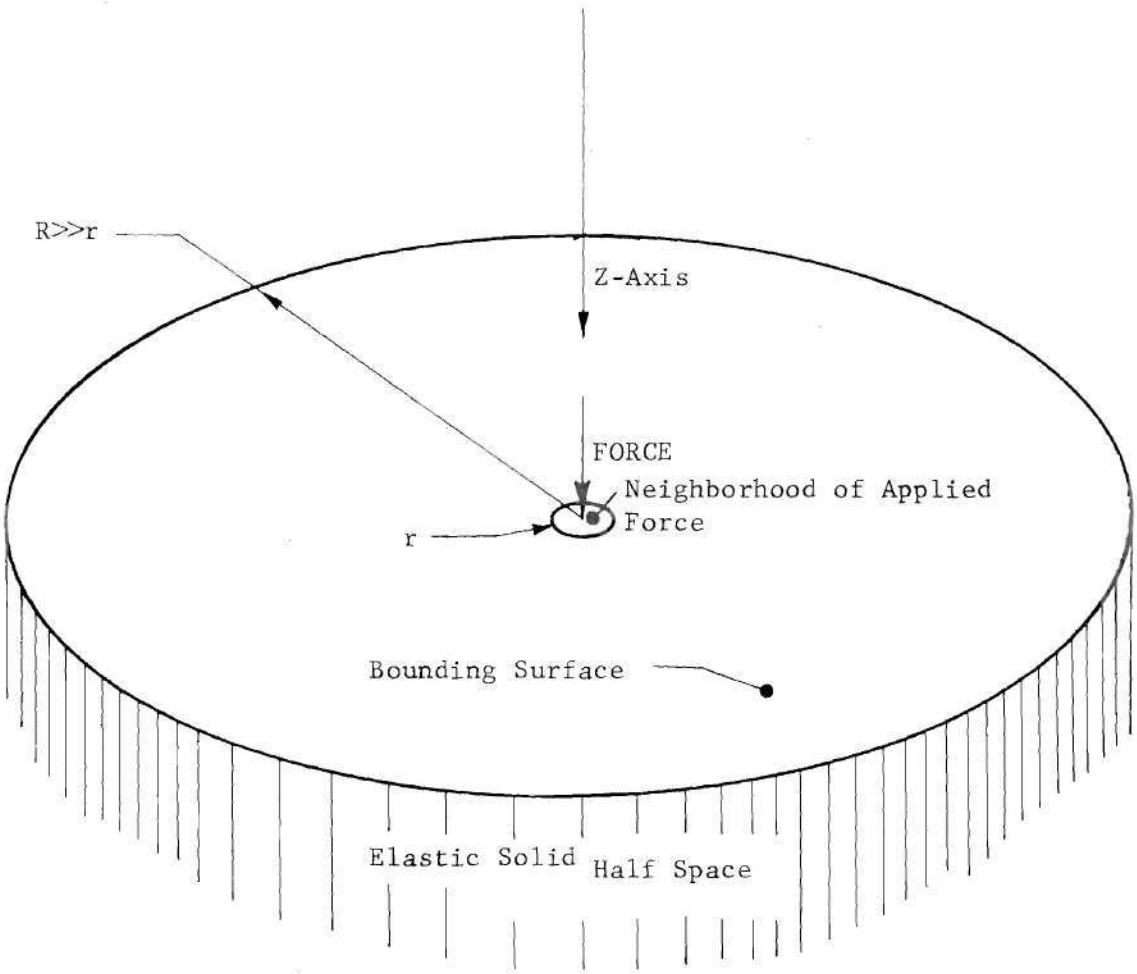

Figure 14. Model for Boussinesq Problem.

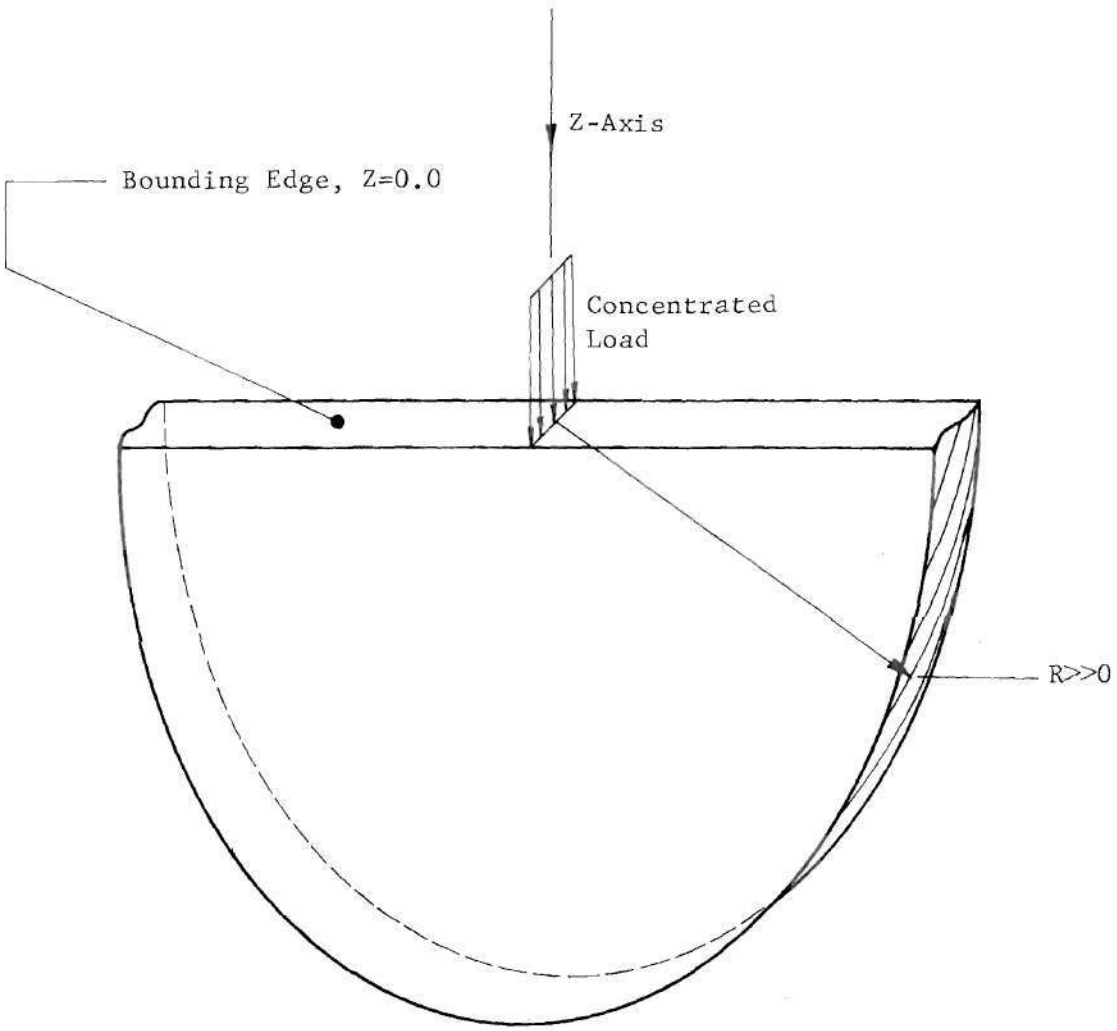

Figure 15. Model for Flammant Problem. Concentrated Load Normal to the Edge of a Half Plane.

1/8 inch load pin

1/2 inch load pin

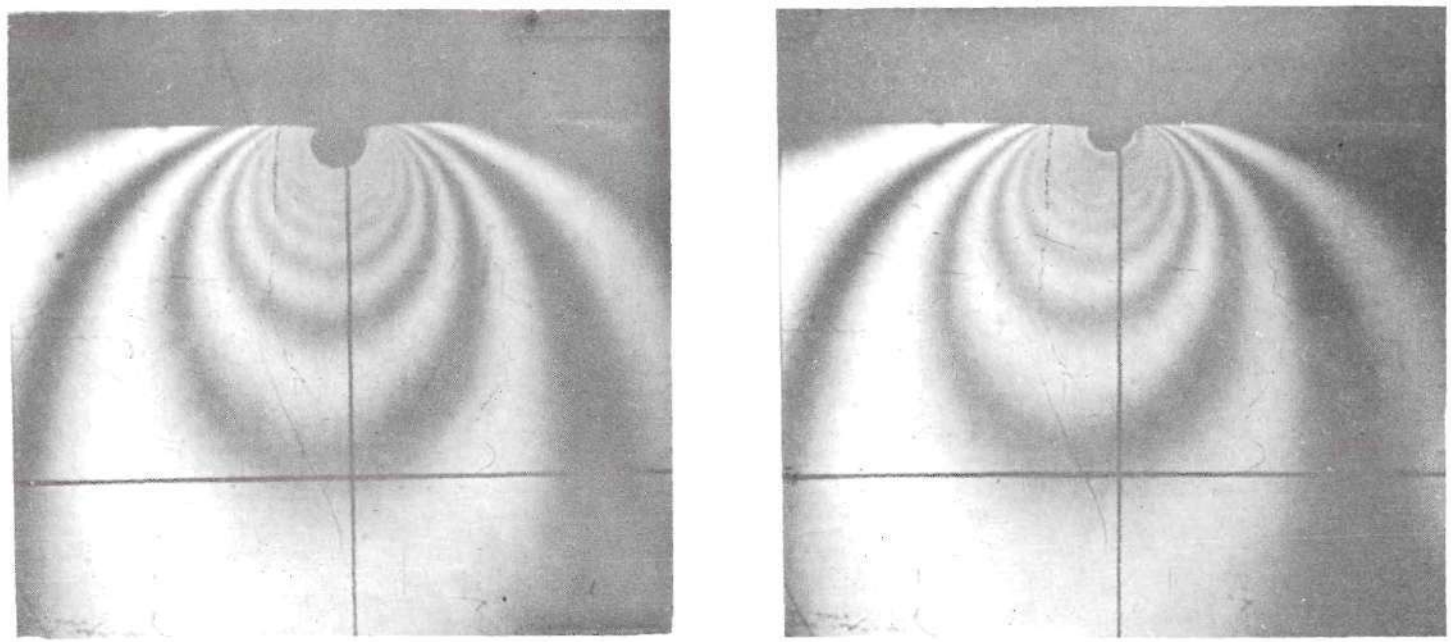

Figure 16. Flammant Problem Isochromatic Fringes Showing Load Pin Size Has No Significant Effect Upon Location of Fringes Away From Load Point.

1/8 inch load pin

1/2 inch load pin

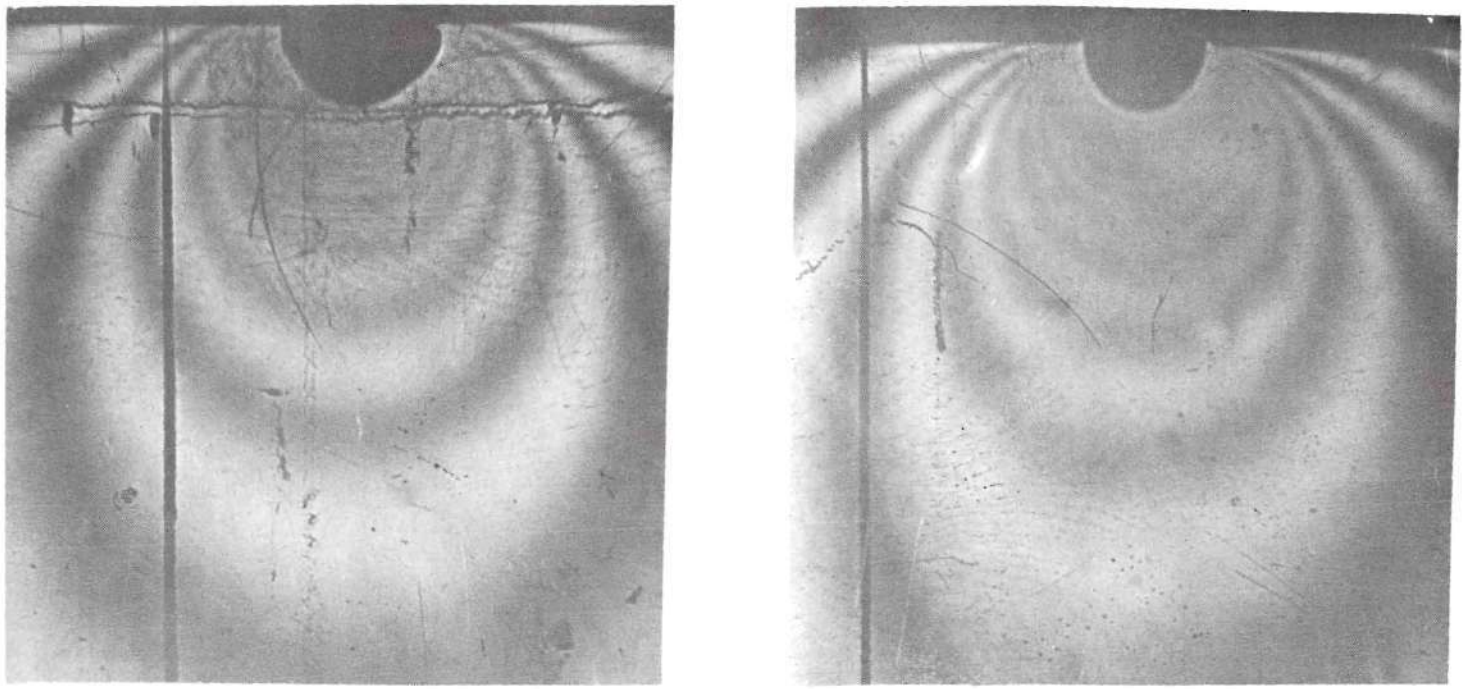

Figure 17. Flammant Problem Isochromatic Fringes Showing Deformed Load Area Caused by 1/8 inch Load Pin Compared to Uniform Load Area Under 1/2 inch Pin.

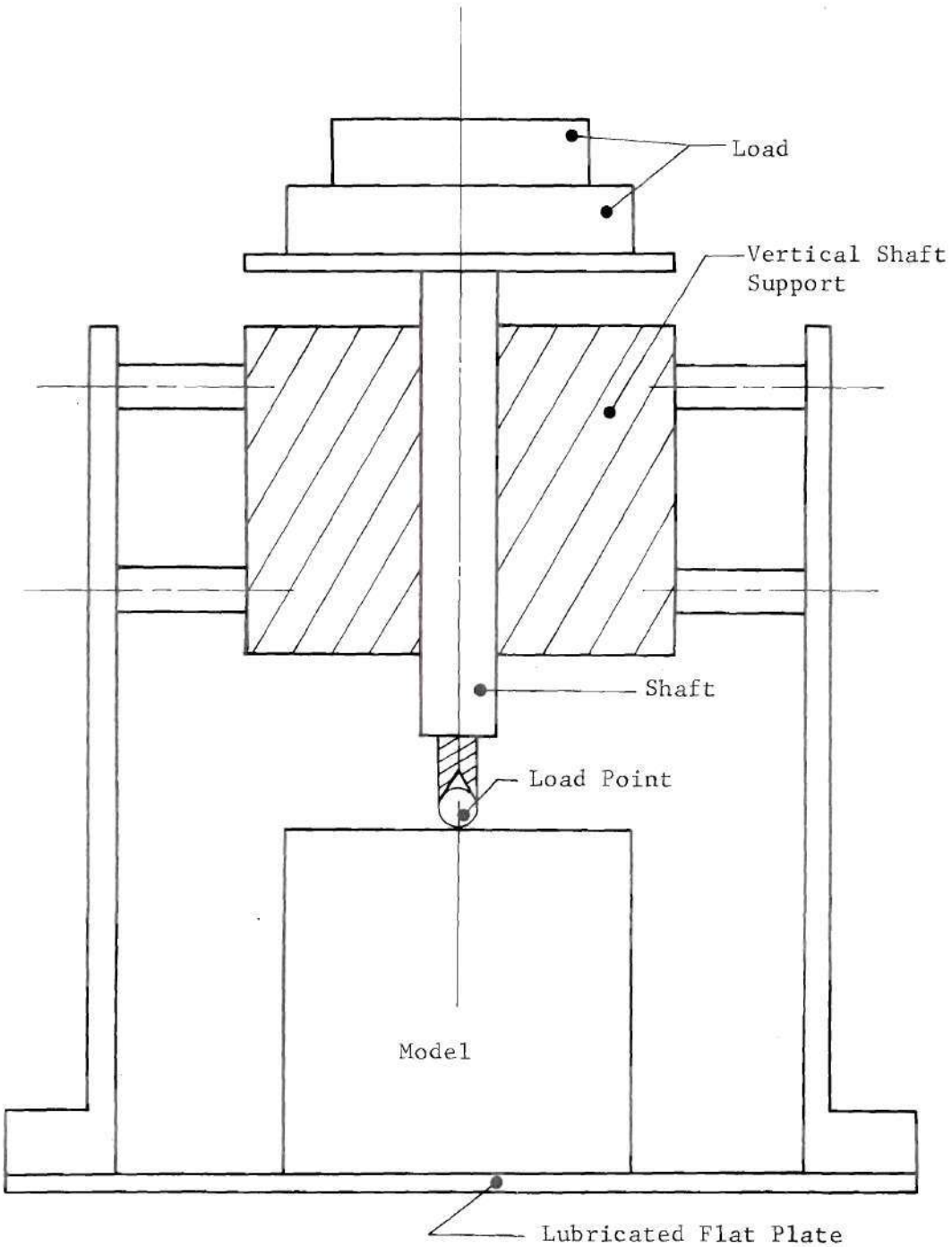

Figure 18. Sketch of Loading Frame.

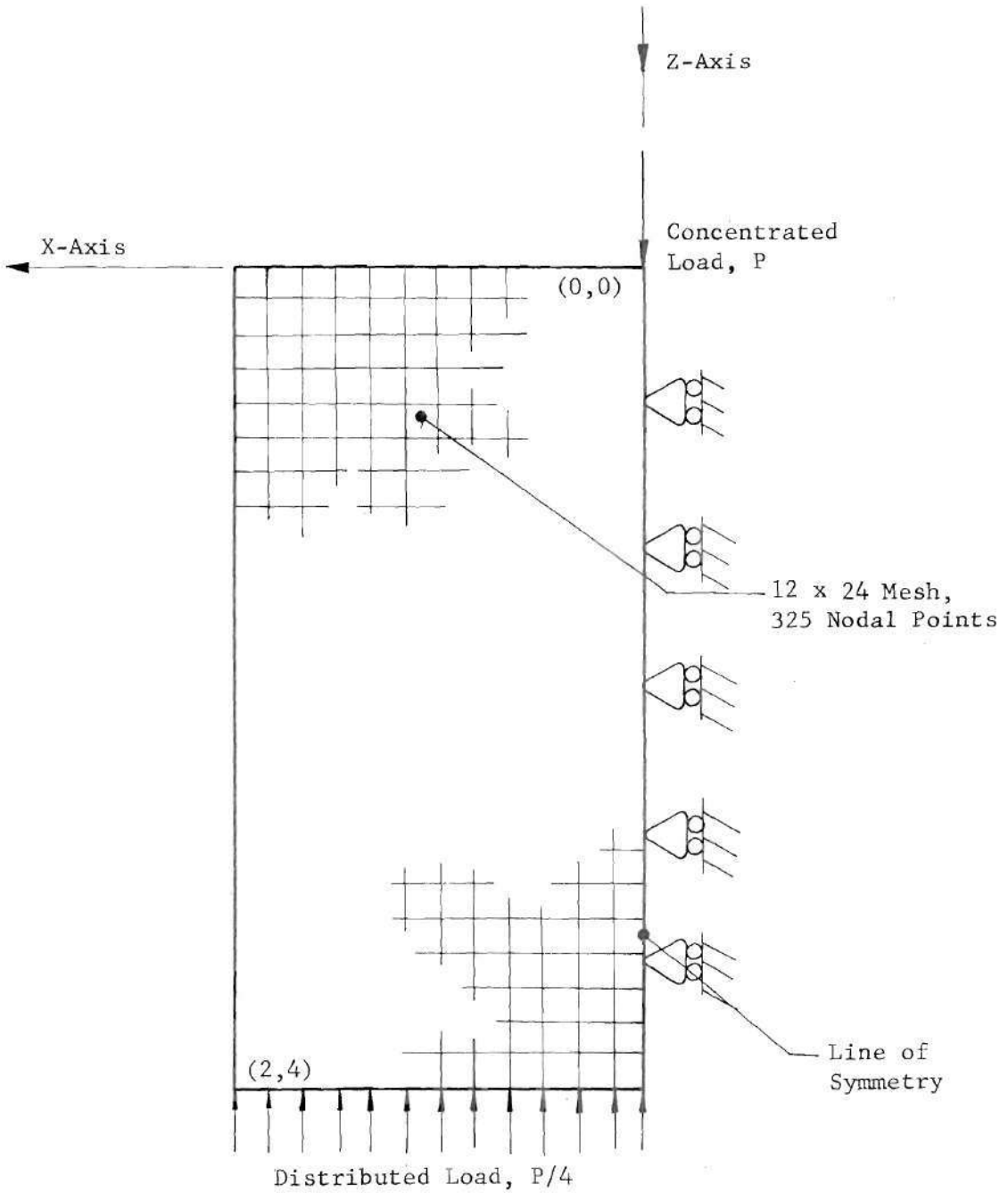

Figure 19. Finite Element Model.

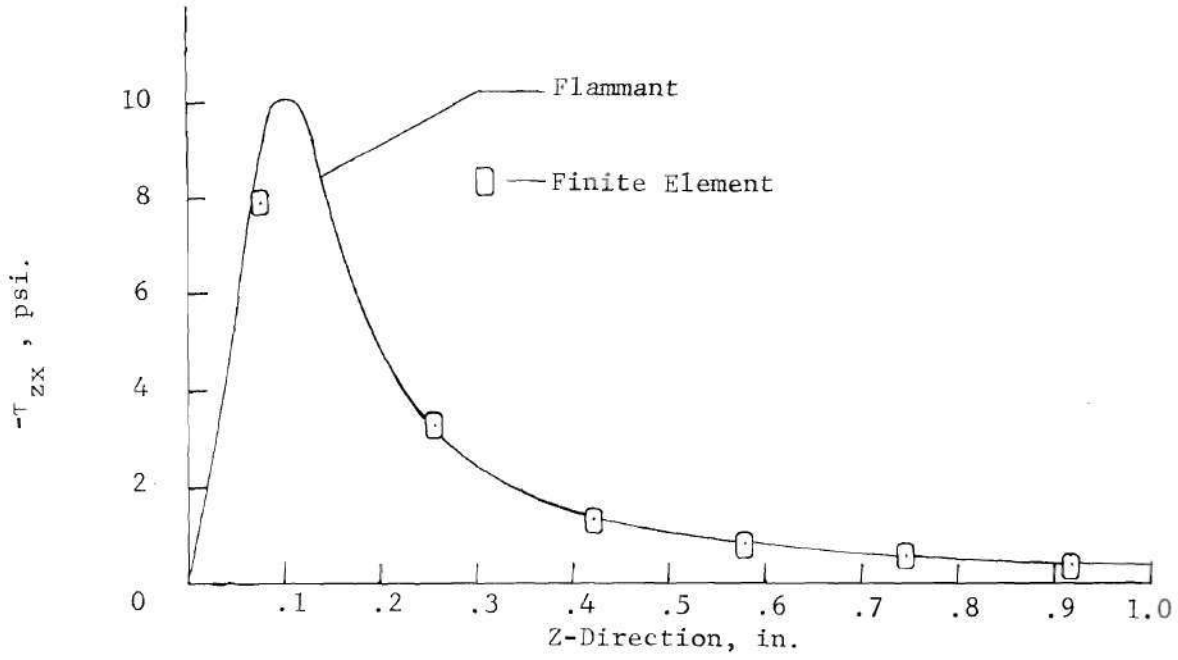

Figure 20. Comparison of τ_{zx} Stress for the Finite Element and Flammant Problems along Line X = .08 in..

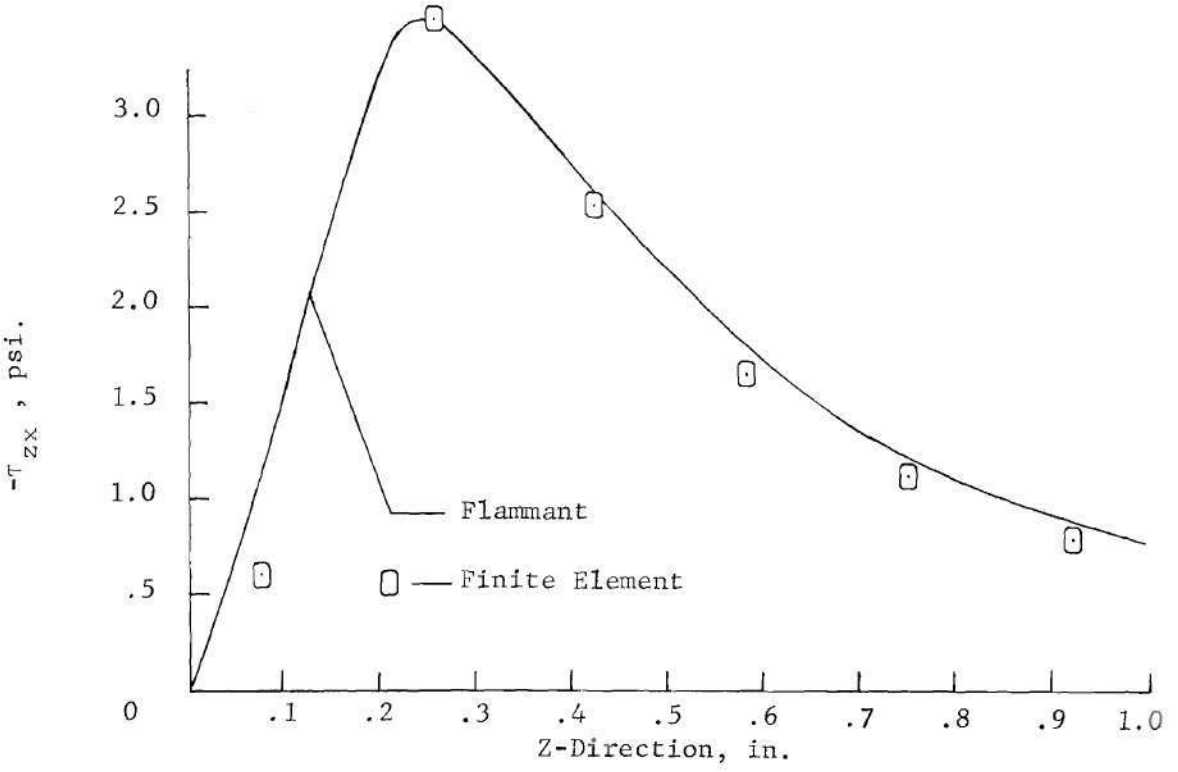

Figure 21. Comparison of τ_{zx} Stress for the Finite Element and Flammant Problems along Line X=.25 in..

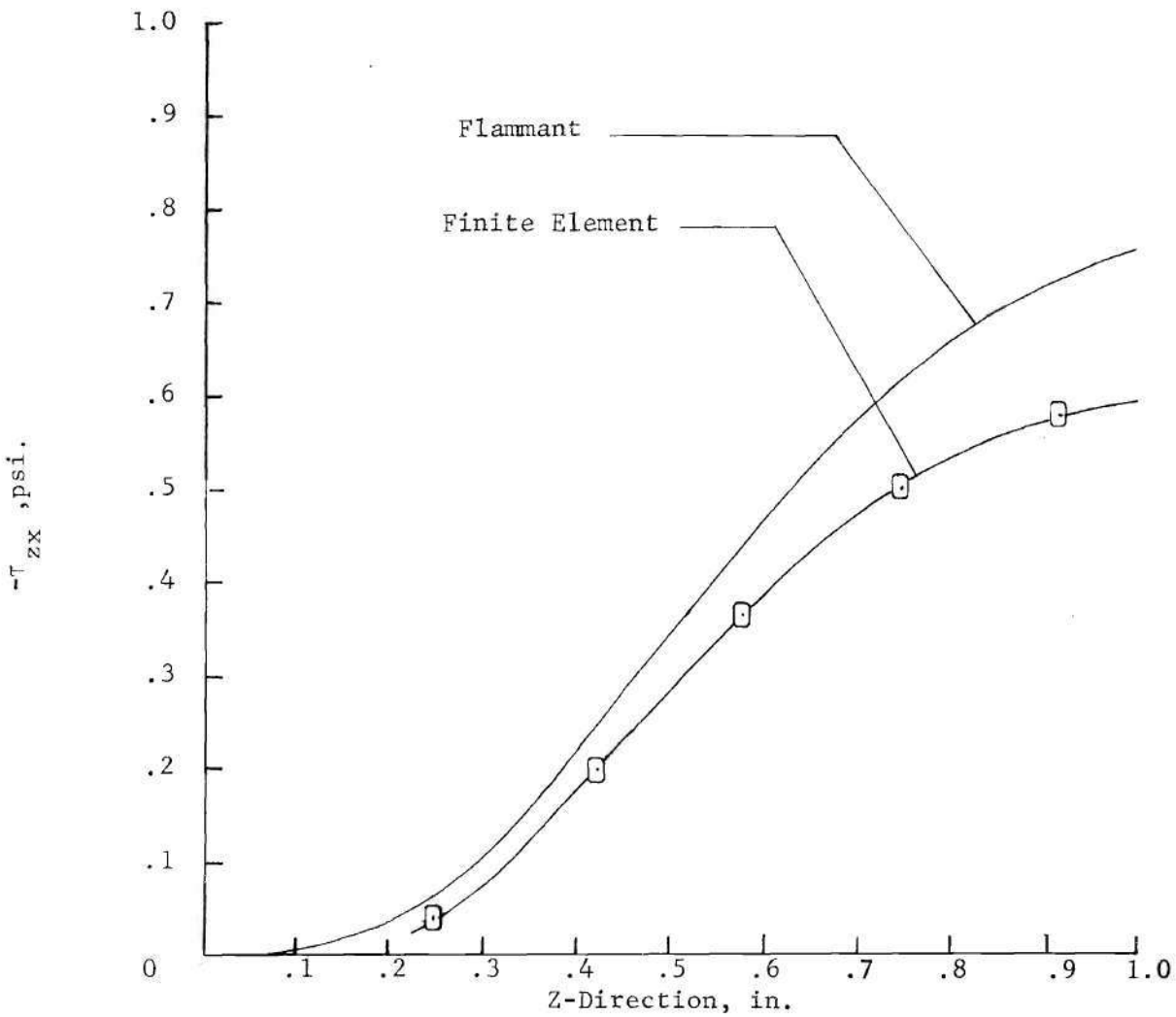

Figure 22. Comparison of τ_{zx} Stress for the Finite Element and Flammant Problems along Line X=1.08 in..

CHAPTER VI

RESULTS

This section is divided into two parts. In the first the results obtained by scattered light and frozen stress techniques are considered. In the second these results are compared with the analytical results for the infinite body problem.

Comparison of the Scattered Light and the Transmitted Light Photoelastic Results

This technique of scattered light photoelasticity was tested by using it to find the shear stresses in the model on the plane $y = .1$ inches, $x \geq .1$ inches (Figure 23) and comparing the stresses as found with those found by slicing and using transmitted light photoelasticity. Both sets of shear stresses (Figure 24) through (Figure 41) are plotted. The plane $y = .1$ inches, $x \geq 0$ inches was sliced from the model (Figure 42) and the τ_{xz} shear stresses were determined at .1 inch increments along lines $x = .1$ through $x = .6$ inches. Three other slices were taken from the model. The τ_{yz} shear stresses along the lines $x = .2$, .3 and .5 inches were determined from these slices (Figure 43). Due to the symmetry of the model τ_{xz} equals τ_{yz} along the line $x = .1$ inches; and hence, a comparison of τ_{yz} by both scattered and transmitted light are shown along line $x = .1$ inches.

A relationship between the two solutions can be directly observed from the plotted points. Freehand curves have been fitted to the sets of results (with the exception of (Figure 24) through

(Figure 26)) to allow ready comparison. However, to reinforce this visual comparison the relationship between the results was next dealt with in a statistical manner. For the greatest confidence in the validity of the process, it was felt that a correlation or degree of relationship between the variables should be demonstrated. This correlation was shown by constructing confidence intervals about a curve which was assumed to best fit the results. In this manner it was possible to say with confidence that the results were very good.

Three typical cases were considered (Figures 24-26). These were the τ_{xz} shear stresses along lines x = .1, .2, and .3 inches. Eighth order polynomials were fitted to the data by the method of least squares. These curves were used to estimate the shear stress τ_{xz} for the statistical calculations of the confidence intervals. If the values from these curves are denoted $\tau_{est.}$ for a given value of z, a measure of the scatter about this constructed curve is supplied by the quantity

$$S = \left(\frac{\sum^{n} (\tau_{actual} - \tau_{est.})^2}{n} \right)^{1/2}$$

which is called the standard error of estimate. Curves are constructed at a normal distance of 2S on both sides of the least squares curve. They correspond to the approximate 95 percent confidence limits (Ref. Kurtz [39]).

It can be seen that the bulk of the results lay within the 95 percent confidence interval. The majority of the results lay within the even more stringent 68 percent confidence limit. Thus it is

evident the results are in excellent agreement.

Experiment Versus Theory

Since the Boussinesq model was used to guide the efforts in the solution of the finite model, the results are compared to the Boussinesq solution. This comparison is shown in Figure 44 through Figure 61. Since the finite model could not approximate the infinite model except in the region of the applied load, it was not surprising that the Boussinesq solution closely approximated the results for the lines x = .1, .2 and .3 inches. Beyond x = .3 inches the comparison was as good as could be expected.

This quality of comparison was expected because the same trend could be determined when the finite element solutions of a point load on a finite plate was compared to the Flammant solution for the infinite plane problem. In the region next to the concentrated load, these two solutions closely approximated each other (Figure 20 and Figure 21). However, as the distance from the concentrated load increased, the difference between the two solutions increased (Figure 22).

Although this trend gave confidence in the results, the prime substantiation that this technique is valid was the comparison with the sub-slicing technique. These results confirm that this method is at least as good as other acceptable techniques of scattered light photoelasticity. It has the distinct advantage over other methods of being able to determine data at any point along the path of the incident light beam. This would be of tremendous use for example in the solution of problems involving composites. With this new technique

more data points and evenly spaced data points could be determined between fibers than with standard scattered light techniques. Furthermore the method developed has been enhanced by the construction of a scattered light polariscope which is considered to be more versatile and more accurate than similar systems (Ref. 23).

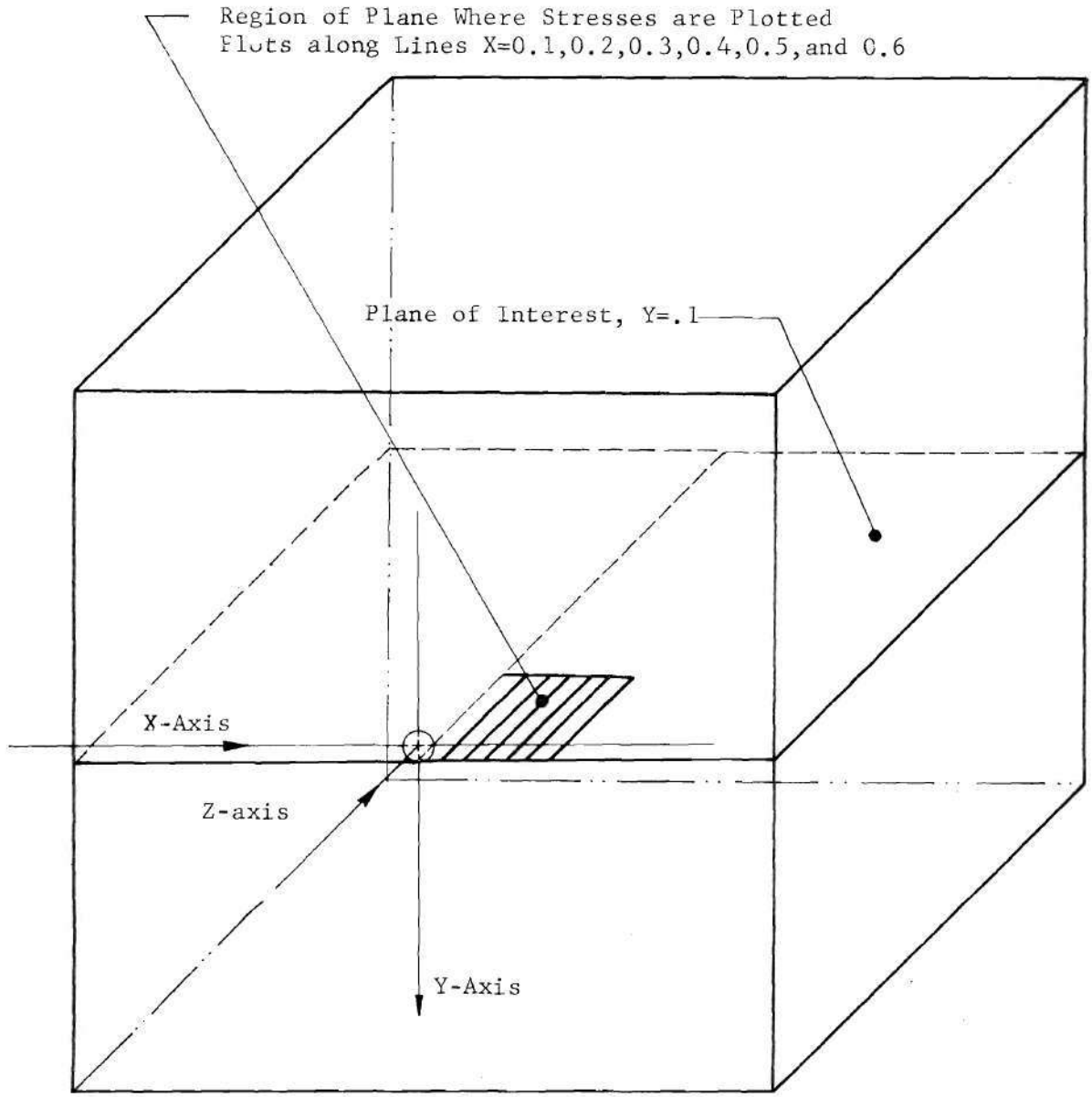

Figure 23. Region of Determined Shear Stress.

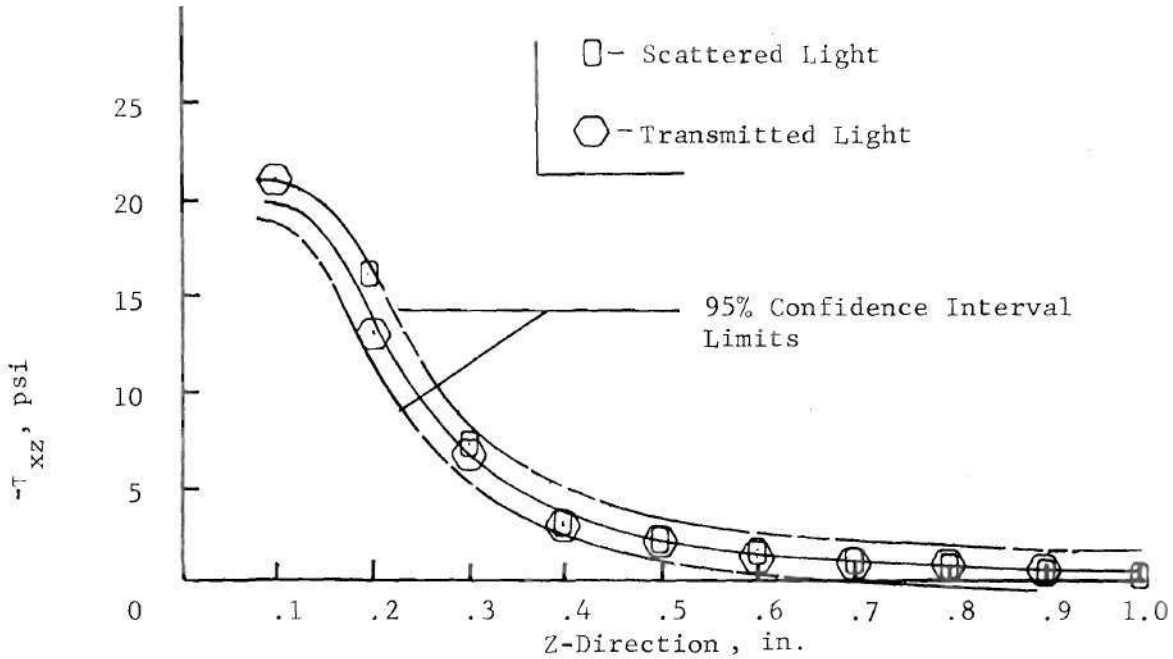

Figure 24. Comparison of τ_{xz} Shear Stresses along Line X = .1 in. as Determined by Two Photoelastic Methods.

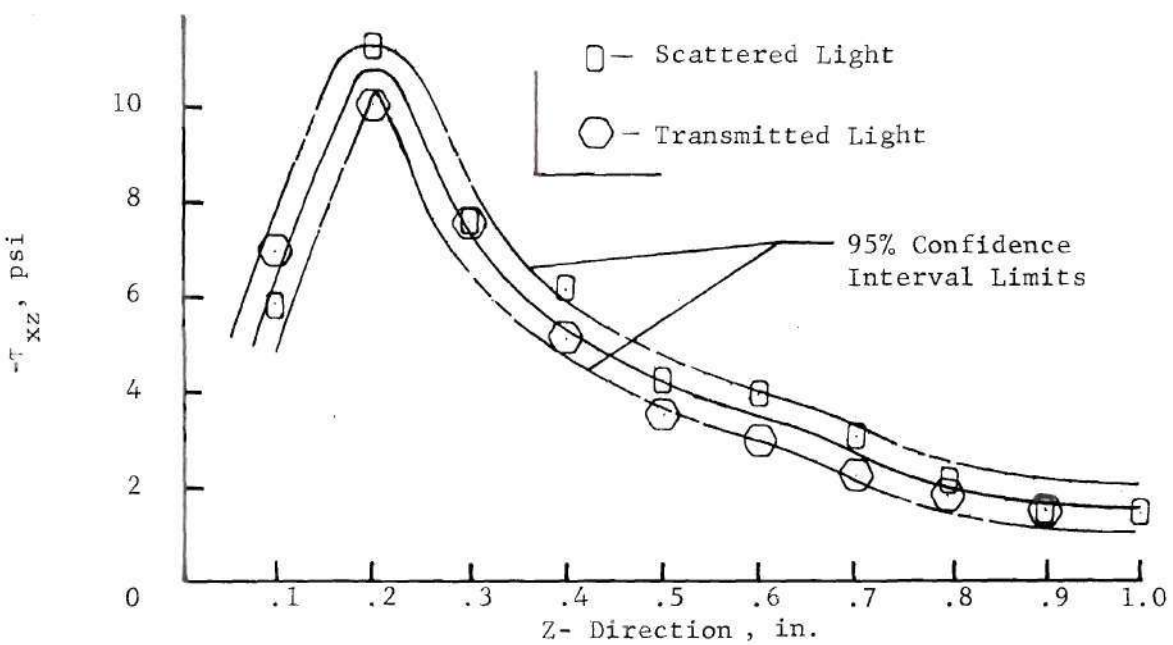

Figure 25. Comparison of τ_{xz} Shear Stresses along Line X = .2 in. as Determined by Two Photoelastic Methods.

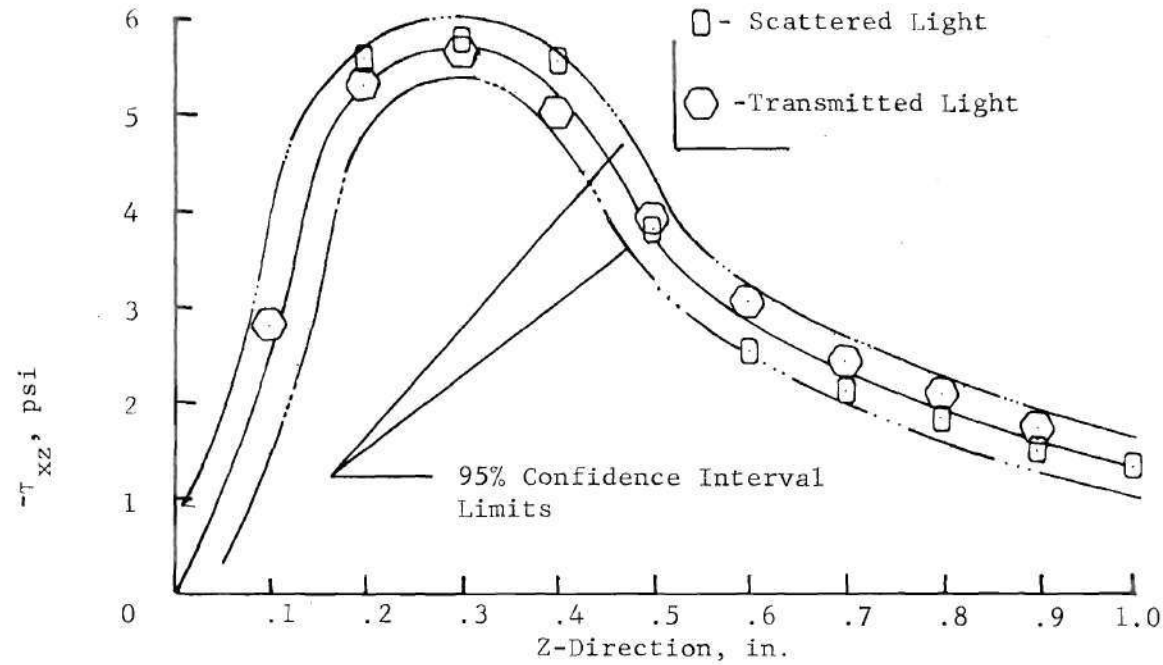

Figure 26. Comparison of τ_{xz} Shear Stresses along Line X = .3 in. as Determined by Two Photoelastic Methods.

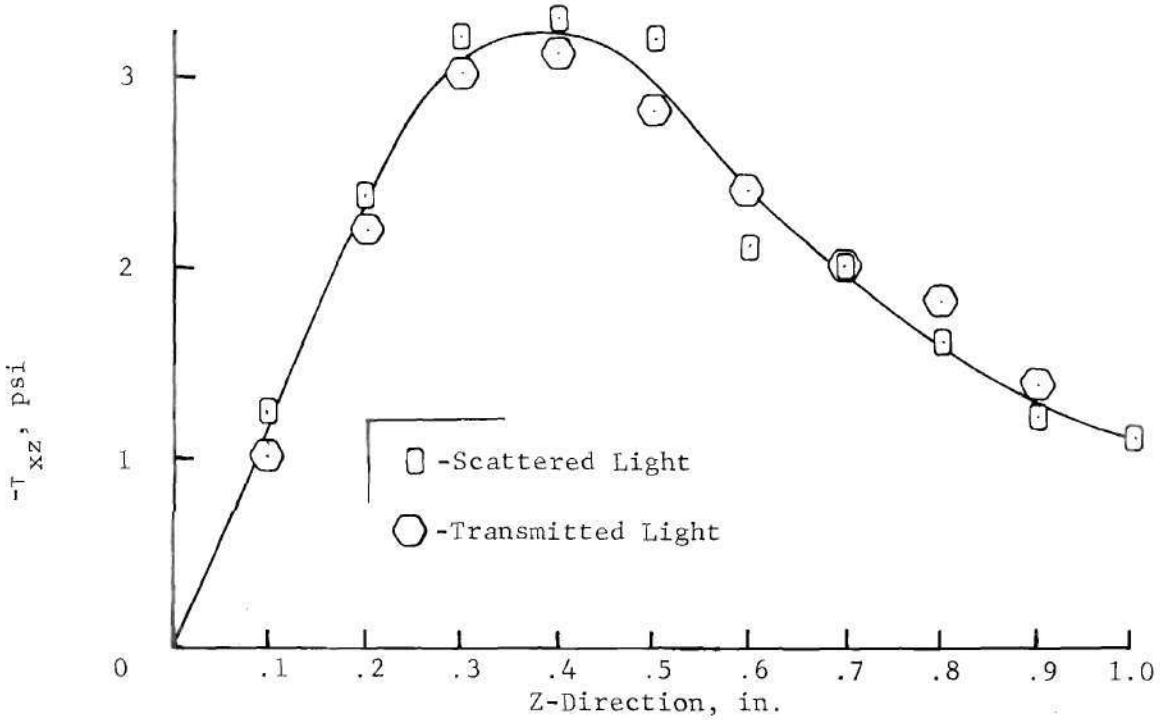

Figure 27. Comparison of τ_{xz} Shear Stresses along Line X = .4 in. as Determined by Two Photoelastic Methods.

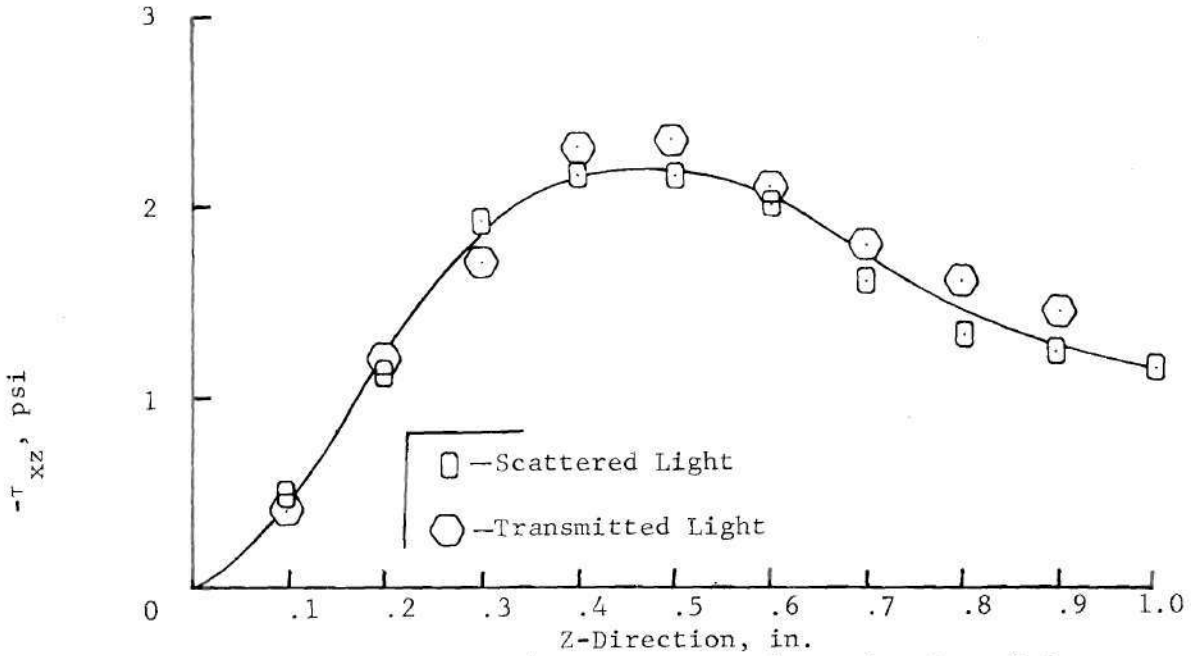

Figure 28. Comparison of τ_{xz} Shear Stresses along Line X = .5 in. as Determined by Two Photoelastic Methods.

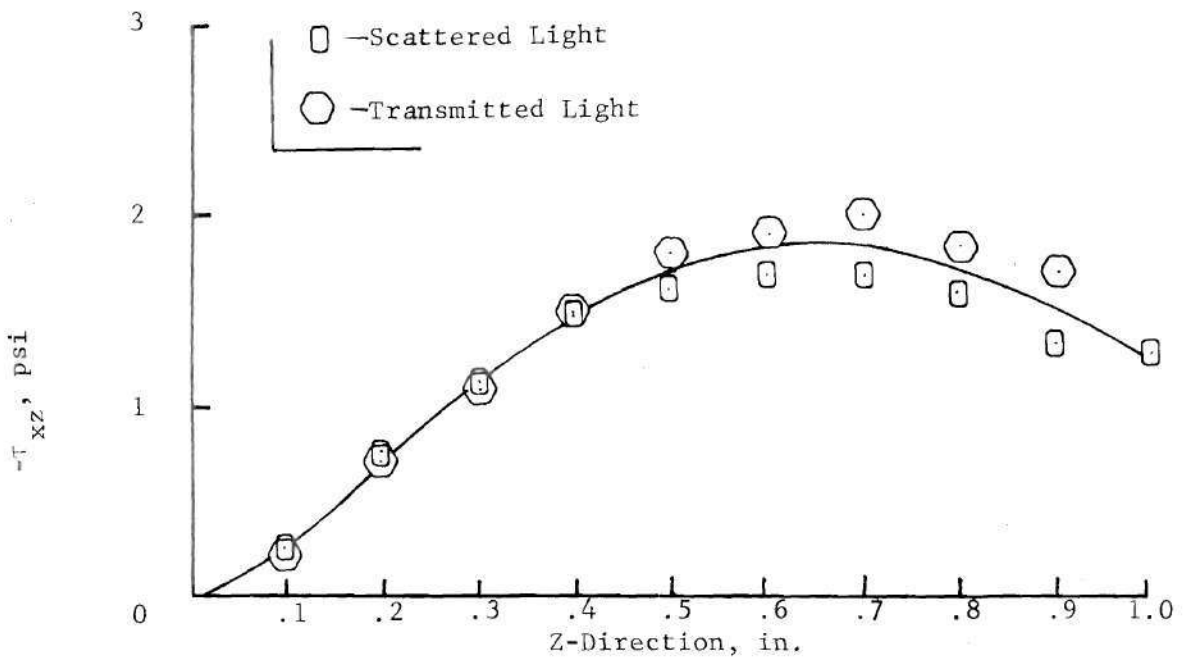

Figure 29. Comparison of τ_{xz} Shear Stresses along Line X = .6 in. as Determined by Two Photoelastic Methods.

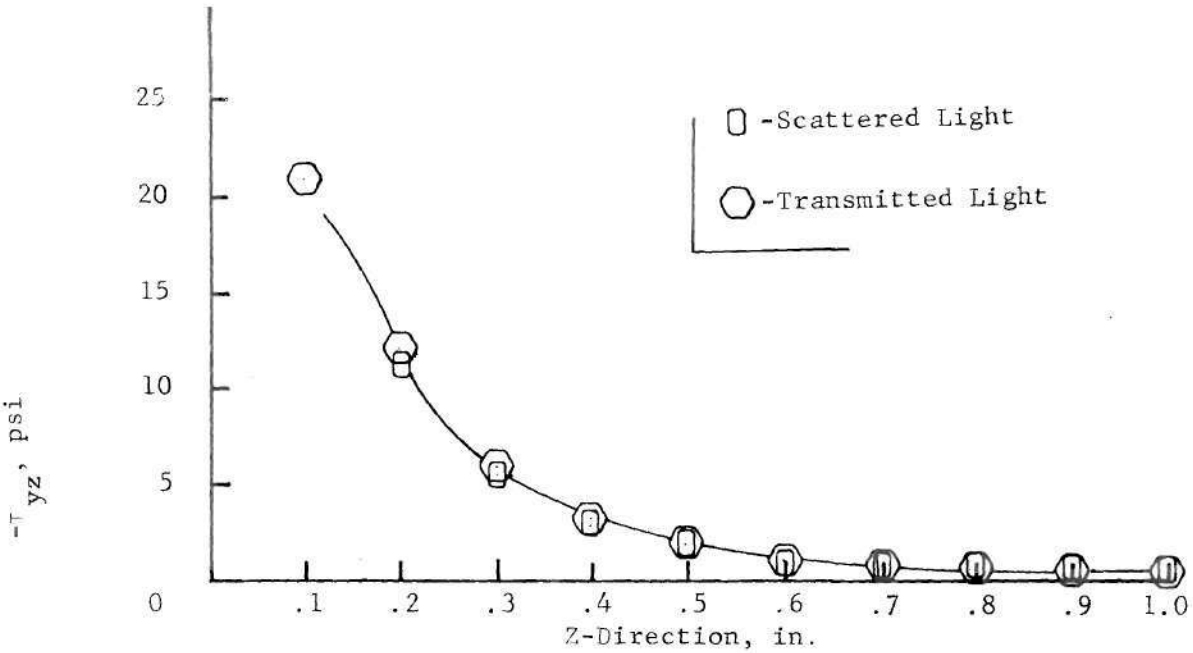

Figure 30. Comparison of τ_{yz} Shear Stresses along Line X = .1 in. as Determined by Two Photoelastic Methods.

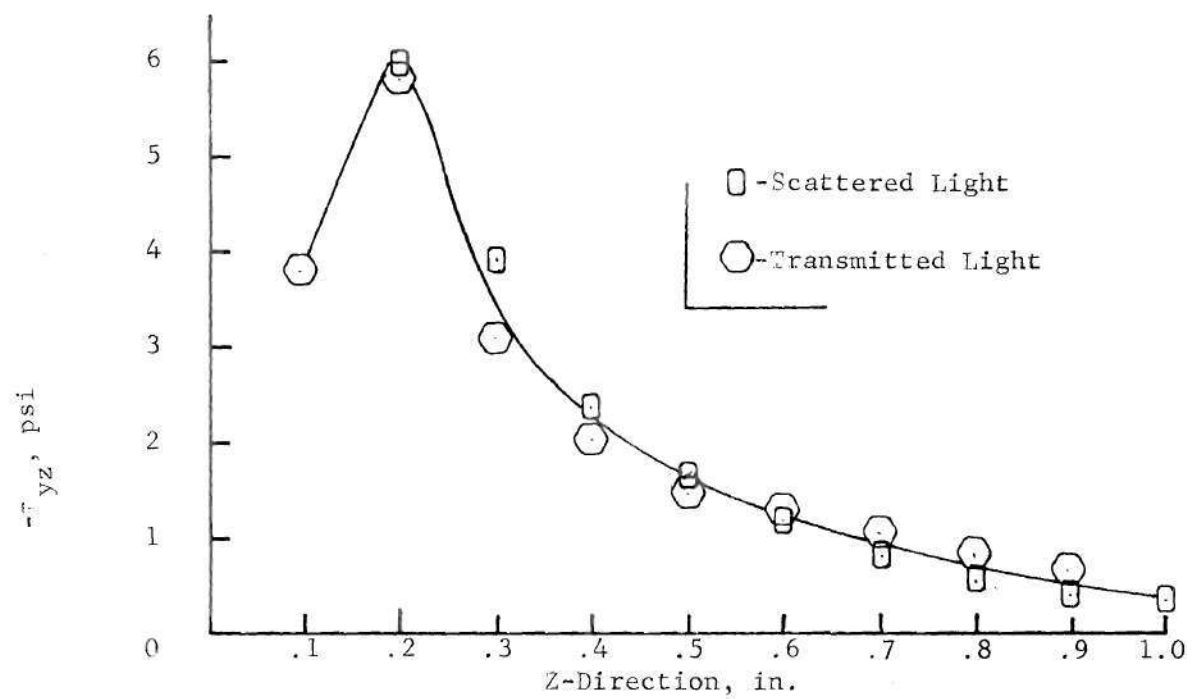

Figure 31. Comparison of τ_{yz} Shear Stresses along Line X = .2 in. as Determined by Two Photoelastic Methods.

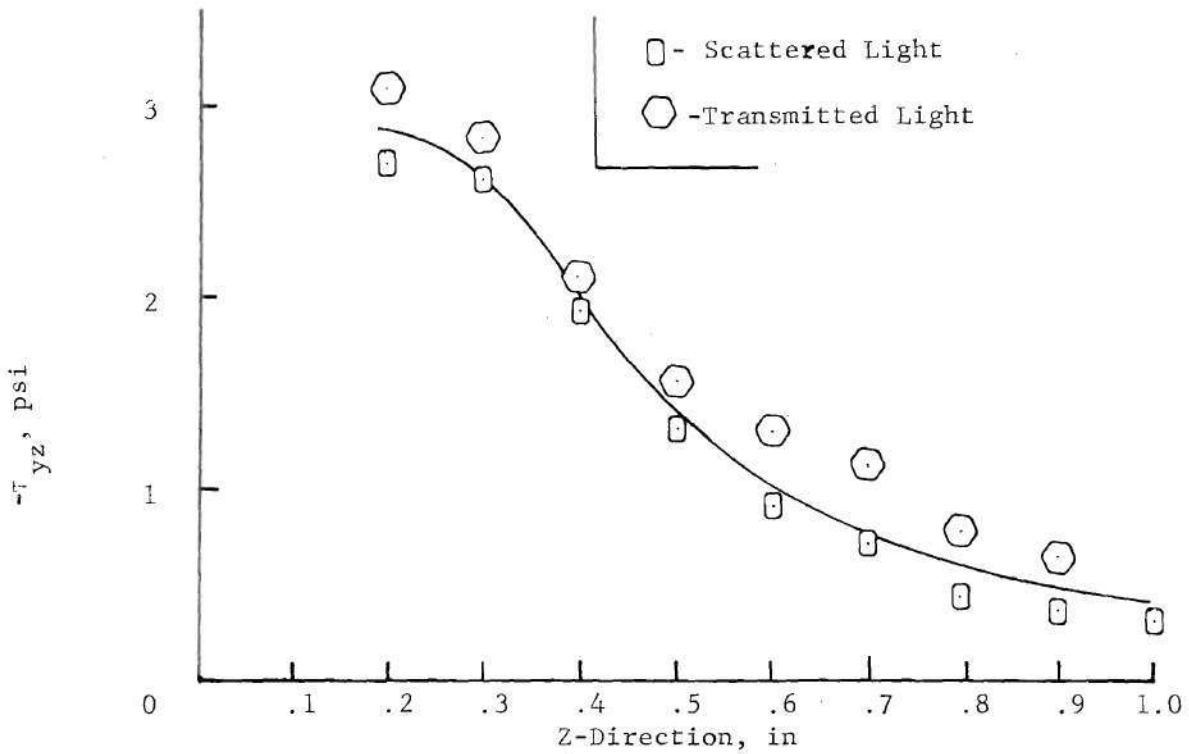

Figure 32. Comparison of τ_{yz} Shear Stresses along Line X = .3 in. as Determined by Two Photoelastic Methods.

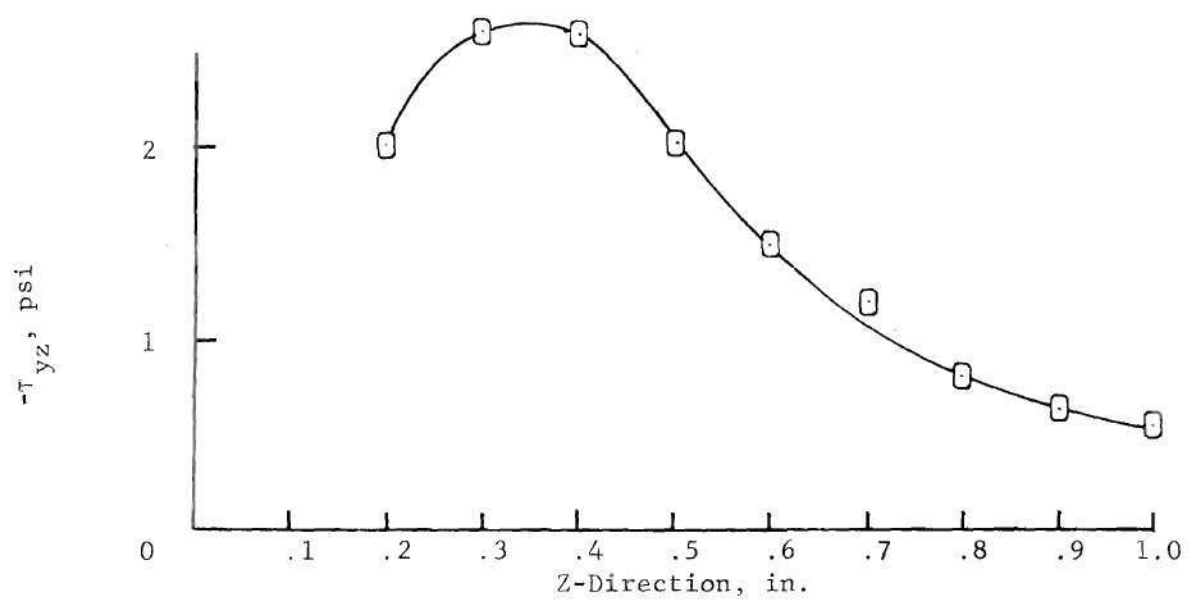

Figure 33. τ_{yz} Shear Stress along Line X = .4 in. as Determined by Scattered Light Photoelasticity.

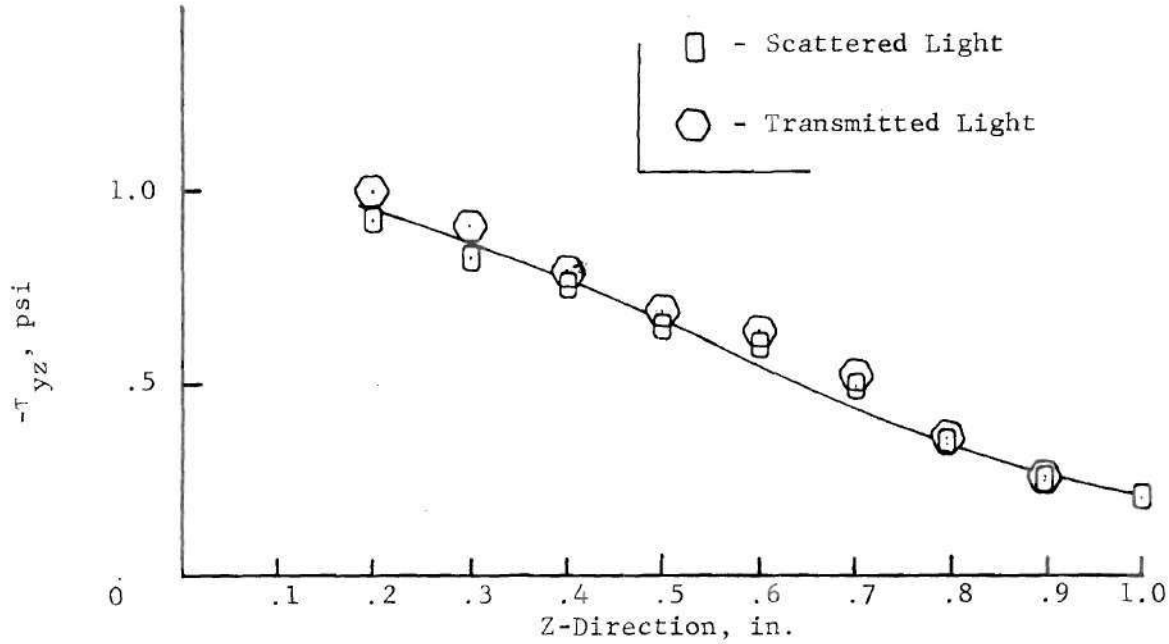

Figure 34. Comparison of τ_{yz} Shear Stresses along Line X = .5 in. as Determined by Two Photoelastic Methods.

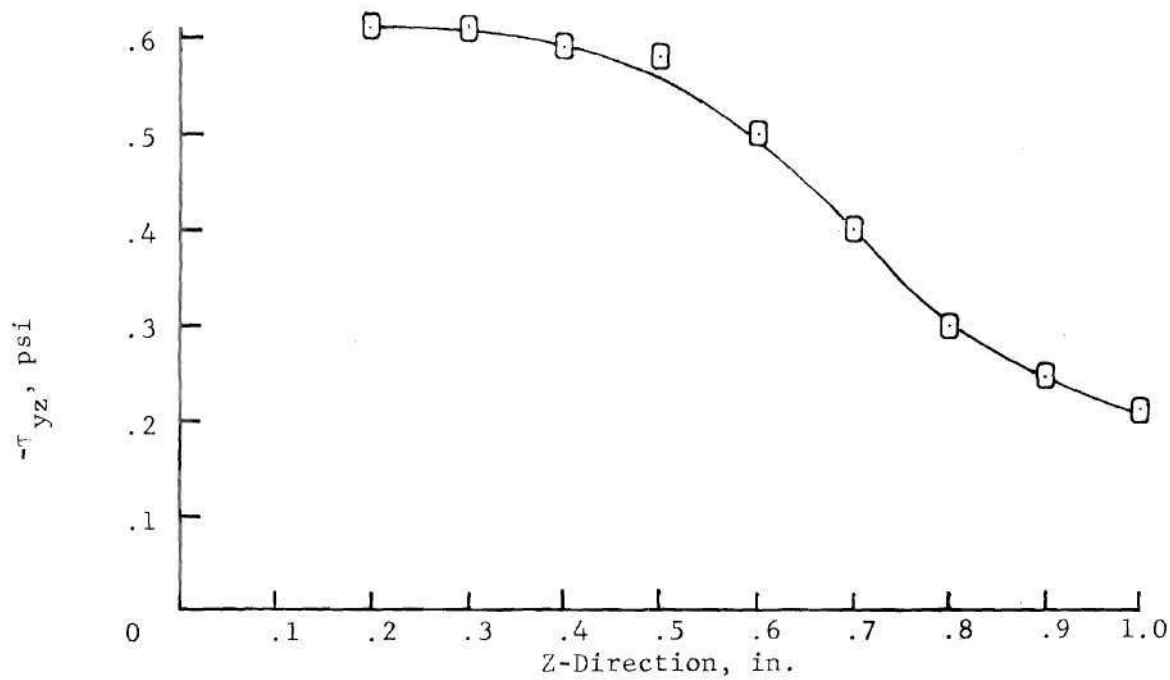

Figure 35. τ_{yz} Shear Stresses along Line X = .6 in. as Determined by Scattered Light Photoelasticity.

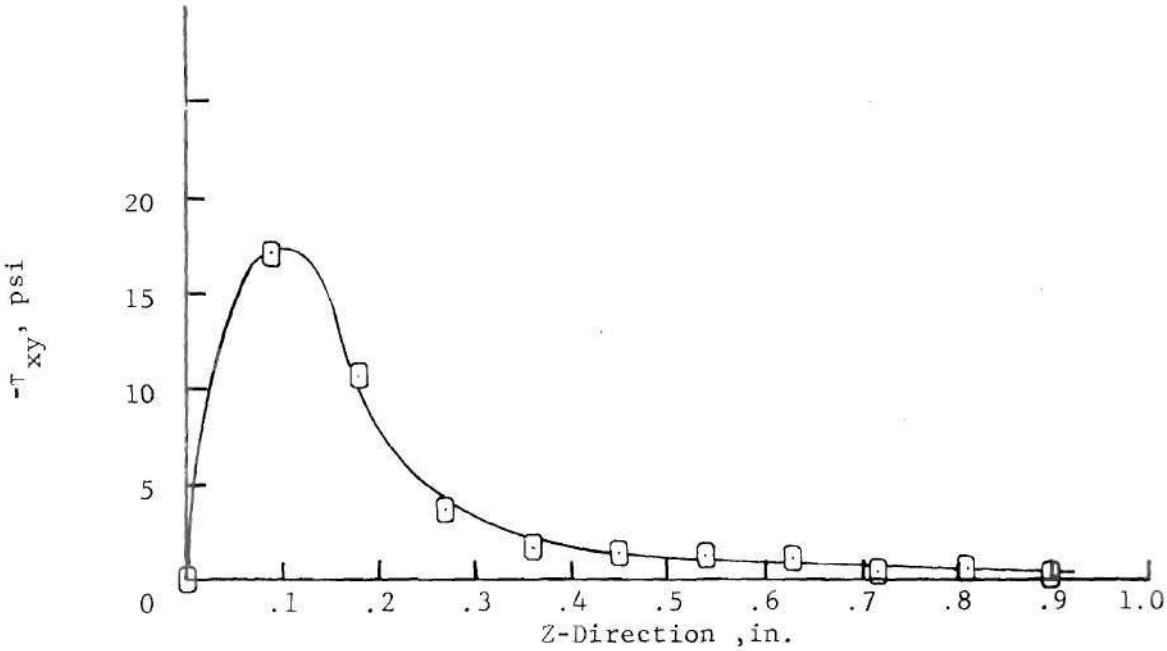

Figure 36. τ_{xy} Shear Stresses along line X = .1 in. as Determined by Scattered Light Photoelasticity.

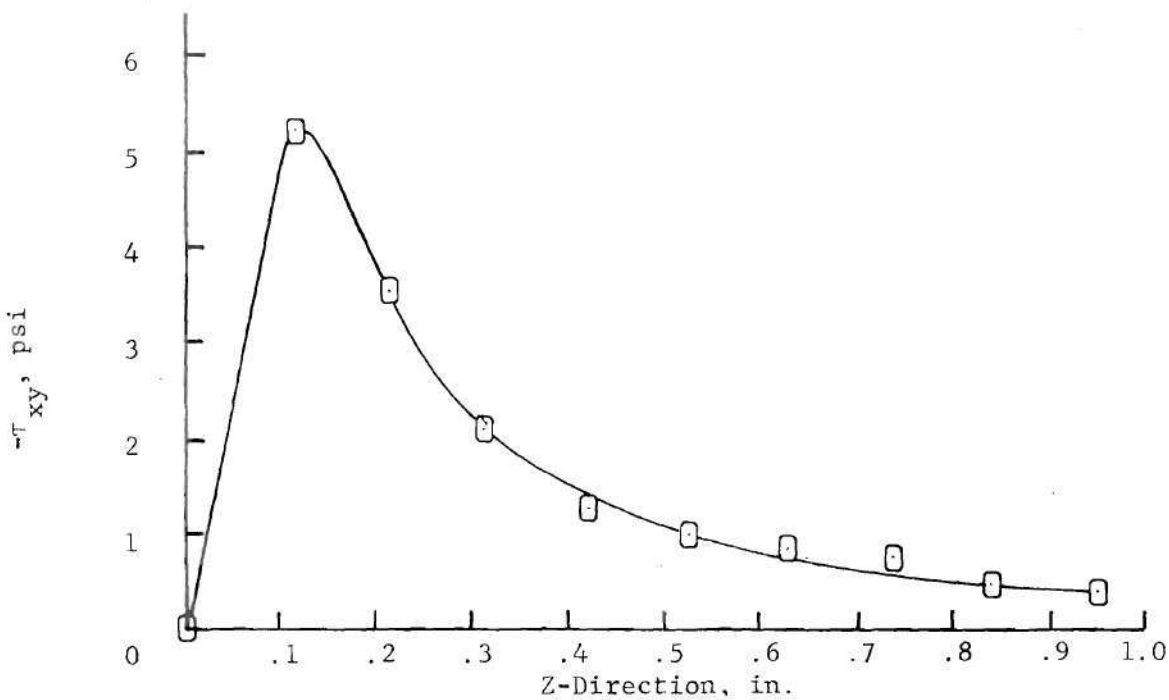

Figure 37. τ_{xy} Shear Stresses along Line X = .2 in. as Determined by Scattered Light Photoelasticity.

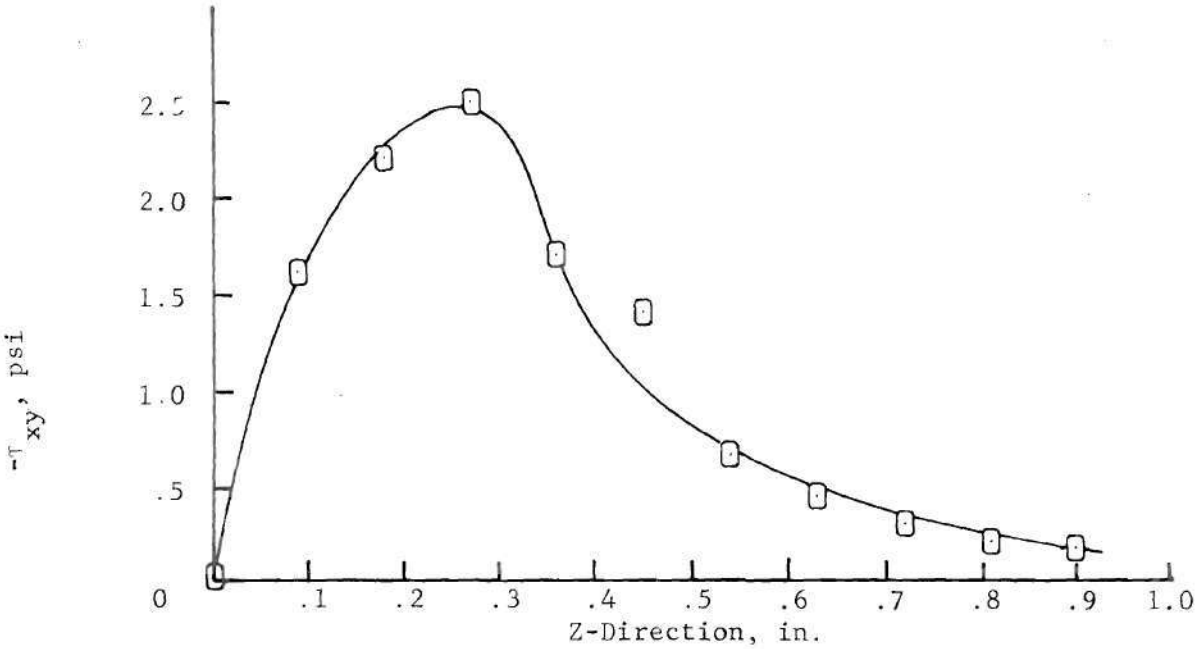

Figure 38. τ_{xy} Shear Stresses along Line X = .3 in. as Determined by Scattered Light Photoelasticity.

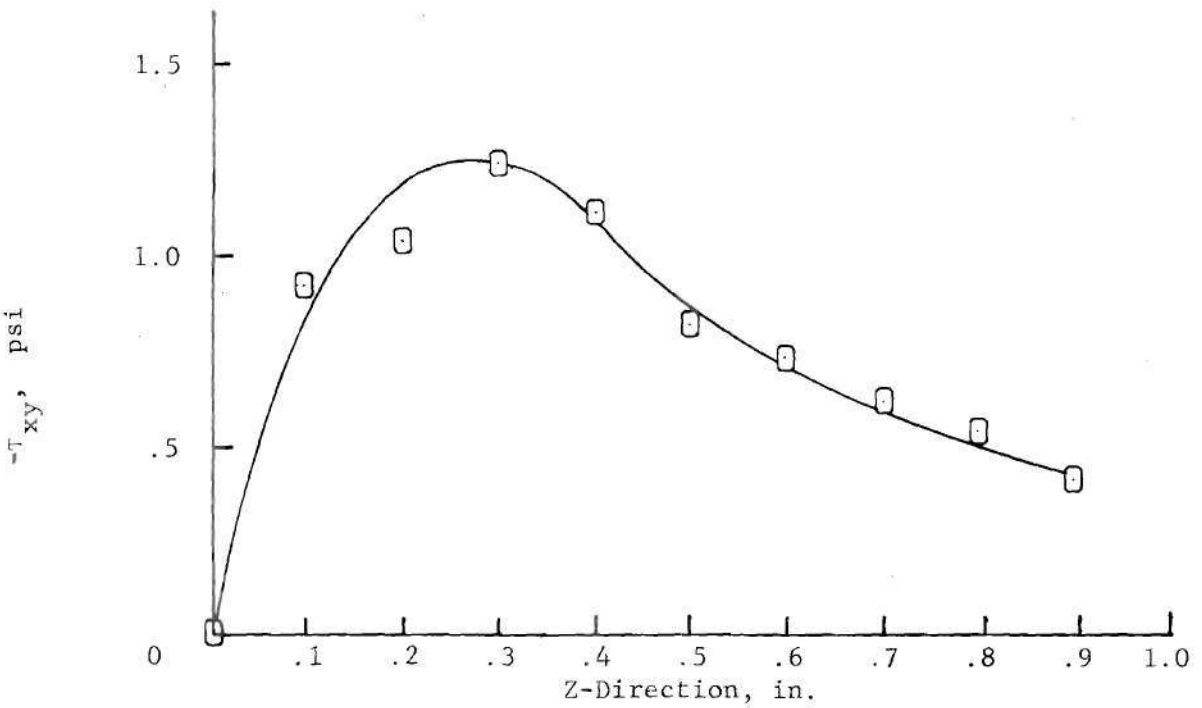

Figure 39. τ_{xy} Shear Stresses along Line X = .4 in. as Determined by Scattered Light Photoelasticity.

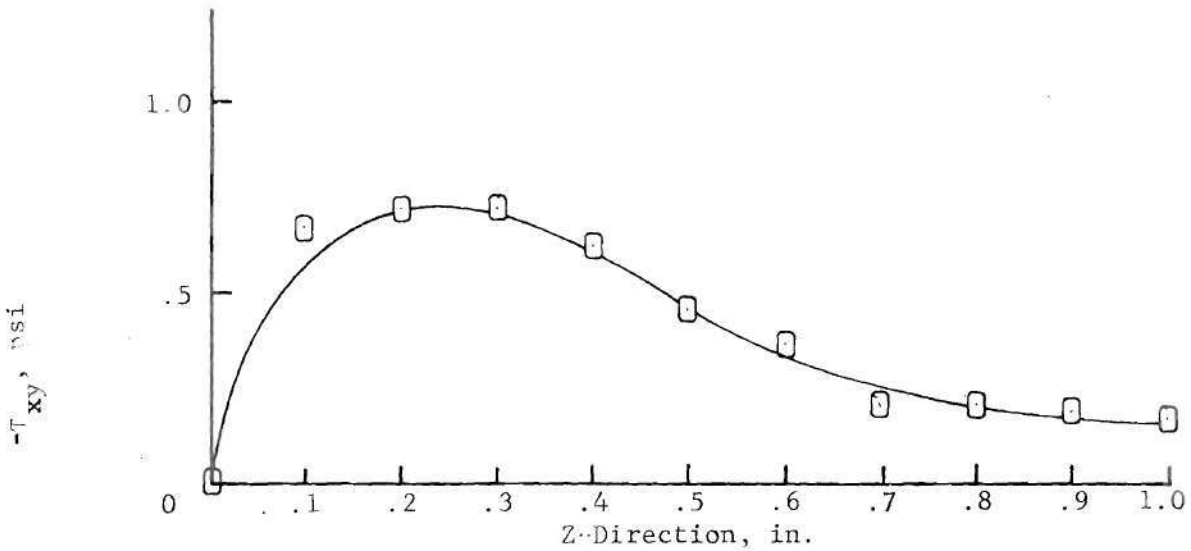

Figure 40. τ_{xy} Shear Stresses along Line X = .5 in. as Determined by Scattered Light Photoelasticity.

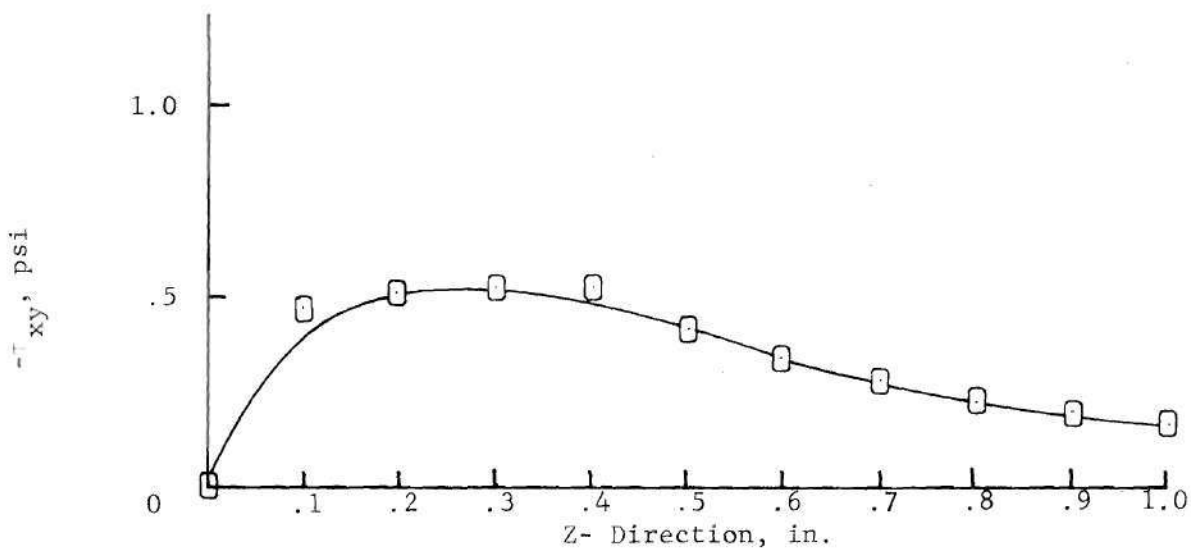

Figure 41. τ_{xy} Shear Stresses along Line X = .6 in. as Determined by Scattered Light Photoelasticity.

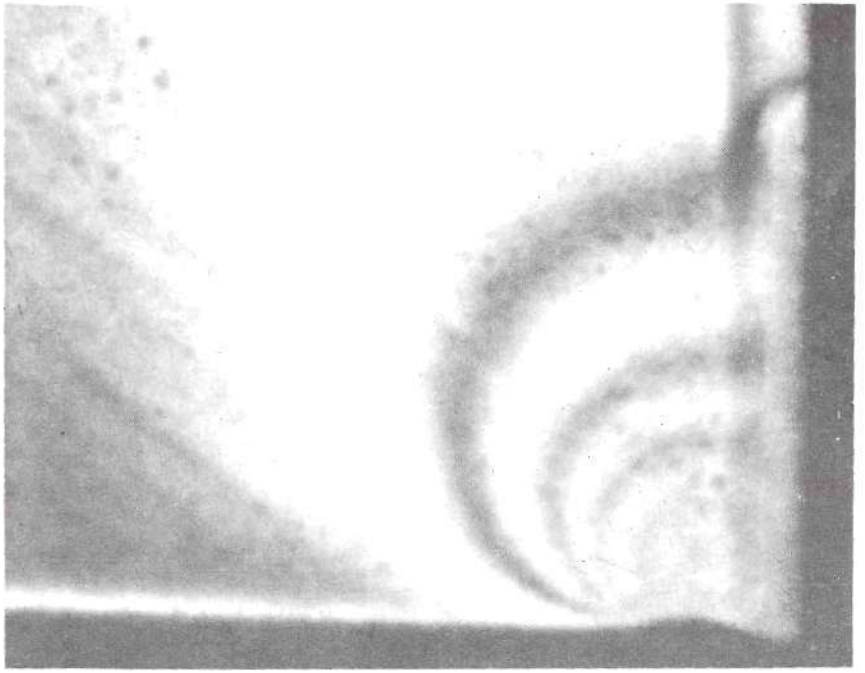

Figure 42. Transmitted Light Photoelastic Slice. Slice is the Plane Y = 0.1 in., X ≥ 0.0 in.. Photograph Shows the Isochromatic Fringe Pattern.

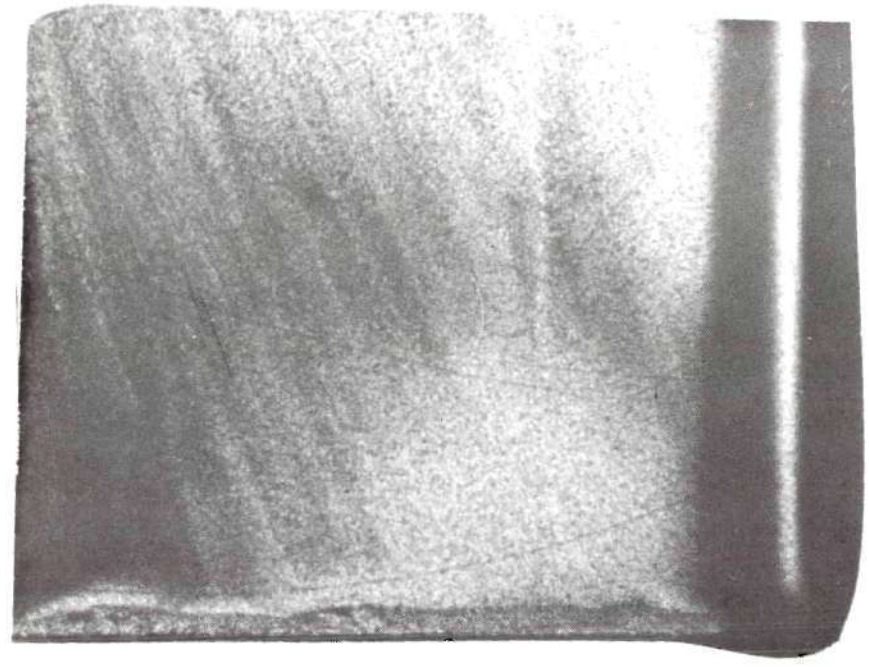

Figure 43. Transmitted Light Photoelastic Slice Used to Determine the τ_{yz} Shear Stresses in the Plane Y = 0.1 in. and Along the Line X = 0.3 in.. Compensation Was Used to Show the Isochromatic in this Photograph.

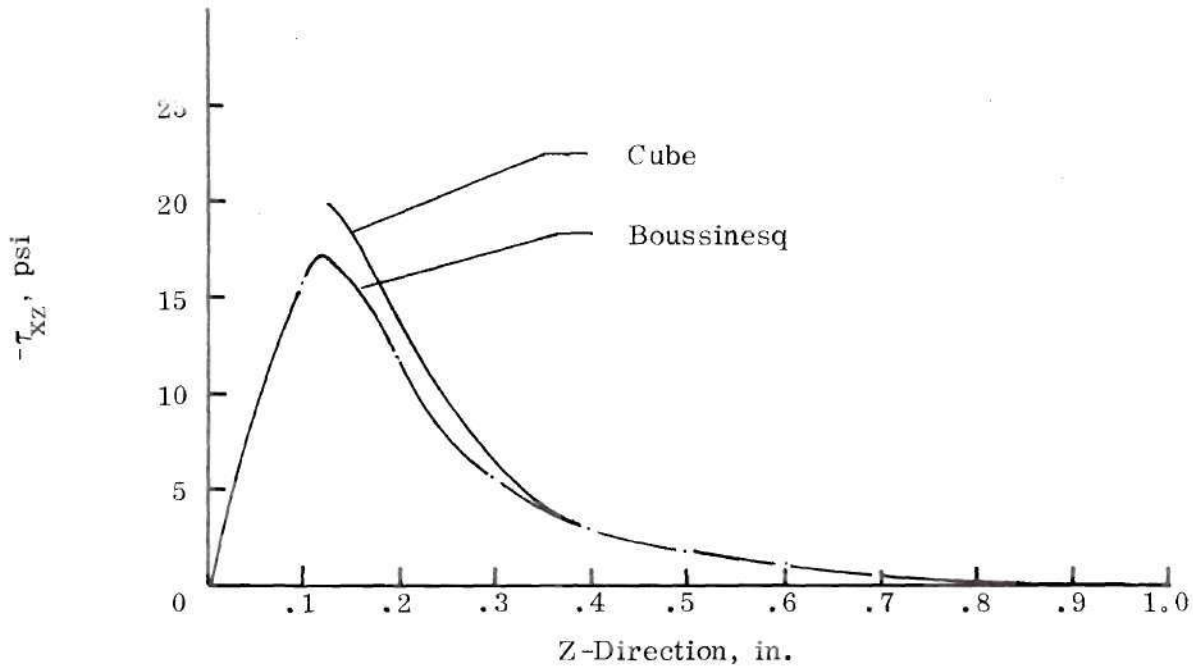

Figure 44. Comparison of τ_{xz} Shear Stress along Line X = .1 in. for the Boussinesq and Cube Problems.

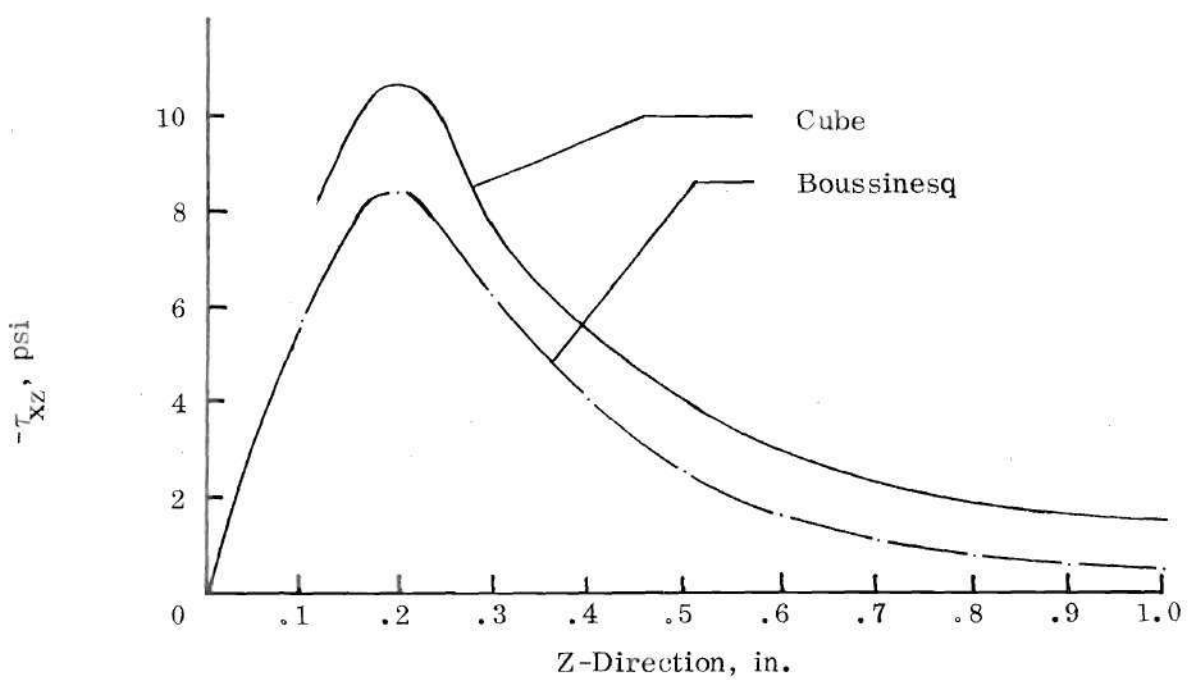

Figure 45. Comparison of τ_{xz} Shear Stress along Line X = .2 in. for the Boussinesq and Cube Problems.

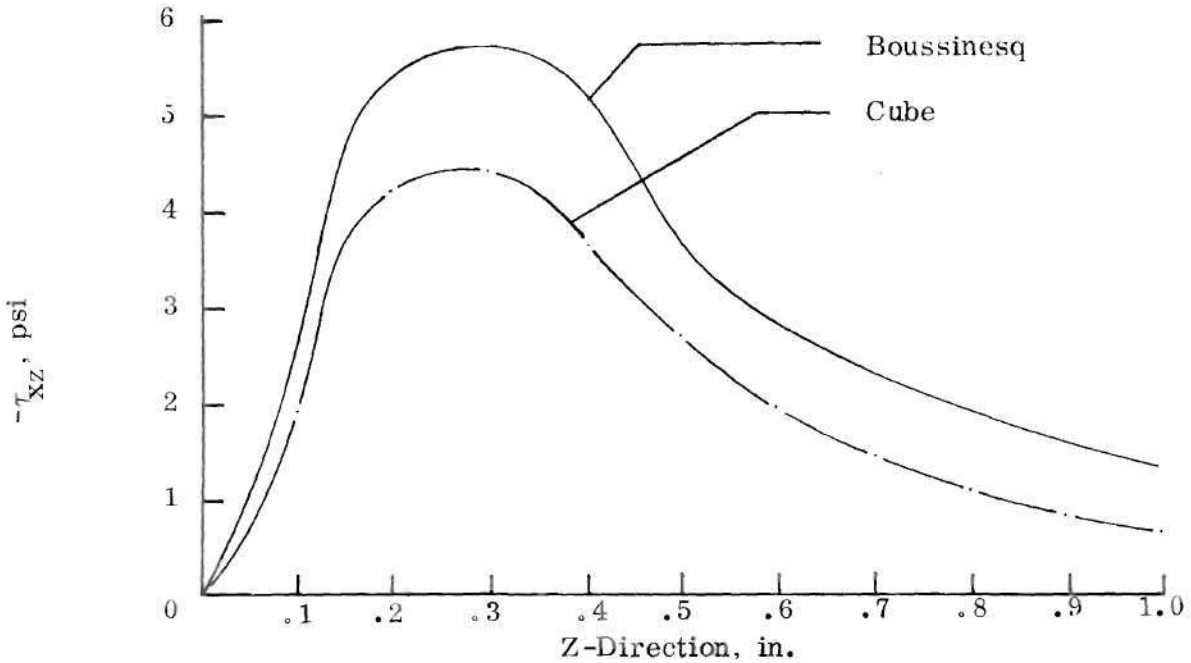

Figure 46. Comparison of τ_{xz} Shear Stress along Line X = .3 in. for the Boussinesq and Cube Problems

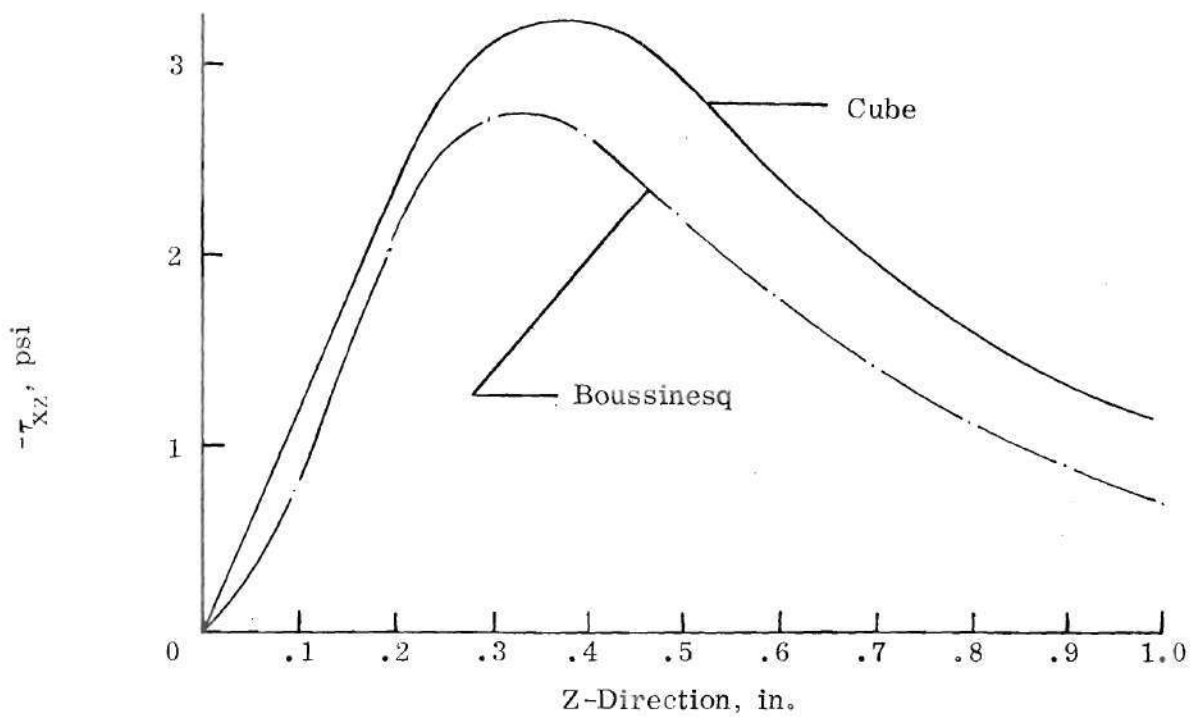

Figure 47. Comparison of τ_{xz} Shear Stress along Line X = .4 in. for the Boussinesq and Cube Problems.

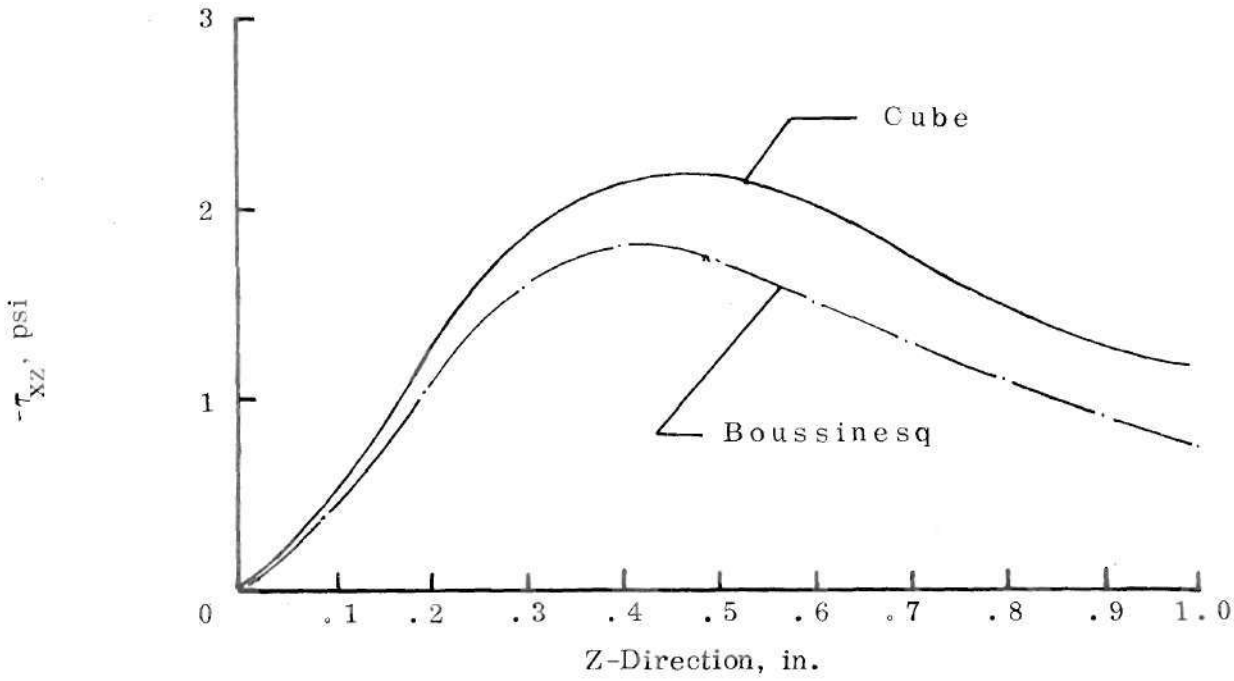

Figure 48. Comparison of τ_{xz} Shear Stress along Line X = .5 in. for the Boussinesq and Cube Problems.

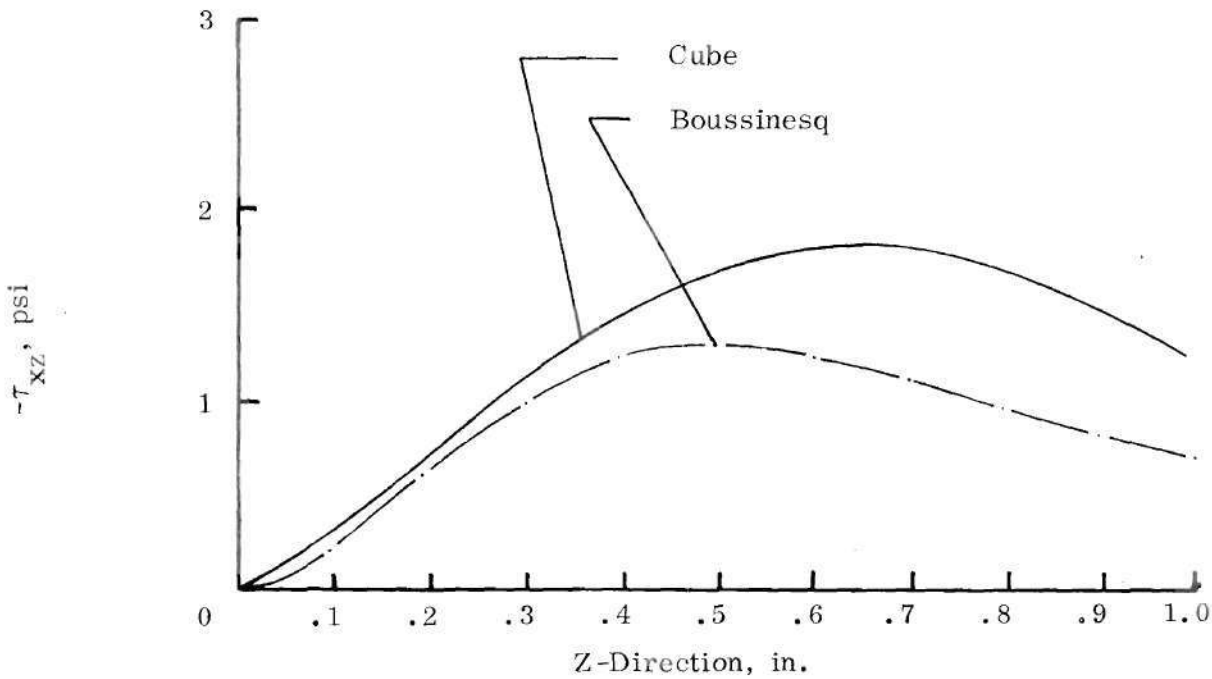

Figure 49. Comparison of τ_{xz} Shear Stress along Line X = .6 in for the Boussinesq and Cube Problems.

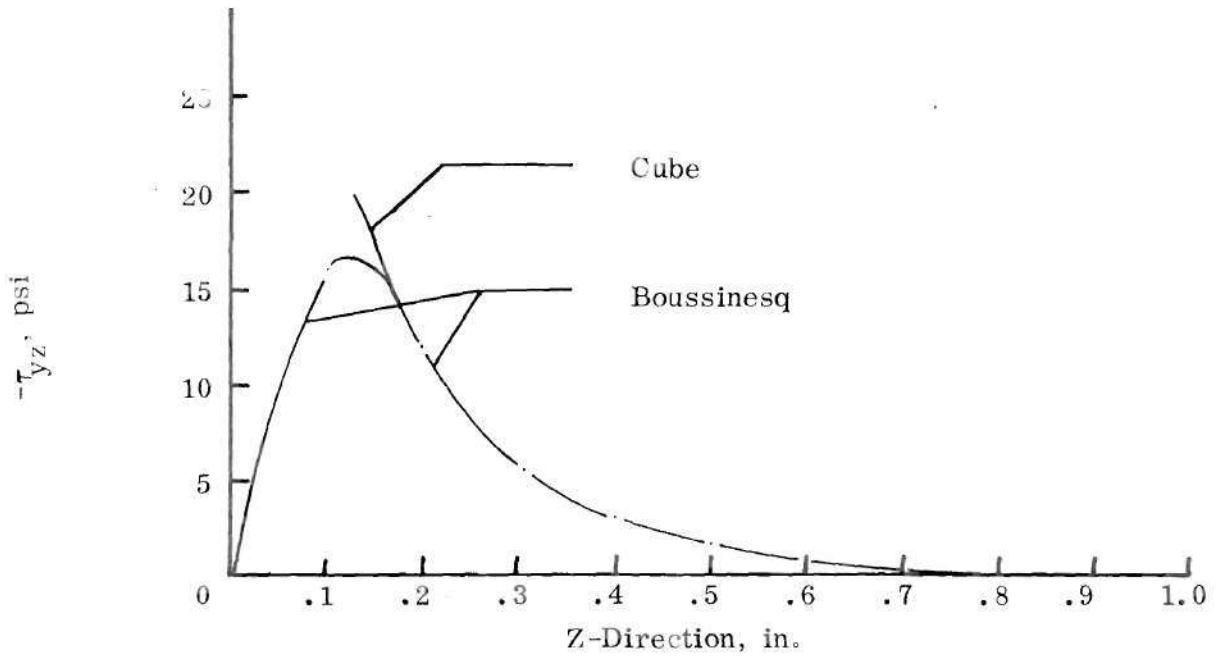

Figure 50. Comparison of τ_{yz} Shear Stress along Line X = .1 in. for the Boussinesq and Cube Problems.

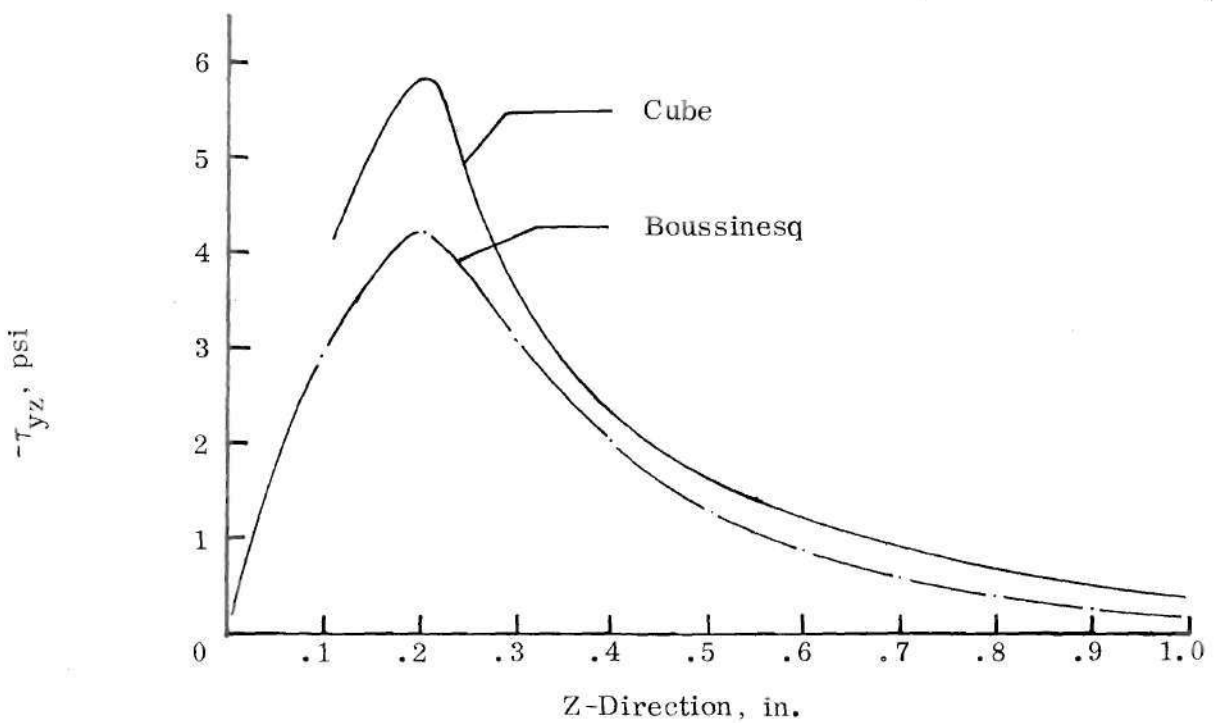

Figure 51. Comparison of τ_{yz} Shear Stress along Line X = .2 in. for the Boussinesq and Cube Problems.

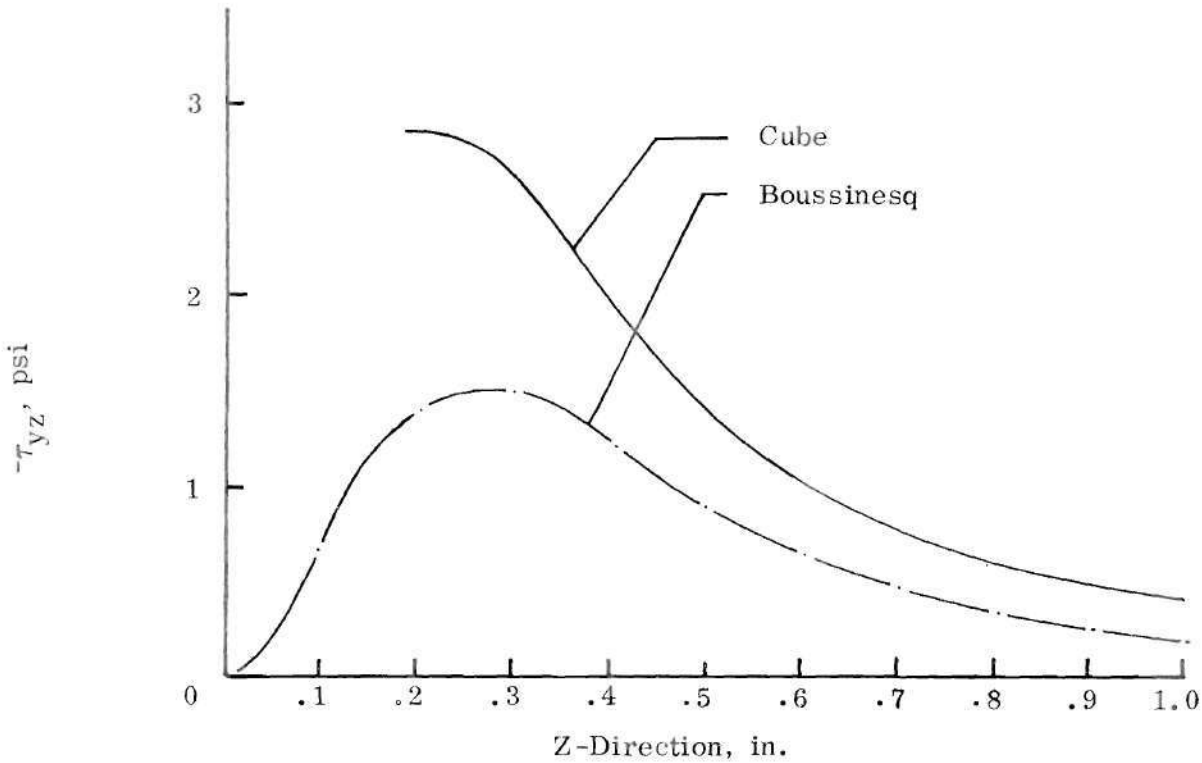

Figure 52. Comparison of τ_{yz} Shear Stress along Line X = .3 in. for the Boussinesq and Cube Problems.

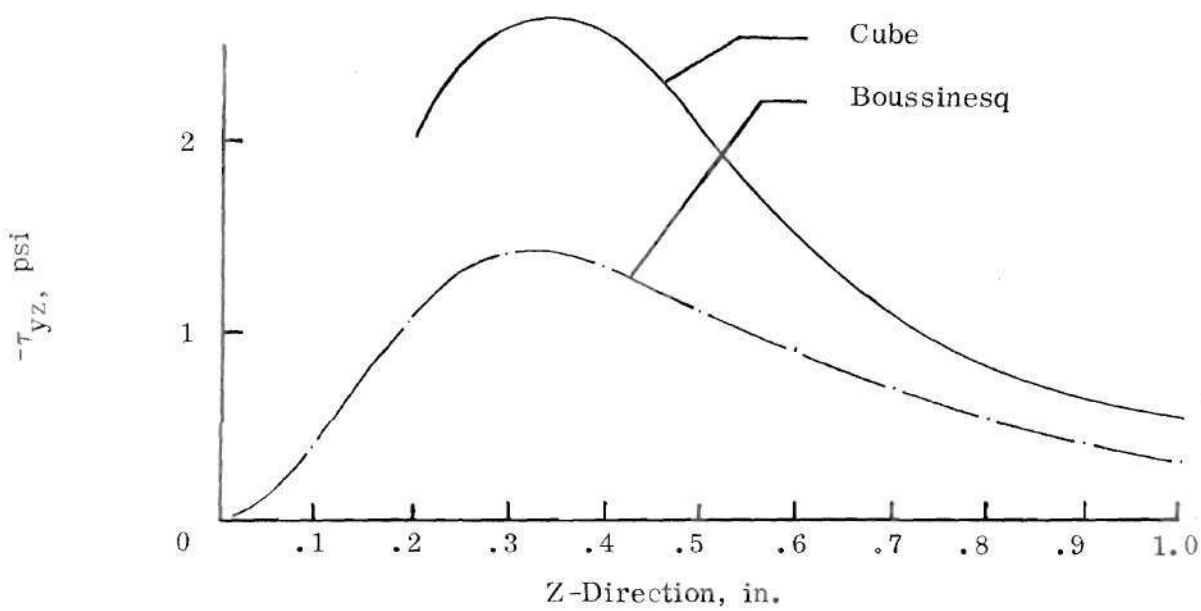

Figure 53. Comparison of τ_{yz} Shear Stress along Line X = .4 in. for the Boussinesq and Cube Problems.

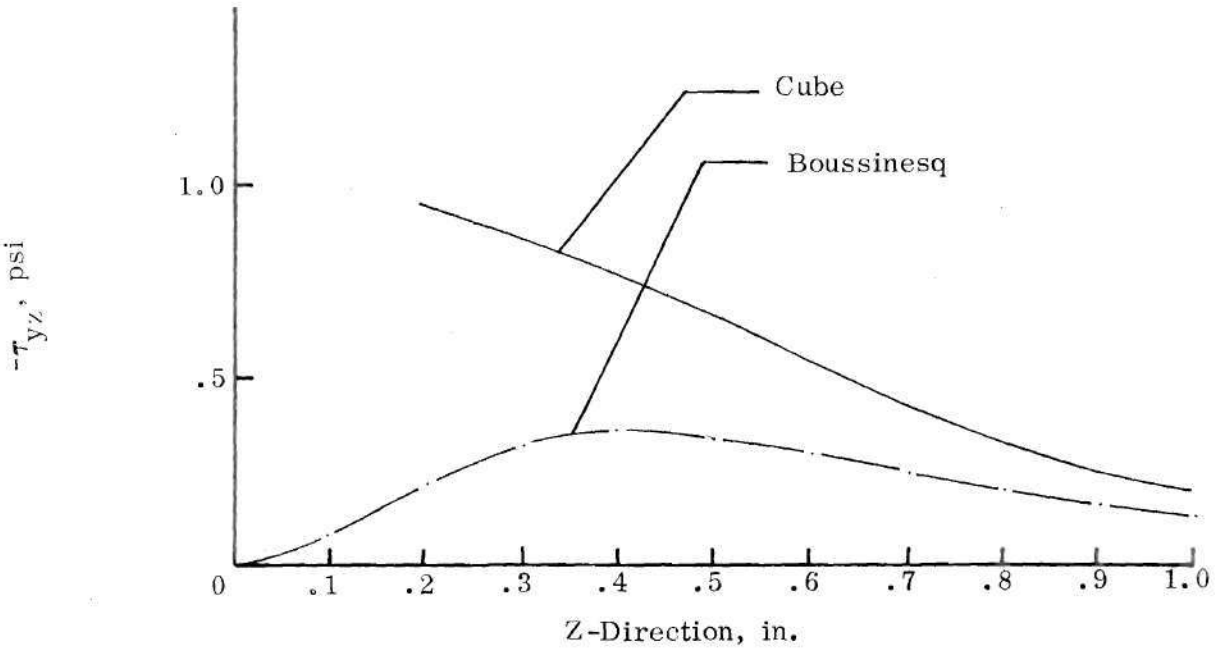

Figure 54. Comparison of τ_{yz} Shear Stress along Line X = .5 in. for the Boussinesq and Cube Problems.

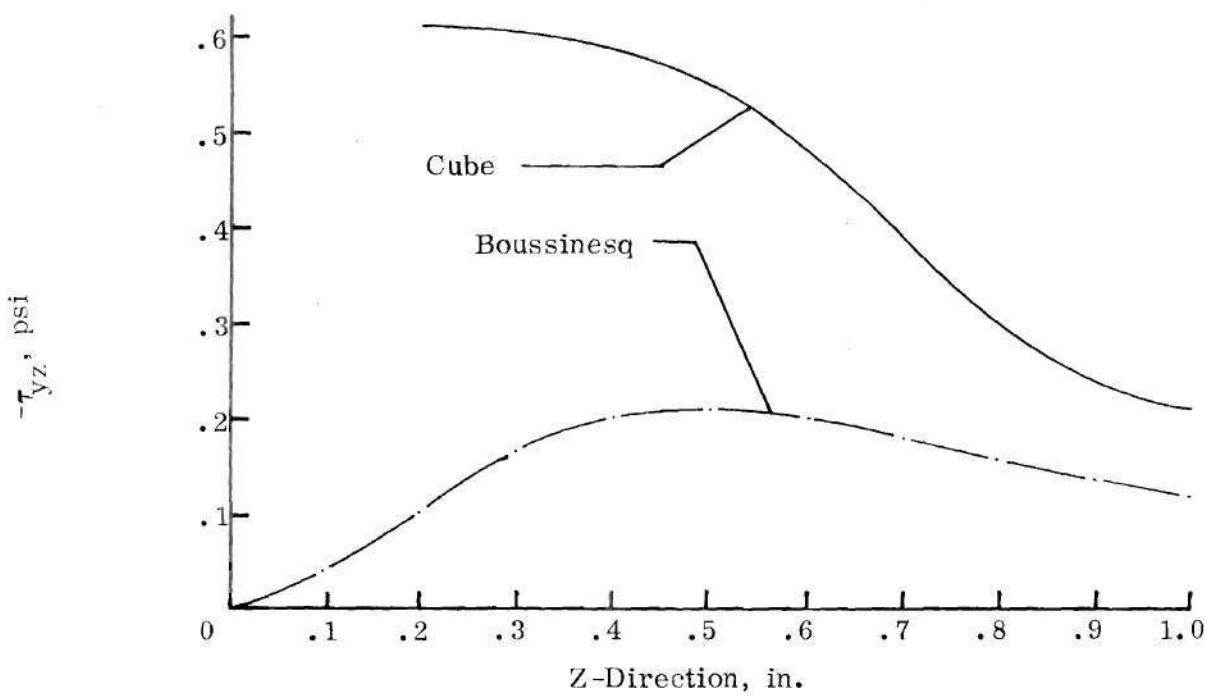

Figure 55. Comparison of τ_{yz} Shear Stress along Line X = .6 in. for the Boussinesq and Cube Problems.

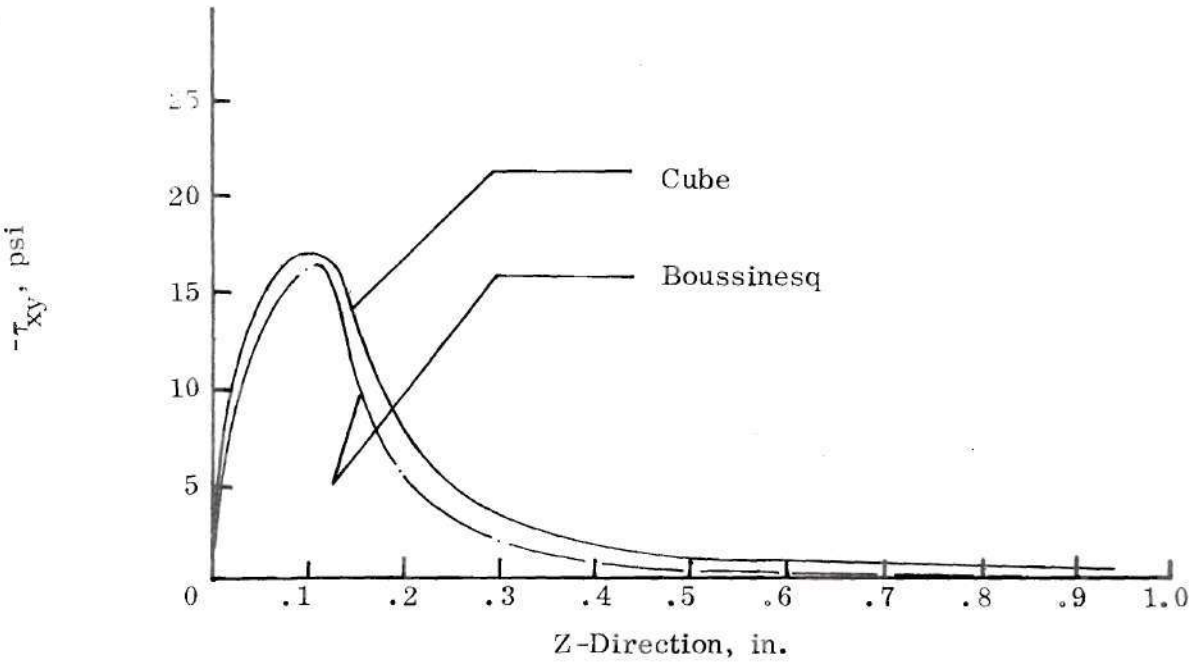

Figure 56. Comparison of τ_{xy} Shear Stress along Line X = .1 in. for the Boussinesq and Cube Problems.

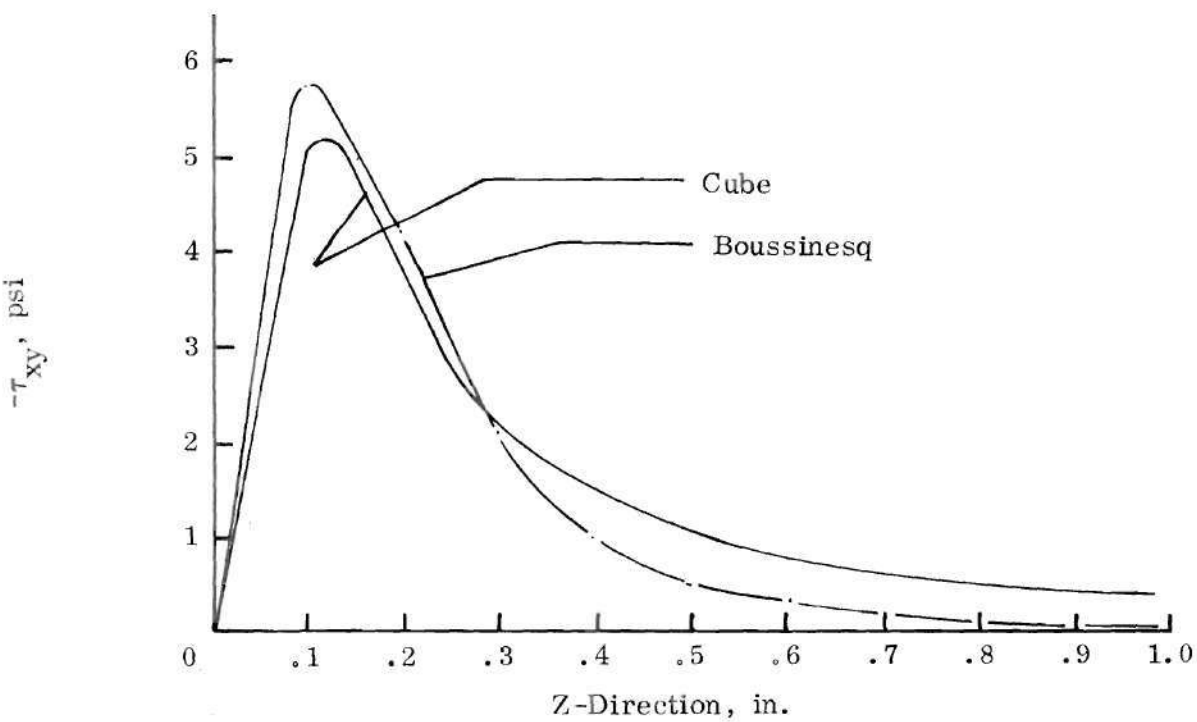

Figure 57. Comparison of τ_{xy} Shear Stress along Line X = .2 in. for the Boussinesq and Cube Problems.

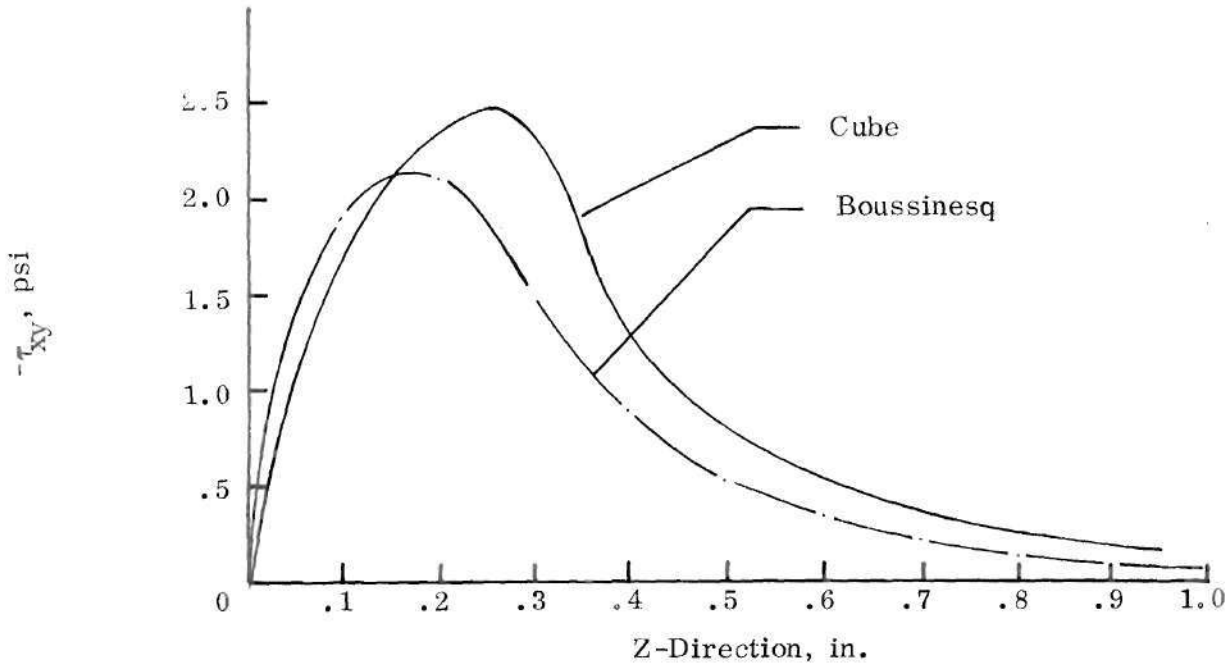

Figure 58. Comparison of τ_{xy} Shear Stress along Line X = .3 in. for the Boussinesq and Cube Problems.

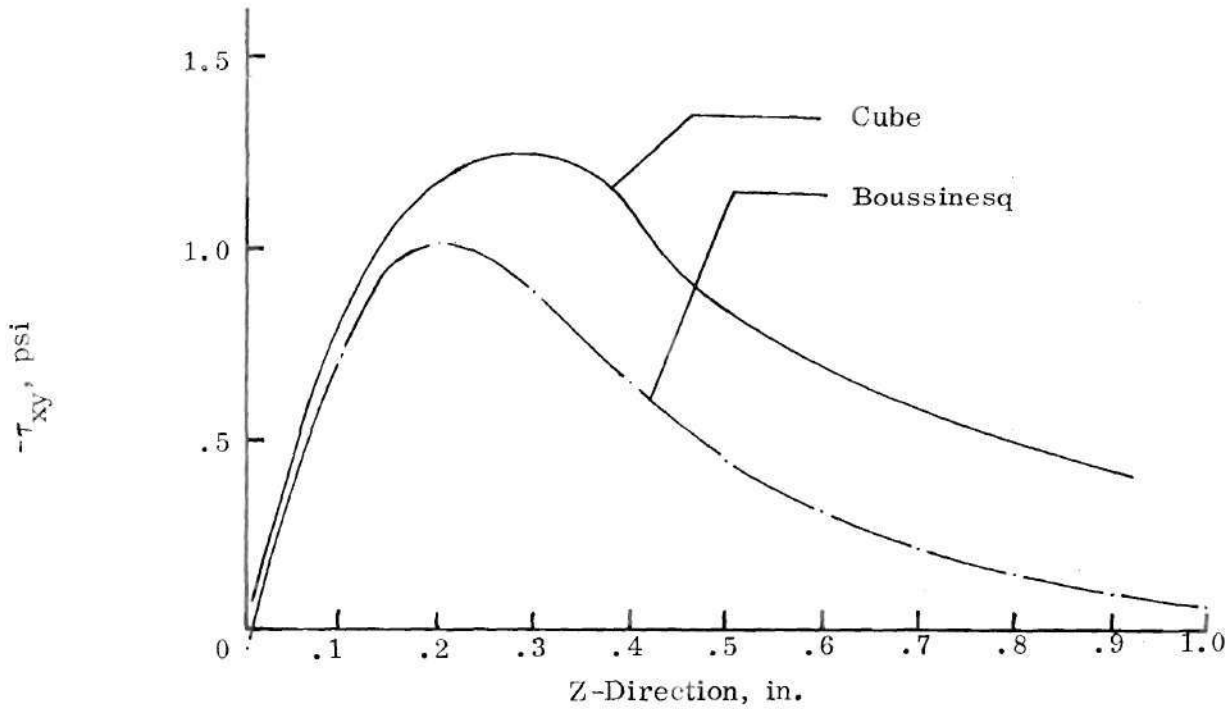

Figure 59. Comparison of τ_{xy} Shear Stress along Line X = .4 in. for the Boussinesq and Cube Problems.

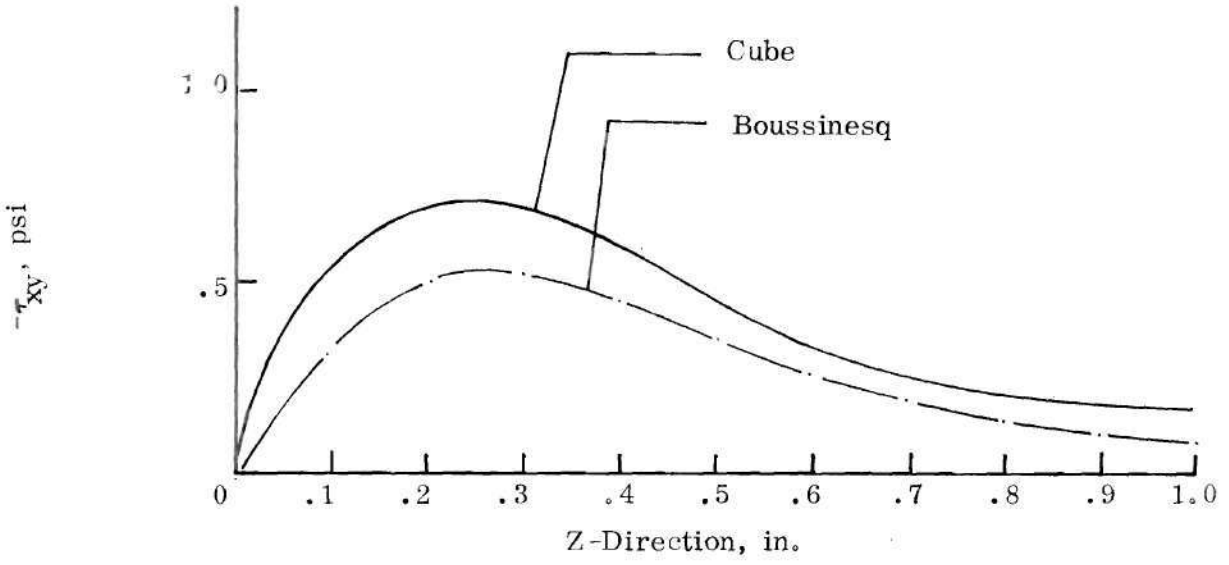

Figure 60. Comparison of τ_{xy} Shear Stress along Line X = .5 in. for the Boussinesq and Cube Problems.

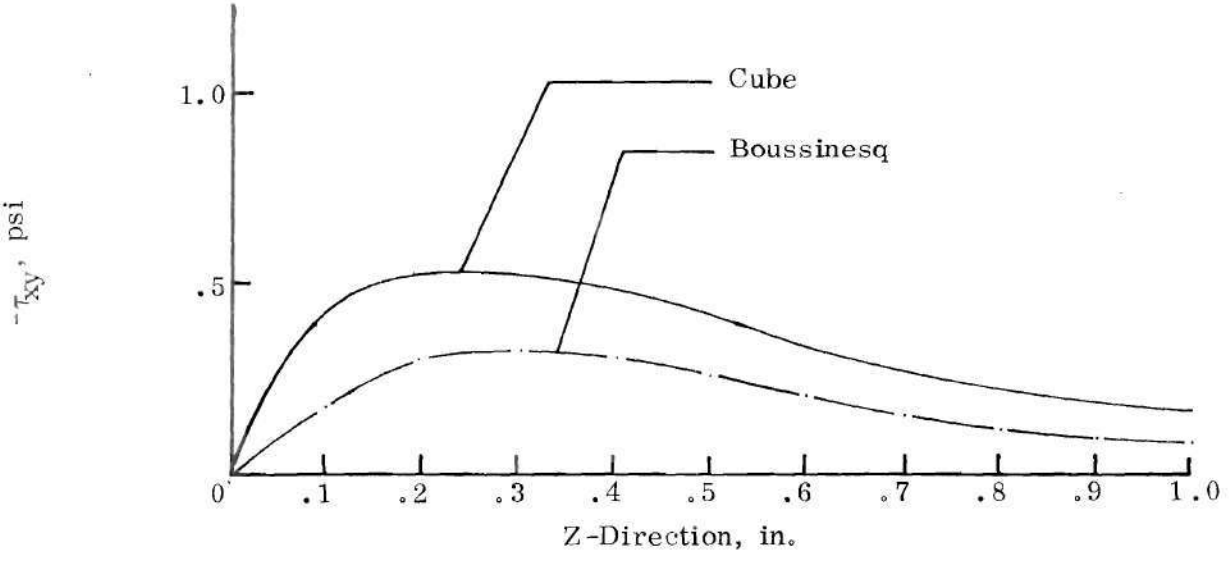

Figure 61. Comparison of τ_{xy} Shear Stress along Line X = .6 in. for the Boussinesq and Cube Problems.

APPENDIX A

LEAST SQUARES DETERMINATION OF THE TOTAL STRESS TENSOR

In all types of photoelasticity, the direct results that can be obtained are the shear stresses and the effective principal stress directions. The total stress tensor is found by using the boundary conditions and some form of numerical integration of the stress equilibrium equations. This determination of the total stress tensor does not determine whether a photoelastic technique is valid. However, it is considered in general, to be part of the total solution to a photoelastic problem. For this reason it is discussed here.

The total stress tensor could not be determined for this problem. Nevertheless an attempt was made to find the total stress tensor for points on the plane $y = .1$ inches, $x \geq .1$ inches using the least squares technique developed by Berghaus [31]. Specifically, interest was focused on the normal stresses along lines $x = .1$ and $x = .2$ inches since a likeness between these normal stresses and those from the Boussinesq solution could be expected.

The problem was two fold. It is generally impossible to determine valid data close to a concentrated load point. In this region the displacements are not infinitesimal and the linearity approximation may not be valid. This also presents problems in obtaining data for neighboring regions if the light beam must pass through the neighborhood of the concentrated load. The second problem lies in

the choice of a mesh size for the finite difference integration scheme. It was hoped that if a mesh sufficiently large could be used, the problem of determining data in the close neighborhood of the concentrated load would be avoided.

In order to determine this, the shear stresses from the Boussinesq solution were used as input data with the least squares technique. In this manner, the computed normal stresses were compared with the normal stresses from the Boussinesq solution. This was done in two ways. First the least squares technique was used with one stress equilibrium equation (15), the boundary conditions (18), and the photoelastic relationships (12-14) and integration carried out along a line. This was repeated for other lines. The program was similar to the shear difference approach of Frocht and Guernsey [30] except it had the smoothing property of an overdetermined system of equations. The program was run using various mesh sizes and computing an rms value comparing the computed normal stresses to the values from the Boussinesq solution. It was determined that a mesh size of .01 inches was necessary for the line x = .1 inches and a mesh size of .02 was necessary for the line x = .2 inches in order to obtain satisfactory results. The following table illustrates this.

The σ_y normal stresses for the line x = .1 inches and mesh sizes .05, .02 and .01 inches, and the line x = .2 inches, mesh size .1, .05, .02 inches are also plotted to more effectively illustrate the result of decreasing the size of the mesh (Figures 62-67).

The rms values were computed using the following equation.

Table 1. RMS Values - One Stress Equilibrium Equation.

Mesh Size	RMS	Line
.1	650.7	x = .1
.05	183.4	x = .1
.02	28.1	x = .1
.01	.41	x = .1
.1	34.7	x = .2
.05	6.7	x = .2
.02	1.0	x = .2
.01	.05	x = .2

$$(\text{RMS})^2 = \frac{1}{n} \sum_{n} \left(\frac{\sigma_x - \sigma_{x\ \text{computed}}}{\sigma_x}\right)^2 + \left(\frac{\sigma_y - \sigma_{y\ \text{computed}}}{\sigma_y}\right)^2 + \left(\frac{\sigma_z - \sigma_{z\ \text{computed}}}{\sigma_z}\right)^2$$

Where

n = the number of solution points.

Next it was decided to investigate the possibility of using a larger mesh size if the least squares technique with two stress equilibrium equations, (15) and (18), was used. In this case, the normal stresses were determined over the region $0 \leq x \leq .5$ inches and $z \leq 1.0$ inches. Again, it was determined that the mesh size necessary for good results would be too small. The rms values for each mesh size was again calculated. The calculations for each rms value was for the solution points along each line in the solution region in order that these values could be compared with those determined using one stress equilibrium equation.

The table shows that when two stress equilibrium equations are used for the solution, better results are obtained with a larger mesh size. By halving the mesh size, the RMS values change by an order of magnitude. However, the maximum mesh size for a reasonable solution to the problem is too small to be practical. A spacing smaller than .05 inches was beyond the present sensitivity of existing equipment. The diameter of the laser light source was approximately

Table 2. RMS Values - Two Stress Equilibrium Equations.

Mesh Size	RMS	Line
.1	20.1	x = .1
.05	2.0	x = .1
.1	18.8	x = .2
.05	1.3	x = .2

.06 inches. Thus beams parallel to one another would contain an overlapping intensity effect with spacing smaller than .06 inches. Obtaining the necessary data with this small spacing in the neighborhood of the concentrated load was also an experimental impossibility. Finally, in order to obtain the necessary data at every solution point, intensity profiles in three orthogonal direction through each point are required. Therefore, the necessary data becomes an insurmountable task as the mesh size is reduced.

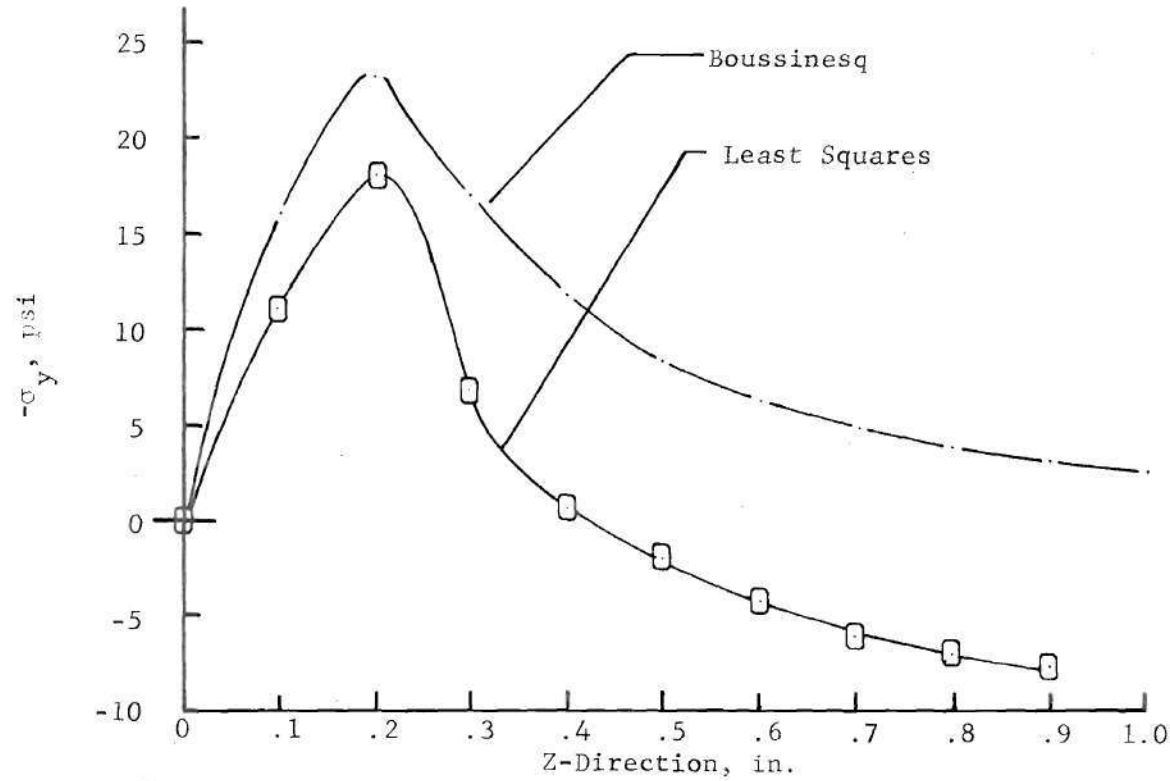

Figure 62. Comparison of σ_y Normal Stresses along Line X = .1 in. for Boussinesq Problem and Least Squares Problem with .05 in. Mesh.

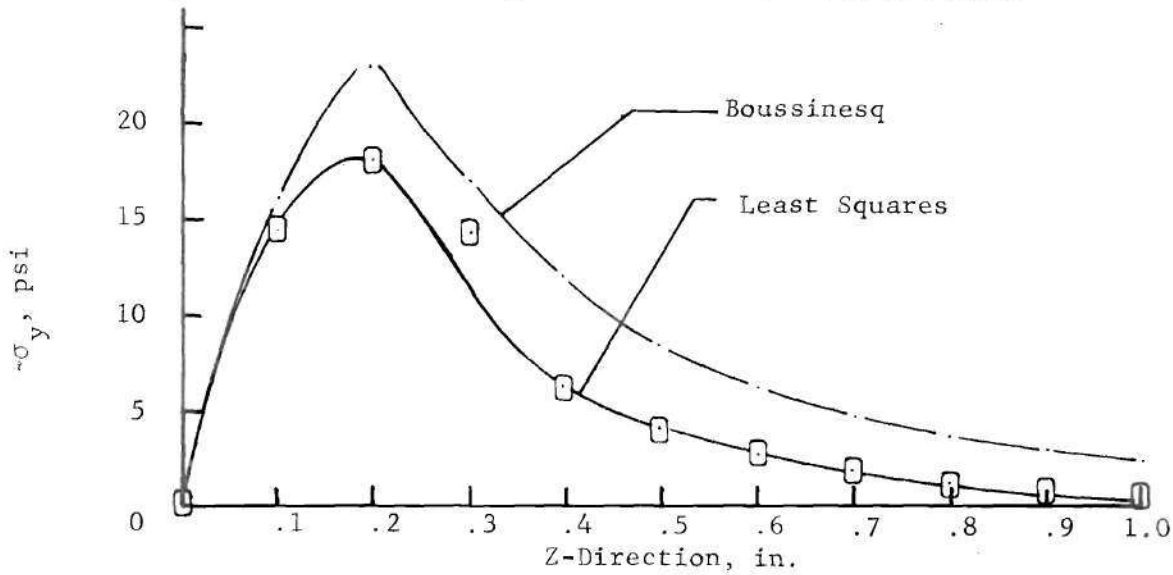

Figure 63. Comparison of σ_y Normal Stresses along Line X =.1 in. for Boussinesq Problem and Least Squares Problem with .02 in. Mesh.

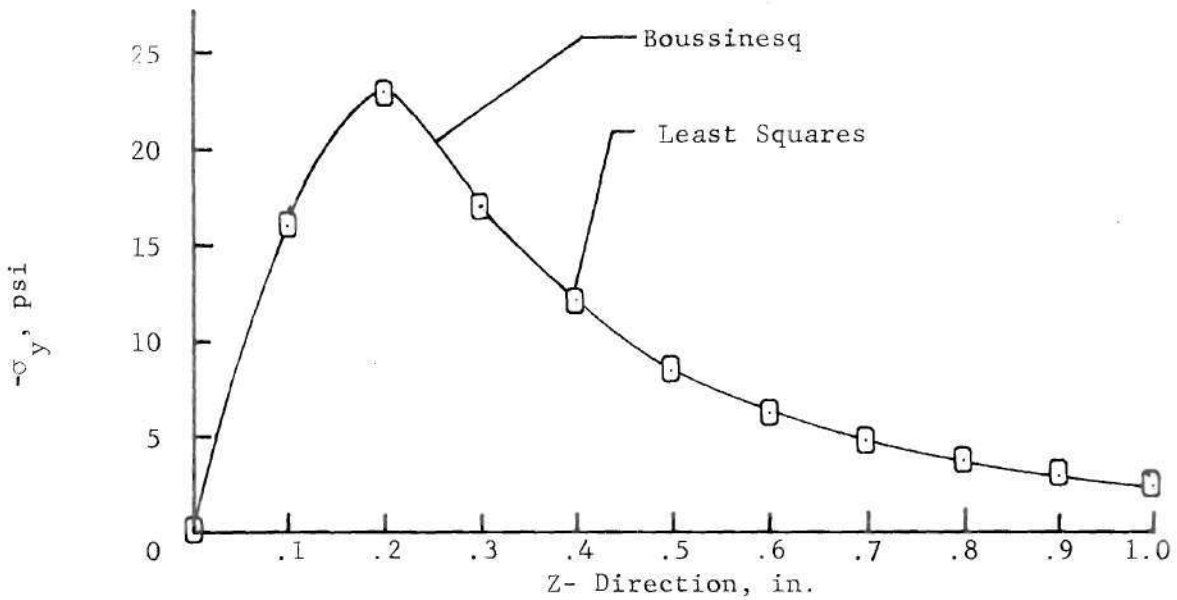

Figure 64. Comparison of σ_y Normal Stresses along Line X = .1 in. for Boussinesq Problem and Least Squares Problem with .01 in Mesh.

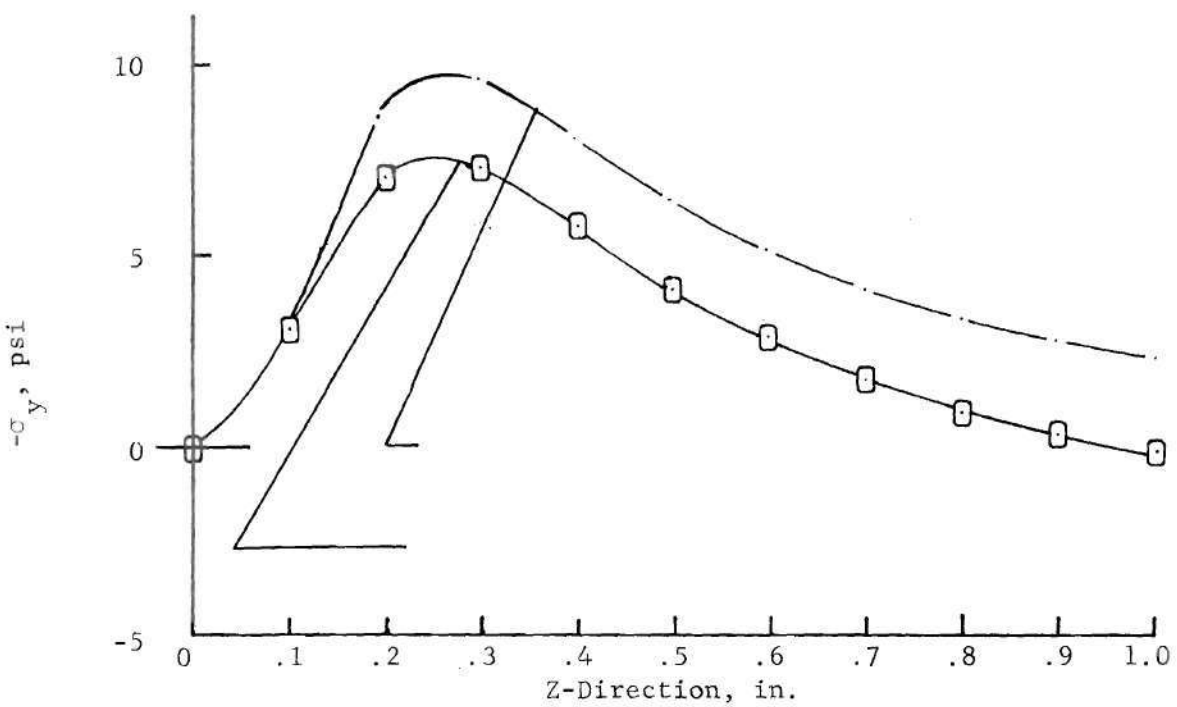

Figure 65. Comparison of σ_y Normal Stresses along Line X = .2 in. for Boussinesq Problem and Least Squares Problem with .1 in. Mesh.

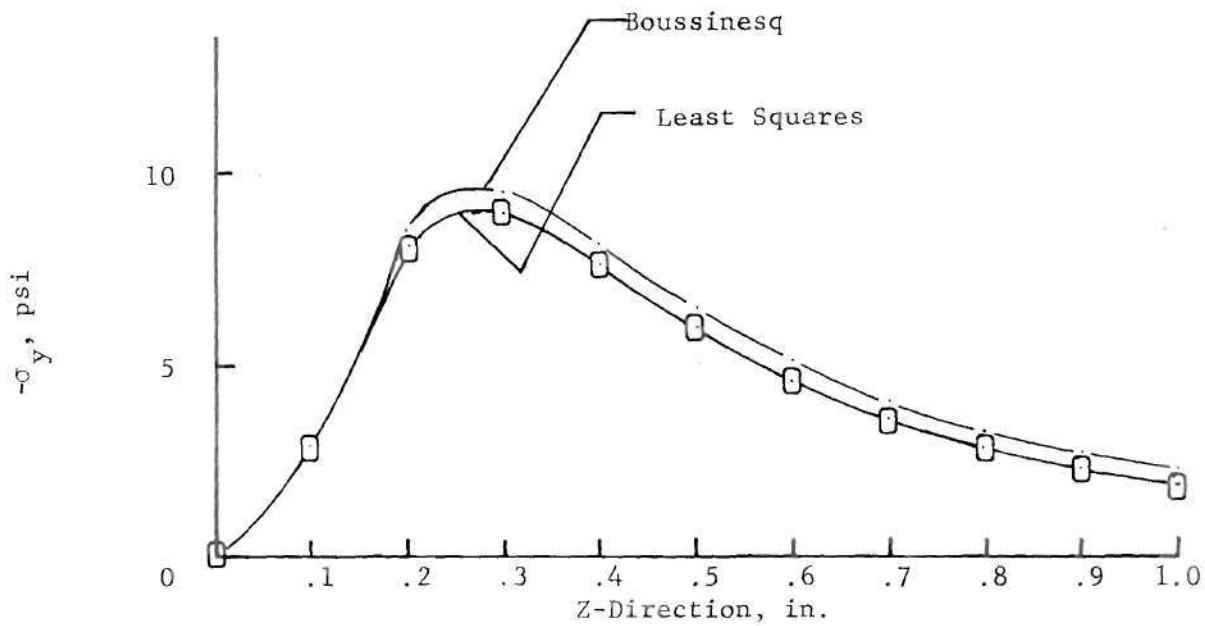

Figure 66. Comparison of σ_y Normal Stresses along Line X = .2 in. for Boussinesq Problem and Least Squares Problem with .05 in. Mesh.

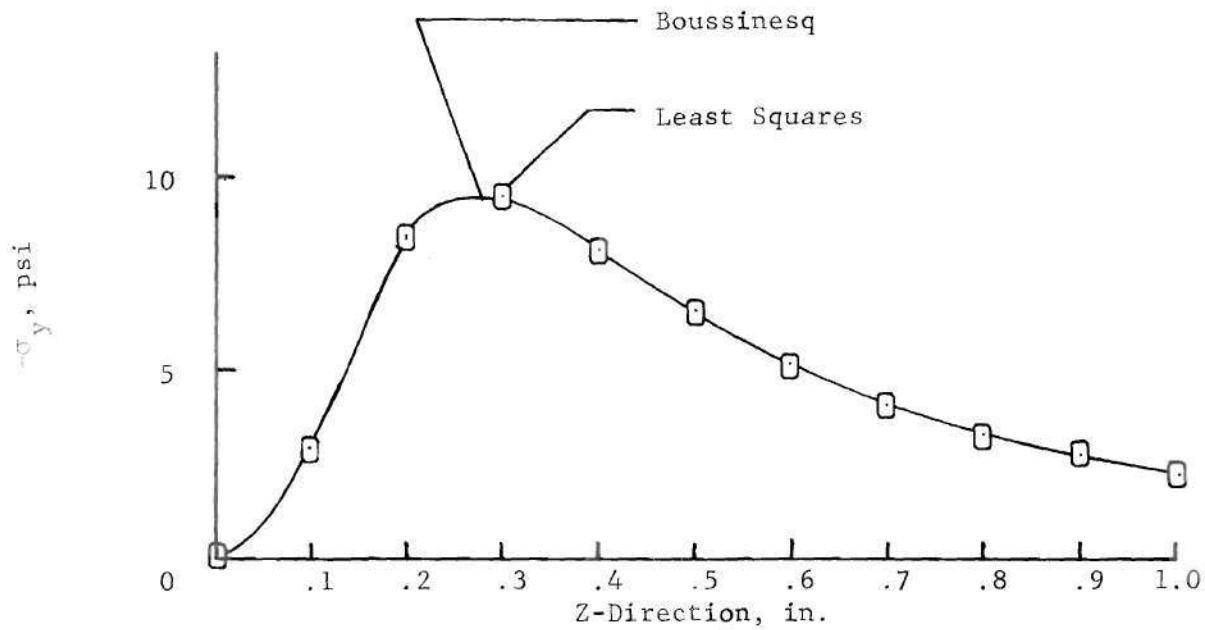

Figure 67. Comparison of σ_y Normal Stresses along Line X = .2 in. for Boussinesq Problem and Least Squares Problem with .02 in. Mesh.

APPENDIX B

DETAILS OF MODEL

Model Manufacture

In order to achieve a successful scattered light photoelastic study, the model material must have four important properties. It must be easily cast, have free machining characteristics, have a high figure of merit and good light scattering properties. (Ref. Dally and Riley [4]). To satisfy these requirements a room temperature cure epoxy was chosen. The casting mixture was that devised by Sampson [40]. It consisted of two parts by weight Bakelite ERL-2774 epoxy resin, two parts by weight Bakelite ERL-2795 epoxy resin and one part by weight Bakelite ZZL-0803 hardener. To improve the light scattering properties of the material 5 milliliters of, Cab-O-Sil, silica powder were added to each pound of mixture.

Room temperature cure epoxies are generally easier to cast and more stable than other types of epoxy resins. Nevertheless, it is still quite difficult to obtain a stress free cube of the size used in this research. Epoxies like all other resins are susceptible to creep; however, the creep rate of the mixture chosen compares favorably with that for the best polymeric material, Catalin 61-893 (Ref. Dally and Riley [4]). Because of the length of time which must necessarily elapse from the construction of the model to the termination of the experiment, creep was an important consideration in material

choice. No actual measurement of the creep rate were made; however, scattered light traces taken during the initial stages of the experiment compared excellently with traces along the same lines taken near to the completion of the experiment. To avoid the common problem of edge effects due to water absorbtion, the model was kept in a dry atmosphere when it was not directly being studied. Slices cut from the model for the transmitted light tests showed that this care had largely alleviated the problem.

The procedure used to construct the model is as follows. The two resins and the silica powder were mixed throughly and the water content removed by heating to 110°F for twelve hours. The hardener was then added and the mixture stirred thoroughly. Air bubbles trapped during mixing were eliminated by degassing in a small vacuum chamber. Such an epoxy mixture can be used for casting purposes up to three hours after it has been made. However the sooner it is used; the less chance there is of having a residual stress problem. Thus the mixture was poured into the mold immediately after degassing. The epoxy was cured for 48 hours at 110°F; then the mold was removed and the cube was post cured for 96 hours at 120°F.

From this $4\frac{1}{2}$" cast cube the finished model was machined. The standard procedure of removing $\frac{1}{4}$" of material from all faces of the model (Ref. Johnson [41]) was followed. The procedure is based upon the fact that the effects of large exothermic reactions from the solidification of the epoxy are generally confined to this region. The model was a $4.000 \pm .005$ inch cube. The sides were parallel within .005 inches and perpendicular within .002 inches. The machining

was done using a single point fly cutter in a Bridgeport vertical milling machine. The tool, which was of the carbide insert type, had the appropriate tool angles as defined by Johnson (Figure 68). A machining speed of 500 surface feet per minute and a feed rate of two inches per minute were used. The finishing cut depth was .010 inches. The tool was kept clear of chips by an appropriate stream of air. Since the model was immersed in fluid for the photoelastic studies, the machined surfaces required no polishing. After machining the model was annealed. A stress freezing cycle was followed for the annealing process. After annealing the surfaces were checked for deformations due to stress relieving. None were found. Although a very small residual stress and slight indications of mottling (non-uniform index of refraction) remain, a good photoelastic model was obtained with this procedure.

The model was loaded through a specially constructed loading fixture (Figure 18, 69, 70). The concentrated load was directed normal to the top surface of the model through a steel ball attached to the end of a vertical shaft. The shaft was held in the vertical position by directing it through a bored hole in an aluminum block. A support to hold the necessary weight was constructed on top of the shaft. The shaft and the weight constituted the appropriate load. The entire model was immersed in a tank of mineral oil and was supported by the flat lubricated plate. The mineral oil bath produced a uniform temperature environment which eliminated edge effects due to thermal gradients.

The loaded model was stress frozen (Ref. Frocht [37]).

A temperature cycle was established from procedures recommended by Photolastic Inc. (Ref. Photolastic [42]). The temperature was raised $4^{\circ}F$ per hour until it reached the critical temperature of this epoxy of $175^{\circ}F$. At that time the load of 5 lb. 6 oz. was applied to the model, and then the model was allowed to soak for 12 hours at this temperature. The temperature was then decreased at $\frac{1}{4}^{\circ}F$ per hour until the oven temperature read $170^{\circ}F$; then the temperature was decreased at $1^{\circ}F$ per hour until the oven temperature was again equal to the room temperature. This process was used to ensure a uniform temperature through the body at all times.

The frozen stress model was viewed through a transmission polariscope upon removing it from the oven. The isochromatic fringe pattern was very symmetrical about the load point. An indentation of approximately .15 inch diameter remained at the load point.

Optical Characteristics

The stress-optic constant for this epoxy mixture was experimentally determined. Along with the model a two inch diameter disk was constructed, 3/8 inches thick. The disk was subjected to a diametral compressive load and stress frozen. The fringe constant was determined by scattered light photoelasticity. The value was $1.5 \frac{\text{psi - in}}{\text{fringe}}$.

This epoxy disk was also used to match the index of refraction of the immersion tank fluid with that of our model. The fluid consists of 50 parts by volume Aroclor (a chlorinated hydrocarbon manufactured by Monsanto) and 15 parts by volume light mineral oil.

Slicing of the Model

In order to obtain slices for the transmitted light photoelastic comparison from the model most efficiently, the size of the model was reduced to include only that area where the stress gradients were highest. This area was within a one inch radius of the concentrated load. Therefore the size of the stress frozen model was reduced to a 2.000 inch cube about the load point (Figure 71). Four slices were taken from this cube. Each slice was approximately 1/8 inch thick. The four slices were layed out on the cube by using a vernier height gage on a surface plate. The center of each slice was lightly scribed and the two lines which established the thickness of the slices were scribed (Figure 72).

The slices were removed from the cube with an eight inch diameter diamond abrasive cut-off saw used in a Do-All surface grinder. The cutting speed was approximately 6000 surface feet per minute. The feed rate was controlled manually and the cut depth was approximately $\frac{1}{2}$ inch. A spray coolant was used. The saw left a very rough surface on the slices; and therefore, the surfaces were polished using a 400 grit abrasive. The four slices were then studied in an optical comparator type transmission polariscope (Ref. Johnson [41], Holliday and Graff [43]).

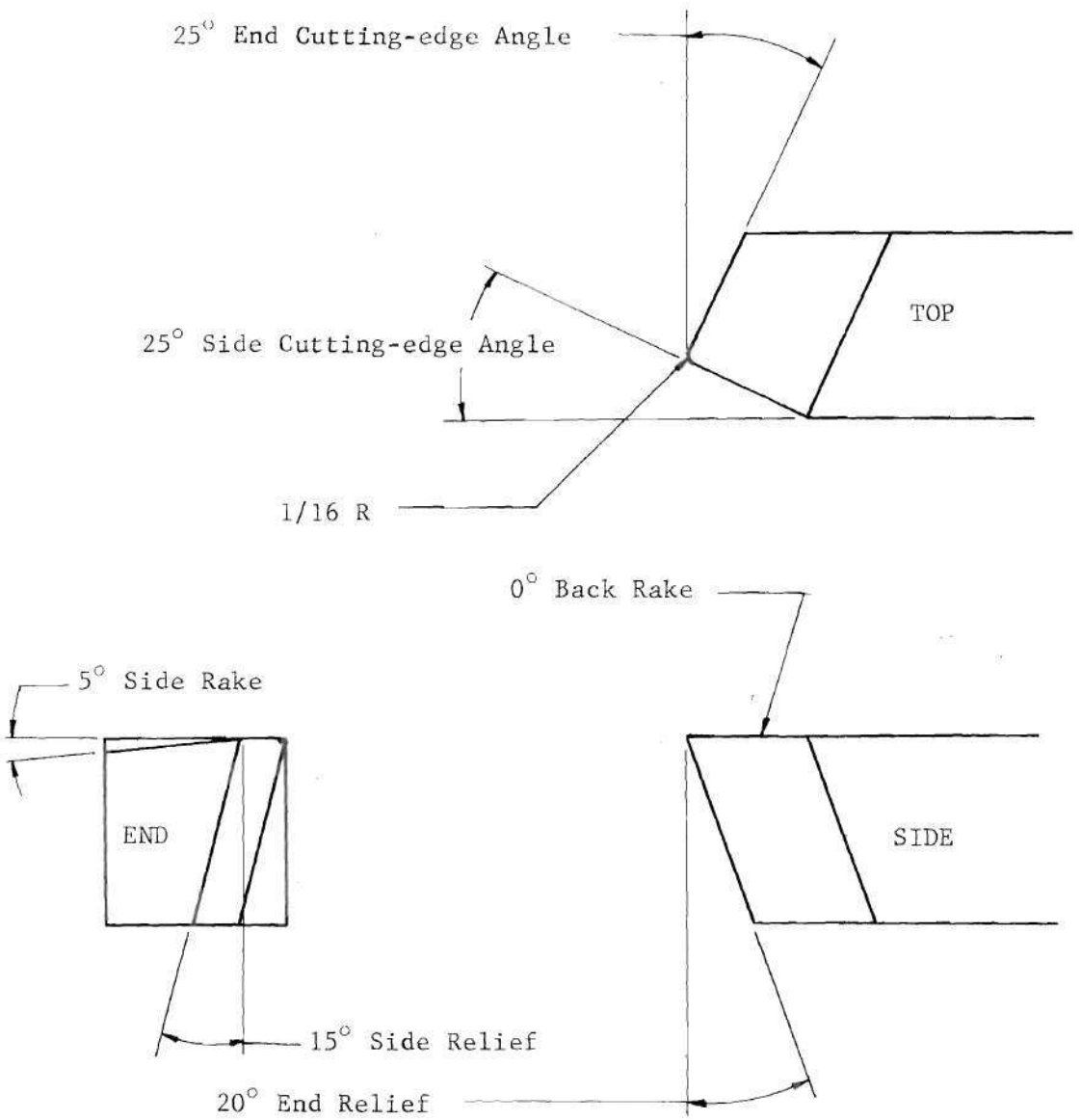

Figure 68. Single Point Cutting Tool for Machining Epoxy Photoelastic Models.

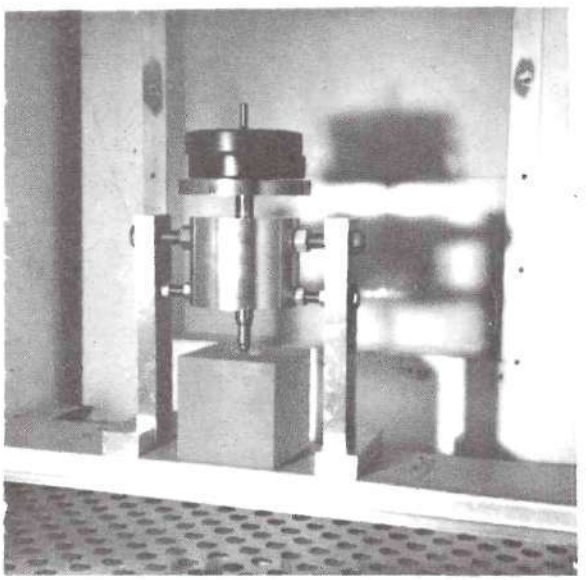

Figure 69. Loading Fixture Constructed to Apply Point Load to Four Inch Epoxy Cube.

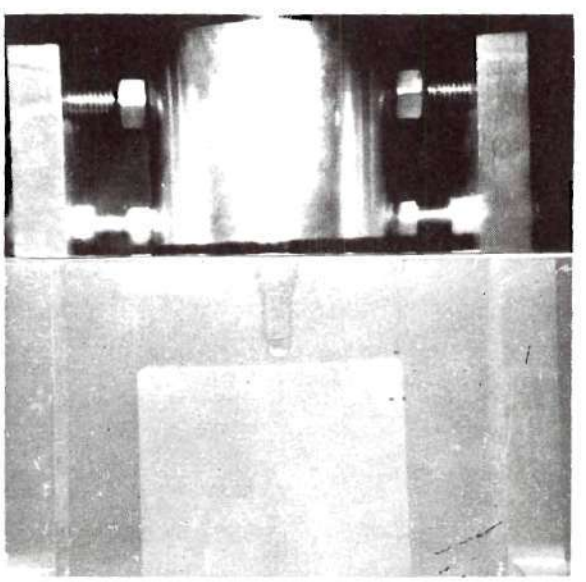

Figure 70. Closer View of Point Load on Epoxy Cube. Cube is Immersed in a Mineral Oil Bath.

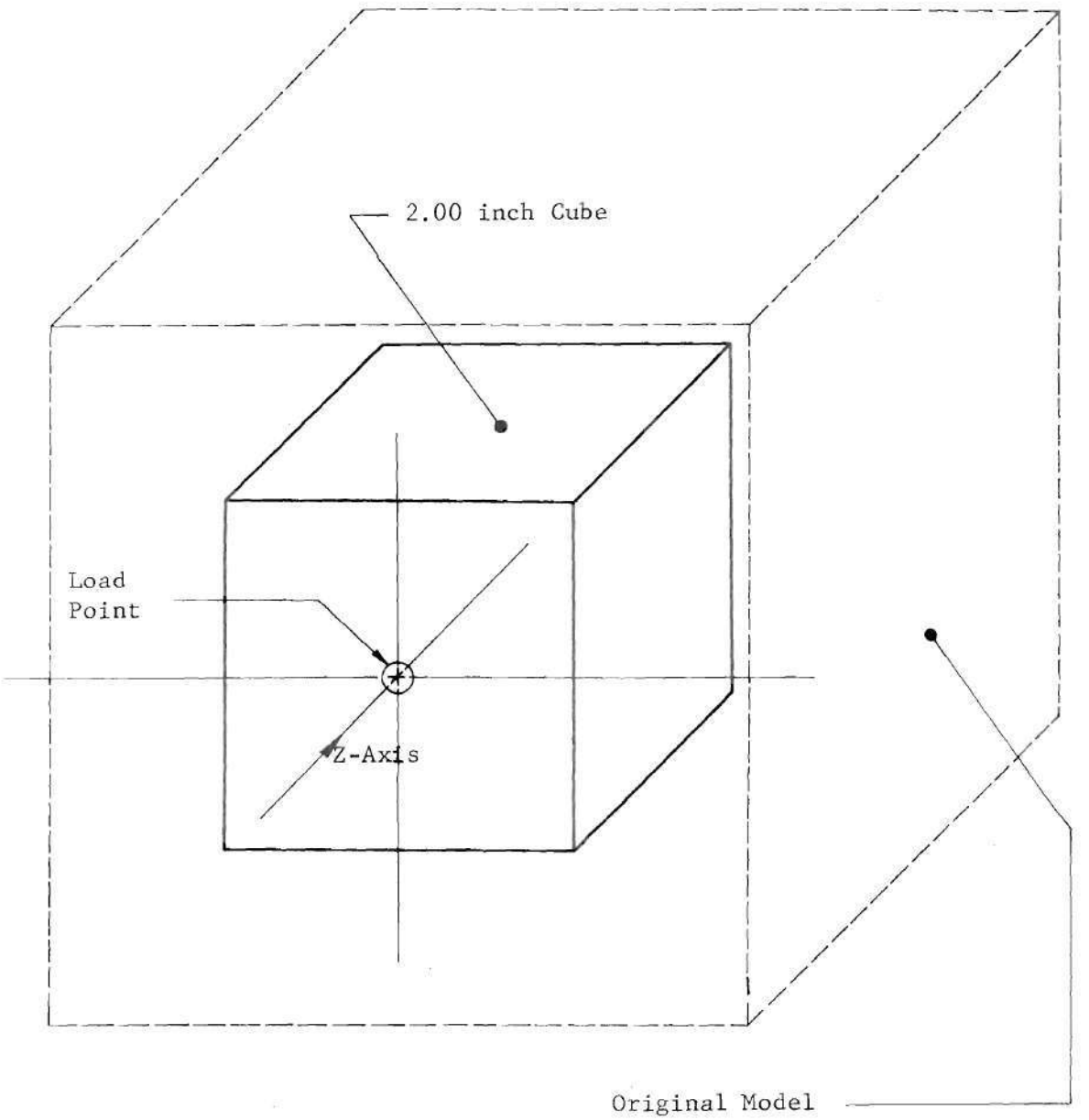

Figure 71. 2 inch Cube Removed from Stress Frozen Model for Slicing.

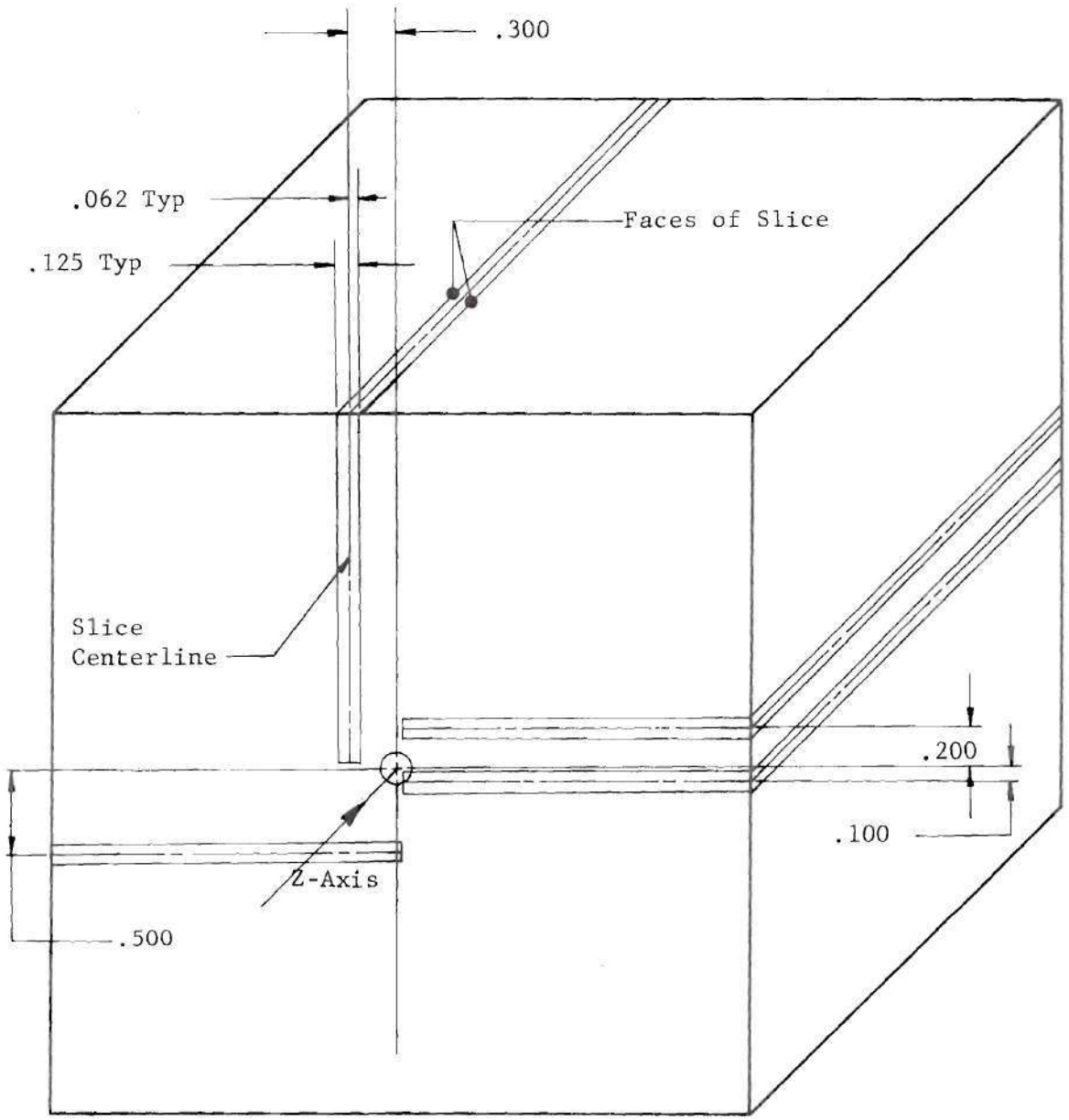

Figure 72. Layout of Slices Cut from Stress Frozen Model.

APPENDIX C

COMPUTER PROGRAMS NECESSARY FOR THE APPLICATION OF THE NEW TECHNIQUE

a) Flowchart and Program for Solution of Equations Describing the State of the Polarized Light.

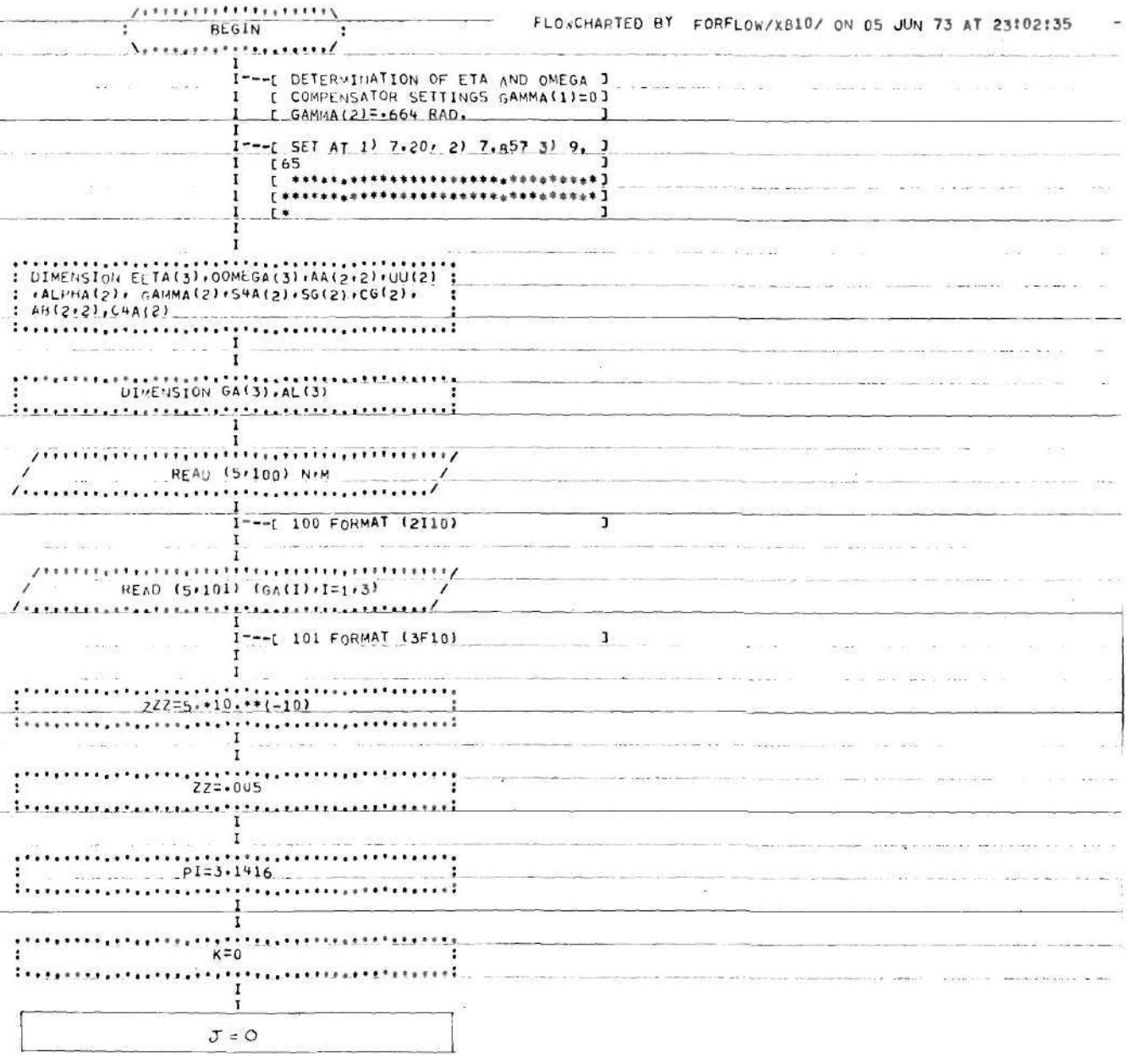
BEGIN
DETERMINATION OF ETA AND OMEGA
COMPENSATOR SETTINGS GAMMA(1)=0
GAMMA(2)=.664 RAD.
SET AT 1) 7.20, 2) 7.857 3) 9,
65
DIMENSION ETA(3),OOMEGA(3),AA(2,2),UU(2)
,ALPHA(2), GAMMA(2),S4A(2),SG(2),CG(2),
AB(2,2),C4A(2)
DIMENSION GA(3),AL(3)
READ (5,100) N,M
100 FORMAT (2I10)
READ (5,101) (GA(I),I=1,3)
101 FORMAT (3F10)
ZZZ=5.*10.**(-10)
ZZ=.005
PI=3.1416
K=0
J=0

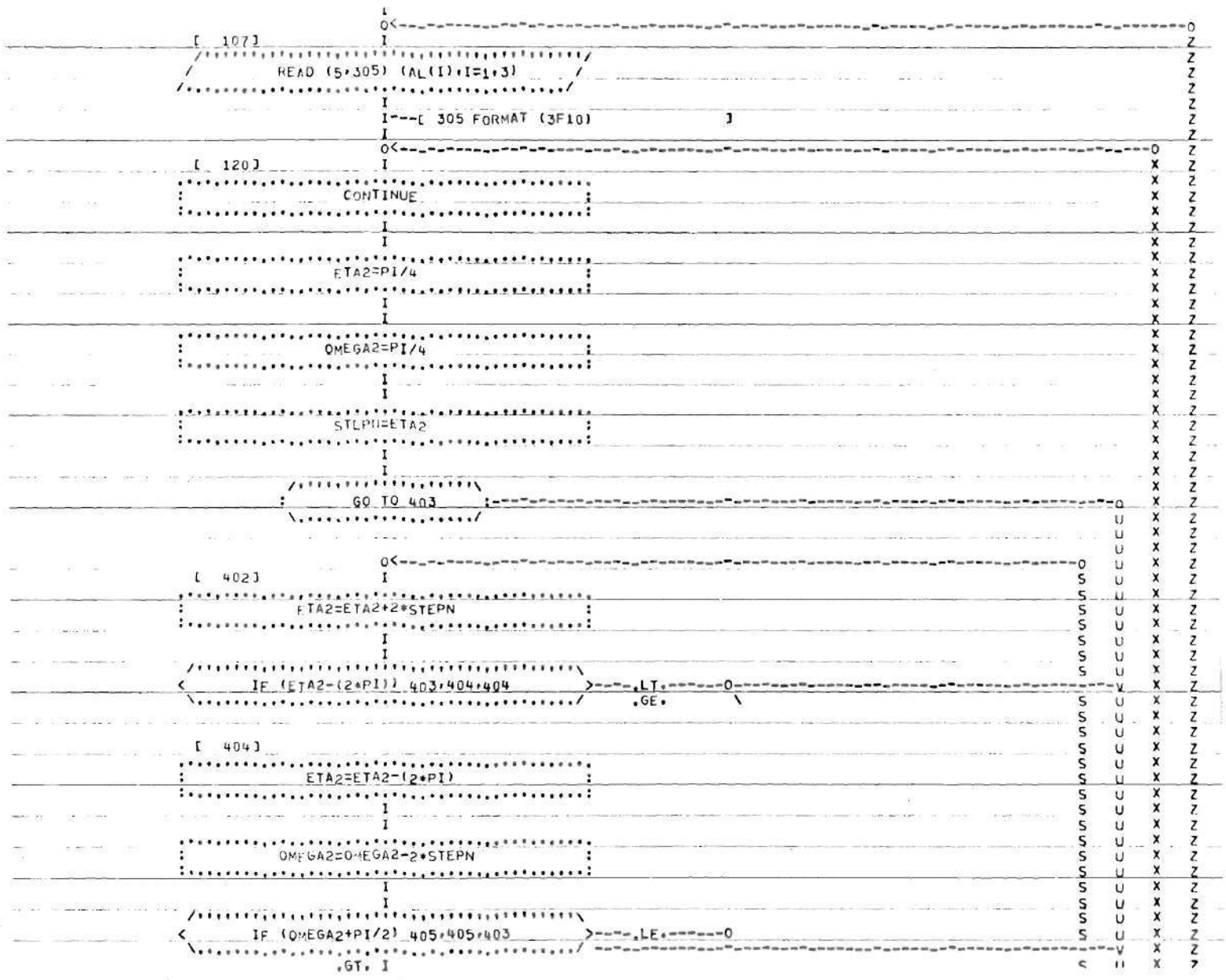
[107]
READ (5,305) (AL(I),I=1,3)
305 FORMAT (3F10)
[120]
CONTINUE
ETA2=PI/4
OMEGA2=PI/4
STEPN=ETA2
GO TO 403
[402]
ETA2=ETA2+2*STEPN
IF (ETA2-(2*PI)) 403,404,404
.LT.
.GE.
[404]
ETA2=ETA2-(2*PI)
OMEGA2=OMEGA2-2*STEPN
IF (OMEGA2+PI/2) 405,405,403
.LE.
.GT.

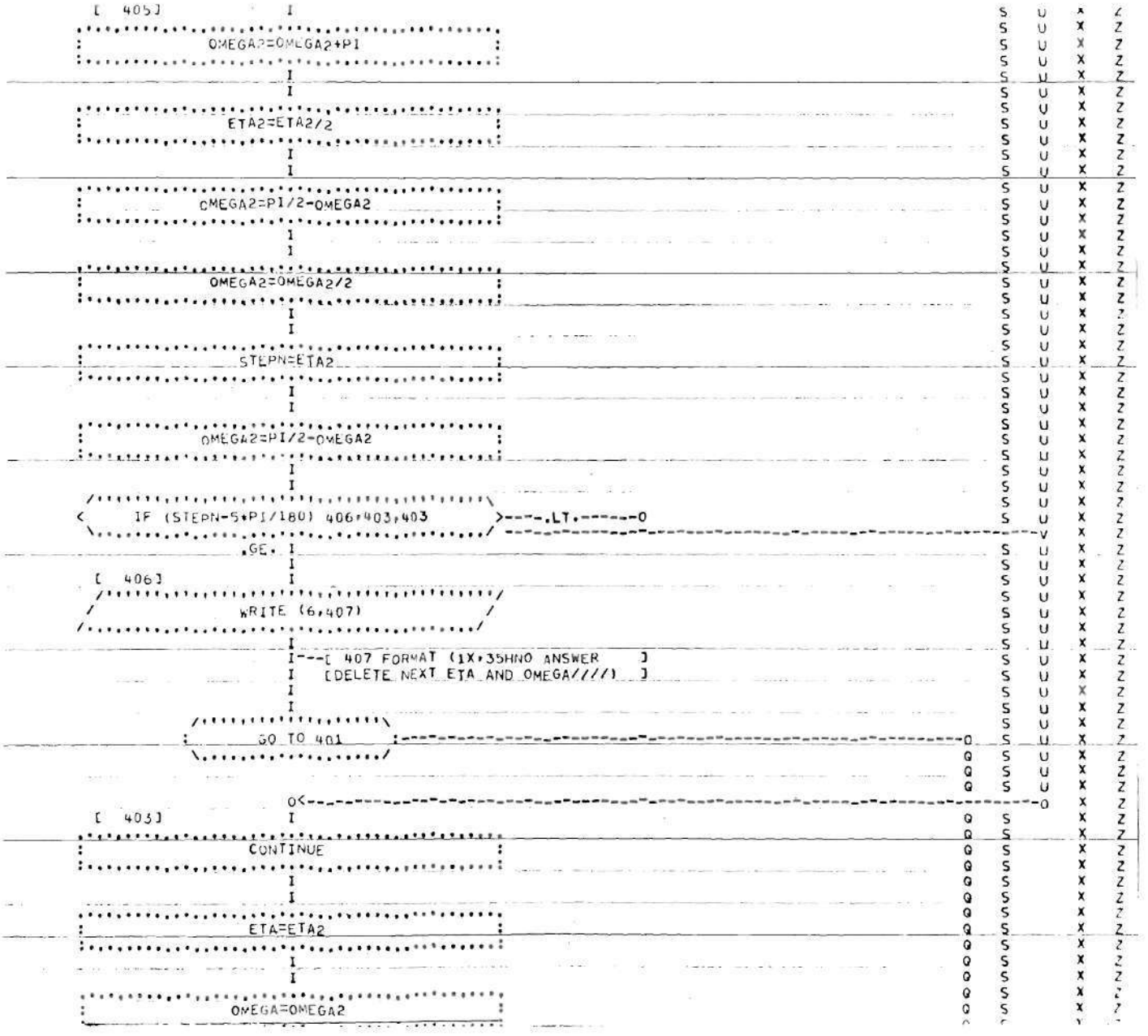
[405]
OMEGA2=OMEGA2+PI
ETA2=ETA2/2
OMEGA2=PI/2-OMEGA2
OMEGA2=OMEGA2/2
STEPN=ETA2
OMEGA2=PI/2-OMEGA2
IF (STEPN-5*PI/180) 406,403,403
.LT.
.GE.
[406]
WRITE (6,407)
[407 FORMAT (1X,35HNO ANSWER
[DELETE NEXT ETA AND OMEGA////)]
GO TO 401
[403]
CONTINUE
ETA=ETA2
OMEGA=OMEGA2

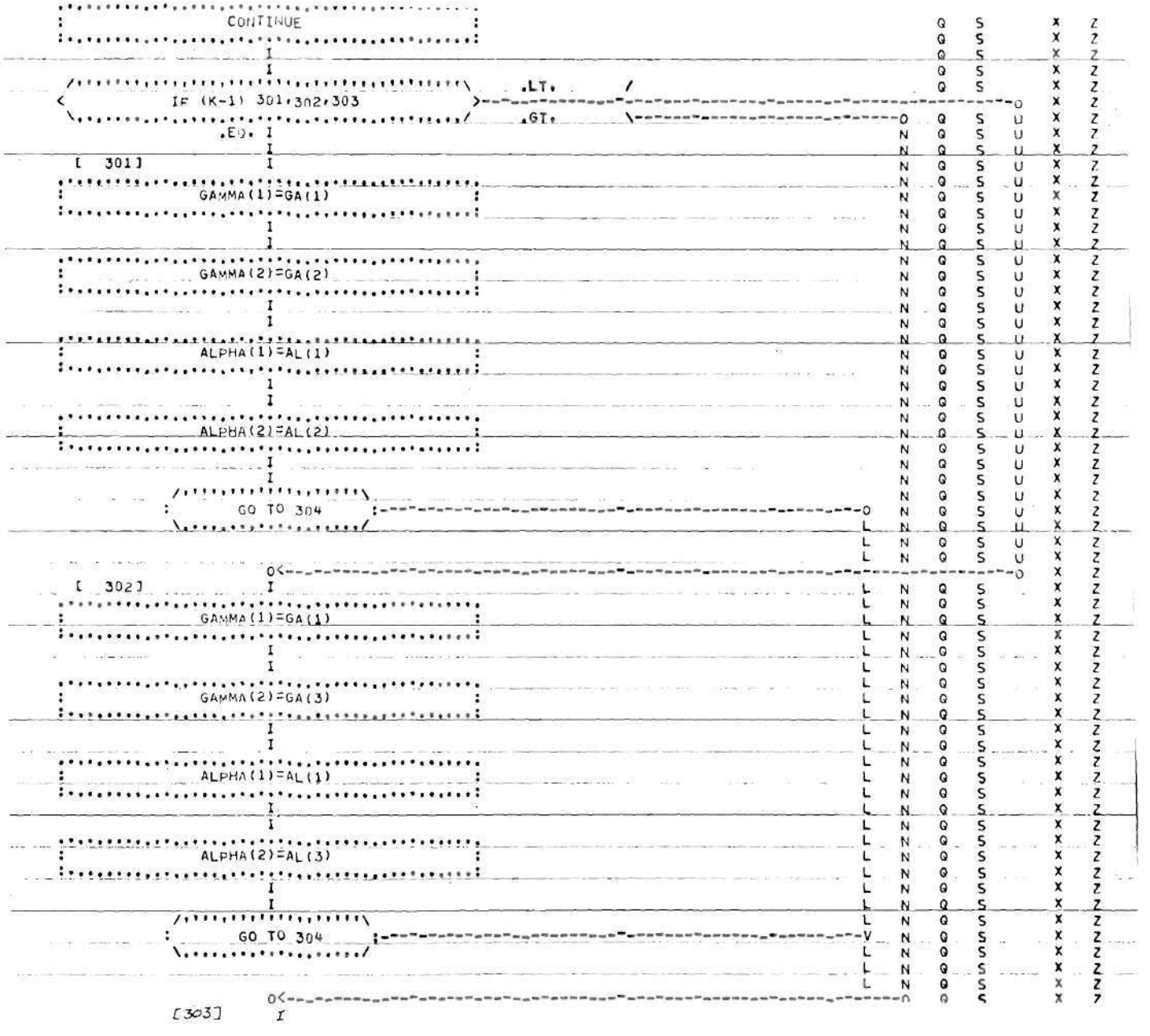
CONTINUE
IF (K-1) 301,302,303
.LT.
.EQ.
.GT.
[301]
GAMMA(1)=GA(1)
GAMMA(2)=GA(2)
ALPHA(1)=AL(1)
ALPHA(2)=AL(2)
GO TO 304
[302]
GAMMA(1)=GA(1)
GAMMA(2)=GA(3)
ALPHA(1)=AL(1)
ALPHA(2)=AL(3)
GO TO 304
[303]

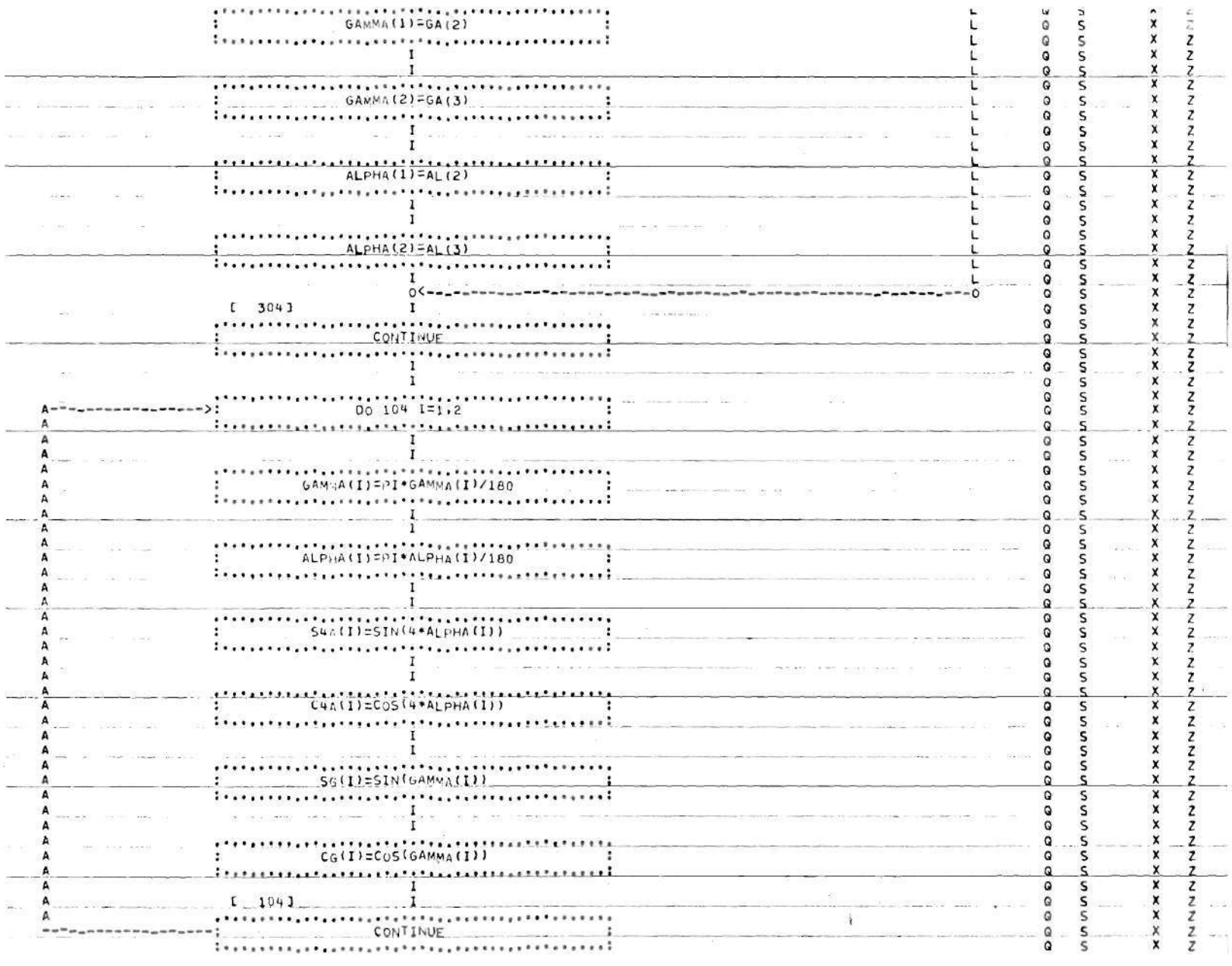
GAMMA(1)=GA(2)
GAMMA(2)=GA(3)
ALPHA(1)=AL(2)
ALPHA(2)=AL(3)
[304]
CONTINUE
DO 104 I=1,2
GAMMA(I)=PI*GAMMA(I)/180
ALPHA(I)=PI*ALPHA(I)/180
S4A(I)=SIN(4*ALPHA(I))
C4A(I)=COS(4*ALPHA(I))
SG(I)=SIN(GAMMA(I))
CG(I)=COS(GAMMA(I))
[104]
CONTINUE

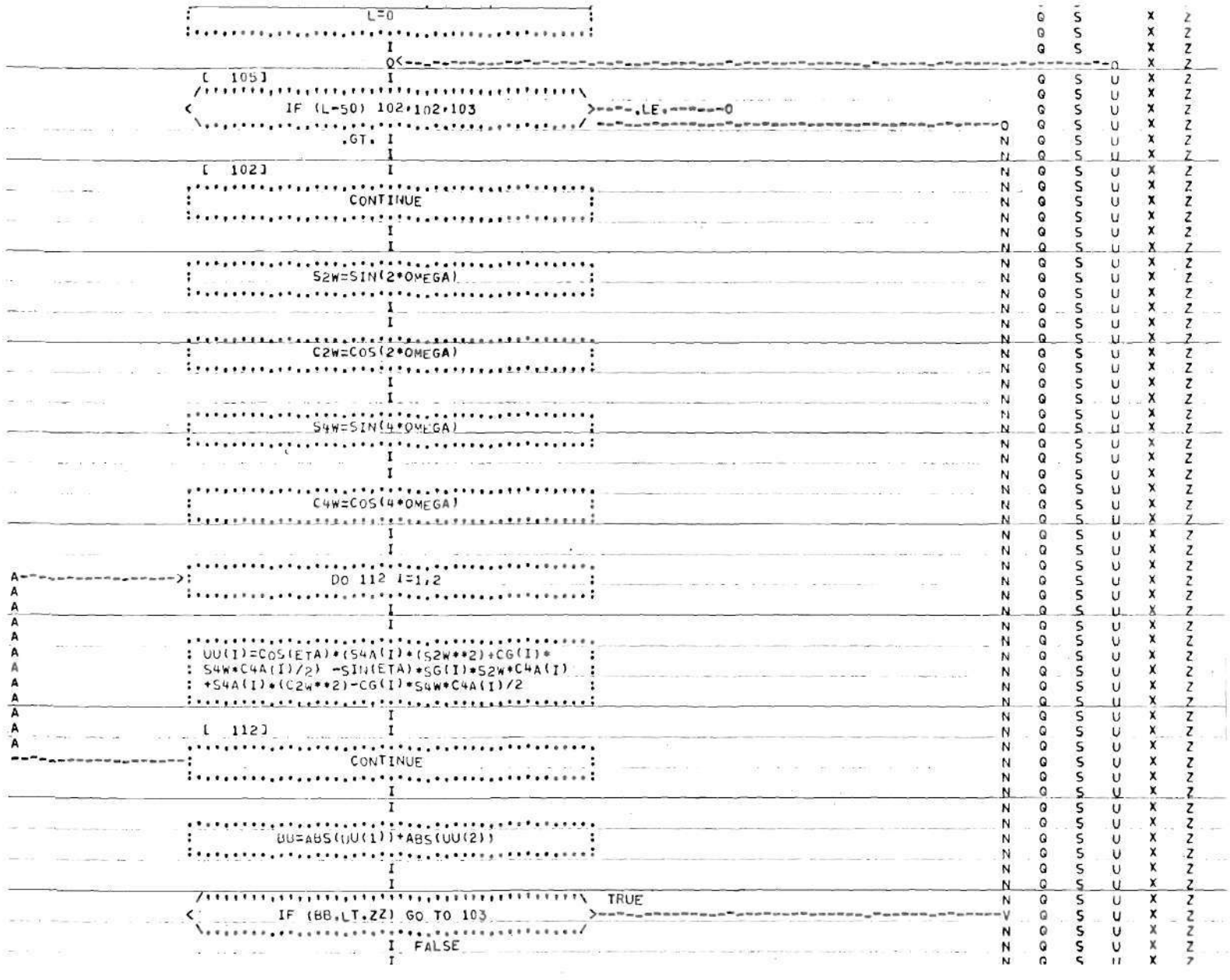
L=0
[105]
IF (L-50) 102,102,103
.LT.
.LE.
.GT.
[102]
CONTINUE
S2W=SIN(2*OMEGA)
C2W=COS(2*OMEGA)
S4W=SIN(4*OMEGA)
C4W=COS(4*OMEGA)
DO 112 I=1,2
UU(I)=COS(ETA)*(S4A(I)*(S2W**2)+CG(I)*
S4W*C4A(I)/2) -SIN(ETA)*SG(I)*S2W*C4A(I)
+S4A(I)*(C2W**2)-CG(I)*S4W*C4A(I)/2
[112]
CONTINUE
BB=ABS(UU(1))+ABS(UU(2))
IF (BB.LT.ZZ) GO TO 103
TRUE
FALSE

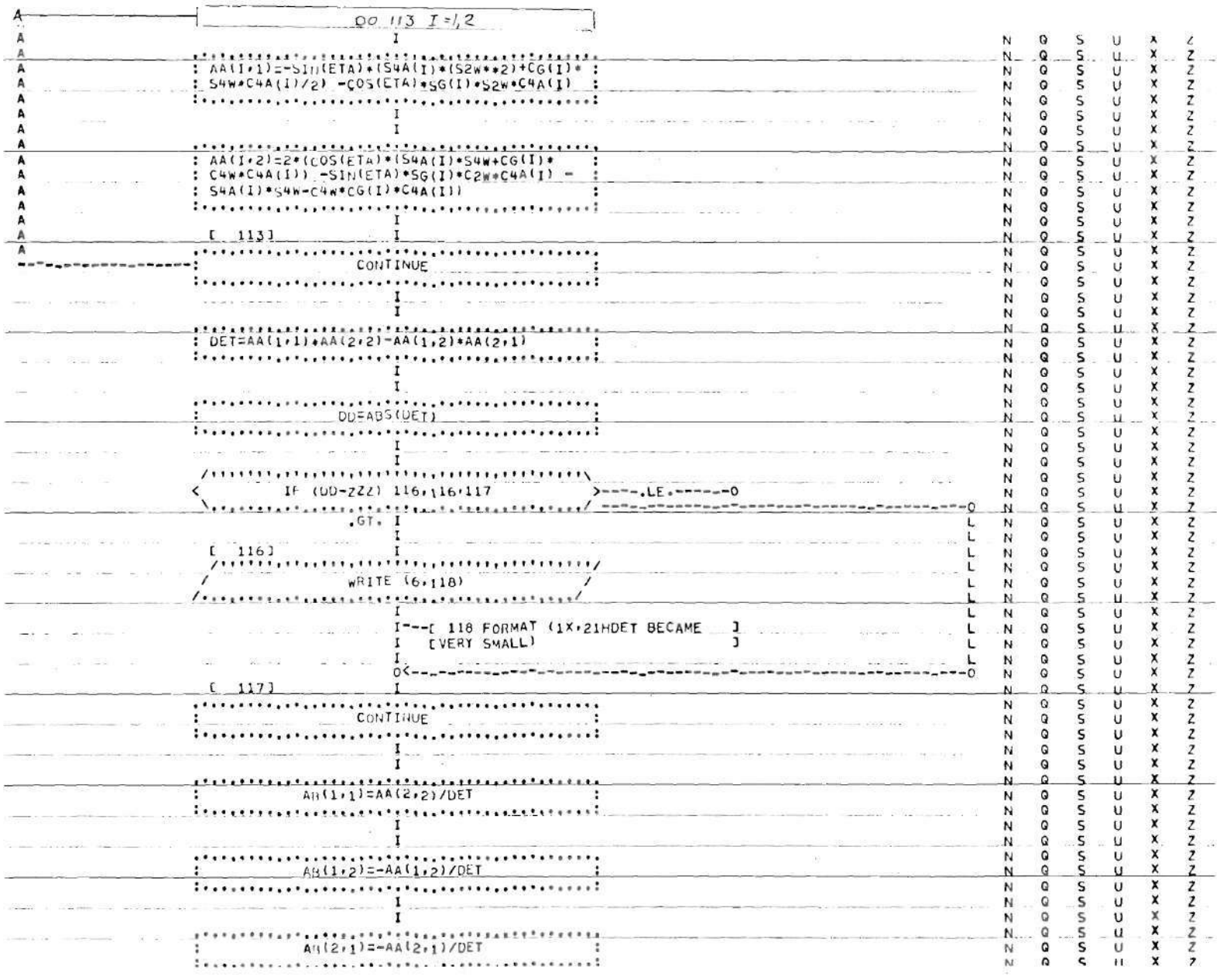
DO 113 I=1,2
AA(I,1)=-SIN(ETA)*(S4A(I)*(S2W**2)+CG(I)*
S4W*C4A(I)/2) -COS(ETA)*SG(I)*S2W*C4A(I)
AA(I,2)=2*(COS(ETA)*(S4A(I)*S4W+CG(I)*
C4W*C4A(I)) -SIN(ETA)*SG(I)*C2W*C4A(I) -
S4A(I)*S4W-C4W*CG(I)*C4A(I))
[113]
CONTINUE
DET=AA(1,1)*AA(2,2)-AA(1,2)*AA(2,1)
DD=ABS(DET)
IF (DD-ZZZ) 116,116,117
.LE.
.GT.
[116]
WRITE (6,118)
[118 FORMAT (1X,21HDET BECAME
[VERY SMALL)
[117]
CONTINUE
AB(1,1)=AA(2,2)/DET
AB(1,2)=-AA(1,2)/DET
AB(2,1)=-AA(2,1)/DET

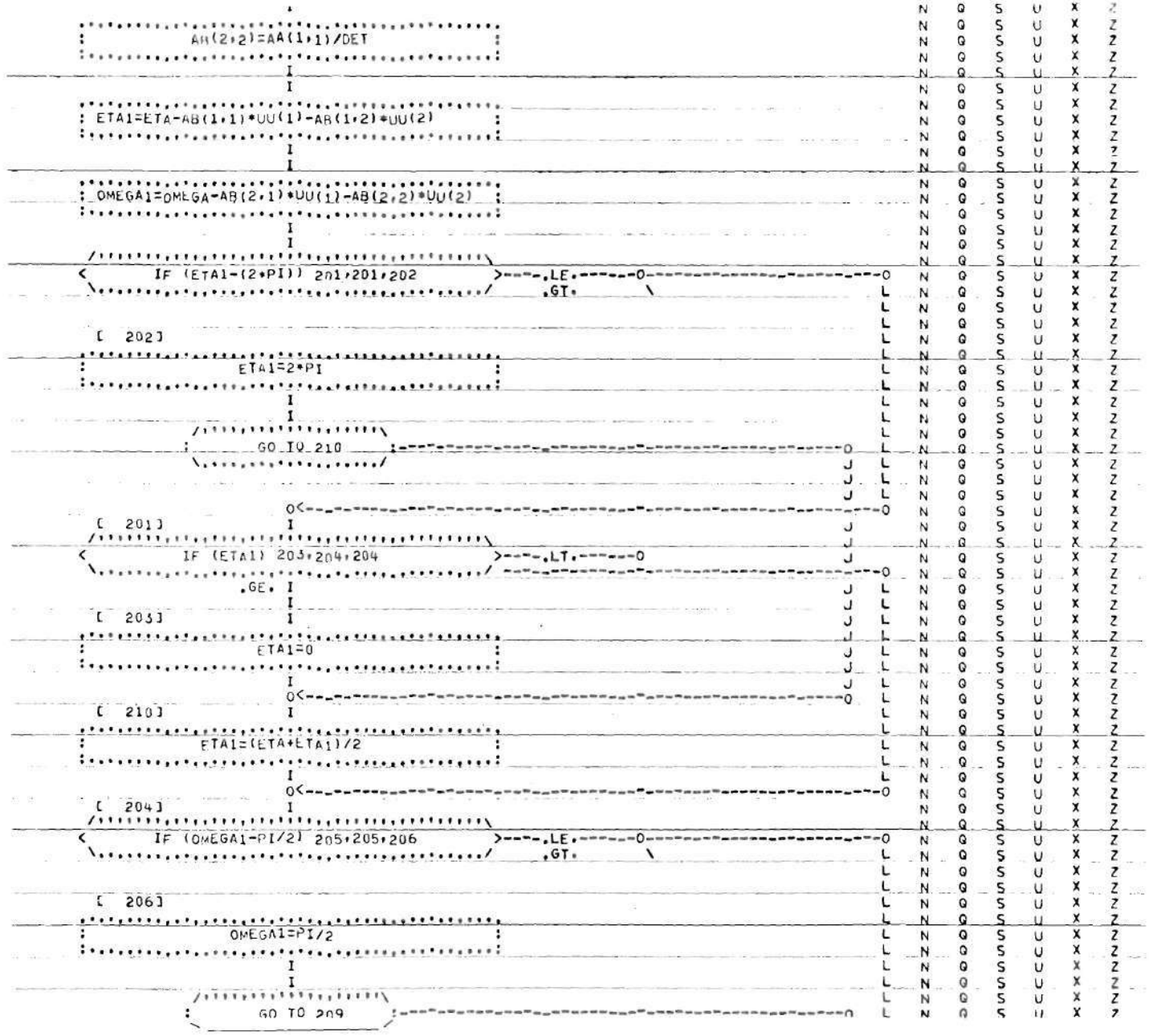
AB(2,2)=AA(1,1)/DET
ETA1=ETA-AB(1,1)*UU(1)-AB(1,2)*UU(2)
OMEGA1=OMEGA-AB(2,1)*UU(1)-AB(2,2)*UU(2)
IF (ETA1-(2*PI)) 201,201,202
.LE.
.GT.
[202]
ETA1=2*PI
GO TO 210
[201]
IF (ETA1) 203,204,204
.LT.
.GE.
[203]
ETA1=0
[210]
ETA1=(ETA+ETA1)/2
[204]
IF (OMEGA1-PI/2) 205,205,206
.LE.
.GT.
[206]
OMEGA1=PI/2
GO TO 209

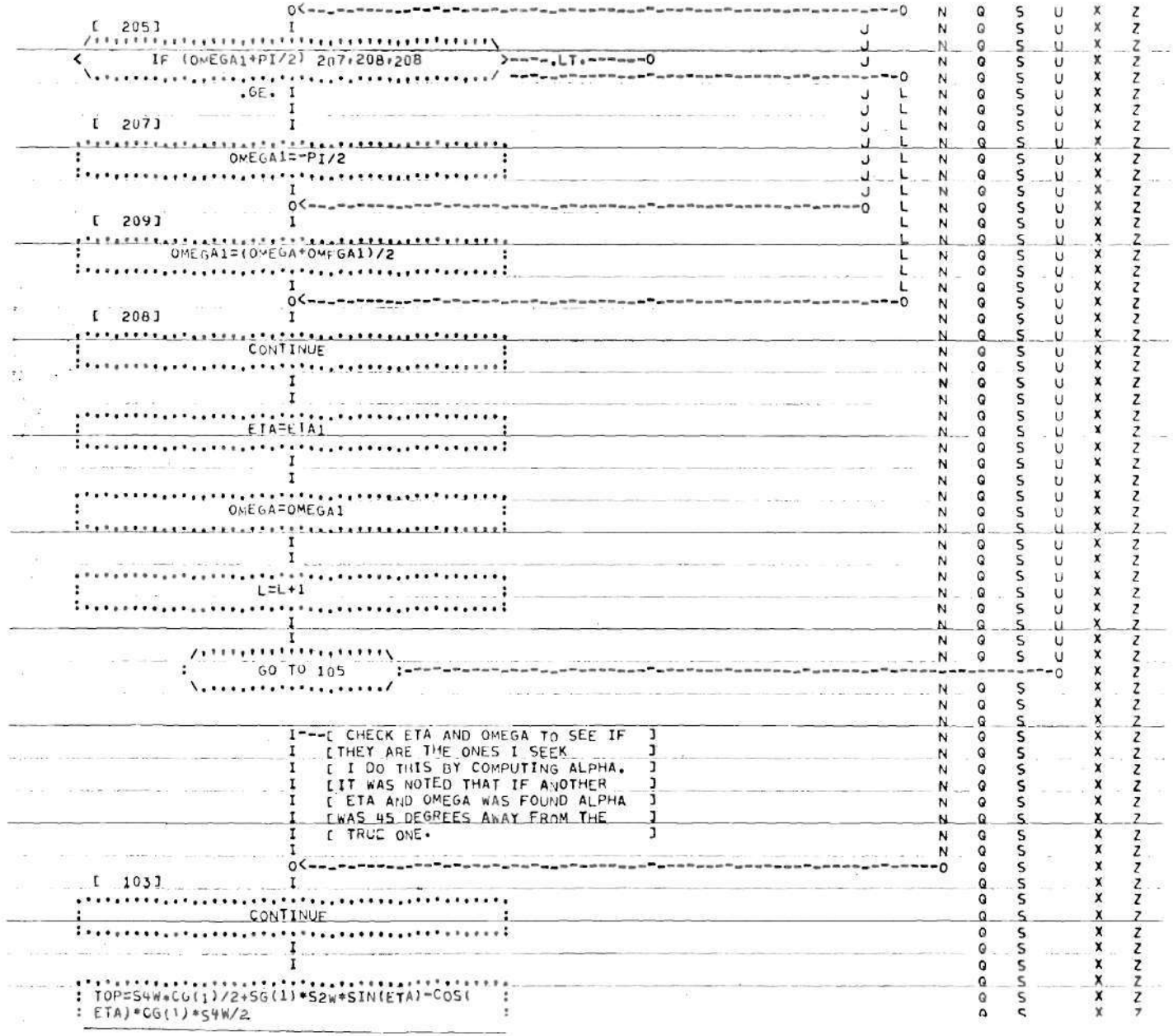
[205]
IF (OMEGA1+PI/2) 207,208,208
.LT.
.GE.
[207]
OMEGA1=-PI/2
[209]
OMEGA1=(OMEGA+OMEGA1)/2
[208]
CONTINUE
ETA=ETA1
OMEGA=OMEGA1
L=L+1
GO TO 105
[CHECK ETA AND OMEGA TO SEE IF
[THEY ARE THE ONES I SEEK
[I DO THIS BY COMPUTING ALPHA.
[IT WAS NOTED THAT IF ANOTHER
[ETA AND OMEGA WAS FOUND ALPHA
[WAS 45 DEGREES AWAY FROM THE
[TRUE ONE.
[103]
CONTINUE
TOP=S4W*CG(1)/2+SG(1)*S2W*SIN(ETA)-COS(
ETA)*CG(1)*S4W/2

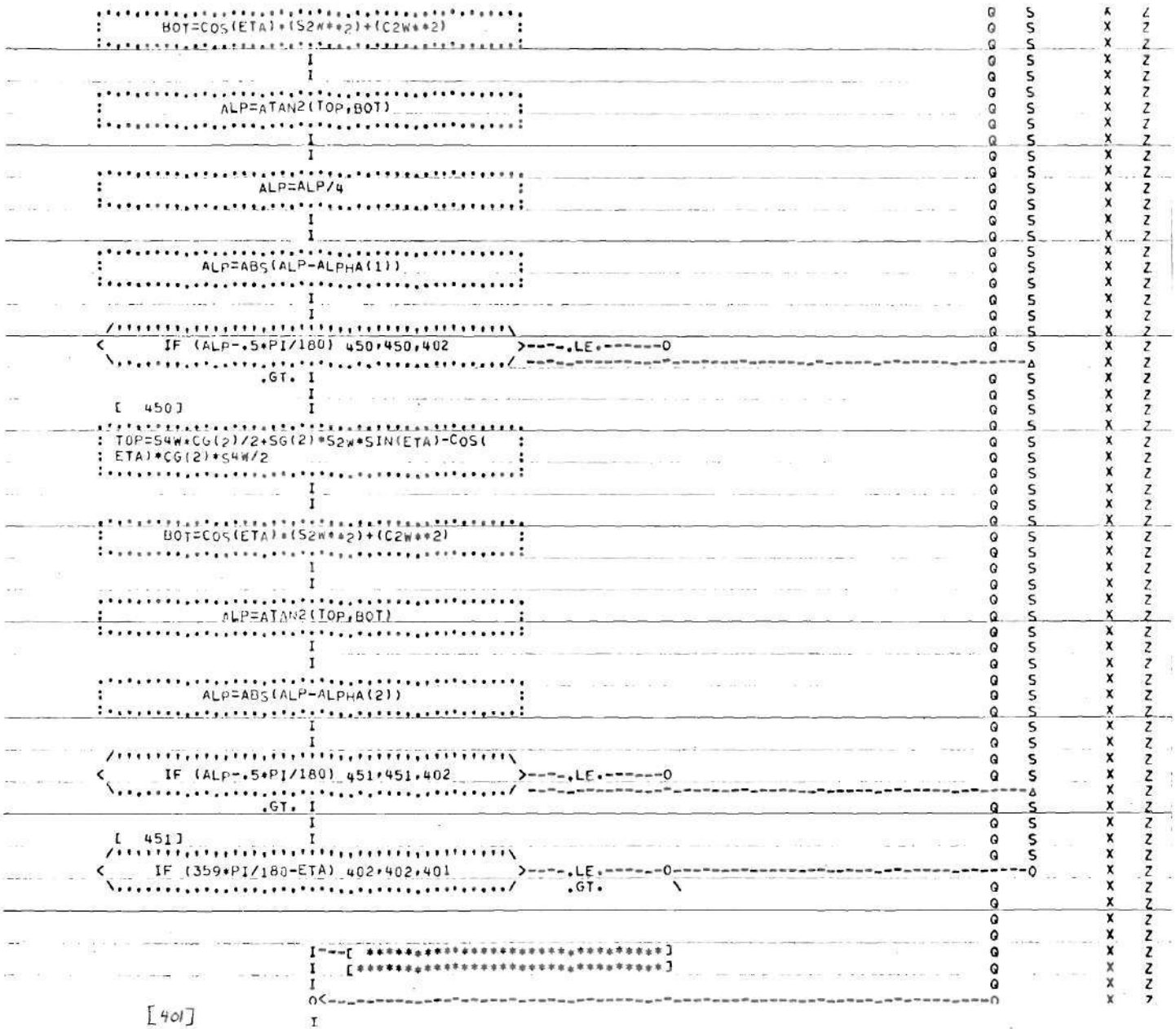
BOT=COS(ETA)*(S2W**2)+(C2W**2)
ALP=ATAN2(TOP,BOT)
ALP=ALP/4
ALP=ABS(ALP-ALPHA(1))
IF (ALP-.5*PI/180) 450,450,402
.GT.
.LE.
0
[450]
TOP=S4W*CG(2)/2+SG(2)*S2W*SIN(ETA)-COS(
ETA)*CG(2)*S4W/2
BOT=COS(ETA)*(S2W**2)+(C2W**2)
ALP=ATAN2(TOP,BOT)
ALP=ABS(ALP-ALPHA(2))
IF (ALP-.5*PI/180) 451,451,402
.GT.
.LE.
0
[451]
IF (359*PI/180-ETA) 402,402,401
.LE.
.GT.
0
[401]

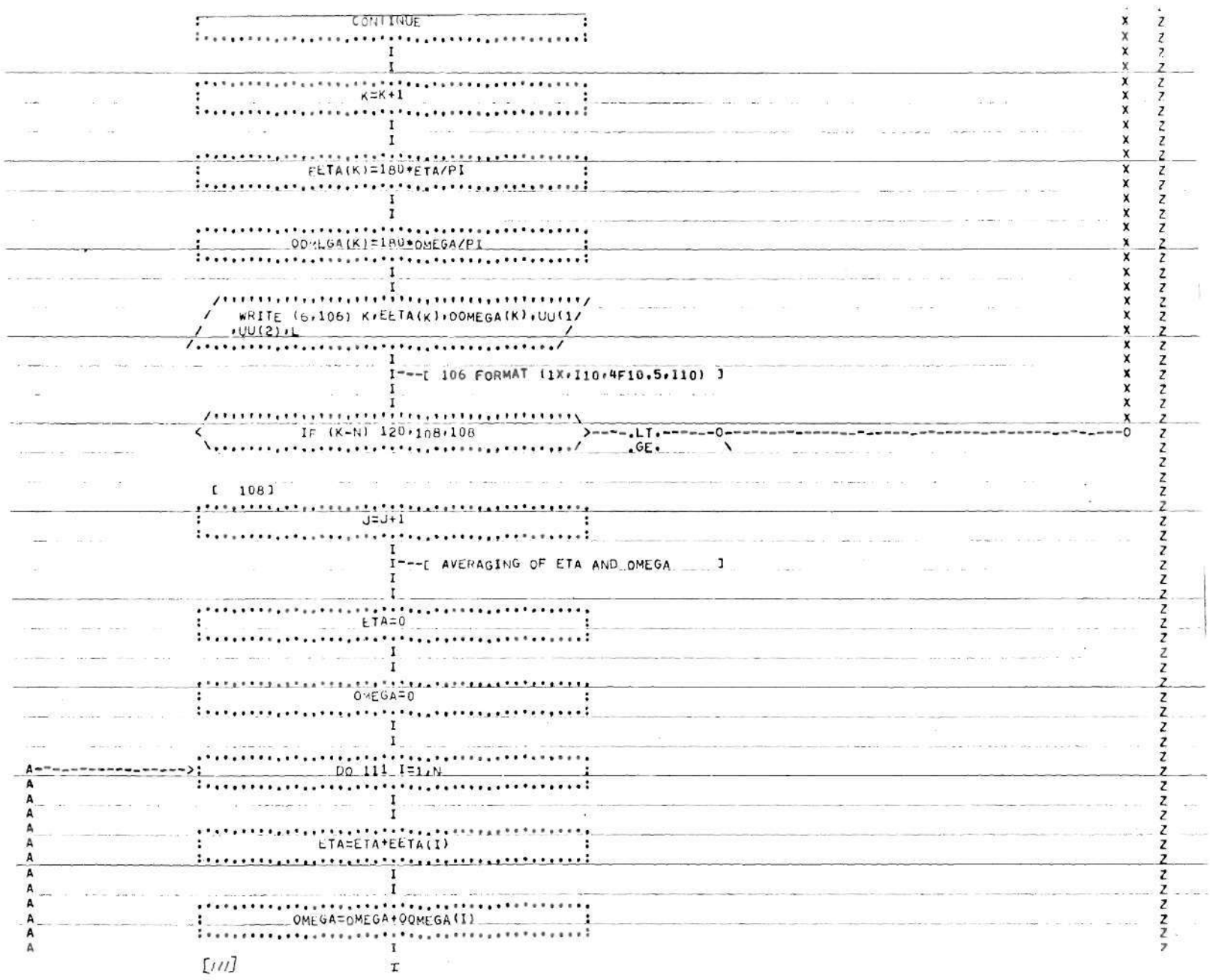
CONTINUE
K=K+1
EETA(K)=180*ETA/PI
OOMEGA(K)=180*OMEGA/PI
WRITE (6,106) K,EETA(K),OOMEGA(K),UU(1/
,UU(2),L
106 FORMAT (1X,I10,4F10.5,110)
IF (K-N) 120,108,108
LT.
GE.
108
J=J+1
AVERAGING OF ETA AND OMEGA
ETA=0
OMEGA=0
DO 111 I=1,N
ETA=ETA+EETA(I)
OMEGA=OMEGA+OOMEGA(I)
111

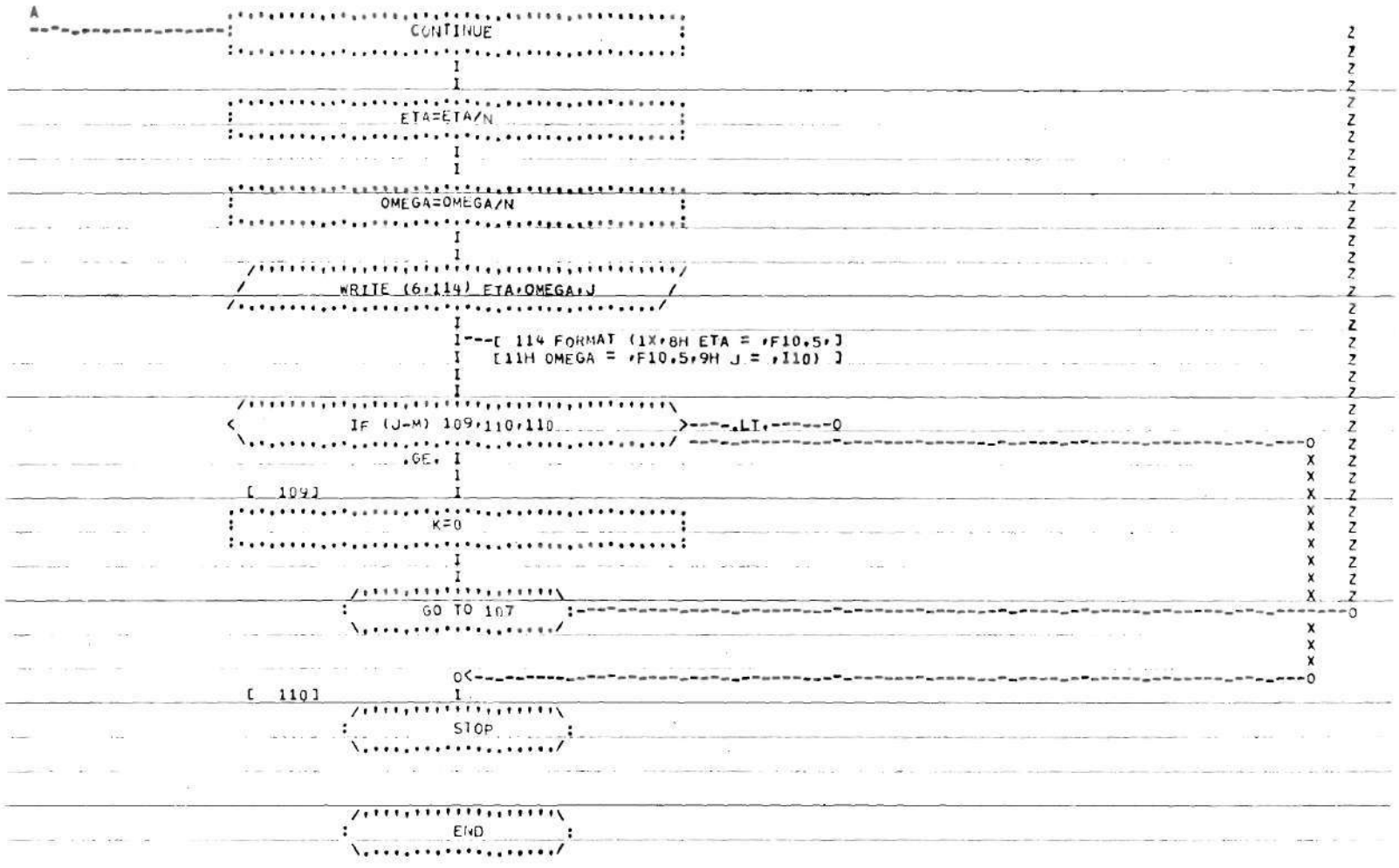
A
CONTINUE
ETA=ETA/N
OMEGA=OMEGA/N
WRITE (6,114) ETA,OMEGA,J
114 FORMAT (1X,8H ETA = ,F10.5,
11H OMEGA = ,F10.5,9H J = ,I10))
IF (J-M) 109,110,110
.LT.
.GE.
109
K=0
GO TO 107
110
STOP
END

```
[illegible]-J-P*BURAN.TRAP
      C     DETERMINATION OF ETA AND OMEGA
      C     COMPENSATOR SETTINGS    GAMMA(1)=0,  GAMMA(2)=.664 RAD
     .
      C                                GAMMA(3)=2.476 RAD.
      C     SET AT  1) 7.20,    2) 7.857    3) 9.65
      C     ***********************************************************
     ***********
      C
      C
      C
            DIMENSION  EETA(3),OOMEGA(3),AA(2,2),UU(2),ALPHA(2),
           1           GAMMA(2),S4A(2),SG(2),CG(2),AB(2,2),C4A(2)
            DIMENSION GA(3),AL(3)
            READ (5,100) N,M
        100 FORMAT (2I10)
            READ (5,101) (GA(I),I=1,3)
        101 FORMAT (3F10)
            ZZZ=5.*10.**(-10)
            ZZ=.005
            PI=3.1416
            K=0
            J=0
        107 READ (5,305) (AL(I),I=1,3)
        305 FORMAT (3F10)
        120 CONTINUE
            ETA2=PI/4
            OMEGA2=PI/4
            STEPN=ETA2
            GO TO 403
        402 ETA2=ETA2+2*STEPN
            IF (ETA2-(2*PI)) 403,404,404
        404 ETA2=ETA2-(2*PI)
            OMEGA2=OMEGA2-2*STEPN
            IF (OMEGA2+PI/2) 405,405,403
        405 OMEGA2=OMEGA2+PI
            ETA2=ETA2/2
            OMEGA2=PI/2-OMEGA2
            OMEGA2=OMEGA2/2
            STEPN=ETA2
            OMEGA2=PI/2-OMEGA2
            IF (STEPN-5*PI/180) 406,403,403
        406 WRITE (6,407)
        407 FORMAT (1X,35HNO ANSWER DELETE NEXT ETA AND OMEGA////)
            GO TO 401
        403 CONTINUE
            ETA=ETA2
            OMEGA=OMEGA2
            CONTINUE
            IF (K-1) 301,302,303
        301 GAMMA(1)=GA(1)
```

```
      GAMMA(2)=GA(2)
      ALPHA(1)=AL(1)
      ALPHA(2)=AL(2)
      GO TO 304
  302 GAMMA(1)=GA(1)
      GAMMA(2)=GA(3)
      ALPHA(1)=AL(1)
      ALPHA(2)=AL(3)
      GO TO 304
  303 GAMMA(1)=GA(2)
      GAMMA(2)=GA(3)
      ALPHA(1)=AL(2)
      ALPHA(2)=AL(3)
  304 CONTINUE
      DO 104 I=1,2
      GAMMA(I)=PI*GAMMA(I)/180
      ALPHA(I)=PI*ALPHA(I)/180
      S4A(I)=SIN(4*ALPHA(I))
      C4A(I)=COS(4*ALPHA(I))
      SG(I)=SIN(GAMMA(I))
      CG(I)=COS(GAMMA(I))
  104 CONTINUE
      L=0
  105 IF (L-50) 102,102,103
  102 CONTINUE
      S2W=SIN(2*OMEGA)
      C2W=COS(2*OMEGA)
      S4W=SIN(4*OMEGA)
      C4W=COS(4*OMEGA)
      DO 112 I=1,2
      UU(I)=COS(ETA)*(S4A(I)*(S2W**2)+CG(I)*S4W*C4A(I)/2)
     1      -SIN(ETA)*SG(I)*S2W*C4A(I)
     2      +S4A(I)*(C2W**2)-CG(I)*S4W*C4A(I)/2
  112 CONTINUE
      BB=ABS(UU(1))+ABS(UU(2))
      IF (BB.LT.ZZ) GO TO 103
      DO 113 I=1,2
      AA(I,1)=-SIN(ETA)*(S4A(I)*(S2W**2)+CG(I)*S4W*C4A(I)/2)
     1        -COS(ETA)*SG(I)*S2W*C4A(I)
      AA(I,2)=2*(COS(ETA)*(S4A(I)*S4W+CG(I)*C4W*C4A(I))
     1        -SIN(ETA)*SG(I)*C2W*C4A(I)
     2        -S4A(I)*S4W-C4W*CG(I)*C4A(I))
  113 CONTINUE
      DET=AA(1,1)*AA(2,2)-AA(1,2)*AA(2,1)
      DD=ABS(DET)
      IF (DD-ZZZ) 116,116,117
  116 WRITE (6,118)
  118 FORMAT (1X,21HDET BECAME VERY SMALL)
  117 CONTINUE
      AB(1,1)=AA(2,2)/DET
      AB(1,2)=-AA(1,2)/DET
```

```
100             AB(2,1)=-AA(2,1)/DET
101             AB(2,2)=AA(1,1)/DET
102             ETA1=ETA-AB(1,1)*UU(1)-AB(1,2)*UU(2)
103             OMEGA1=OMEGA-AB(2,1)*UU(1)-AB(2,2)*UU(2)
104             IF (ETA1-(2*PI)) 201,201,202
105         202 ETA1=2*PI
106             GO TO 210
107         201 IF (ETA1) 203,204,204
108         203 ETA1=0
109         210 ETA1=(ETA+ETA1)/2
110         204 IF (OMEGA1-PI/2) 205,205,206
111         206 OMEGA1=PI/2
112             GO TO 209
113         205 IF (OMEGA1+PI/2) 207,208,208
114         207 OMEGA1=-PI/2
115         209 OMEGA1=(OMEGA+OMEGA1)/2
116         208 CONTINUE
117             ETA=ETA1
118             OMEGA=OMEGA1
119             L=L+1
120             GO TO 105
121       C     CHECK ETA AND OMEGA TO SEE IF THEY ARE THE ONES I SEEK
122       C     I DO THIS BY COMPUTING ALPHA. IT WAS NOTED THAT IF ANO
    THER
123       C     ETA AND OMEGA WAS FOUND ALPHA WAS 45 DEGREES AWAY FROM
     THE
124       C     TRUE ONE.
125         103 CONTINUE
126             TOP=S4W*CG(1)/2+SG(1)*S2W*SIN(ETA)-COS(ETA)*CG(1)*S4W/
    2
127             BOT=COS(ETA)*(S2W**2)+(C2W**2)
128             ALP=ATAN2(TOP,BOT)
129             ALP=ALP/4
130             ALP=ABS(ALP-ALPHA(1))
131             IF (ALP-.5*PI/180) 450,450,402
132         450 TOP=S4W*CG(2)/2+SG(2)*S2W*SIN(ETA)-COS(ETA)*CG(2)*S4W/
    2
133             BOT=COS(ETA)*(S2W**2)+(C2W**2)
134              ALP=ATAN2(TOP,BOT)
135             ALP=ABS(ALP-ALPHA(2))
136             IF (ALP-.5*PI/180) 451,451,402
137         451 IF (359*PI/180-ETA) 402,402,401
138       C     ************************************************************
    ************
139         401 CONTINUE
140             K=K+1
141             BETA(K)=180*ETA/PI
142             OOMEGA(K)=180*OMEGA/PI
143             WRITE (6,106) K,BETA(K),OOMEGA(K),UU(1),UU(2),L
144         106 FORMAT (1X,I10,4F10.5,I10)
145             IF (K-N) 120,108,108
```

```
      108 J=J+1
C         AVERAGING OF ETA AND OMEGA
          ETA=0
          OMEGA=0
          DO 111 I=1,K
          ETA=ETA+EETA(I)
          OMEGA=OMEGA+OOMEGA(I)
      111 CONTINUE
          ETA=ETA/K
          OMEGA=OMEGA/K
          WRITE (6,114) ETA,OMEGA,J
      114 FORMAT (1X,8H  ETA = ,F10.5,11H   OMEGA = ,F10.5,9H
     J = ,I10)
          IF (J-M) 109,110,110
      109 K=0
          GO TO 107
      110 STOP
          END
```

b) Flowchart and Program for the Smoothed-Spline Derivatives.

BEGIN
DIMENSION X(70),Y(70),DY(70),CP0(70),CP1(70),CP2(70),CP3(70),XLS(10),YLS(10)
PI=3.1416
[999]
CONTINUE
READ (5,101) THETA
[101 FORMAT (F10)]
THETA=THETA*PI/180
WRITE (6,501) THETA
[501 FORMAT (1X,8HTHETA = ,F4.1)]
READ (5,950) N,EPS,S,ND,NLS
RND=ND
WRITE (6,968) N,EPS,S,NLS,ND
NP1=N+1

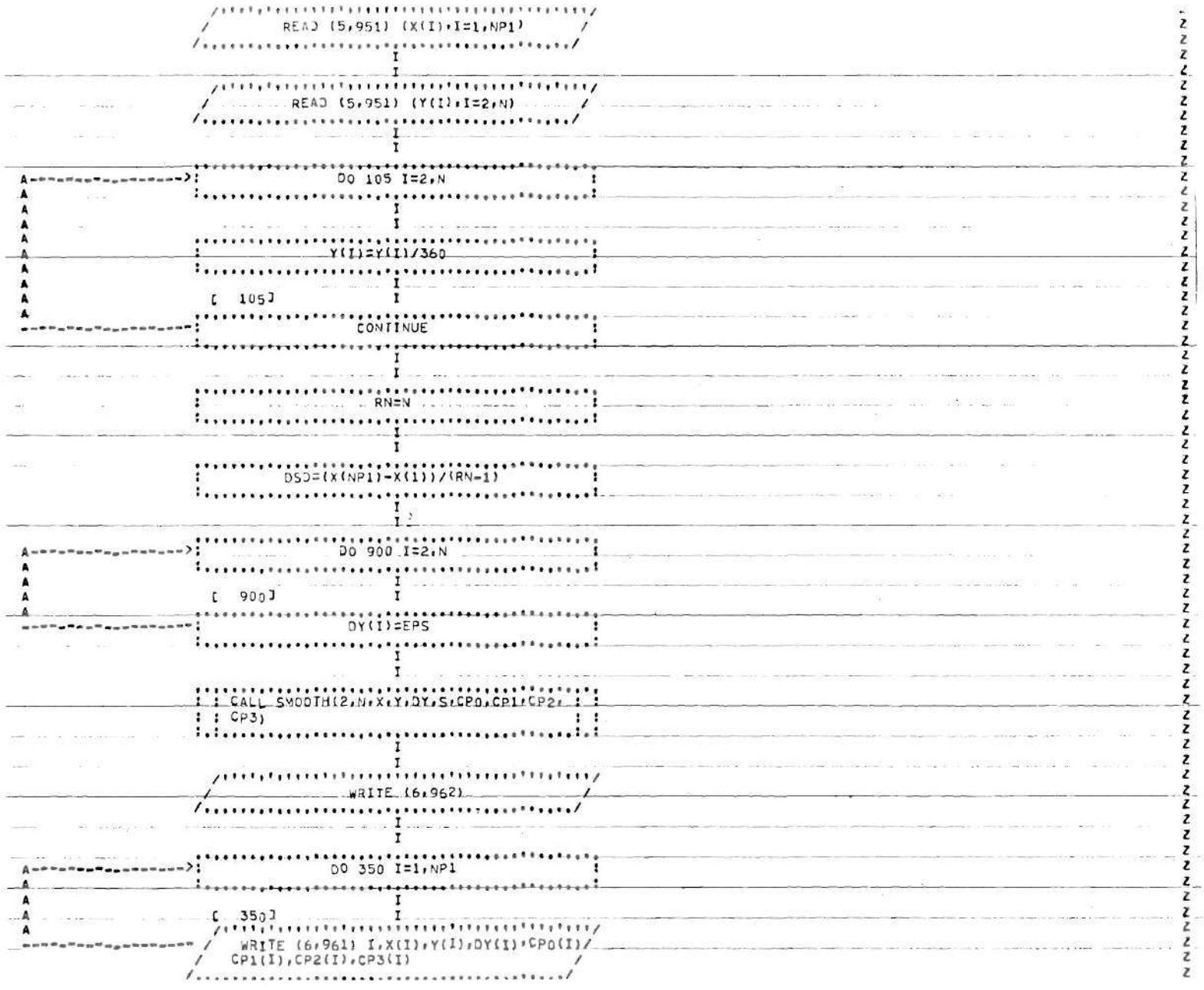
READ (5,951) (X(I),I=1,NP1)
READ (5,951) (Y(I),I=2,N)
DO 105 I=2,N
Y(I)=Y(I)/360
105
CONTINUE
RN=N
DSD=(X(NP1)-X(1))/(RN-1)
DO 900 I=2,N
900
DY(I)=EPS
CALL SMOOTH(2,N,X,Y,DY,S,CP0,CP1,CP2,CP3)
WRITE (6,962)
DO 350 I=1,NP1
350
WRITE (6,961) I,X(I),Y(I),DY(I),CP0(I),CP1(I),CP2(I),CP3(I)

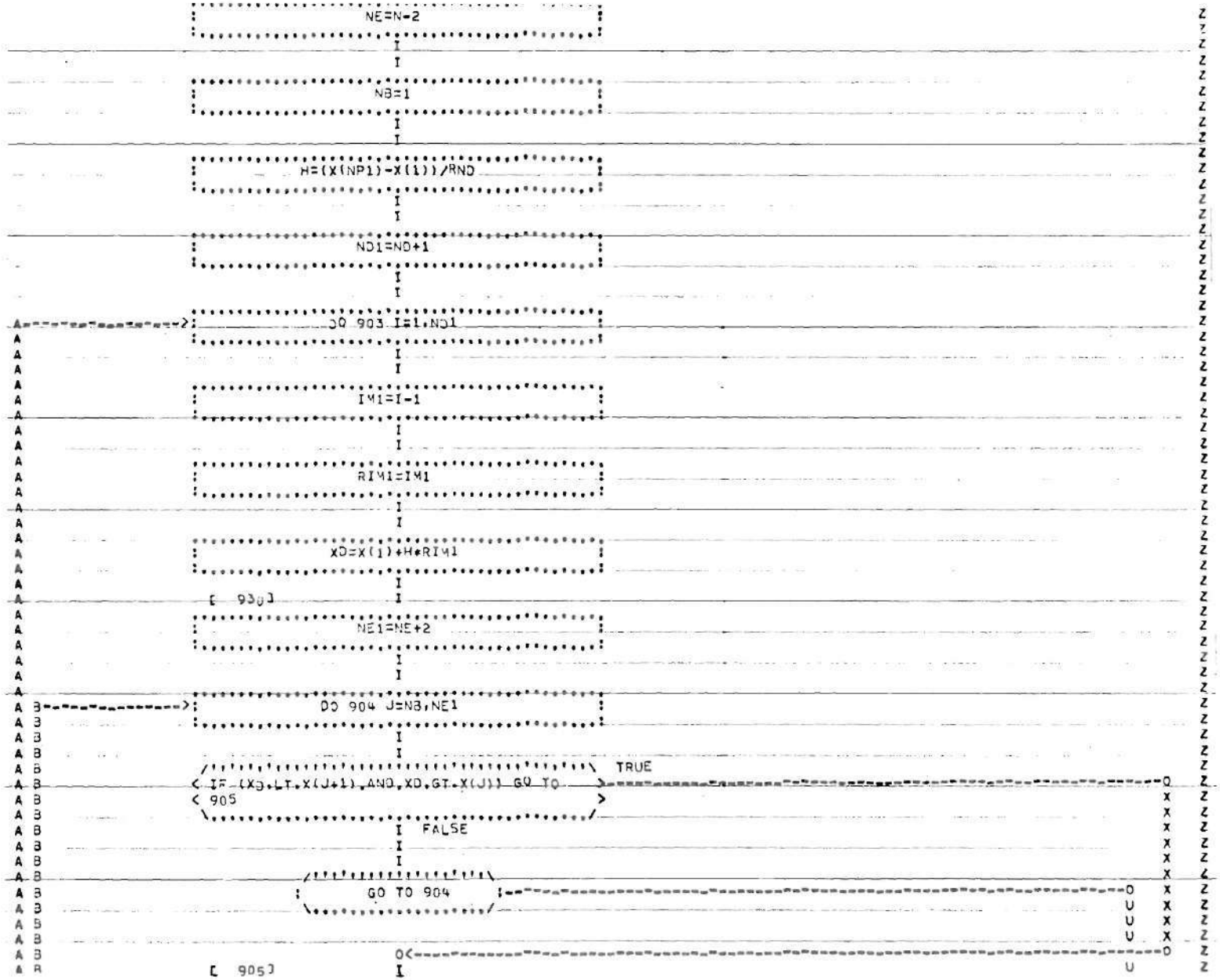
NE=N-2
NB=1
H=(X(NP1)-X(1))/RND
ND1=ND+1
DO 903 I=1,ND1
IM1=I-1
RIM1=IM1
XD=X(1)+H*RIM1
[930]
NE1=NE+2
DO 904 J=NB,NE1
IF (XD.LT.X(J+1).AND.XD.GT.X(J)) GO TO 905
TRUE
FALSE
GO TO 904
[905]

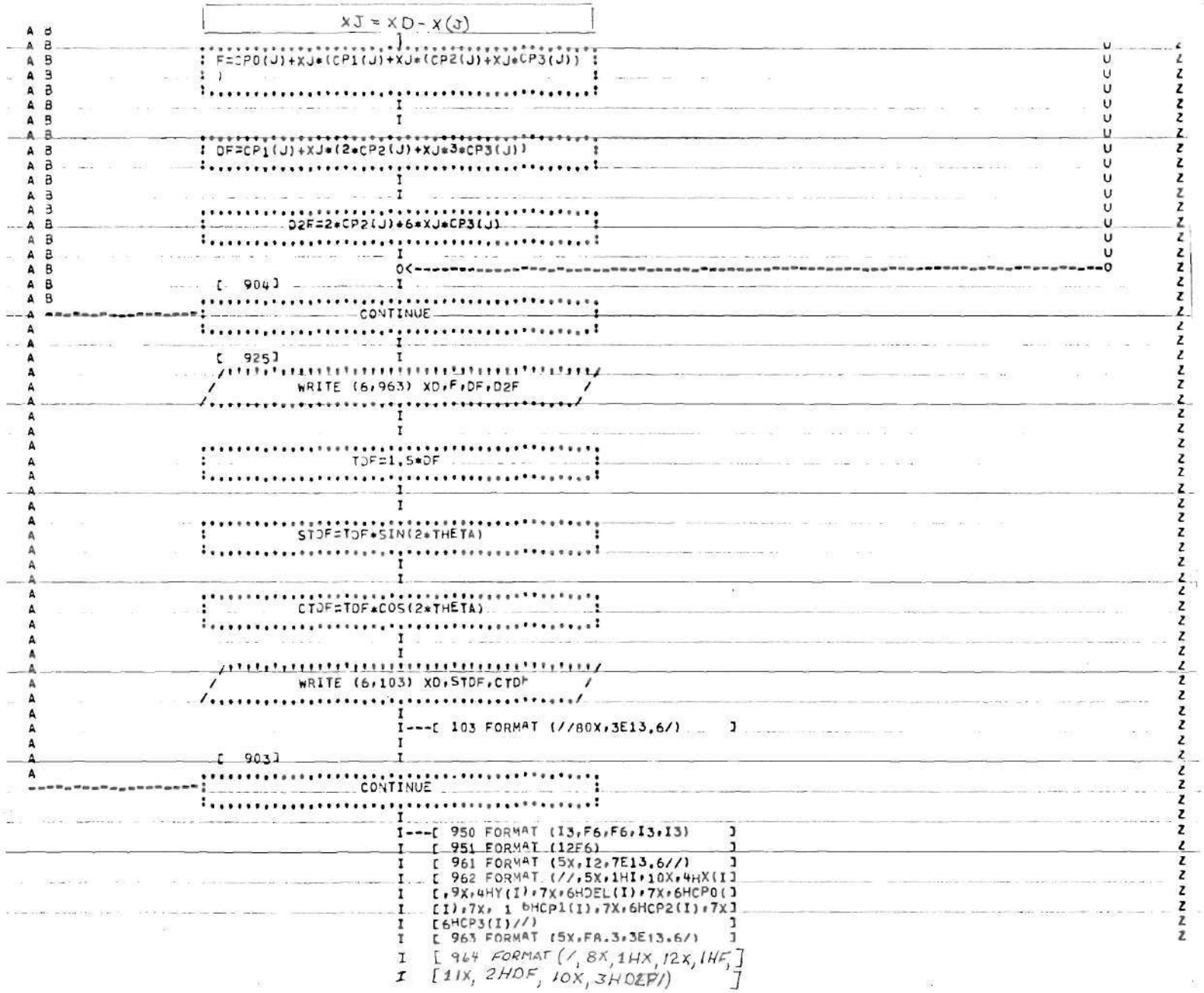
XJ = XD - X(J)
F=CP0(J)+XJ*(CP1(J)+XJ*(CP2(J)+XJ*CP3(J))
DF=CP1(J)+XJ*(2*CP2(J)+XJ*3*CP3(J))
D2F=2*CP2(J)+6*XJ*CP3(J)
[904]
CONTINUE
[925]
WRITE (6,963) XD,F,DF,D2F
TDF=1.5*DF
STDF=TDF*SIN(2*THETA)
CTDF=TDF*COS(2*THETA)
WRITE (6,103) XD,STDF,CTDF
[103 FORMAT (//80X,3E13.6/)
[903]
CONTINUE
[950 FORMAT (I3,F6,F6,I3,I3)
[951 FORMAT (12F6)
[961 FORMAT (5X,I2,7E13.6//)
[962 FORMAT (//,5X,1HI,10X,4HX(I)
[,9X,4HY(I),7X,6HDEL(I),7X,6HCP0(I)
[I),7X, 1 6HCP1(I),7X,6HCP2(I),7X]
[6HCP3(I)//)
[963 FORMAT (5X,F8.3,3E13.6/)
[964 FORMAT (/, 8X, 1HX, 12X, 1HF,
[11X, 2HDF, 10X, 3HD2F/)

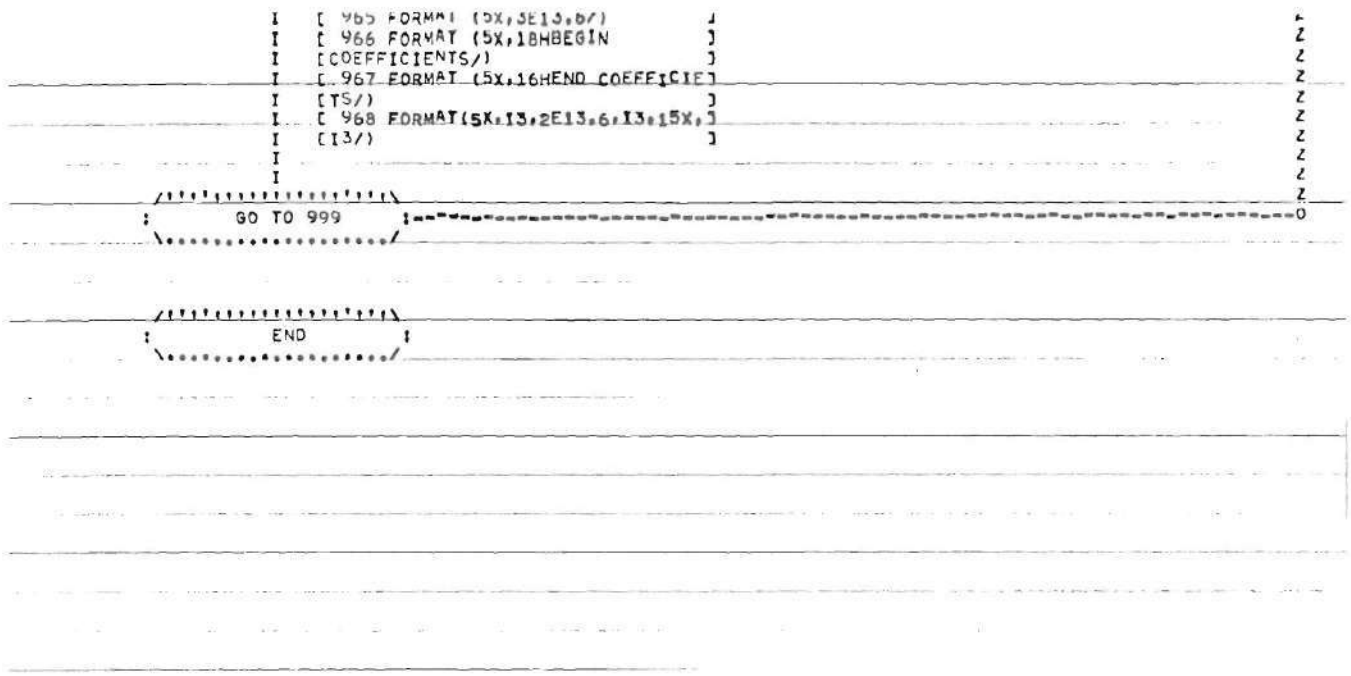
[965 FORMAT (5X,3E13.6/)
[966 FORMAT (5X,18HBEGIN
[COEFFICIENTS/)
[967 FORMAT (5X,16HEND COEFFICIE
[TS/)
[968 FORMAT(5X,I3,2E13.6,I3,15X,
[I3/)
GO TO 999
END

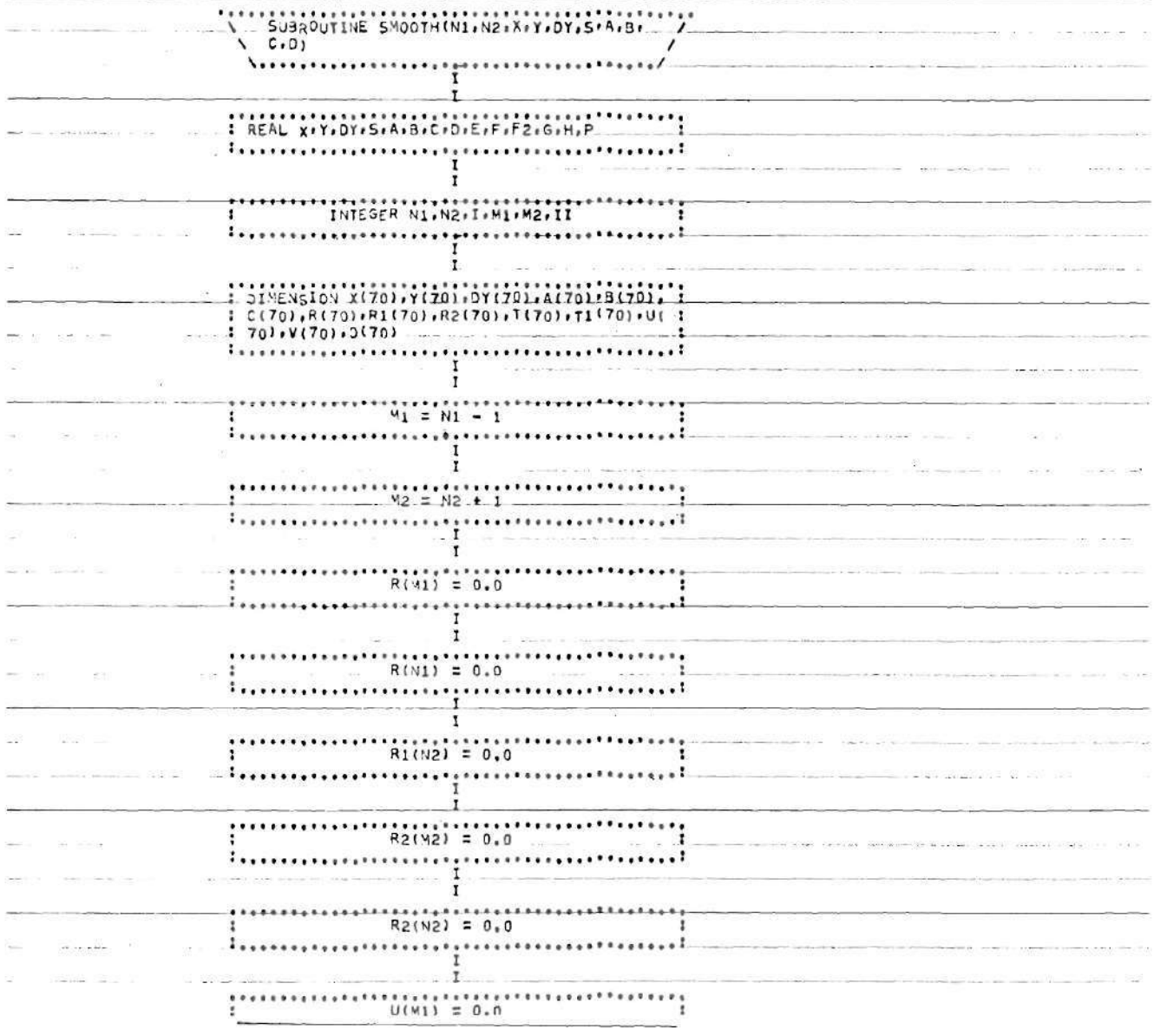
SUBROUTINE SMOOTH(N1,N2,X,Y,DY,S,A,B,
C,D)
REAL X,Y,DY,S,A,B,C,D,E,F,F2,G,H,P
INTEGER N1,N2,I,M1,M2,II
DIMENSION X(70),Y(70),DY(70),A(70),B(70),
C(70),R(70),R1(70),R2(70),T(70),T1(70),U(
70),V(70),D(70)
M1 = N1 - 1
M2 = N2 + 1
R(M1) = 0.0
R(N1) = 0.0
R1(N2) = 0.0
R2(M2) = 0.0
R2(N2) = 0.0
U(M1) = 0.0

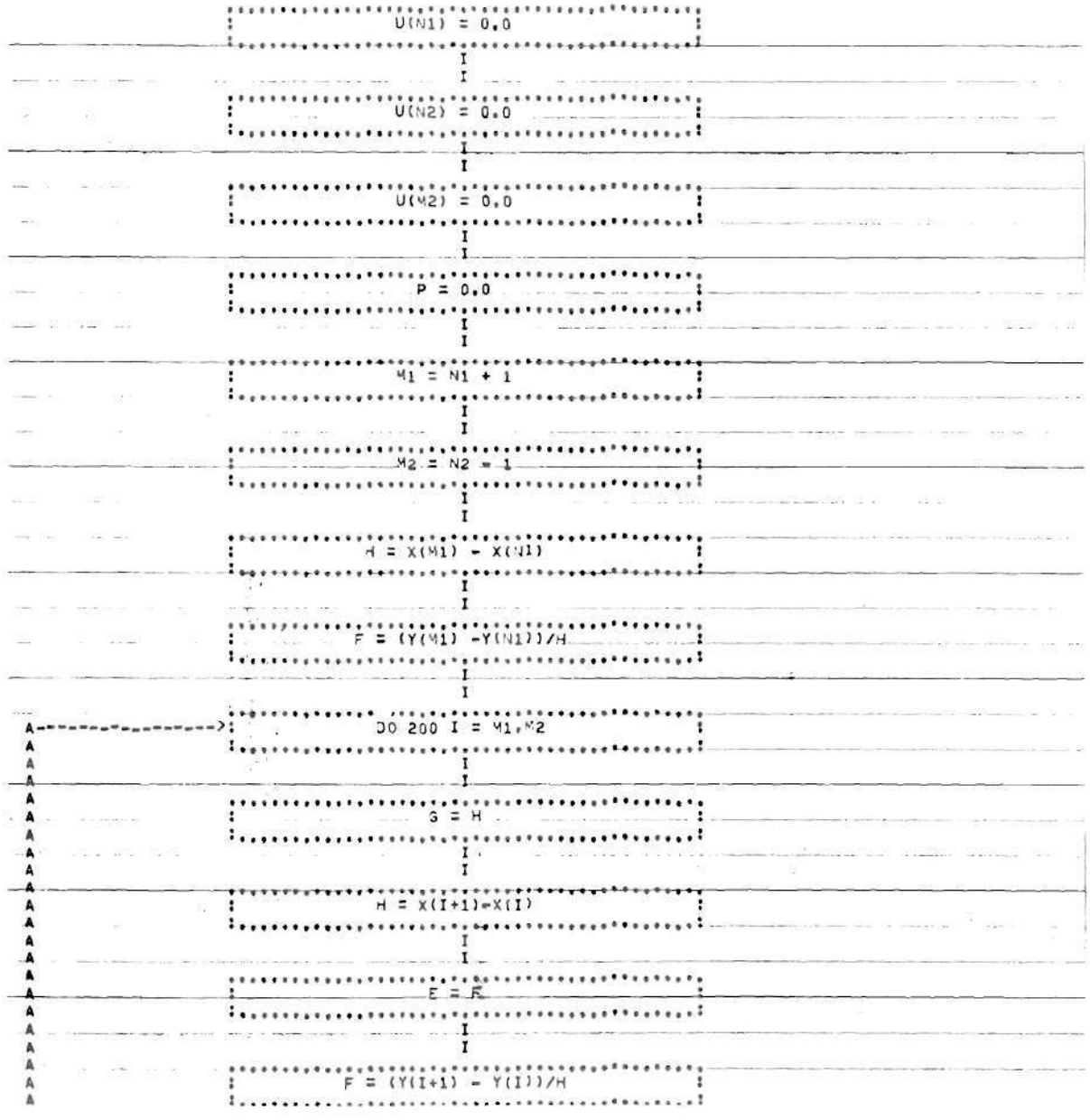
U(N1) = 0.0
U(N2) = 0.0
U(M2) = 0.0
P = 0.0
M1 = N1 + 1
M2 = N2 + 1
H = X(M1) - X(N1)
F = (Y(M1) -Y(N1))/H
DO 200 I = M1,M2
S = H
H = X(I+1)-X(I)
F = F
F = (Y(I+1) - Y(I))/H

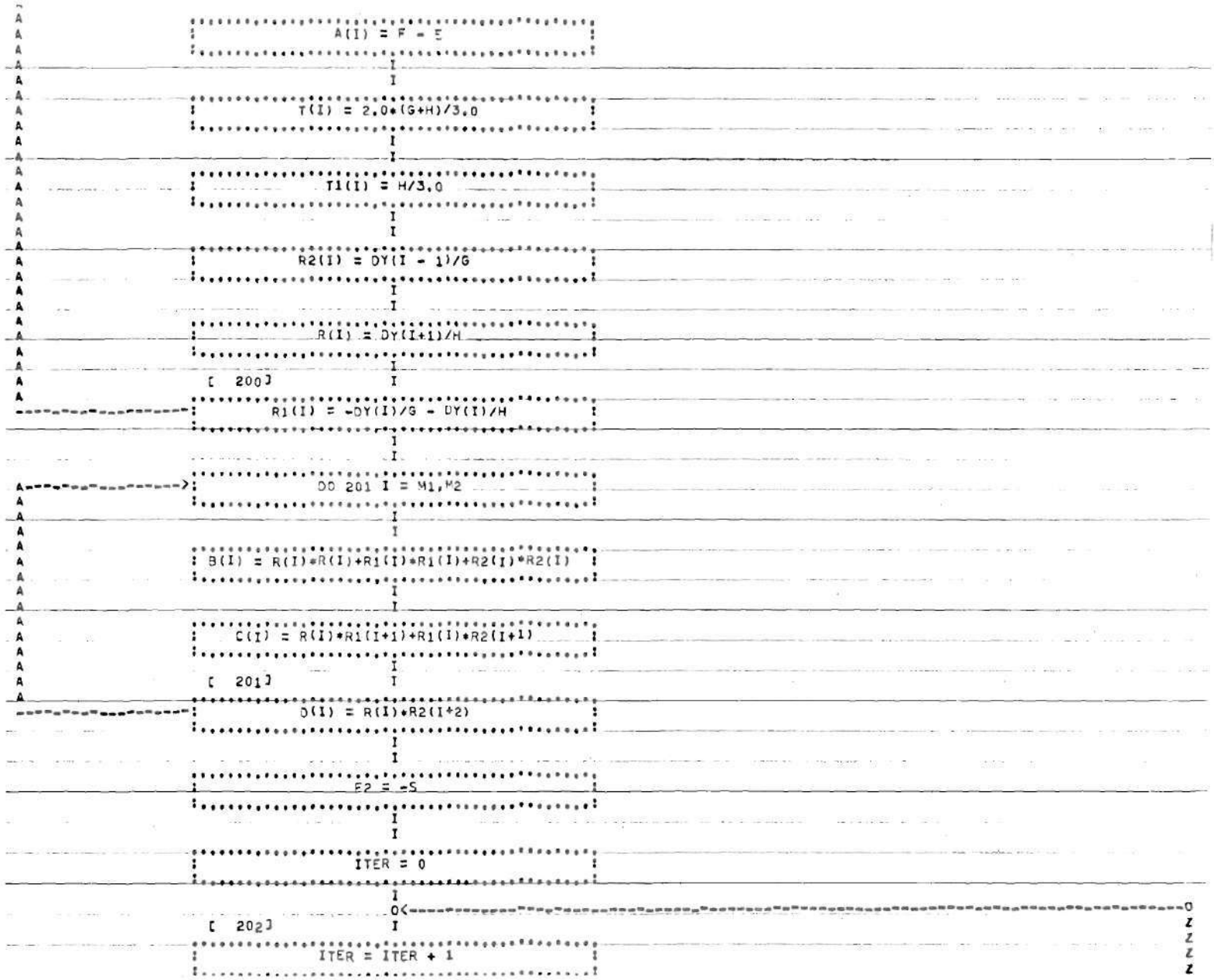
A(I) = F - E
T(I) = 2.0*(G+H)/3.0
T1(I) = H/3.0
R2(I) = DY(I - 1)/G
R(I) = DY(I+1)/H
[200]
R1(I) = -DY(I)/G - DY(I)/H
DO 201 I = M1,M2
B(I) = R(I)*R(I)+R1(I)*R1(I)+R2(I)*R2(I)
C(I) = R(I)*R1(I+1)+R1(I)*R2(I+1)
[201]
D(I) = R(I)*R2(I+2)
F2 = -S
ITER = 0
[202]
ITER = ITER + 1

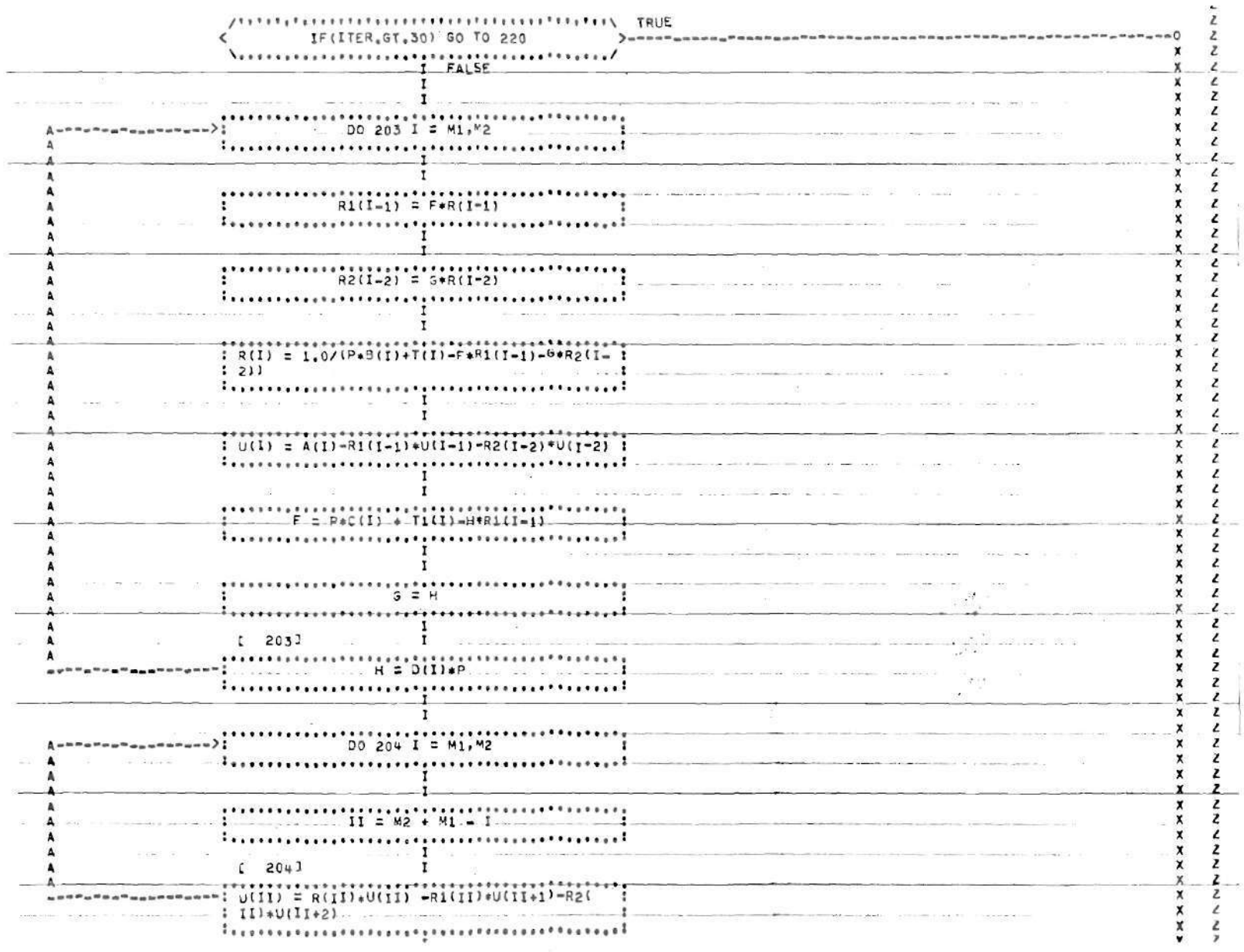
IF(ITER.GT.30) GO TO 220
TRUE
FALSE
DO 203 I = M1,M2
R1(I-1) = F*R(I-1)
R2(I-2) = G*R(I-2)
R(I) = 1.0/(P*B(I)+T(I)-F*R1(I-1)-G*R2(I-2))
U(I) = A(I)-R1(I-1)*U(I-1)-R2(I-2)*U(I-2)
F = P*C(I) + T1(I)-H*R1(I-1)
G = H
[203]
H = D(I)*P
DO 204 I = M1,M2
II = M2 + M1 - I
[204]
U(II) = R(II)*U(II) -R1(II)*U(II+1)-R2(II)*U(II+2)

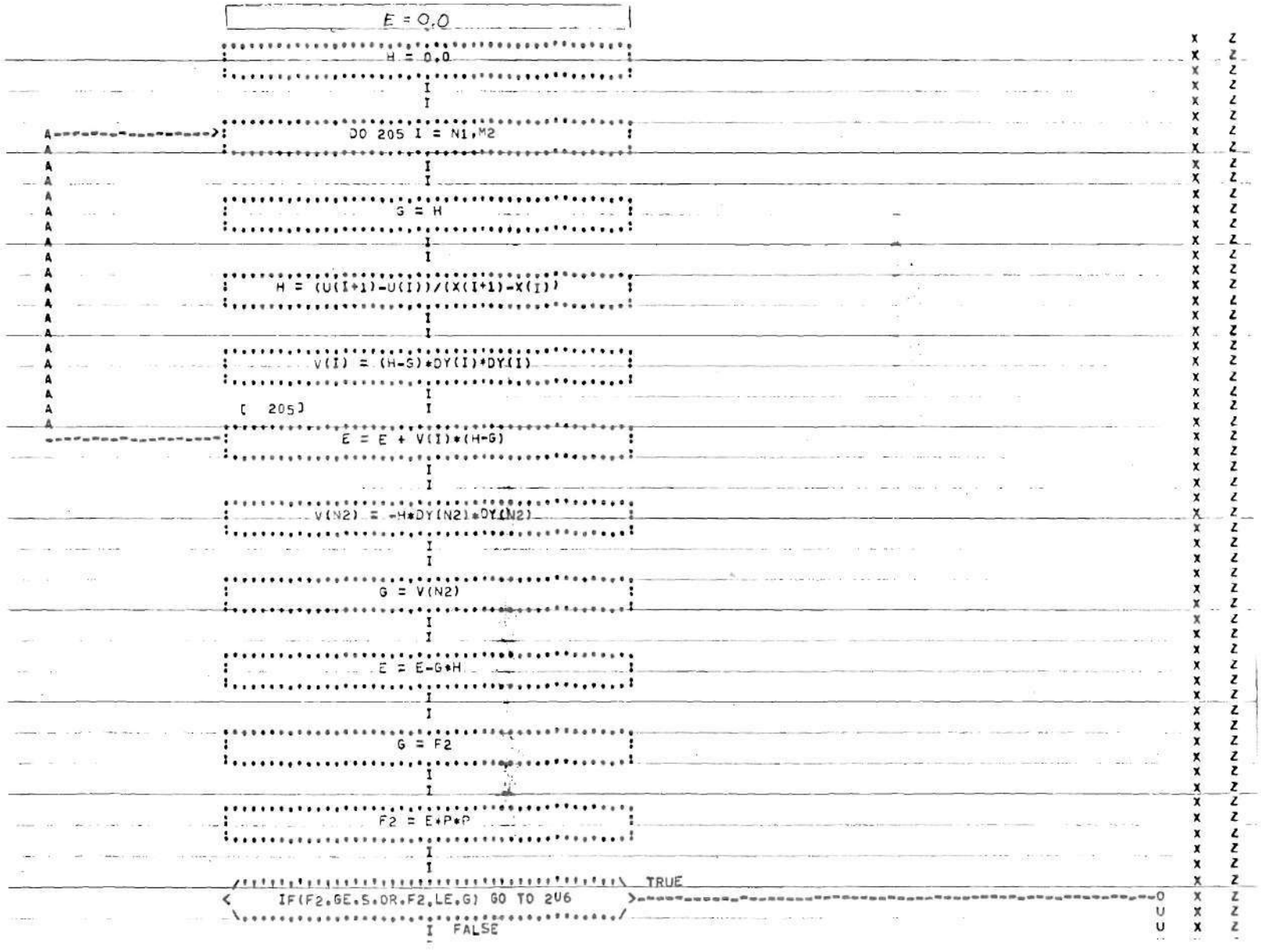
E = 0.0
H = 0.0
DO 205 I = N1,M2
G = H
H = (U(I+1)-U(I))/(X(I+1)-X(I))
V(I) = (H-G)*DY(I)*DY(I)
[205]
E = E + V(I)*(H-G)
V(N2) = -H*DY(N2)*DY(N2)
G = V(N2)
E = E-G*H
G = F2
F2 = E*P*P
IF(F2.GE.S.OR.F2.LE.G) GO TO 206
TRUE
FALSE

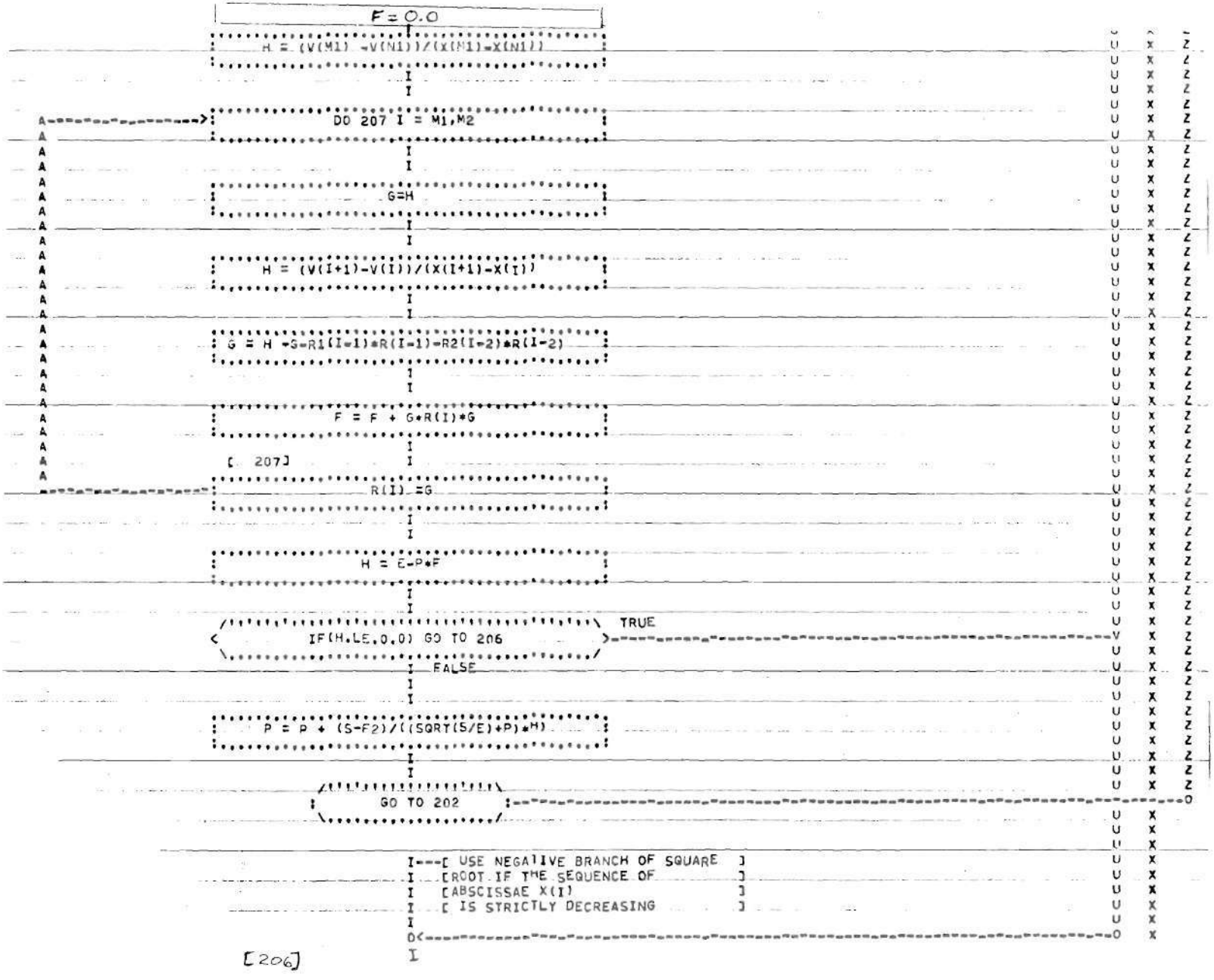
F = 0.0
H = (V(M1) -V(N1))/(X(M1)-X(N1))
DO 207 I = M1,M2
G=H
H = (V(I+1)-V(I))/(X(I+1)-X(I))
G = H -S-R1(I-1)*R(I-1)-R2(I-2)*R(I-2)
F = F + G*R(I)*G
[207]
R(I) =G
H = E-P*F
IF(H.LE.0.0) GO TO 206
TRUE
FALSE
P = P + (S-F2)/((SQRT(S/E)+P)*H)
GO TO 202
[USE NEGATIVE BRANCH OF SQUARE]
[ROOT IF THE SEQUENCE OF]
[ABSCISSAE X(I)]
[IS STRICTLY DECREASING]
[206]

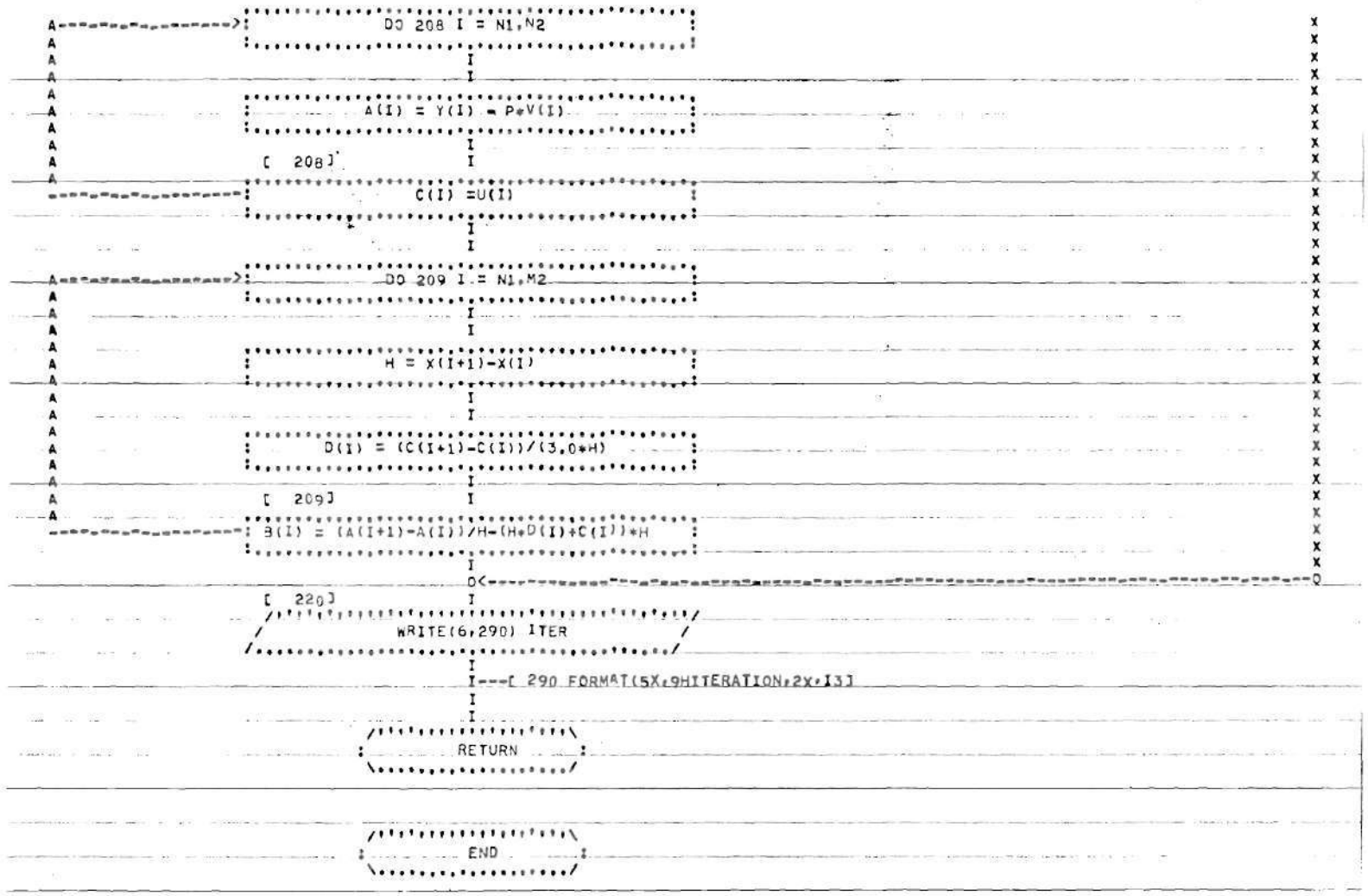
DO 208 I = N1,N2
A(I) = Y(I) + P*V(I)
[208]
C(I) =U(I)
DO 209 I = N1,M2
H = X(I+1)-X(I)
D(I) = (C(I+1)-C(I))/(3.0*H)
[209]
B(I) = (A(I+1)-A(I))/H-(H*D(I)+C(I))*H
[220]
WRITE(6,290) ITER
290 FORMAT(5X,9HITERATION,2X,I3)
RETURN
END

```
HUBAN-J-P*BUBAN.DERIV1
     1            DIMENSION X(70),Y(70),DY(70),CP0(70),CP1(70),CP2(70),C
      P3(70),
     2           1          XLS(10),YLS(10)
     3            PI=3.1416
     4          999 CONTINUE
     5            READ (5,101) THETA
     6          101 FORMAT (F10)
     7            THETA=THETA*PI/180
     8            WRITE (6,501) THETA
     9          501 FORMAT (1X,8HTHETA = ,F4.1)
    10            READ (5,950) N,EPS,S,ND,NLS
    11            RND=ND
    12            WRITE (6,968) N,EPS,S,NLS,ND
    13            NP1=N+1
    14            READ (5,951) (X(I),I=1,NP1)
    15            READ (5,951) (Y(I),I=2,N)
    16            DO 105 I=2,N
    17            Y(I)=Y(I)/360
    18          105 CONTINUE
    19            RN=N
    20            DSD=(X(NP1)-X(1))/(RN-1)
    21            DO 900 I=2,N
    22          900 DY(I)=EPS
    23            CALL SMOOTH(2,N,X,Y,DY,S,CP0,CP1,CP2,CP3)
    24            WRITE (6,962)
    25            DO 350 I=1,NP1
    26          350 WRITE (6,961) I,X(I),Y(I),DY(I),CP0(I),CP1(I),CP2(I),C
      P3(I)
    27            NE=N-2
    28            NB=1
    29            H=(X(NP1)-X(1))/RND
    30            ND1=ND+1
    31            DO 903 I=1,ND1
    32            IM1=I-1
    33            RIM1=IM1
    34            XD=X(1)+H*RIM1
    35          930 NE1=NE+2
    36            DO 904 J=NB,NE1
    37            IF (XD.LT.X(J+1).AND.XD.GT.X(J)) GO TO 905
    38            GO TO 904
    39          905 XJ=XD-X(J)
    40            F=CP0(J)+XJ*(CP1(J)+XJ*(CP2(J)+XJ*CP3(J)))
    41            DF=CP1(J)+XJ*(2*CP2(J)+XJ*3*CP3(J))
    42            D2F=2*CP2(J)+6*XJ*CP3(J)
    43          904 CONTINUE
    44          925 WRITE (6,963) XD,F,DF,D2F
    45            TDF=1.5*DF
    46            STDF=TDF*SIN(2*THETA)
    47            CTDF=TDF*COS(2*THETA)
    48            WRITE (6,103) XD,STDF,CTDF
```

```
 40          103 FORMAT (//80X,3E13.6/)
 50          903 CONTINUE
 51          950 FORMAT (I3,F6,F6,I3,I3)
 52          951 FORMAT (12F6)
 53          961 FORMAT (5X,I2,7E13.6//)
 54          962 FORMAT (//,5X,1HI,10X,4HX(I),9X,4HY(I),7X,6HDEL(I),7X,
   6HCP0(I),7X,
 55             1       6HCP1(I),7X,6HCP2(I),7X,6HCP3(I)//)
 56          963 FORMAT (5X,F8.3,3E13.6/)
 57          964 FORMAT (/,8X,1HX,12X,1HF,11X,2HDF,10X,3HD2F/)
 58          965 FORMAT (5X,3E13.6/)
 59          966 FORMAT (5X,18HBEGIN COEFFICIENTS/)
 60          967 FORMAT (5X,16HEND COEFFICIENTS/)
 61          968 FORMAT(5X,I3,2E13.6,I3,15X,I3/)
 62              GO TO 999
 63              END
END PRT
@PP-RT BUBAN.SMOOTH


BUBAN-J-P*BUBAN.SMOOTH
  1              SUBROUTINE SMOOTH(N1,N2,X,Y,DY,S,A,B,C,D)
  2              REAL X,Y,DY,S,A,B,C,D,E,F,F2,G,H,P
  3              INTEGER N1,N2,I,M1,M2,II
  4              DIMENSION X(70),Y(70),DY(70),A(70),B(70),C(70),R(70),R
   1(70),R2(70)
  5             $,T(70),T1(70),U(70),V(70),D(70)
  6              M1 = N1 - 1
  7              M2 = N2 + 1
  8              R(M1) = 0.0
  9              R(N1) = 0.0
 10              R1(N2) = 0.0
 11              R2(M2) = 0.0
 12              R2(N2) = 0.0
 13              U(M1) = 0.0
 14              U(N1) = 0.0
 15              U(N2) = 0.0
 16              U(M2) = 0.0
 17              P = 0.0
 18              M1 = N1 + 1
 19              M2 = N2 - 1
 20              H = X(M1) - X(N1)
 21              F = (Y(M1) -Y(N1))/H
 22              DO 200 I = M1,M2
 23              G = H
 24              H = X(I+1)-X(I)
 25              E = F
 26              F = (Y(I+1) - Y(I))/H
 27              A(I) = F - E
 28              T(I) = 2.0*(G+H)/3.0
 29              T1(I) = H/3.0
```

```
30            R(I) = D(I - 1)/G
31            R(I) = DY(I+1)/H
32          200 R1(I) = -DY(I)/G - DY(I)/H
33            DO 201 I = M1,M2
34            B(I) = R(I)*R(I)+R1(I)*R1(I)+R2(I)*R2(I)
35            C(I) = R(I)*R1(I+1)+R1(I)*R2(I+1)
36          201 D(I) = R(I)*R2(I+2)
37            F2 = -S
38            ITER = 0
39          202 ITER = ITER + 1
40            IF(ITER.GT.30) GO TO 220
41            DO 203 I = M1,M2
42            R1(I-1) = F*R(I-1)
43            R2(I-2) = G*R(I-2)
44            R(I) = 1.0/(P*B(I)+T(I)-F*R1(I-1)-G*R2(I-2))
45            U(I) = A(I)-R1(I-1)*U(I-1)-R2(I-2)*U(I-2)
46            F = P*C(I) + T1(I)-H*R1(I-1)
47            G = H
48          203 H = D(I)*P
49            DO 204 I = M1,M2
50            II = M2 + M1 - I
51          204 U(II) = R(II)*U(II) -R1(II)*U(II+1)-R2(II)*U(II+2)
52            E = 0.0
53            H = 0.0
54            DO 205 I = N1,M2
55            G = H
56            H = (U(I+1)-U(I))/(X(I+1)-X(I))
57            V(I) = (H-G)*DY(I)*DY(I)
58          205 E = E + V(I)*(H-G)
59            V(N2) = -H*DY(N2)*DY(N2)
60            G = V(N2)
61            E = E-G*H
62            G = F2
63            F2 = E*P*P
64            IF(F2.GE.S.OR.F2.LE.G) GO TO 206
65            F = 0.0
66            H = (V(M1) -V(N1))/(X(M1)-X(N1))
67            DO 207 I = M1,M2
68            G=H
69            H = (V(I+1)-V(I))/(X(I+1)-X(I))
70            G = H -G-R1(I-1)*R(I-1)-R2(I-2)*R(I-2)
71            F = F + G*R(I)*G
72          207 R(I) =G
73            H = E-P*F
74            IF(H.LE.0.0) GO TO 206
75            P = P + (S-F2)/((SQRT(S/E)+P)*H)
76            GO TO 202
77        C USE NEGATIVE BRAMCH OF SQUARE ROOT IF THE SEQUENCE OF ABSC
  ISSAE X(I)
78        C   IS STRICTLY DECREASING
79          206 DO 208 I = N1,N2
```

```
    80            A(I) = Y(I) - P*V(I)
    81        208 C(I) =U(I)
    82            DO 209 I = N1,M2
    83            H = X(I+1)-X(I)
    84            D(I) = (C(I+1)-C(I))/(3.0*H)
    85        209 B(I) = (A(I+1)-A(I))/H-(H*D(I)+C(I))*H
    86        220 WRITE(6,290) ITER
    87        290 FORMAT(5X,9HITERATION,2X,I3)
    88            RETURN
    89            END
END PRT
```

c) Flowchart and Program for the Least Squares Determination for the Total Stress Tensor.

BEGIN
LOGICAL BANC
COMMON AM(256,166)
DIMENSION X(11,7),Z(11,7),TAY(11,7,3),
TYZ(11,7,3),TXZ(11,7)
DIMENSION LM(11,7,3),IN(166),JN(166),LN(
166) ,AV(256), AMS(166), CX(11,7),SY(11,
7),SZ(11,7)
DIMENSION SXX(11,7),SYY(11,7),SZZ(11,7)
DY=.2
P=5.375
U=.49
PI=3.1416
II=0
0
0
3027
READ (5,501) Y,K

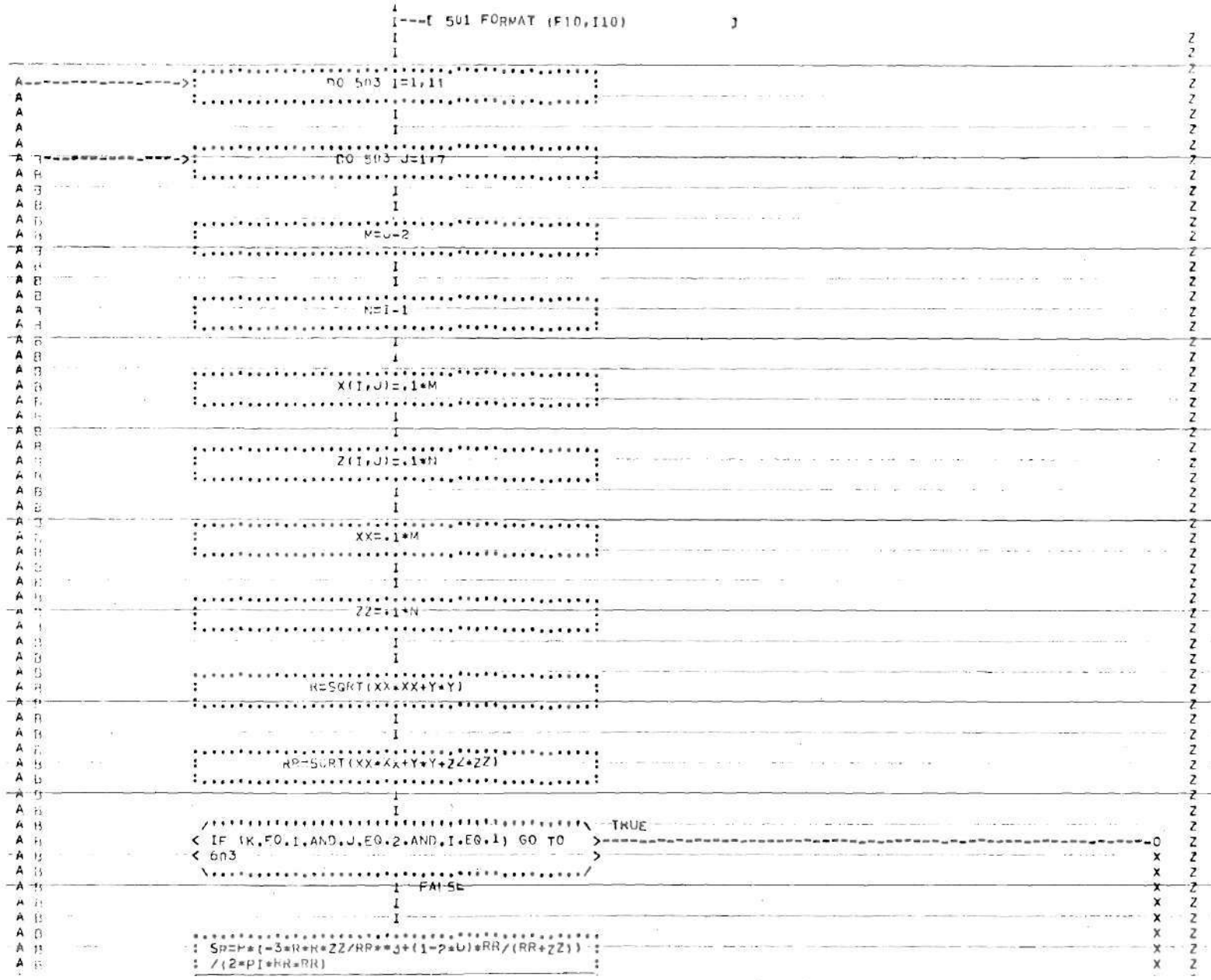
501 FORMAT (F10,I10)
DO 503 I=1,11
DO 503 J=1,7
M=J-2
N=I-1
X(I,J)=.1*M
Z(I,J)=.1*N
XX=.1*M
ZZ=.1*N
R=SQRT(XX*XX+Y*Y)
RR=SQRT(XX*XX+Y*Y+ZZ*ZZ)
IF (K.EQ.1.AND.J.EQ.2.AND.I.EQ.1) GO TO 603
TRUE
FALSE
SR=M*(-3*R*R*ZZ/RR**5+(1-2*U)*RR/(RR+ZZ))
/(2*PI*RR*RR)

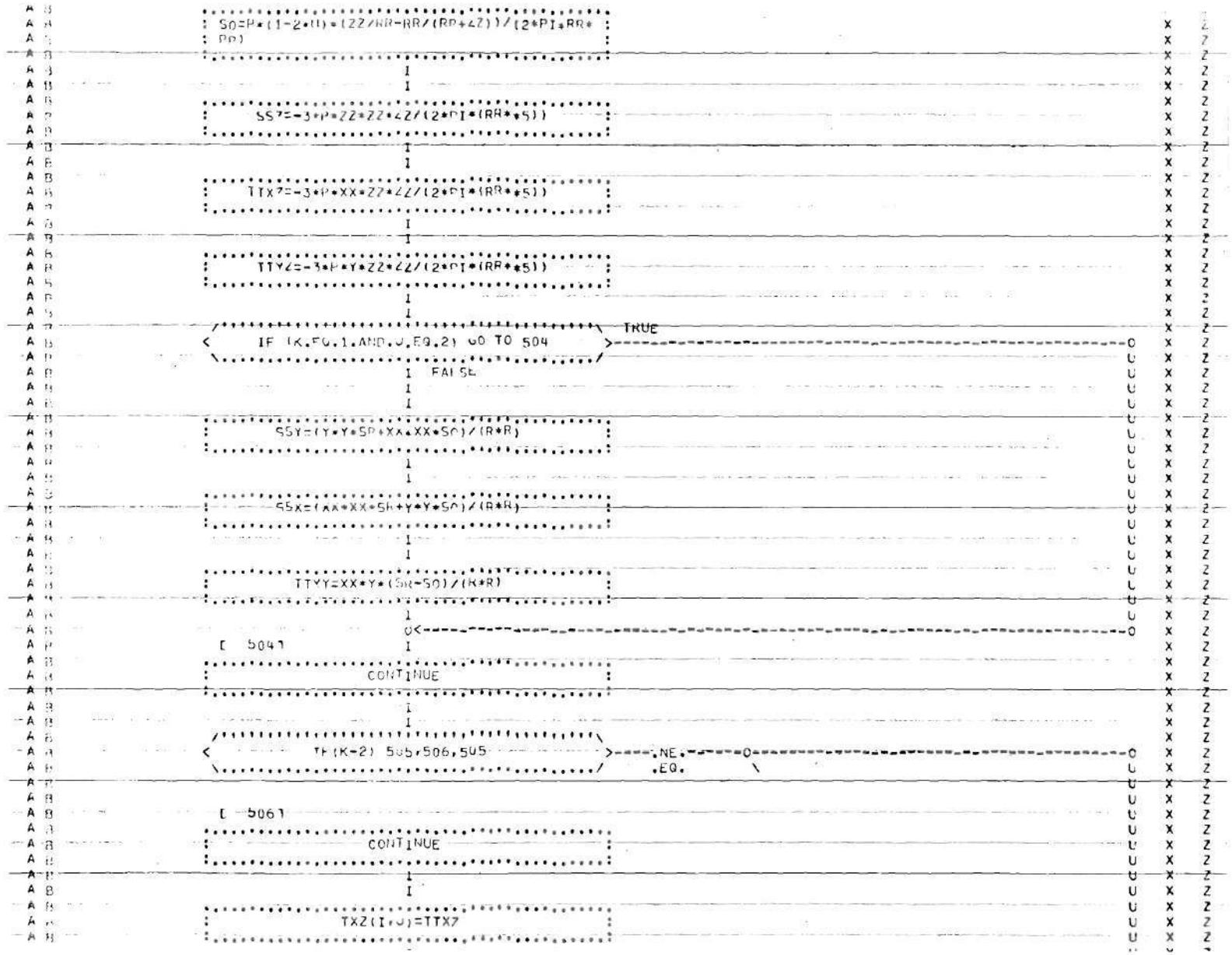
SO=P*(1-2*U)*(ZZ/RR-RR/(RR+ZZ))/(2*PI*RR*
PP)
SSZ=-3*P*ZZ*ZZ*ZZ/(2*PI*(RR**5))
TTX7=-3*P*XX*ZZ*ZZ/(2*PI*(RR**5))
TTY7=-3*P*Y*ZZ*ZZ/(2*PI*(RR**5))
IF (K.EQ.1.AND.J.EQ.2) GO TO 504
TRUE
FALSE
SSY=(Y*Y*SP+XX*XX*SO)/(R*R)
SSX=(XX*XX*SP+Y*Y*SO)/(R*R)
TTYY=XX*Y*(SP-SO)/(R*R)
[5049
CONTINUE
IF(K-2) 505,506,505
.NE.
.EQ.
[5061
CONTINUE
TXZ(I,J)=TTX7

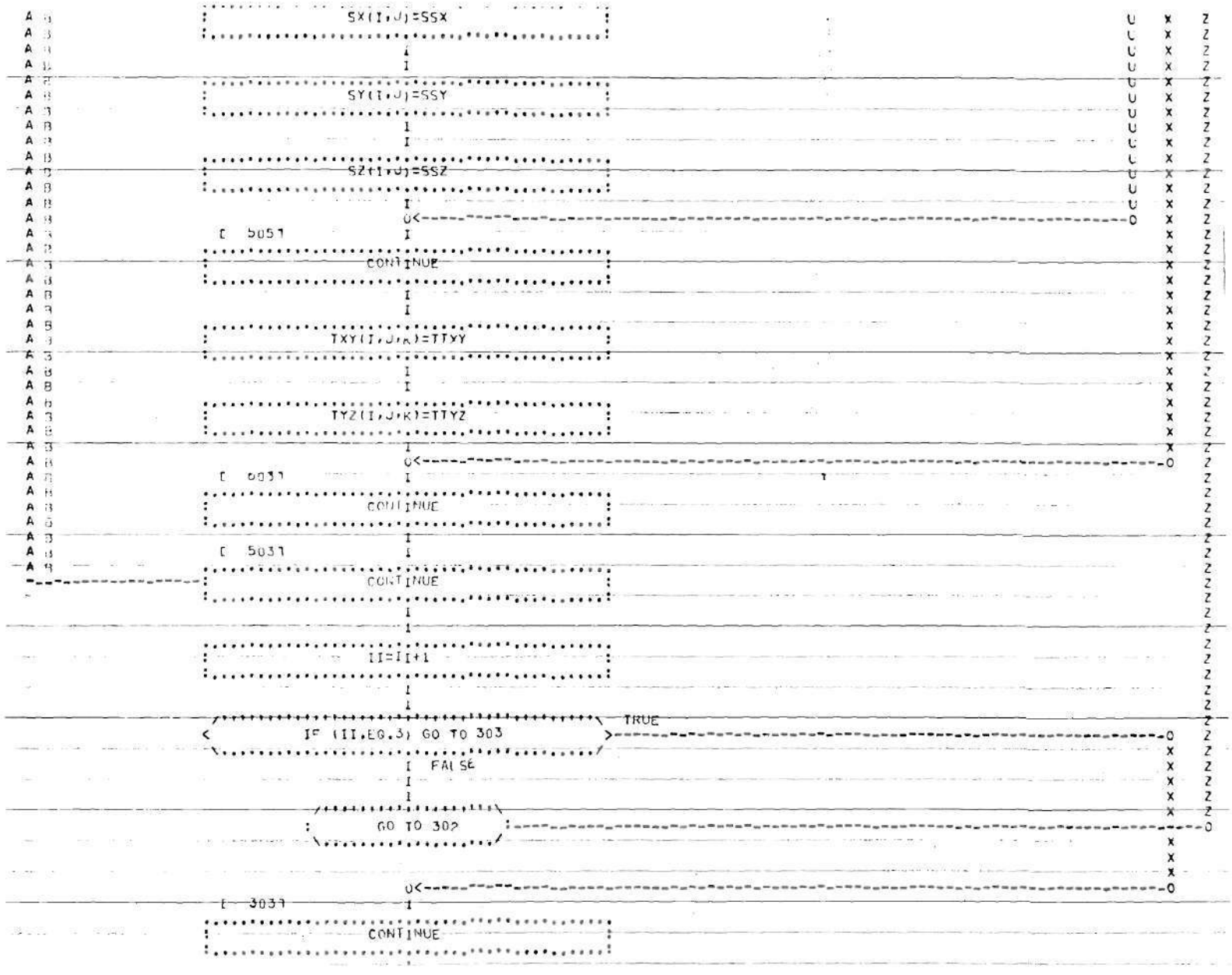
SX(I,J)=SSX
SY(I,J)=SSY
SZ(I,J)=SSZ
TXY(I,J,K)=TTXY
TYZ(I,J,K)=TTYZ
CONTINUE
CONTINUE
CONTINUE
II=I+1
IF (II.EQ.3) GO TO 303
TRUE
FALSE
GO TO 302
CONTINUE
5051
6031
5031
3031

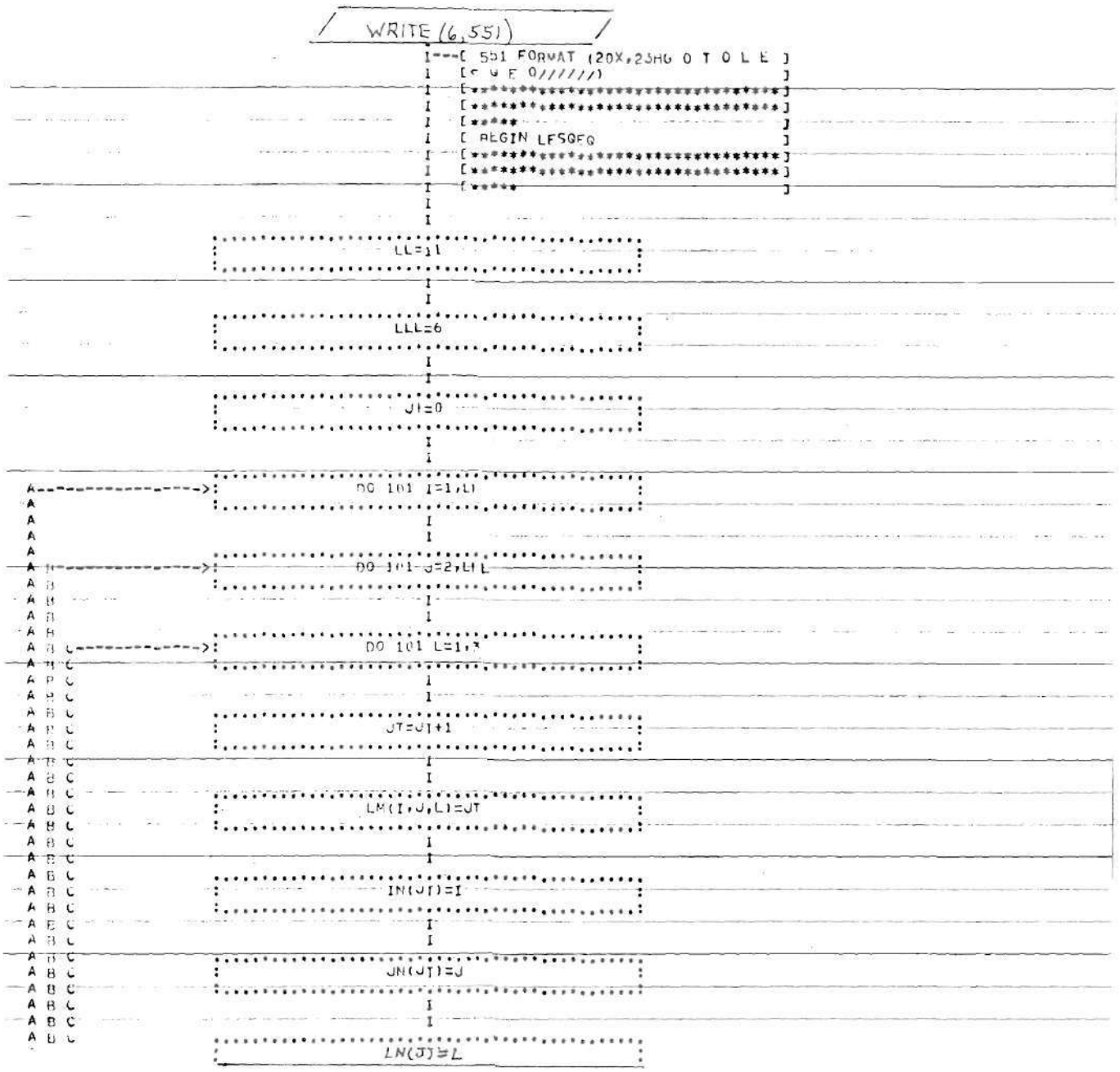
WRITE (6,55)
55 FORMAT (20X,23HG O T O L E
BEGIN LFSQFQ
LL=11
LLL=6
JT=0
DO 101 I=1,LL
DO 101 J=2,LLL
DO 101 L=1,*
JT=JT+1
LM(I,J,L)=JT
IN(JT)=I
JN(JT)=J
LN(JT)=L

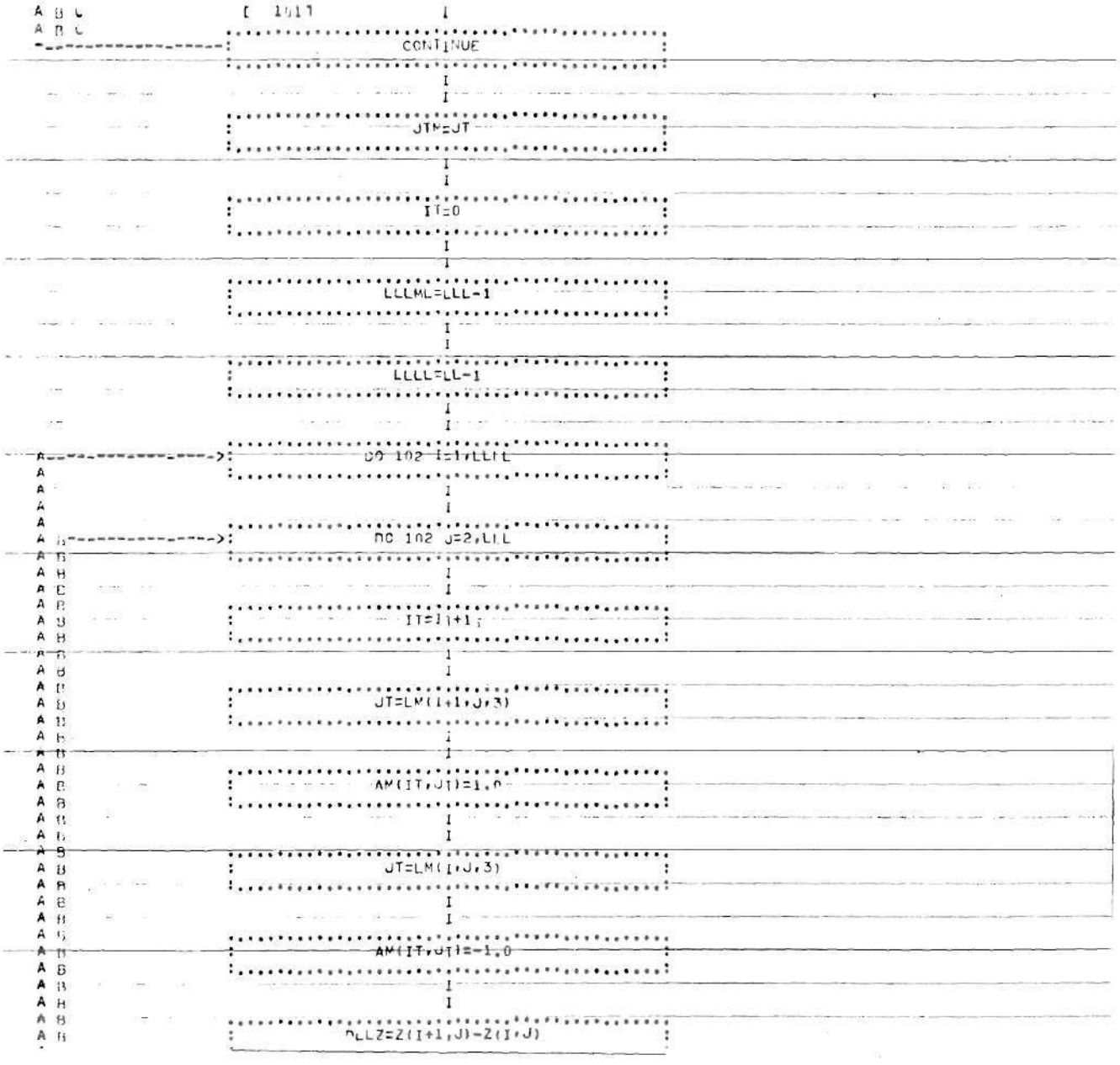
1017
CONTINUE
JTM=JT
IT=0
LLLML=LLL-1
LLLL=LL-1
DO 102 I=1,LLLL
DO 102 J=2,LLL
IT=I+1;
JT=LM(I+1,J,3)
AM(IT,JT)=1.0
JT=LM(I,J,3)
AM(IT,JT)=-1.0
DLLZ=Z(I+1,J)-Z(I,J)

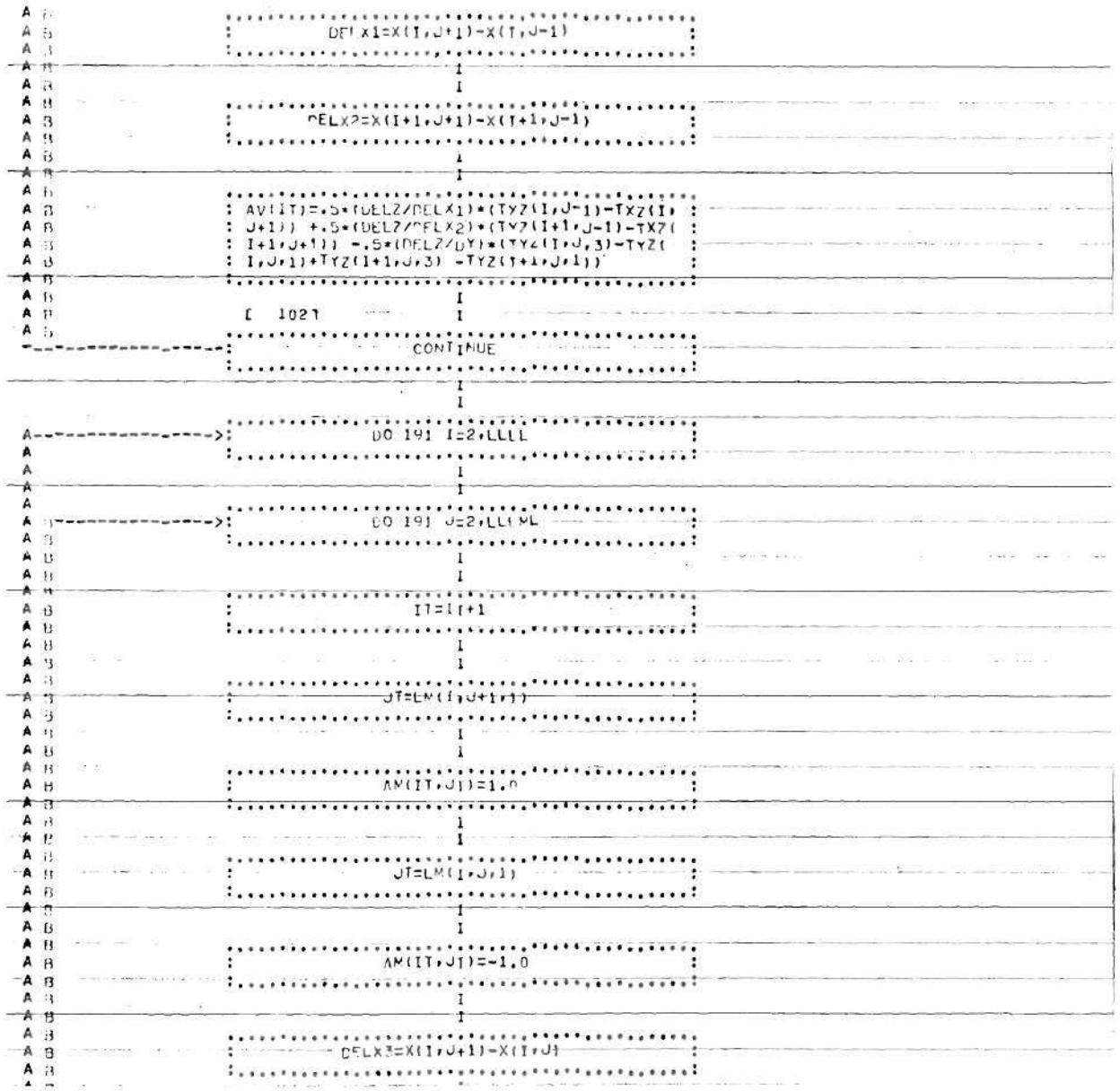
DELX1=X(I,J+1)-X(I,J-1)
DELX2=X(I+1,J+1)-X(I+1,J-1)
AV(IT)=.5*(DELZ/DELX1)*(TYZ(I,J-1)-TXZ(I,
J+1)) +.5*(DELZ/DELX2)*(TYZ(I+1,J-1)-TXZ(
I+1,J+1)) -.5*(DELZ/DY)*(TYZ(I,J,3)-TYZ(
I,J,1)+TYZ(I+1,J,3) -TYZ(I+1,J,1))
1021 CONTINUE
DO 191 I=2,LLLL
DO 191 J=2,LLLML
IT=IT+1
JT=LM(I,J+1,1)
AM(IT,JT)=1.0
JT=LM(I,J,1)
AM(IT,JT)=-1.0
DELX3=X(I,J+1)-X(I,J)

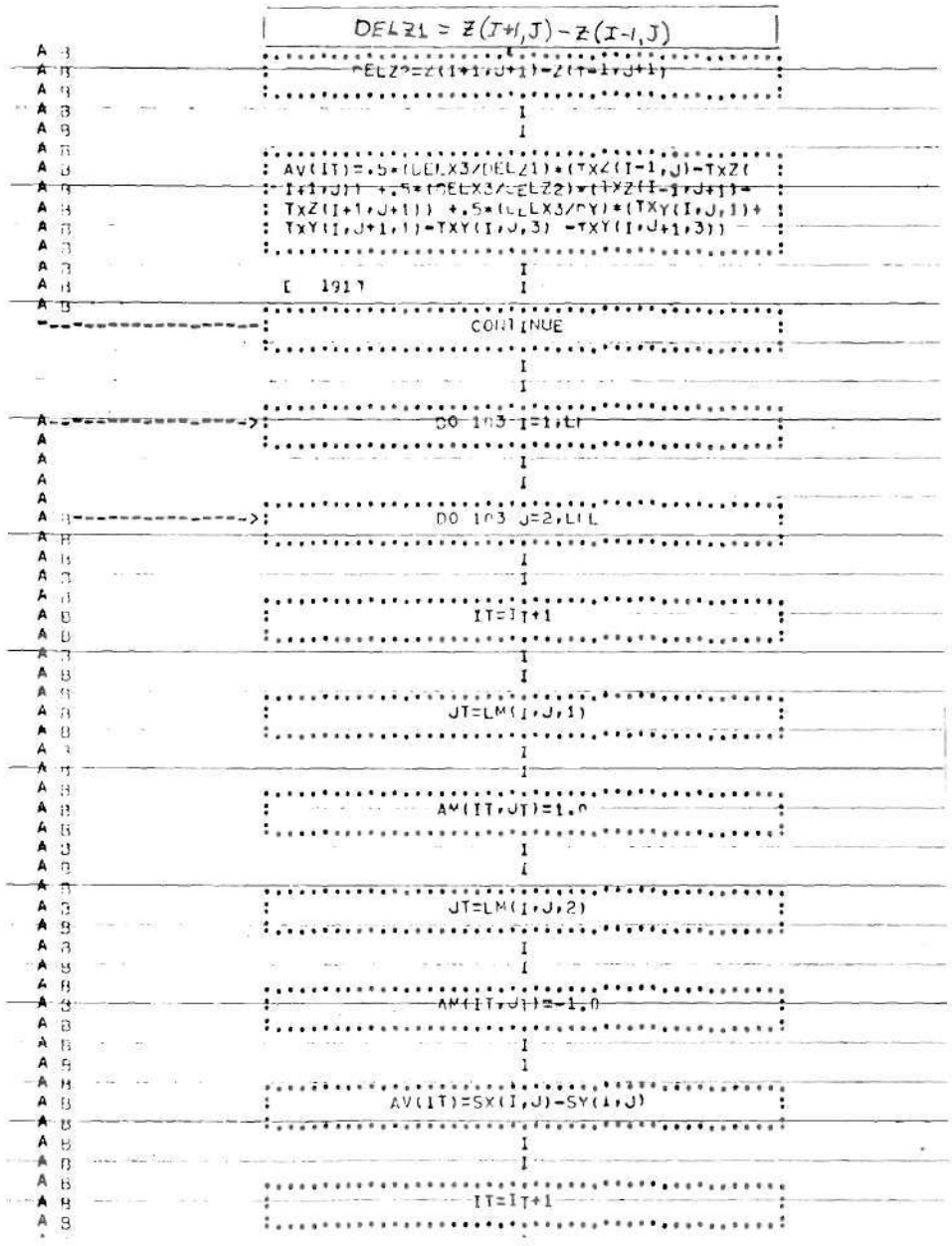
DELZ1 = Z(I+1,J) - Z(I-1,J)
DELZ2=Z(I+1,J+1)-Z(I-1,J+1)
AV(IT)=.5*(DELX3/DELZ1)*(TXZ(I-1,J)-TXZ(
I+1,J)) +.5*(DELX3/DELZ2)*(TXZ(I-1,J+1)-
TXZ(I+1,J+1)) +.5*(DELX3/DY)*(TXY(I,J,1)+
TXY(I,J+1,1)-TXY(I,J,3) -TXY(I,J+1,3))
[1917
CONTINUE
DO 103 I=1,LI
DO 103 J=2,LIL
IT=IT+1
JT=LM(I,J,1)
AM(IT,JT)=1.0
JT=LM(I,J,2)
AM(IT,JT)=-1.0
AV(IT)=SX(I,J)-SY(I,J)
IT=IT+1

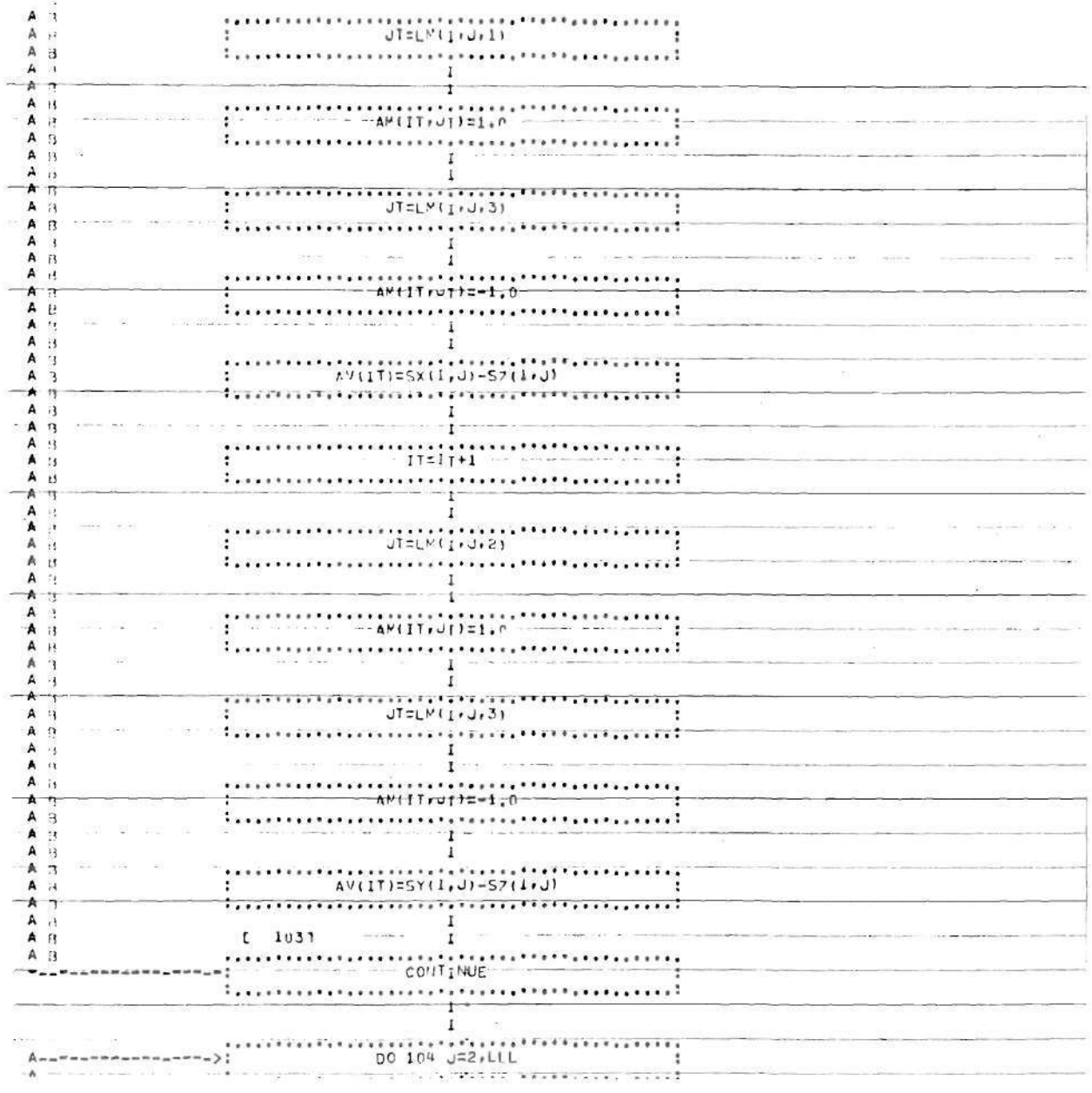
JT=LM(I,J,1)
AM(IT,JT)=1.0
JT=LM(I,J,3)
AM(IT,JT)=-1.0
AV(IT)=SX(I,J)-S7(I,J)
IT=IT+1
JT=LM(I,J,2)
AM(IT,JT)=1.0
JT=LM(I,J,3)
AM(IT,JT)=-1.0
AV(IT)=SY(I,J)-S7(I,J)
[1031
CONTINUE
DO 104 J=2,LLL

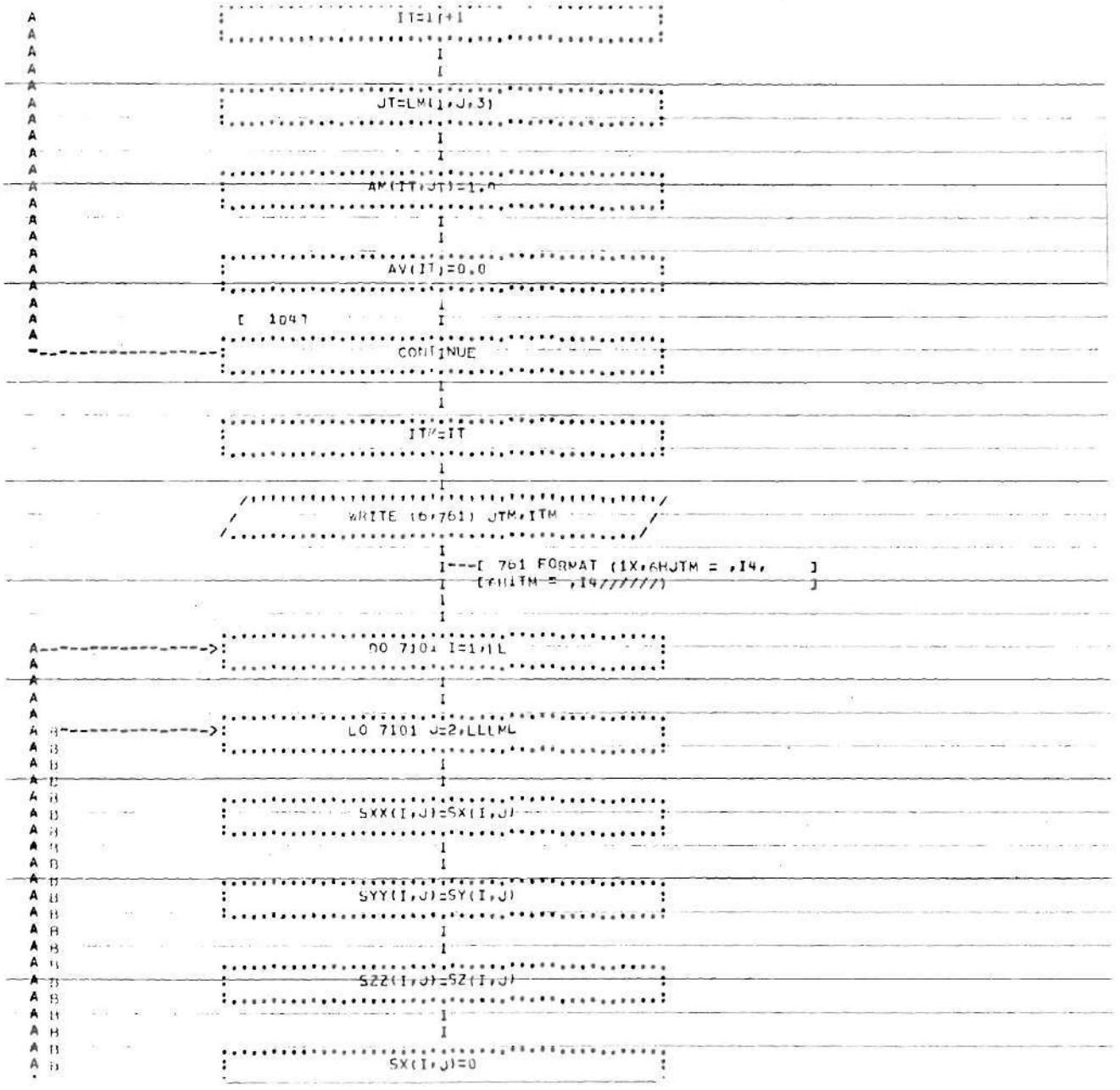
IT=1(+1
JT=LM(1,J,3)
AM(IT,JT)=1.0
AV(IT)=0.0
[1047
CONTINUE
ITM=IT
WRITE (6,761) JTM,ITM
[761 FORMAT (1X,6HJTM = ,I4,
ITM = ,I4///////)
DO 7101 I=1,IL
DO 7101 J=2,LLLML
SXX(I,J)=SX(I,J)
SYY(I,J)=SY(I,J)
SZZ(I,J)=SZ(I,J)
SX(I,J)=0

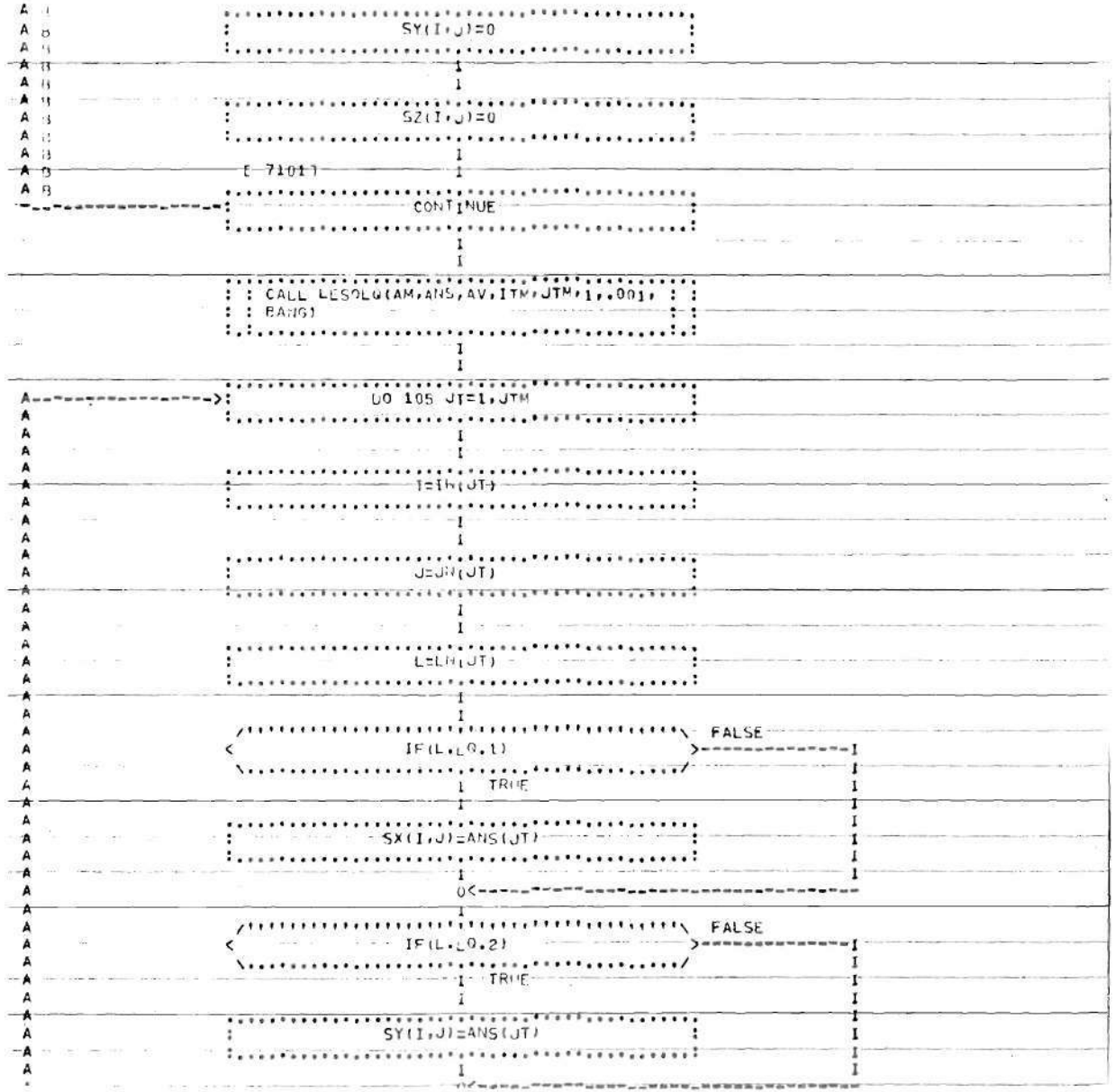
SY(I,J)=0
SZ(I,J)=0
[7101]
CONTINUE
CALL LESOLG(AM,ANS,AV,ITM,JTM,1,.001, BAND)
DO 105 JT=1,JTM
I=IH(JT)
J=JN(JT)
L=LH(JT)
IF(L.LQ.1)
FALSE
TRUE
SX(I,J)=ANS(JT)
IF(L.LQ.2)
FALSE
TRUE
SY(I,J)=ANS(JT)

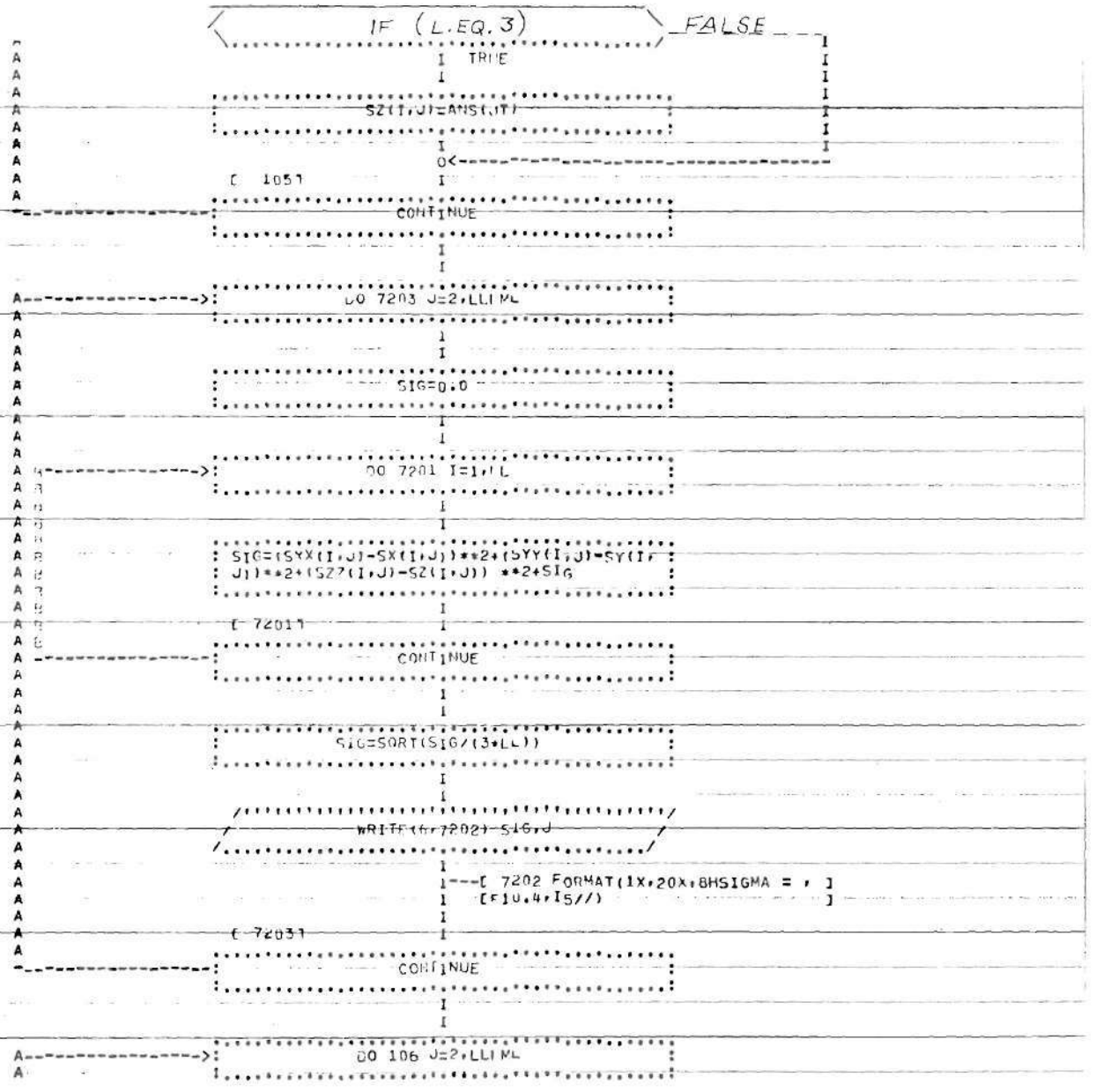
IF (L.EQ.3)
FALSE
TRUE
SZ(I,J)=ANS(JT)
[1051
CONTINUE
DO 7203 J=2,LLIML
SIG=0.0
DO 7201 I=1,IL
SIG=(SYX(I,J)-SX(I,J))**2+(SYY(I,J)-SY(I,
J))**2+(SZ?(I,J)-SZ(I,J)) **2+SIG
[72011
CONTINUE
SIG=SQRT(SIG/(3*LL))
WRITE(6,7202) SIG,J
[7202 FORMAT(1X,20X,8HSIGMA = ,]
[F10.4,I5//)]
[72031
CONTINUE
DO 106 J=2,LLIML

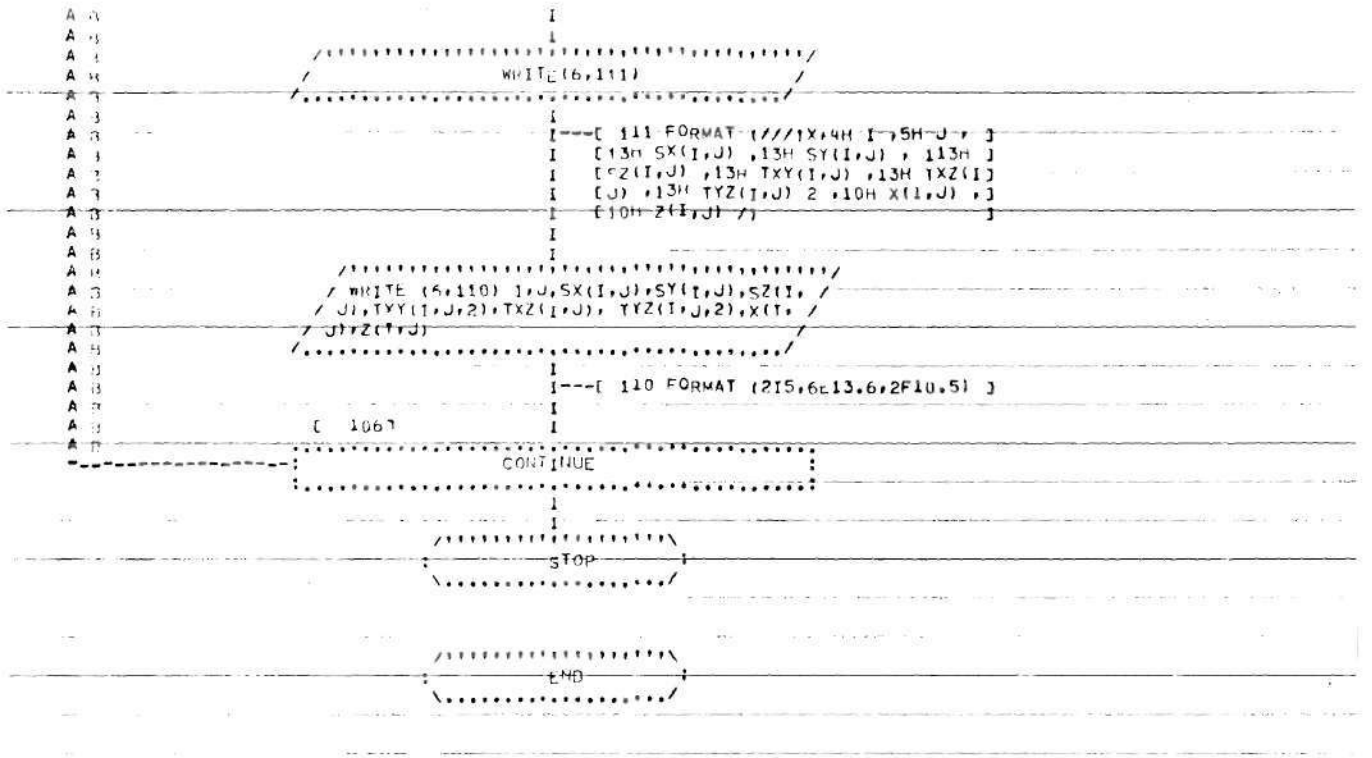
WRITE(6,111)
111 FORMAT (///1X,4H I ,5H J ,
13H SX(I,J) ,13H SY(I,J) , 13H
SZ(I,J) ,13H TXY(I,J) ,13H TXZ(I
J) ,13H TYZ(I,J) 2 ,10H X(I,J) ,
10H Z(I,J) /)
WRITE (6,110) I,J,SX(I,J),SY(I,J),SZ(I,
J),TXY(I,J,2),TXZ(I,J), TYZ(I,J,2),X(I,
J),Z(I,J)
110 FORMAT (2I5,6E13.6,2F10.5)
106
CONTINUE
STOP
END

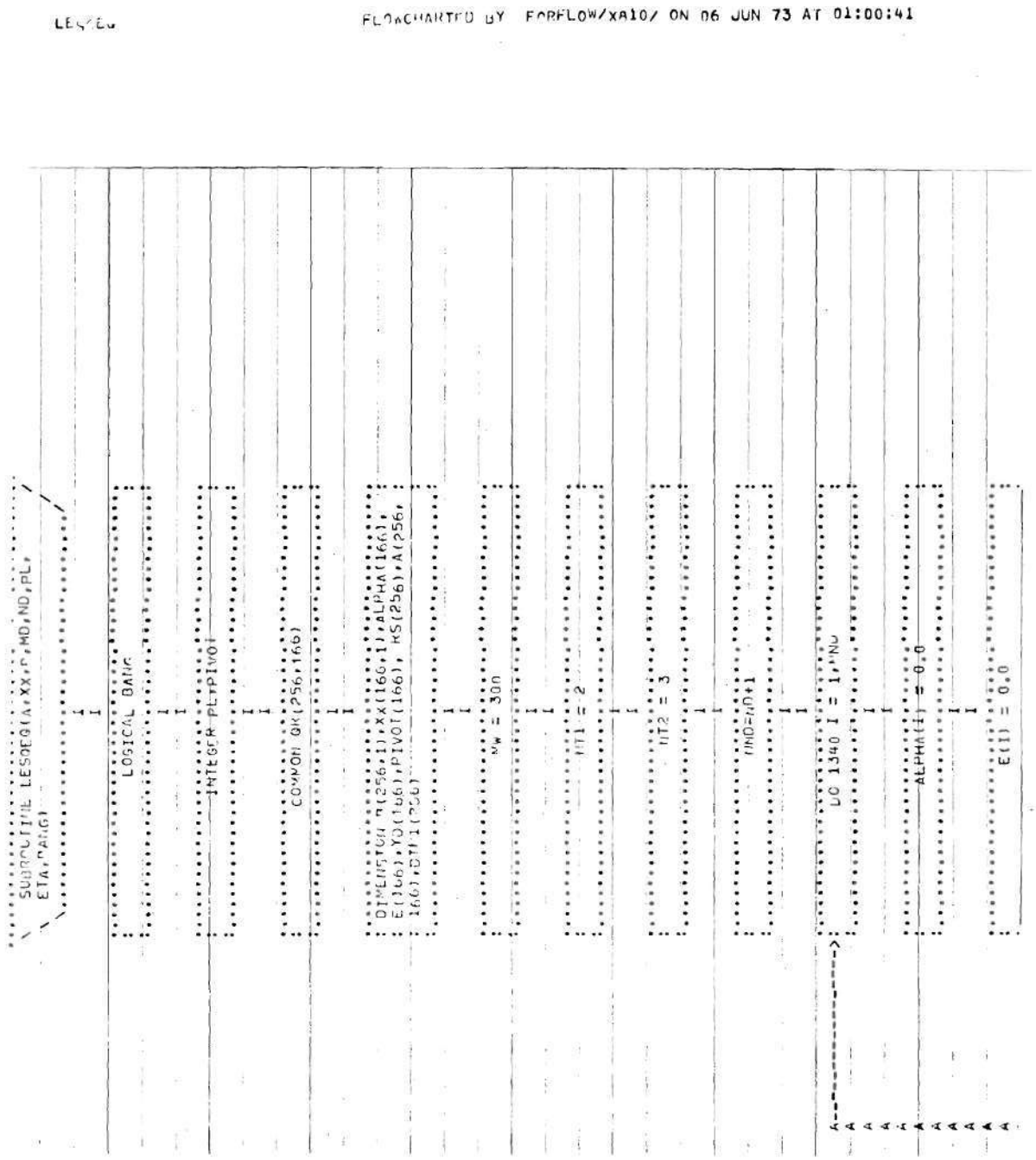
FLOWCHARTED BY FORFLOW/XA10/ ON 06 JUN 73 AT 01:00:41
SUBROUTINE LESOEQN(A,XX,P,MD,ND,PL,
ETA,RANG)
LOGICAL BANK
INTEGER PIVOT
COMMON QK(256,166)
DIMENSION P(256,1),XX(166,1),ALPHA(166),
E(166),YO(166),PIVOT(166),WS(256),A(256,
166),DT1(256)
MW = 300
IT1 = 2
IT2 = 3
IND=ND+1
DO 1340 I = 1,IND
ALPHA(I) = 0.0
E(I) = 0.0


YD(I) = 0.0
[13401
PIVOT(I) = 0
DO 13541 I = 1,MD
RS(I) = 0.0
[13541
DIFF(I) = 0.0
WRITE(2) ((A(I,J),J=1,MD),I=1,MD)
WRITE(6,1504) MD,ND
RL.IND ?
CALL DECOMP(MD,ND,GR,ALPHA,PIVOT,
BANG)
IF(MD.LE.MW) GO TO 13541
TRUE
FALSE
WRITE(6,1504) (PIVOT(J),J = 1,ND)
WRITE(6,1503) ((GR(I,J),J = 1,ND), I =
1,MD)

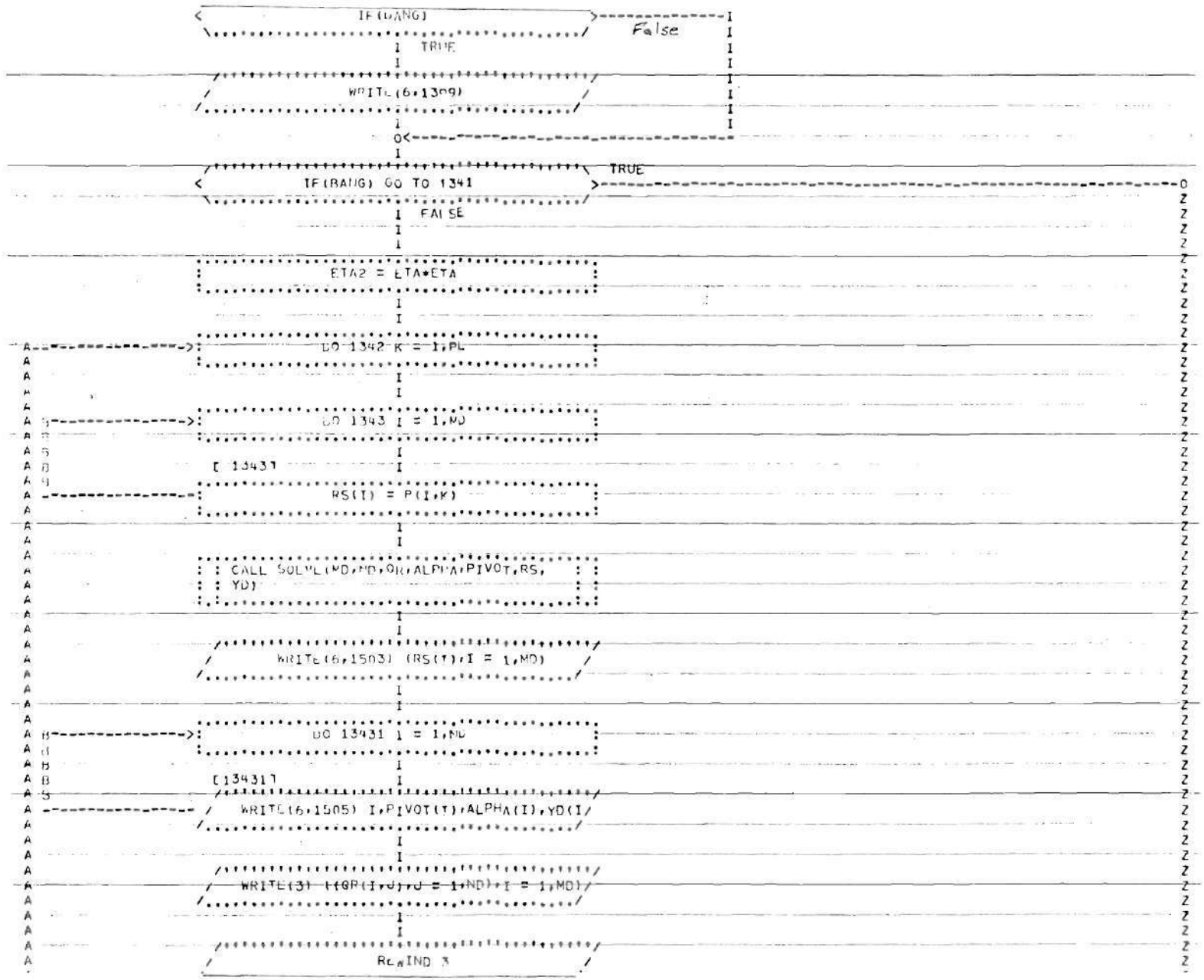
IF(DANG)
False
TRUE
WRITE(6,1309)
IF(BANG) GO TO 1341
TRUE
FALSE
ETA2 = ETA*ETA
DO 1342 K = 1,PL
DO 1343 I = 1,MD
[13437
RS(I) = P(I,K)
CALL SOLVE(MD,MD,QR,ALPHA,PIVOT,RS,
YD)
WRITE(6,1503) (RS(I),I = 1,MD)
DO 13431 I = 1,MD
[134317
WRITE(6,1505) I,PIVOT(I),ALPHA(I),YD(I)
WRITE(3) ((QR(I,J),J = 1,MD),I = 1,MD)
RETURN 3

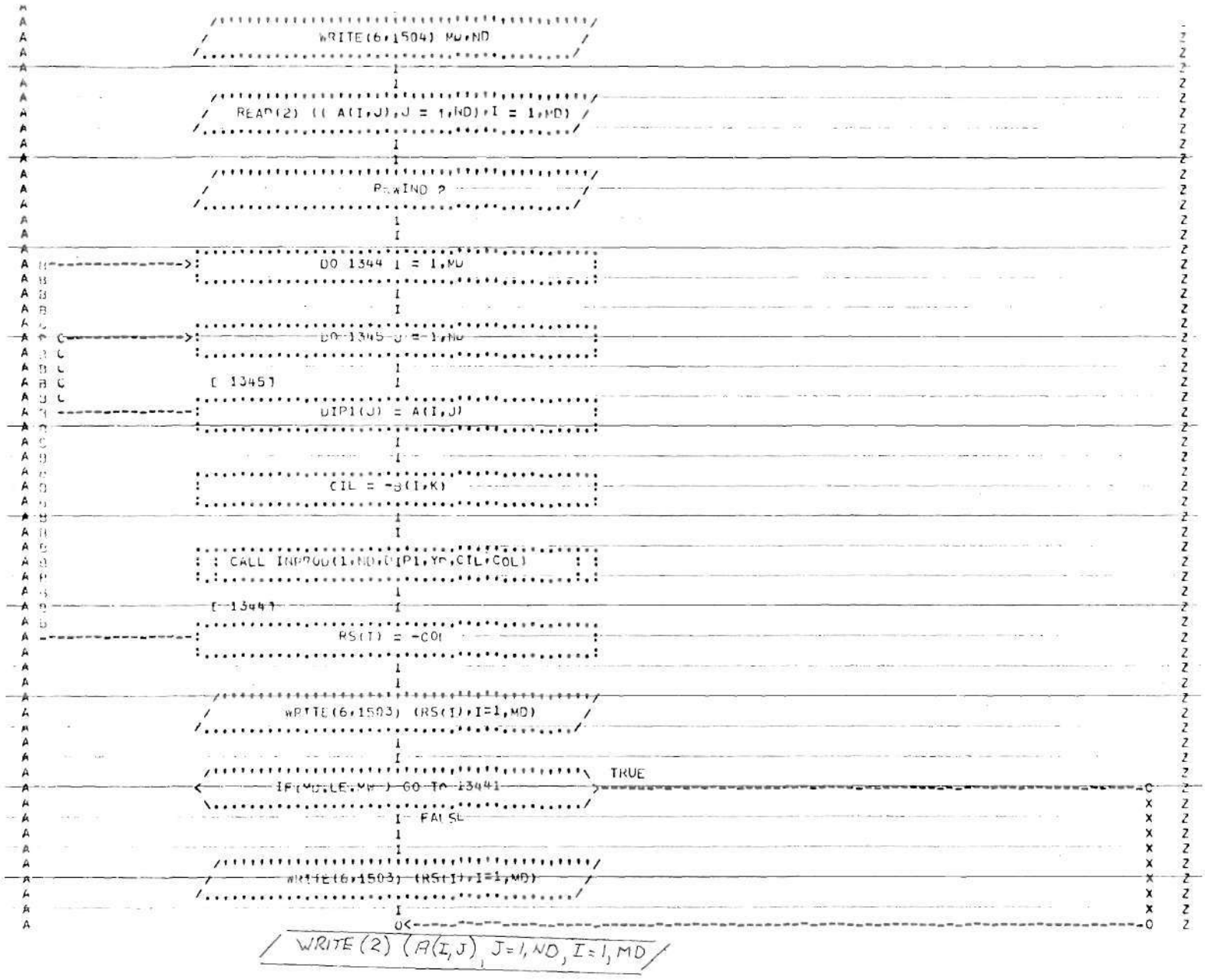
WRITE(6,1504) MD,ND
READ(2) ((A(I,J),J = 1,ND),I = 1,MD)
ROWIND ?
DO 1344 I = 1,MD
DO 1345 J = 1,ND
[1345]
DIP1(J) = A(I,J)
CIL = -B(I,K)
CALL INPROD(1,ND,DIP1,YP,CIL,COL)
[1344]
RS(I) = -COL
WRITE(6,1503) (RS(I),I=1,MD)
IF(MD.LE.MW) GO TO 1344
TRUE
FALSE
WRITE(6,1503) (RS(I),I=1,MD)
WRITE (2) (A(I,J), J=1,ND, I=1,MD)

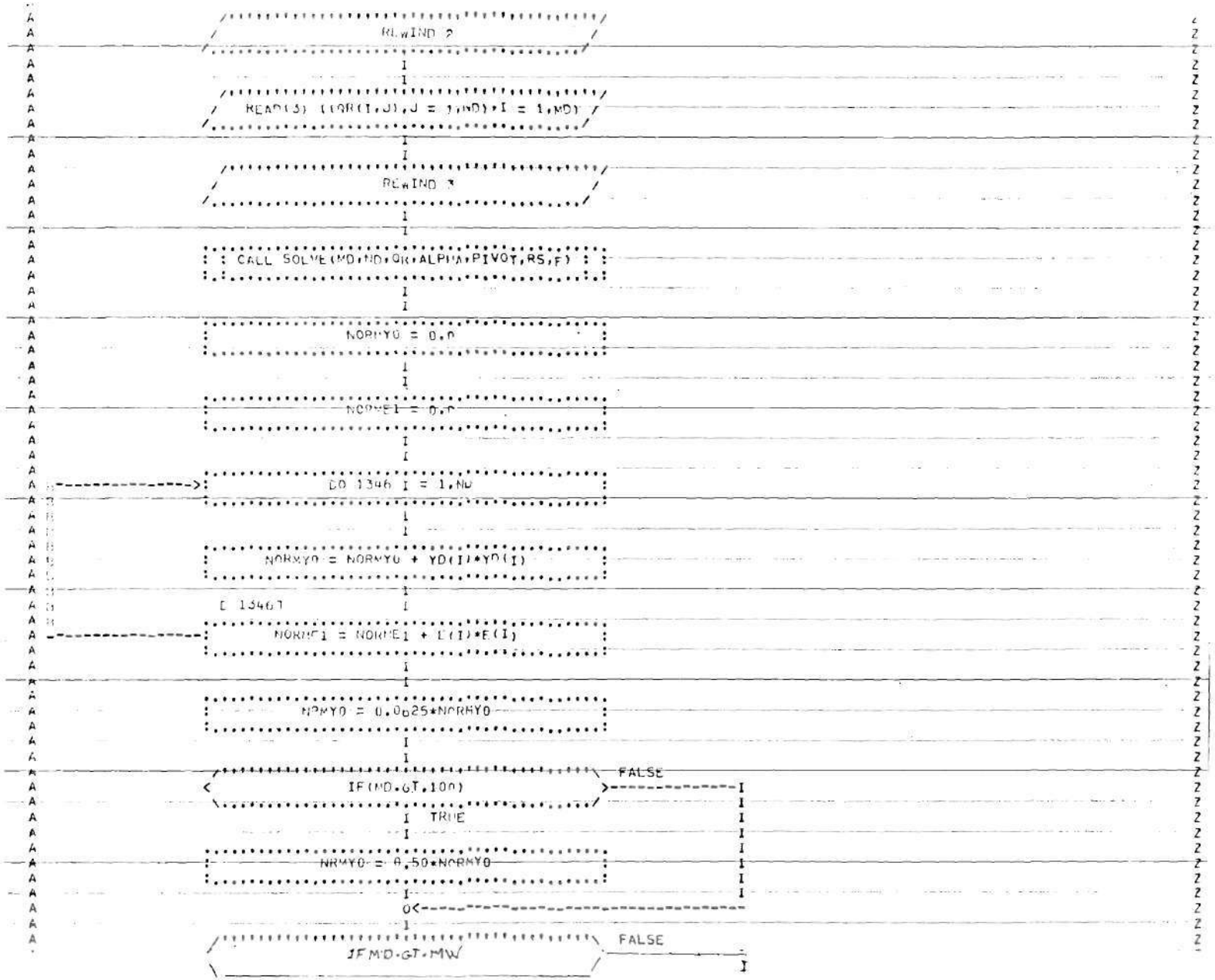
REWIND 2
READ(3) ((QR(I,J),J = 1,ND),I = 1,MD)
REWIND 3
CALL SOLVE(MD,ND,QR,ALPHA,PIVOT,RS,F)
NORMY0 = 0.0
NORME1 = 0.0
DO 1346 I = 1,ND
NORMY0 = NORMY0 + YD(I)*YD(I)
1346
NORME1 = NORME1 + E(I)*E(I)
NORMY0 = 0.0625*NORMY0
IF(MD.GT.100)
FALSE
TRUE
NRMY0 = 0.50*NORMY0
IF MD.GT.MW
FALSE

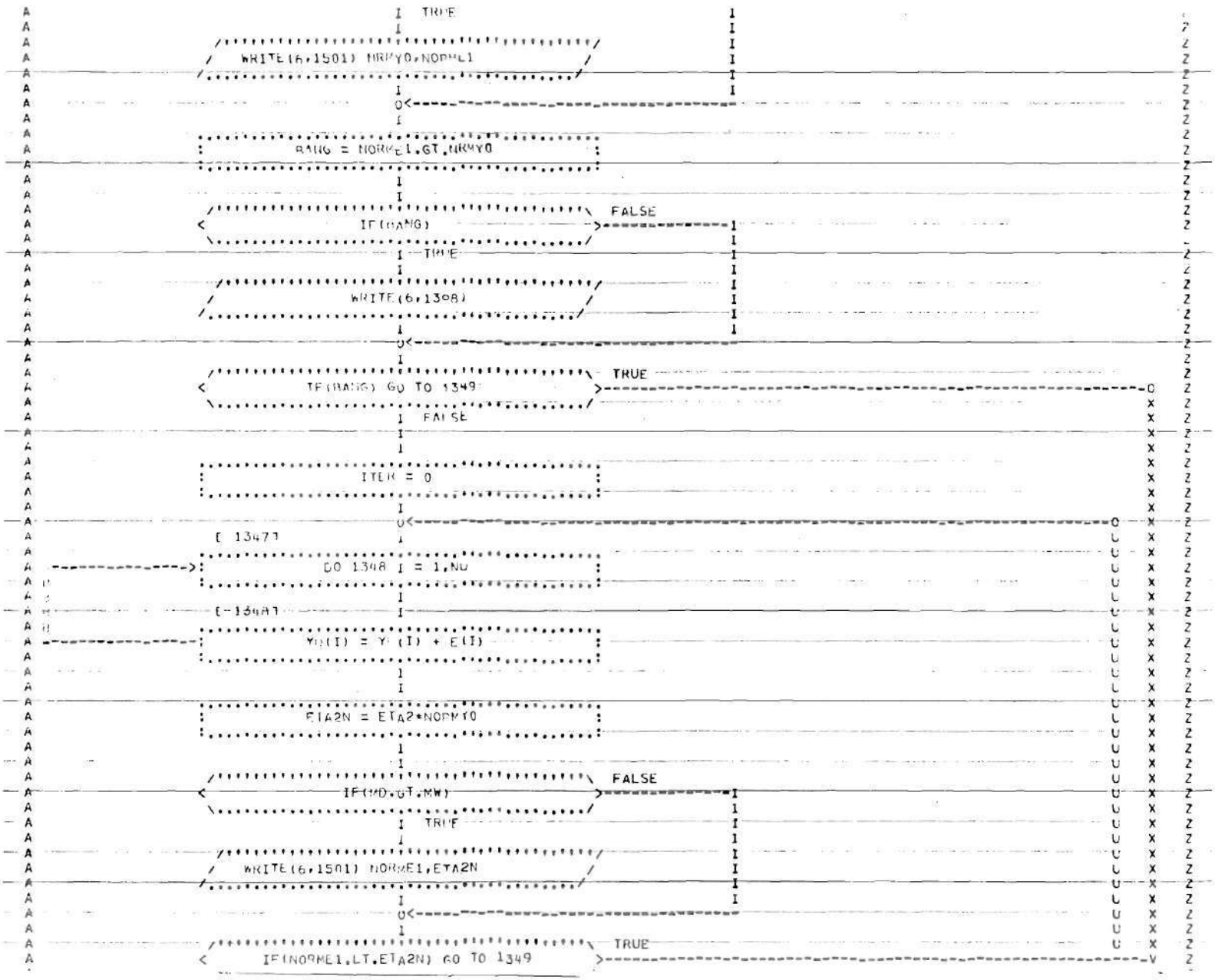
WRITE(6,1501) NORMY0,NORME1
BANG = NORME1.GT.NORMY0
IF(BANG)
TRUE
FALSE
WRITE(6,1308)
IF(BANG) GO TO 1349
FALSE
ITER = 0
[1347
DO 1348 I = 1,NU
[-1348]
YU(I) = Y (I) + E(I)
ETA2N = ETA2*NORMY0
IF(NU.GT.MW)
TRUE
WRITE(6,1501) NORME1,ETA2N
IF(NORME1.LT.ETA2N) GO TO 1349
TRUE

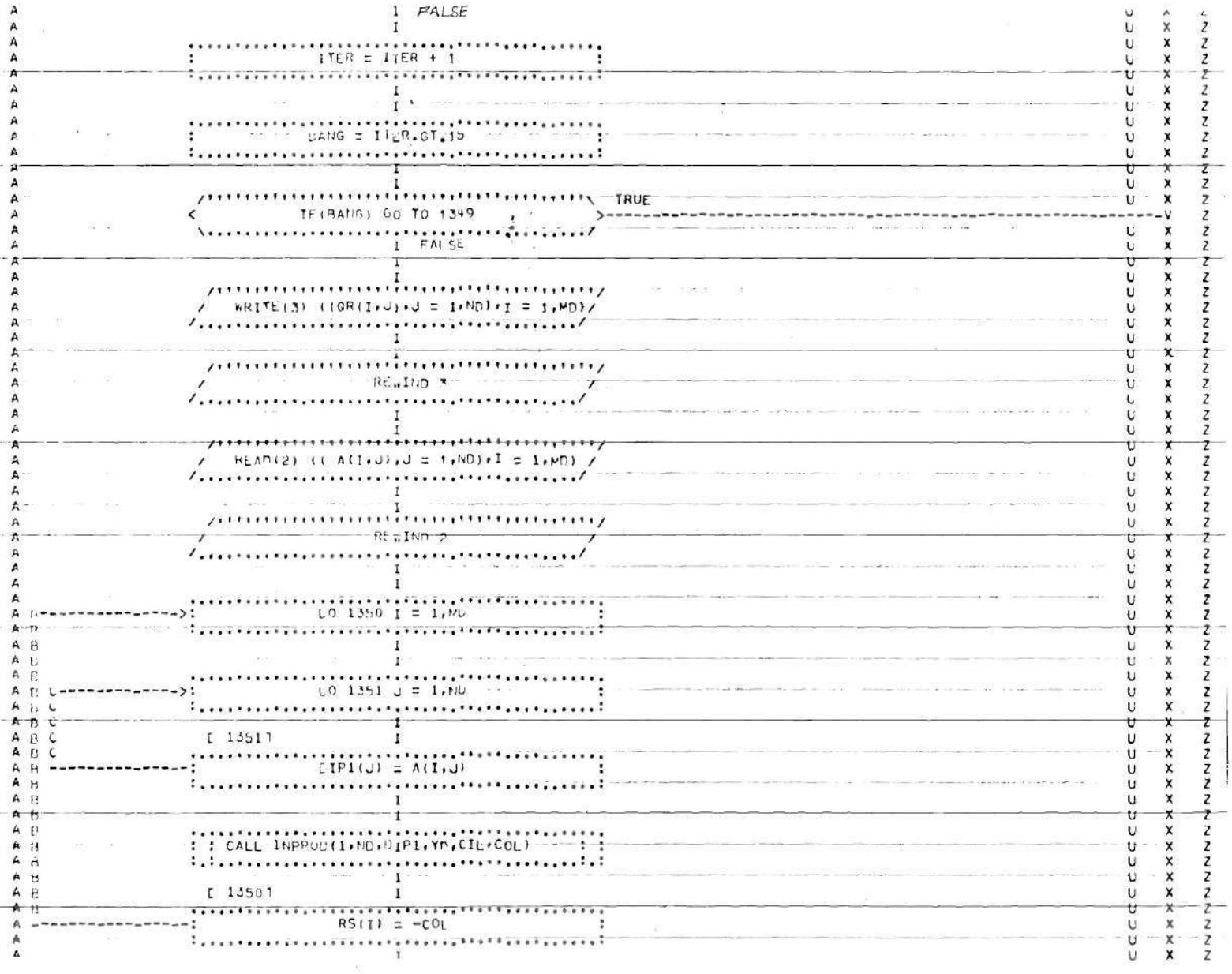
1 FALSE
ITER = ITER + 1
BANG = ITER.GT.15
TRUE
IF(BANG) GO TO 1349
FALSE
WRITE(3) ((GR(I,J),J = 1,ND),I = 1,MD)
REWIND 3
READ(2) ((A(I,J),J = 1,ND),I = 1,MD)
REWIND 2
DO 1350 I = 1,MD
DO 1351 J = 1,ND
[13517
CIP1(J) = A(I,J)
CALL INPROD(1,ND,0,IP1,YP,CIL,COL)
[13501
RS(I) = -COL

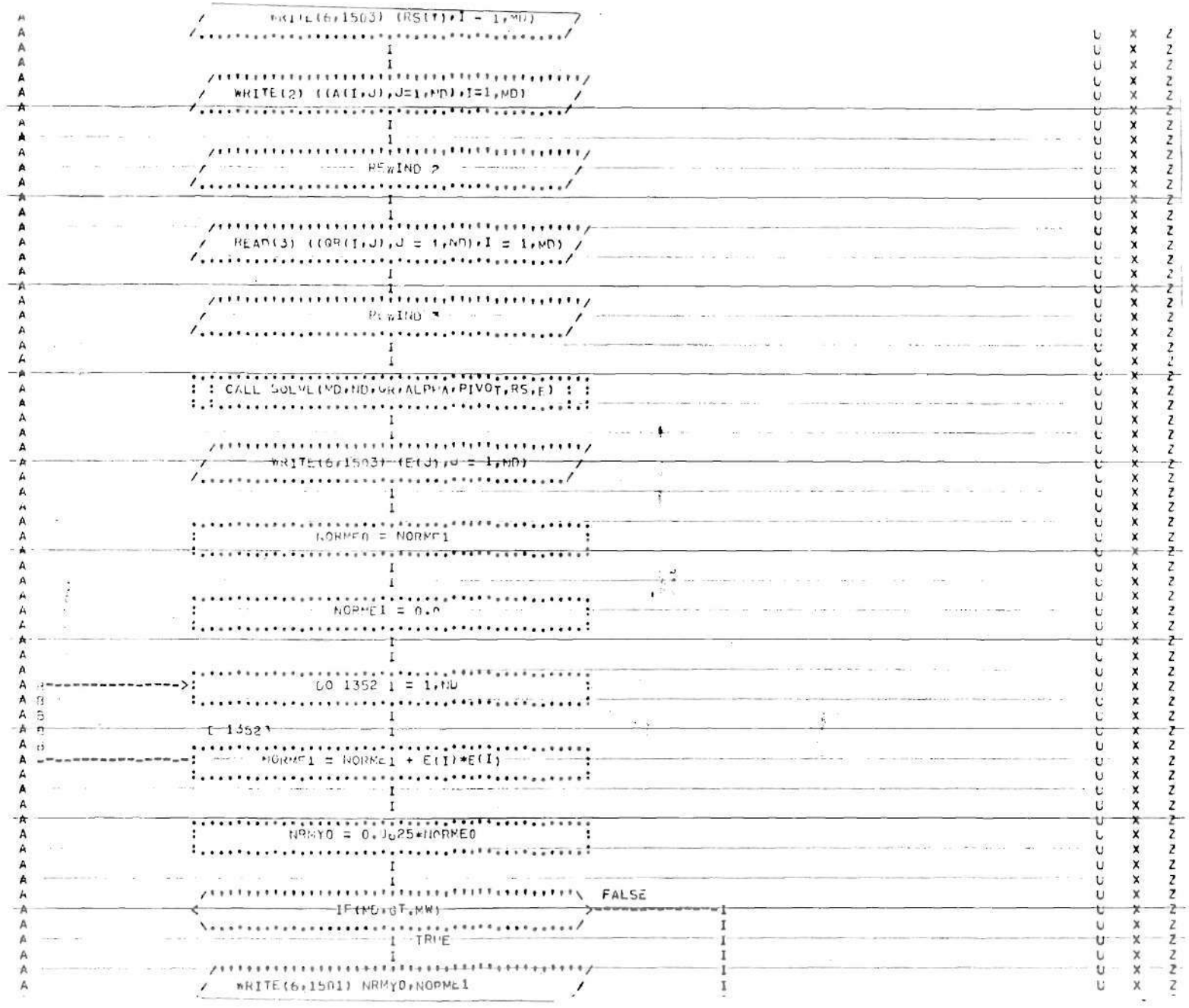
WRITE(6,1503) (RS(I),I = 1,MD)
WRITE(2) ((A(I,J),J=1,MD),I=1,MD)
REWIND 2
READ(3) ((QR(I,J),J = 1,MD),I = 1,MD)
REWIND 3
CALL SOLVE(MD,ND,QR,ALPHA,PIVOT,RS,E)
WRITE(6,1503) (E(J),J = 1,MD)
NORME0 = NORME1
NORME1 = 0.0
DO 1352 I = 1,ND
1352
NORME1 = NORME1 + E(I)*E(I)
NRMY0 = 0.025*NORME0
IF(ND.GT.MW)
FALSE
TRUE
WRITE(6,1501) NRMY0,NORME1

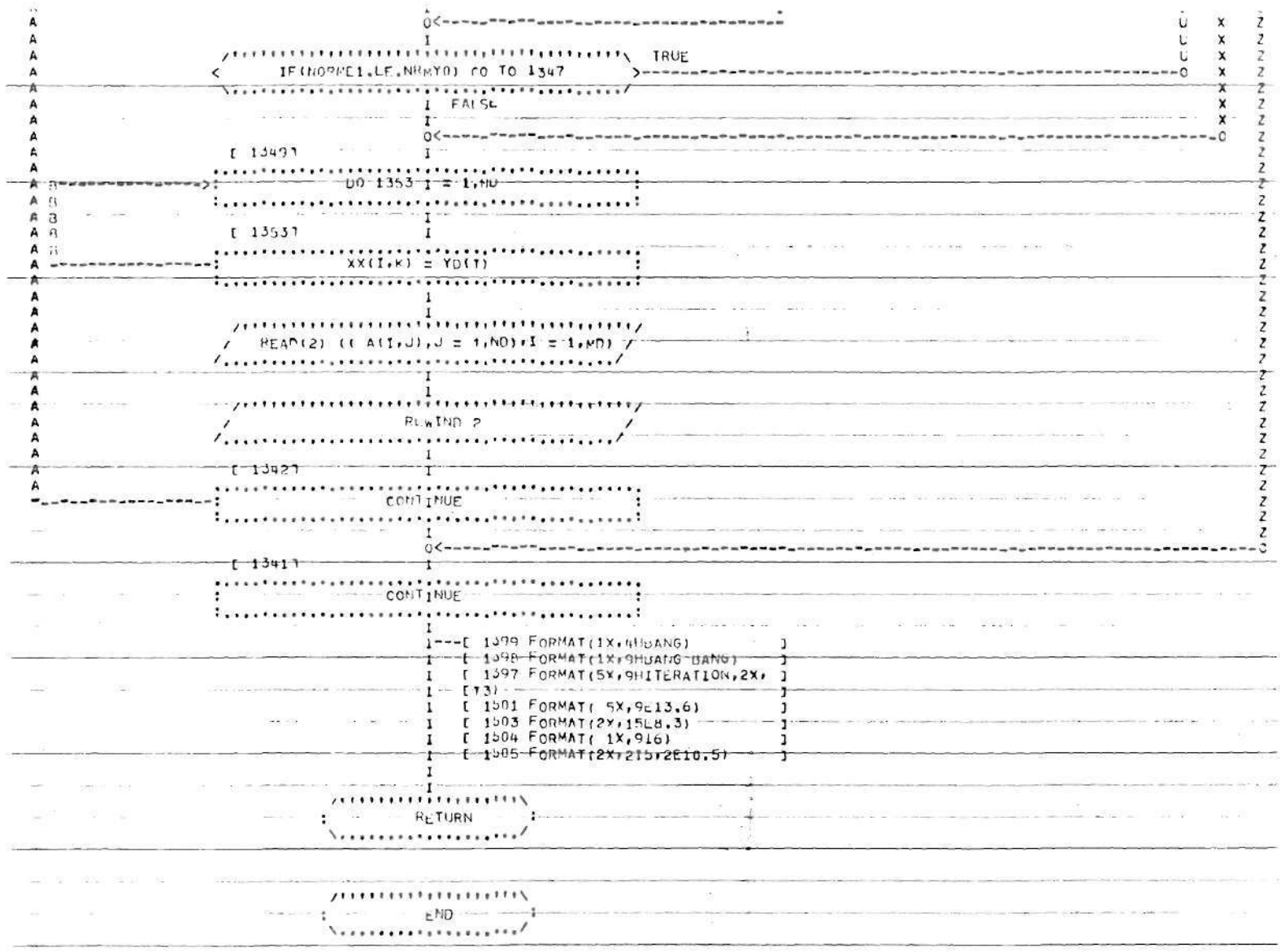
IF(NORME1.LE.NRMYD) GO TO 1347
TRUE
FALSE
[13497
DO 1353 I = 1,ND
[13537
XX(I,K) = YD(I)
READ(2) ((A(I,J),J = 1,ND),I = 1,MD)
REWIND 2
[13427
CONTINUE
[13417
CONTINUE
[1599 FORMAT(1X,6HBANG)
[1598 FORMAT(1X,9HBANG BANG)
[1597 FORMAT(5X,9HITERATION,2X,
[13]
[1501 FORMAT(5X,9E13.6)
[1503 FORMAT(2X,15L8.3)
[1504 FORMAT(1X,916)
[1505 FORMAT(2X,2I5,2E10.5)
RETURN
END

DECOMP FLOWCHARTED BY FORFLOW/X810/ ON 06 JUN 73 AT 01:03:00

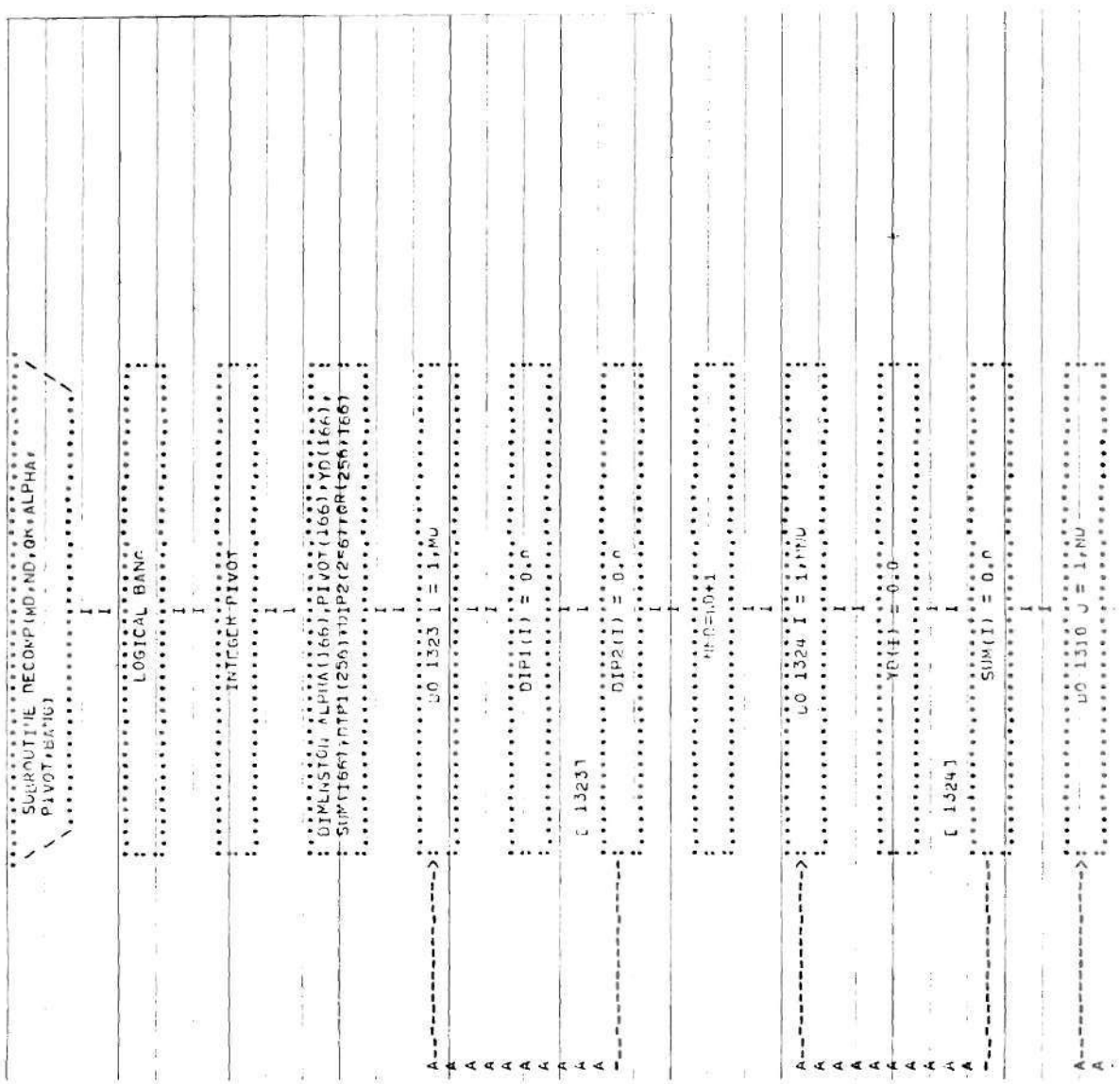

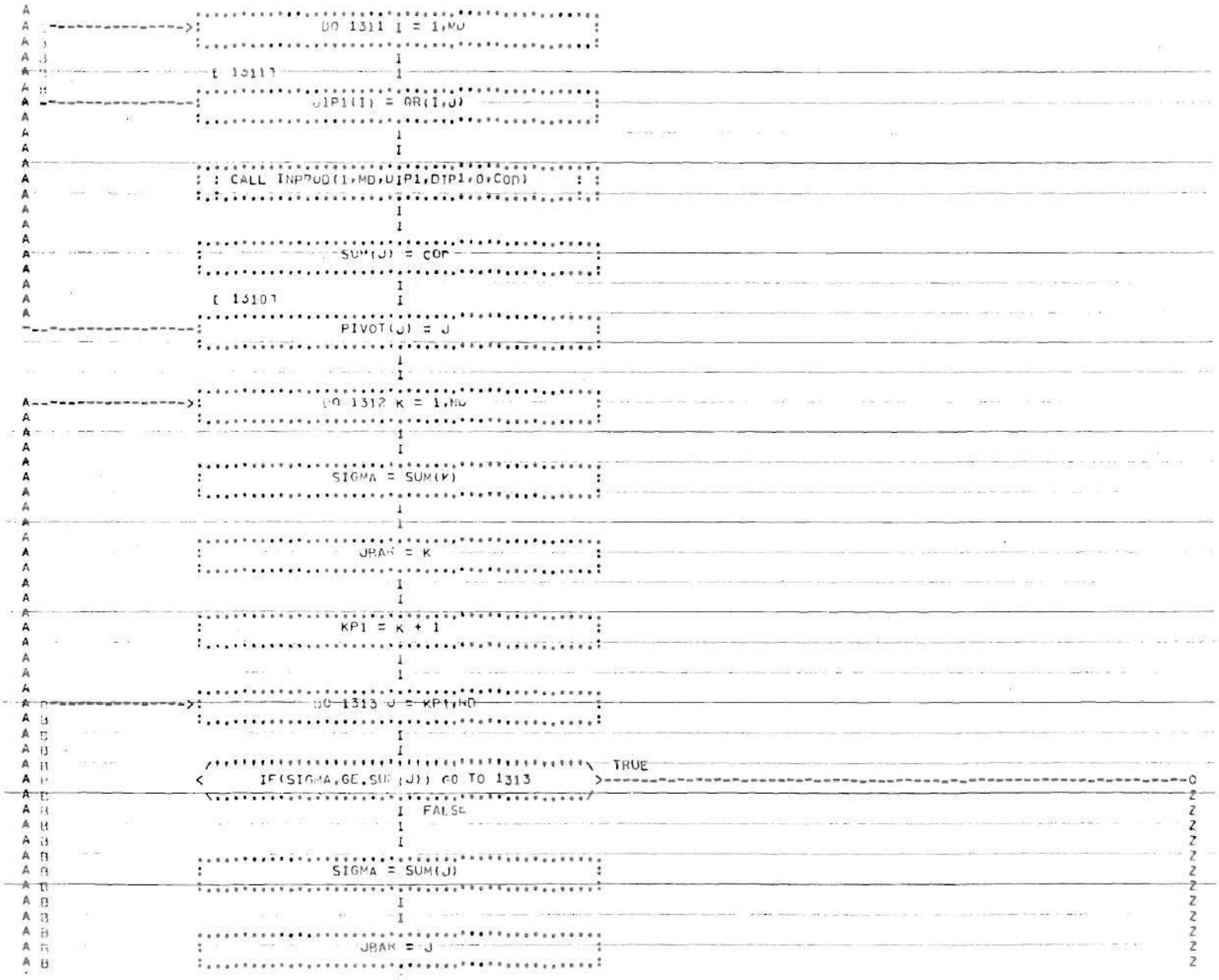
DO 1311 I = 1,ND
(13111
DIP1(I) = OR(I,J)
CALL INPROD(1,ND,DIP1,DIP1,0,COR)
SUM(J) = COR
(13107
PIVOT(J) = J
DO 1312 K = 1,ND
SIGMA = SUM(K)
JBAR = K
KP1 = K + 1
DO 1313 J = KP1,ND
IF(SIGMA,GE,SUM(J)) GO TO 1313
TRUE
FALSE
SIGMA = SUM(J)
JBAR = J

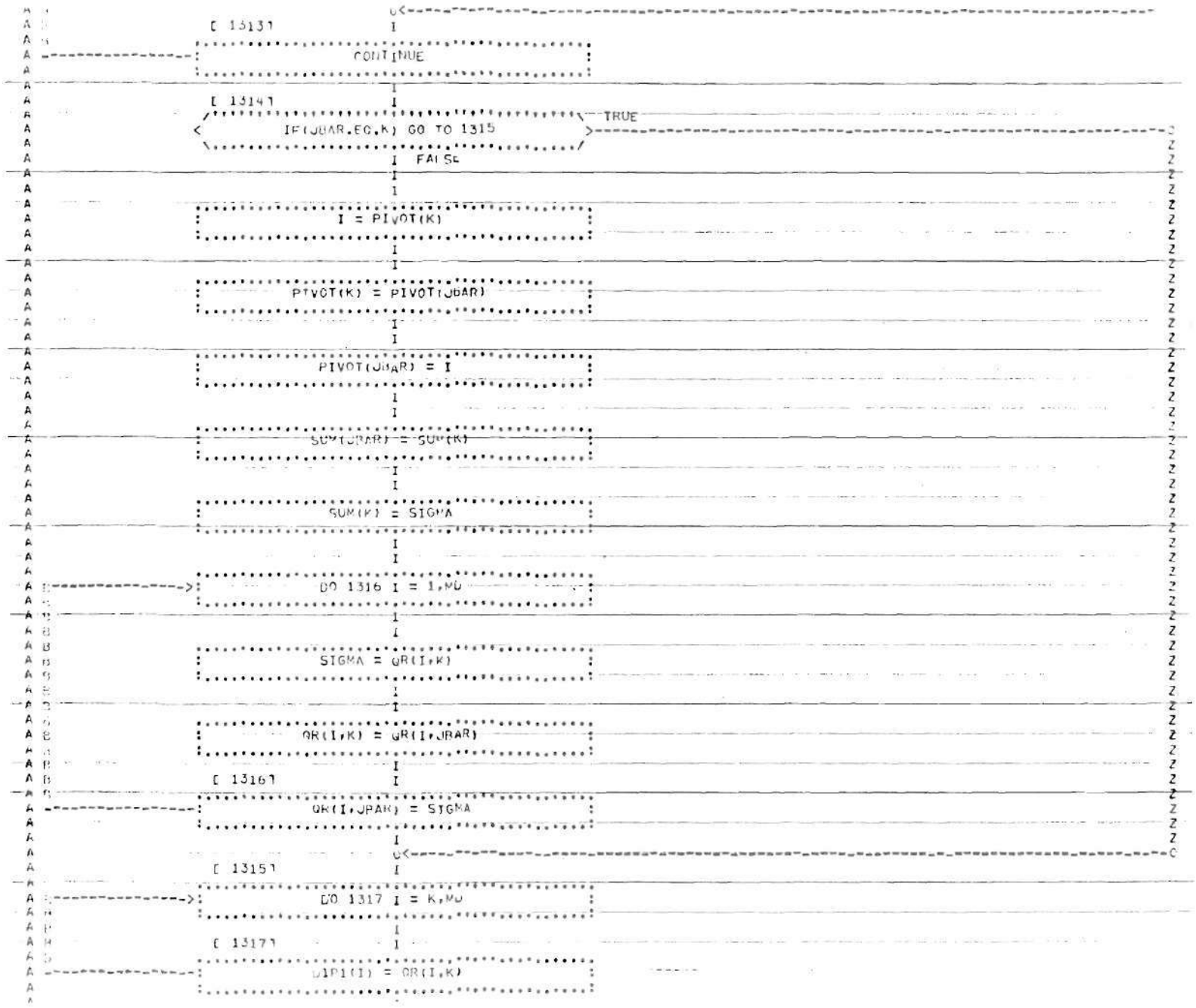
[13131
CONTINUE
[13141
IF(JBAR.EQ.K) GO TO 1315
TRUE
FALSE
I = PIVOT(K)
PIVOT(K) = PIVOT(JBAR)
PIVOT(JBAR) = I
SUM(JBAR) = SUM(K)
SUM(K) = SIGMA
DO 1316 I = 1,MD
SIGMA = QR(I,K)
QR(I,K) = QR(I,JBAR)
[13161
QR(I,JBAR) = SIGMA
[13151
DO 1317 I = K,MD
[13171
DIP1(I) = QR(I,K)

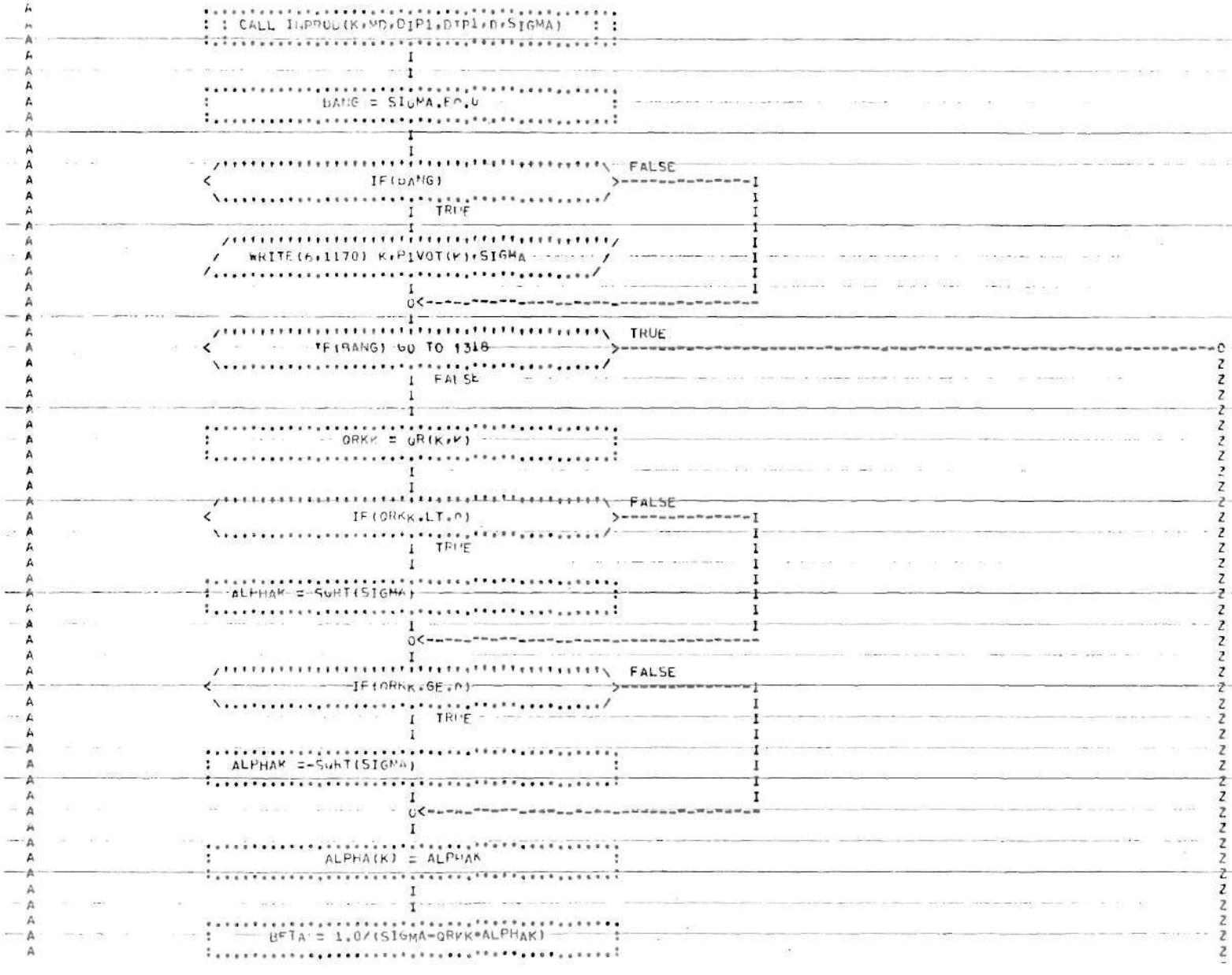
CALL INPROD(K,MD,DIP1,DIP1,D,SIGMA)
DANG = SIGMA.EQ.0
IF(DANG)
FALSE
TRUE
WRITE(6,1170) K,PIVOT(K),SIGMA
IF(DANG) GO TO 1318
TRUE
FALSE
ORKK = OR(K,K)
IF(ORKK.LT.0)
FALSE
TRUE
ALPHAK = SQRT(SIGMA)
IF(ORKK.GE.0)
FALSE
TRUE
ALPHAK =-SQRT(SIGMA)
ALPHA(K) = ALPHAK
BETA = 1.0/(SIGMA-ORKK*ALPHAK)

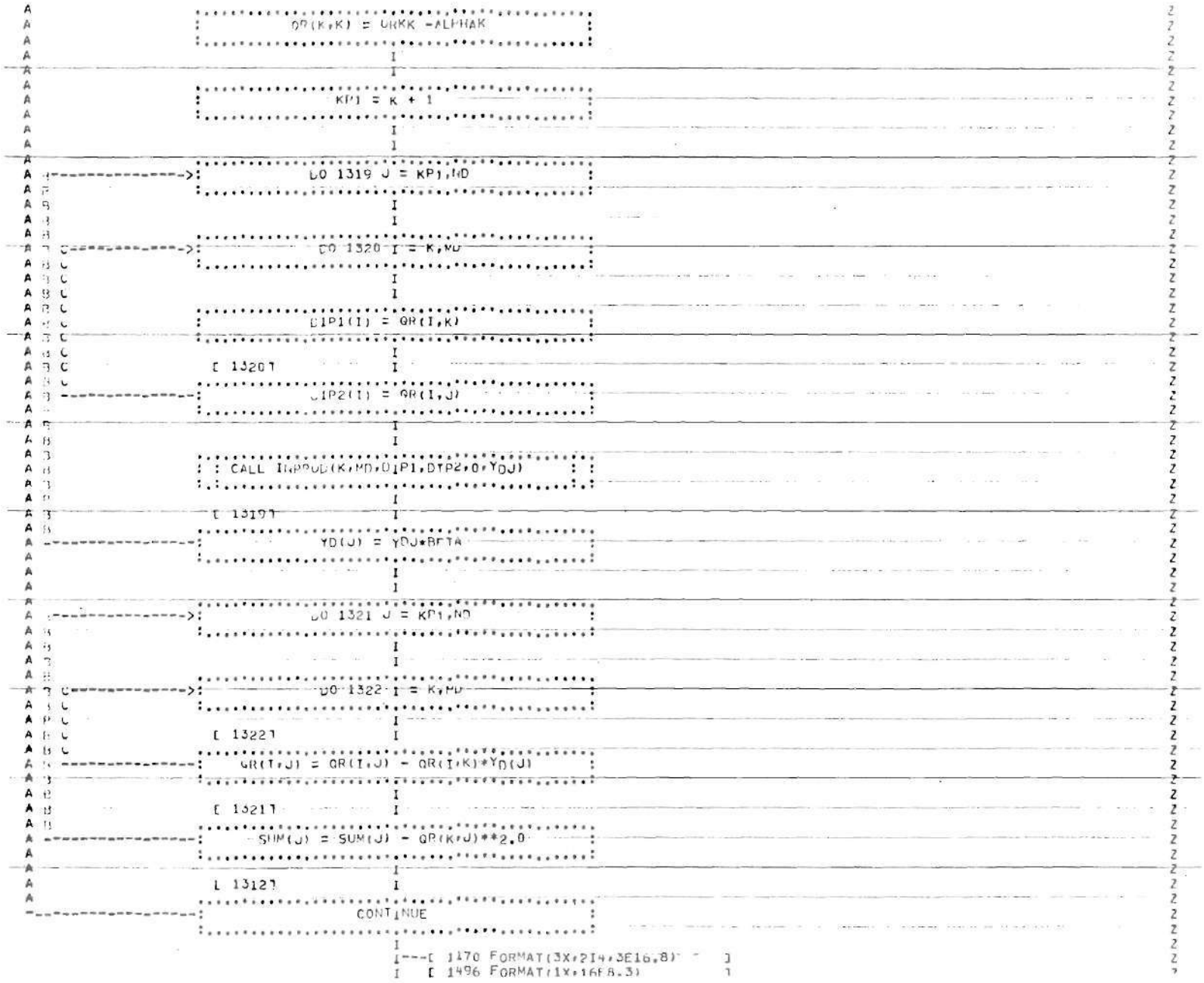
QR(K,K) = QRKK -ALPHAK
KP1 = K + 1
DO 1319 J = KP1,ND
DO 1320 I = K,MD
[13207
VIP1(I) = QR(I,K)
VIP2(I) = QR(I,J)
CALL INPROD(K,MD,VIP1,VIP2,0,YDJ)
[13197
YD(J) = YDJ*BETA
DO 1321 J = KP1,ND
DO 1322 I = K,MD
[13227
QR(I,J) = QR(I,J) - QR(I,K)*YD(J)
[13217
SUM(J) = SUM(J) - QR(K,J)**2.0
[13127
CONTINUE
[1170 FORMAT(3X,2I4,3E16.8)
[1496 FORMAT(1X,16F8.3)

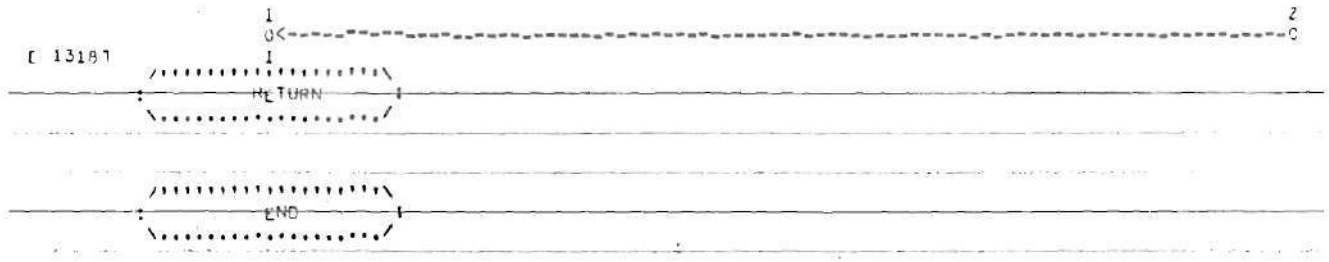
[13187
RETURN
END

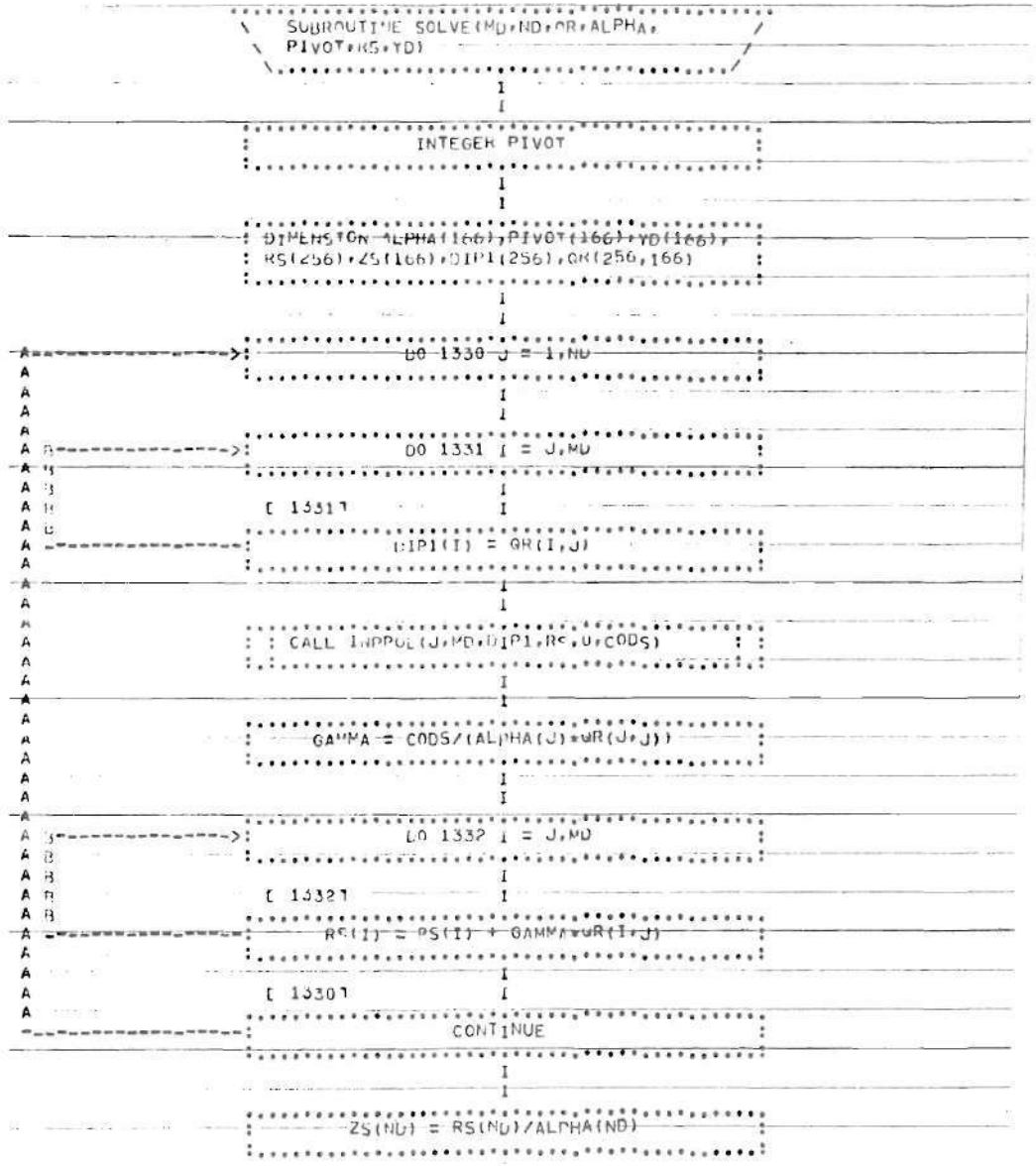
SUBROUTINE SOLVE(MD,ND,QR,ALPHA,
PIVOT,RS,YD)
INTEGER PIVOT
DIMENSION ALPHA(166),PIVOT(166),YD(166),
RS(256),ZS(166),DIP1(256),QR(256,166)
DO 1330 J = 1,ND
DO 1331 I = J,MD
[1331]
DIP1(I) = QR(I,J)
CALL IMPPOL(J,MD,DIP1,RS,U,CODS)
GAMMA = CODS/(ALPHA(J)*QR(J,J))
DO 1332 I = J,MD
[1332]
RS(I) = RS(I) + GAMMA*QR(I,J)
[1330]
CONTINUE
ZS(ND) = RS(ND)/ALPHA(ND)

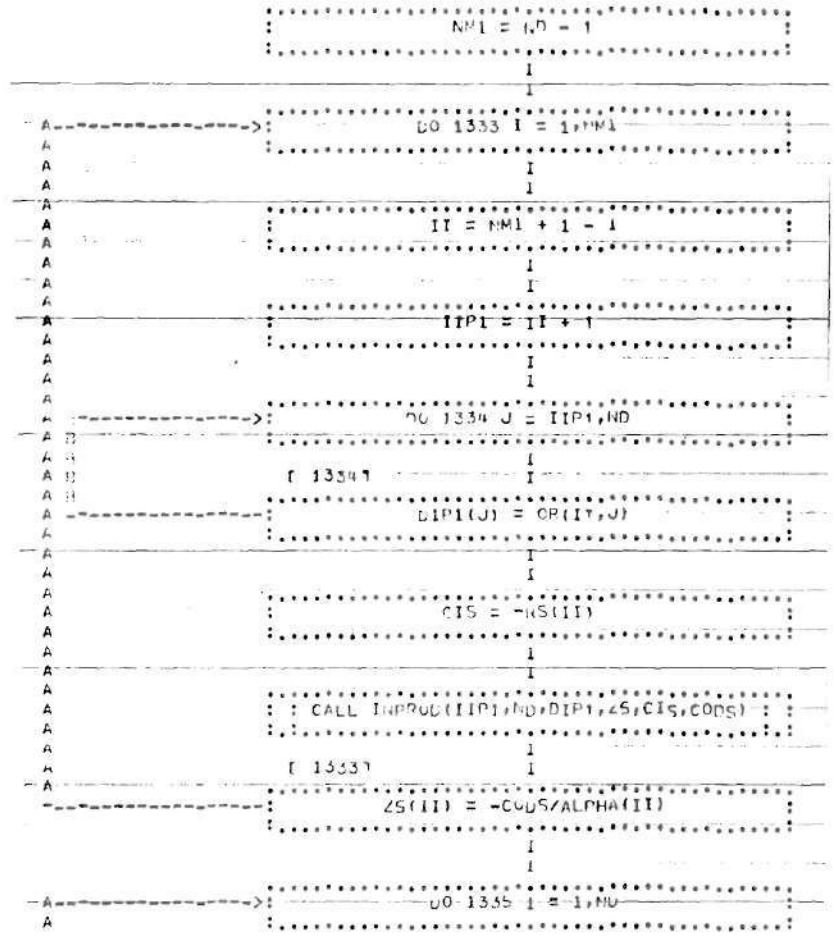
NM1 = ND - 1
DO 1333 I = 1,NM1
II = NM1 + 1 - I
IIP1 = II + 1
DO 1334 J = IIP1,ND
[1334]
DIP1(J) = OP(II,J)
CIS = -RS(II)
CALL INPROD(IIP1,ND,DIP1,ZS,CIS,CODS)
[1333]
ZS(II) = -CODS/ALPHA(II)
DO 1335 I = 1,ND

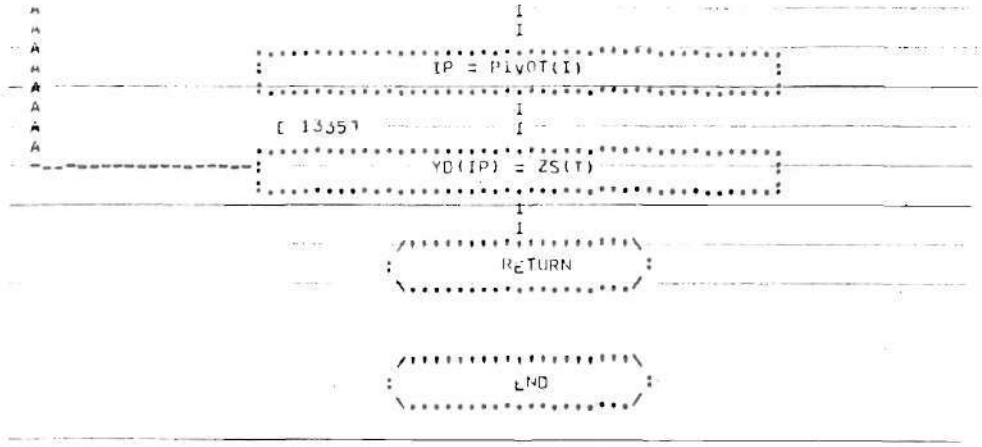
IP = PIVOT(I)
[1355]
YD(IP) = ZS(I)
RETURN
END

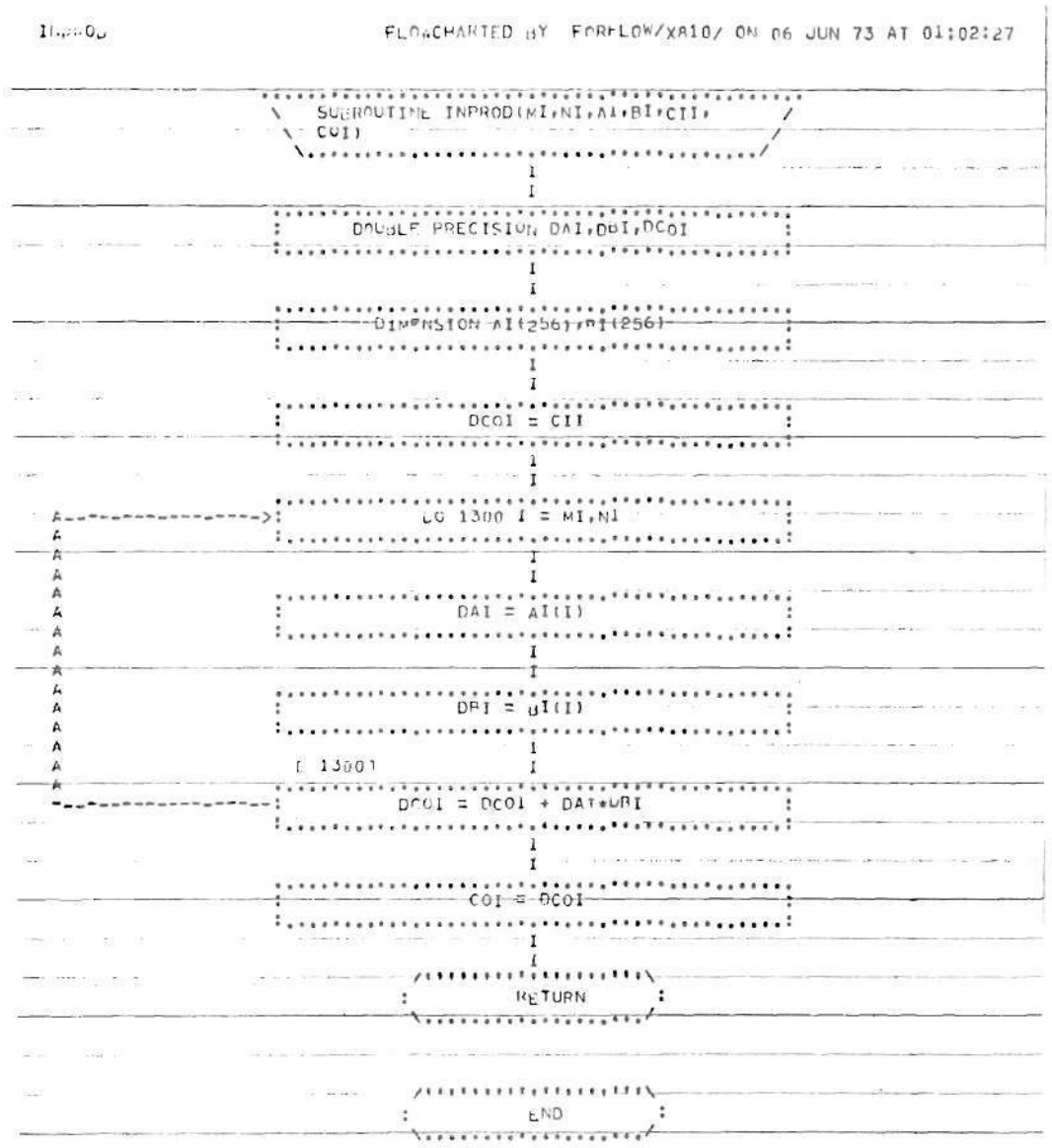
FLOWCHARTED BY FORFLOW/X810/ ON 06 JUN 73 AT 01:02:27
SUBROUTINE INPROD(MI,NI,AI,BI,CII,
CCI)
DOUBLE PRECISION DAI,DBI,DCOI
DIMENSION AI(256),BI(256)
DCOI = CII
DO 1300 I = MI,NI
DAI = AI(I)
DBI = BI(I)
1300
DCOI = DCOI + DAI*DBI
CCI = DCOI
RETURN
END

```
BUBAN-J-P*BUBAN.MAIN
     1            LOGICAL BANG
     2            COMMON AM(256,166)
     3            DIMENSION X(11,7),Z(11,7),TXY(11,7,3),TYZ(11,7,3),TXZ(
      11,7)
     4            DIMENSION LM(11,7,3),IN(166),JN(166),LN(166)
     5           1         ,AV(256), ANS(166),  SX(11,7),SY(11,7),SZ(11,
      7)
     6            DIMENSION SXX(11,7),SYY(11,7),SZZ(11,7)
     7            DY=.2
     8            P=5.375
     9            U=.49
    10            PI=3.1416
    11            II=0
    12        302 READ (5,501) Y,K
    13        501 FORMAT (F10,I10)
    14            DO 503 I=1,11
    15            DO 503 J=1,7
    16            M=J-2
    17            N=I-1
    18            X(I,J)=.1*M
    19            Z(I,J)=.1*N
    20            XX=.1*M
    21            ZZ=.1*N
    22            R=SQRT(XX*XX+Y*Y)
    23            RR=SQRT(XX*XX+Y*Y+ZZ*ZZ)
    24            IF (K.EQ.1.AND.J.EQ.2.AND.I.EQ.1) GO TO 603
    25            SR=P*(-3*R*R*ZZ/RR**3+(1-2*U)*RR/(RR+ZZ))/(2*PI*RR*RR)
    26            SO=P*(1-2*U)*(ZZ/RR-RR/(RR+ZZ))/(2*PI*RR*RR)
    27            SSZ=-3*P*ZZ*ZZ*ZZ/(2*PI*(RR**5))
    28            TTXZ=-3*P*XX*ZZ*ZZ/(2*PI*(RR**5))
    29            TTYZ=-3*P*Y*ZZ*ZZ/(2*PI*(RR**5))
    30            IF (K.EQ.1.AND.J.EQ.2) GO TO 504
    31            SSY=(Y*Y*SR+XX*XX*SO)/(R*R)
    32            SSX=(XX*XX*SR+Y*Y*SO)/(R*R)
    33            TTXY=XX*Y*(SR-SO)/(R*R)
    34        504 CONTINUE
    35            IF(K-2) 505,506,505
    36        506 CONTINUE
    37            TXZ(I,J)=TTXZ
    38            SX(I,J)=SSX
    39            SY(I,J)=SSY
    40            SZ(I,J)=SSZ
    41        505 CONTINUE
    42            TXY(I,J,K)=TTXY
    43            TYZ(I,J,K)=TTYZ
    44        603 CONTINUE
    45        503 CONTINUE
    46            II=II+1
    47            IF (II.EQ.3) GO TO 303
    48            GO TO 302
```

```
      303 CONTINUE
          WRITE (6,551)
      551 FORMAT (20X,23HG O   T O   L E S Q E Q//////)
     C*****************************************************************
     ********************
     C       BEGIN LESQEQ
     C*****************************************************************
     ********************
          LL=11
          LLL=6
          JT=0
          DO 101 I=1,LL
          DO 101 J=2,LLL
          DO 101 L=1,3
          JT=JT+1
          LM(I,J,L)=JT
          IN(JT)=I
          JN(JT)=J
          LN(JT)=L
      101 CONTINUE
          JTM=JT
          IT=0
          LLLML=LLL-1
          LLLL=LL-1
          DO 102 I=1,LLLL
          DO 102 J=2,LLL
          IT=IT+1
          JT=LM(I+1,J,3)
          AM(IT,JT)=1.0
          JT=LM(I,J,3)
          AM(IT,JT)=-1.0
          DELZ=Z(I+1,J)-Z(I,J)
          DELX1=X(I,J+1)-X(I,J-1)
          DELX2=X(I+1,J+1)-X(I+1,J-1)
          AV(IT)=.5*(DELZ/DELX1)*(TXZ(I,J-1)-TXZ(I,J+1))
         1       +.5*(DELZ/DELX2)*(TXZ(I+1,J-1)-TXZ(I+1,J+1))
         2       -.5*(DELZ/DY)*(TYZ(I,J,3)-TYZ(I,J,1)+TYZ(I+1,J,
     3)
         3       -TYZ(I+1,J,1))
      102 CONTINUE
          DO 191 I=2,LLLL
          DO 191 J=2,LLLML
          IT=IT+1
          JT=LM(I,J+1,1)
          AM(IT,JT)=1.0
          JT=LM(I,J,1)
          AM(IT,JT)=-1.0
          DELX3=X(I,J+1)-X(I,J)
          DELZ1=Z(I+1,J)-Z(I-1,J)
          DELZ2=Z(I+1,J+1)-Z(I-1,J+1)
          AV(IT)=.5*(DELX3/DELZ1)*(TXZ(I-1,J)-TXZ(I+1,J))
```

```
     1       +.5*(DELX3/DELZ2)*(TXZ(I-1,J+1)-TXZ(I+1,J+1))
     2       +.5*(DELX3/DY)*(TXY(I,J,1)+TXY(I,J+1,1)-TXY(I,J
,3)
     3      -TXY(I,J+1,3))
 191 CONTINUE
     DO 103 I=1,LL
     DO 103 J=2,LLL
     IT=IT+1
     JT=LM(I,J,1)
     AM(IT,JT)=1.0
     JT=LM(I,J,2)
     AM(IT,JT)=-1.0
     AV(IT)=SX(I,J)-SY(I,J)
     IT=IT+1
     JT=LM(I,J,1)
     AM(IT,JT)=1.0
     JT=LM(I,J,3)
     AM(IT,JT)=-1.0
     AV(IT)=SX(I,J)-SZ(I,J)
     IT=IT+1
     JT=LM(I,J,2)
     AM(IT,JT)=1.0
     JT=LM(I,J,3)
     AM(IT,JT)=-1.0
     AV(IT)=SY(I,J)-SZ(I,J)
 103 CONTINUE
     DO 104 J=2,LLL
     IT=IT+1
     JT=LM(1,J,3)
     AM(IT,JT)=1.0
     AV(IT)=0.0
 104 CONTINUE
     ITM=IT
     WRITE (6,761) JTM,ITM
 761 FORMAT (1X,6HJTM = ,I4,6HITM = ,I4//////)
     DO 7101 I=1,LL
     DO 7101 J=2,LLLML
     SXX(I,J)=SX(I,J)
     SYY(I,J)=SY(I,J)
     SZZ(I,J)=SZ(I,J)
     SX(I,J)=0
     SY(I,J)=0
     SZ(I,J)=0
7101 CONTINUE
     CALL LESQEQ(AM,ANS,AV,ITM,JTM,1,.001,BANG)
     DO 105 JT=1,JTM
     I=IN(JT)
     J=JN(JT)
     L=LN(JT)
     IF(L.EQ.1)    SX(I,J)=ANS(JT)
     IF(L.EQ.2)    SY(I,J)=ANS(JT)
```

```
  147            IF(L.EQ.3)    SZ(I,J)=ANS(JT)
  148        105 CONTINUE
  149            DO 7203 J=2,LLLML
  150            SIG=0.0
  151            DO 7201 I=1,LL
  152            SIG=(SXX(I,J)-SX(I,J))**2+(SYY(I,J)-SY(I,J))**2+(SZZ(I
     ,J)-SZ(I,J))
  153           1     **2+SIG
  154       7201 CONTINUE
  155            SIG=SQRT(SIG/(3*LL))
  156            WRITE(6,7202) SIG,J
  157       7202 FORMAT(1X,20X,8HSIGMA = ,E10.4,I5//)
  158       7203 CONTINUE
  159            DO 106 J=2,LLLML
  160            DO 106 I=1,LL
  161            WRITE(6,111)
  162        111 FORMAT (///1X,4H I  ,5H  J  ,13H   SX(I,J)   ,13H   SY
     (I,J)   ,
  163           113H   SZ(I,J)   ,13H  TXY(I,J)   ,13H  TXZ(I,J)   ,13H
       TYZ(I,J)
  164           2 ,10H  X(I,J)  ,10H  Z(I,J)  /)
  165            WRITE (6,110) I,J,SX(I,J),SY(I,J),SZ(I,J),TXY(I,J,2),T
     XZ(I,J),
  166           1            TYZ(I,J,2),X(I,J),Z(I,J)
  167        110 FORMAT (2I5,6E13.6,2F10.5)
  168        106 CONTINUE
  169            STOP
  170            END
END PRT
@PRT BUBAN.LESQEQ


BUBAN-J-P*BUBAN.LESQEQ
    1            SUBROUTINE LESQEQ(A,XX,B,MD,ND,PL,ETA,BANG)
    2            LOGICAL BANG
    3            INTEGER PL,PIVOT
    4            COMMON QR(256,166)
    5            DIMENSION B(256,1),XX(166,1),ALPHA(166),E(166),YD(166)
     ,PIVOT(166),
    6           1 RS(256),A(256,166),DIP1(256)
    7            MW = 300
    8            NT1 = 2
    9             NT2 = 3
   10            NND=ND+1
   11            DO 1340 I = 1,NND
   12            ALPHA(I) = 0.0
   13            E(I) = 0.0
   14            YD(I) = 0.0
   15       1340 PIVOT(I) = 0
   16            DO 1354 I = 1,MD
   17            RS(I) = 0.0
```

```
 1354 DIP1(I) = 0.0
      WRITE(2)   ((A(I,J),J=1,ND),I=1,MD)
      WRITE(6,1504) MD,ND
      REWIND 2
      CALL DECOMP(MD,ND,QR,ALPHA,PIVOT,BANG)
      IF(MD.LE.MW) GO TO 13541
      WRITE(6,1504) (PIVOT(J),J = 1,ND)
      WRITE(6,1503) ((QR(I,J),J = 1,MD), I = 1,MD)
13541 IF(BANG) WRITE(6,1399)
      IF(BANG) GO TO 1341
      ETA2 = ETA*ETA
      DO 1342 K = 1,PL
      DO 1343 I = 1,MD
 1343 RS(I) = B(I,K)
      CALL SOLVE(MD,ND,QR,ALPHA,PIVOT,RS,YD)
      WRITE(6,1503) (RS(I),I = 1,MD)
      DO 13431 I = 1,ND
13431 WRITE(6,1505) I,PIVOT(I),ALPHA(I),YD(I)
      WRITE(3)   ((QR(I,J),J = 1,ND),I = 1,MD)
      REWIND 3
      WRITE(6,1504) MD,ND
      READ(2)     ((A(I,J),J = 1,ND),I = 1,MD)
      REWIND 2
      DO 1344 I = 1,MD
      DO 1345 J = 1,ND
 1345 DIP1(J) = A(I,J)
      CIL = -B(I,K)
      CALL INPROD(1,ND,DIP1,YD,CIL,COL)
 1344 RS(I) = -COL
      WRITE(6,1503) (RS(I),I=1,MD)
      IF(MD.LE.MW  ) GO TO 13441
      WRITE(6,1503) (RS(I),I=1,MD)
13441 WRITE(2) ((A(I,J),J=1,ND),I=1,MD)
      REWIND 2
      READ(3)   ((QR(I,J),J = 1,ND),I = 1,MD)
      REWIND 3
      CALL SOLVE(MD,ND,QR,ALPHA,PIVOT,RS,E)
      NORMYO = 0.0
      NORME1 = 0.0
      DO 1346 I = 1,ND
      NORMYO = NORMYO + YD(I)*YD(I)
 1346 NORME1 = NORME1 + E(I)*E(I)
      NRMYO = 0.0625*NORMYO
      IF(MD.GT.100) NRMYO = 0.50*NORMYO
      IF(MD.GT.MW) WRITE(6,1501) NRMYO,NORME1
      BANG = NORME1.GT.NRMYO
      IF(BANG) WRITE(6,1398)
      IF(BANG) GO TO 1349
      ITER = 0
 1347 DO 1348 I = 1,ND
 1348 YD(I) = YD(I) + E(I)
```

```
     69              ETA2N = ETA2*NORMYO
     70              IF(MD.GT.MW) WRITE(6,1501) NORME1,ETA2N
     71              IF(NORME1.LT.ETA2N) GO TO 1349
     72              ITER = ITER + 1
     73              BANG = ITER.GT.15
     74              IF(BANG) GO TO 1349
     75              WRITE(3)   ((QR(I,J),J = 1,ND),I = 1,MD)
     76              REWIND 3
     77              READ(2)     (( A(I,J),J = 1,ND),I = 1,MD)
     78              REWIND 2
     79              DO 1350 I = 1,MD
     80              DO 1351 J = 1,ND
     81         1351 DIP1(J) = A(I,J)
     82              CALL INPROD(1,ND,DIP1,YD,CIL,COL)
     83         1350 RS(I) = -COL
     84              WRITE(6,1503) (RS(I),I = 1,MD)
     85              WRITE(2)   ((A(I,J),J=1,ND),I=1,MD)
     86              REWIND 2
     87              READ(3)   ((QR(I,J),J = 1,ND),I = 1,MD)
     88              REWIND 3
     89              CALL SOLVE(MD,ND,QR,ALPHA,PIVOT,RS,E)
     90              WRITE(6,1503) (E(J),J = 1,ND)
     91              NORME0 = NORME1
     92              NORME1 = 0.0
     93              DO 1352 I = 1,ND
     94         1352 NORME1 = NORME1 + E(I)*E(I)
     95              NRMYO = 0.0625*NORME0
     96              IF(MD.GT.MW) WRITE(6,1501) NRMYO,NORME1
     97              IF(NORME1.LE.NRMYO) GO TO 1347
     98         1349 DO 1353 I = 1,ND
     99         1353 XX(I,K) = YD(I)
    100              READ(2)     (( A(I,J),J = 1,ND),I = 1,MD)
    101              REWIND 2
    102         1342 CONTINUE
    103         1341 CONTINUE
    104         1399 FORMAT(1X,4HBANG)
    105         1398 FORMAT(1X,9HBANG BANG)
    106         1397 FORMAT(5X,9HITERATION,2X,I3)
    107         1501 FORMAT(  5X,9E13.6)
    108         1503 FORMAT(2X,15E8.3)
    109         1504 FORMAT(  1X,9I6)
    110         1505 FORMAT(2X,2I5,2E10.5)
    111              RETURN
    112              END
END PRT
@PRT BUBAN.DECOMP


BUBAN-J-P*BUBAN.DECOMP
      1              SUBROUTINE DECOMP(MD,ND,QR,ALPHA,PIVOT,BANG)
```

```
      LOGICAL BANG
      INTEGER PIVOT
      DIMENSION ALPHA(166),PIVOT(166),YD(166),SUM(166),DIP1(
     256),
     $DIP2(256),QR(256,166)
      DO 1323 I = 1,MD
      DIP1(I) = 0.0
 1323 DIP2(I) = 0.0
      NND=ND+1
      DO 1324 I = 1,NND
      YD(I) = 0.0
 1324 SUM(I) = 0.0
      DO 1310 J = 1,ND
      DO 1311 I = 1,MD
 1311 DIP1(I) = QR(I,J)
      CALL INPROD(1,MD,DIP1,DIP1,0,COD)
      SUM(J) = COD
 1310 PIVOT(J) = J
      DO 1312 K = 1,ND
      SIGMA = SUM(K)
      JBAR = K
      KP1 = K + 1
      DO 1313 J = KP1,ND
      IF(SIGMA.GE.SUM(J)) GO TO 1313
      SIGMA = SUM(J)
      JBAR = J
 1313 CONTINUE
 1314 IF(JBAR.EQ.K) GO TO 1315
      I = PIVOT(K)
      PIVOT(K) = PIVOT(JBAR)
      PIVOT(JBAR) = I
      SUM(JBAR) = SUM(K)
      SUM(K) = SIGMA
      DO 1316 I = 1,MD
      SIGMA = QR(I,K)
      QR(I,K) = QR(I,JBAR)
 1316 QR(I,JBAR) = SIGMA
 1315 DO 1317 I = K,MD
 1317 DIP1(I) = QR(I,K)
      CALL INPROD(K,MD,DIP1,DIP1,0,SIGMA)
      BANG = SIGMA.EQ.0
      IF(BANG) WRITE(6,1170) K,PIVOT(K),SIGMA
      IF(BANG) GO TO  1318
      QRKK = QR(K,K)
      IF(QRKK.LT.0) ALPHAK = SQRT(SIGMA)
      IF(QRKK.GE.0) ALPHAK =-SQRT(SIGMA)
      ALPHA(K) = ALPHAK
      BETA = 1.0/(SIGMA-QRKK*ALPHAK)
      QR(K,K) = QRKK -ALPHAK
      KP1 = K + 1
      DO 1319 J = KP1,ND
```

```
    52              DO 1320 I = K,MD
    53              DIP1(I) = QR(I,K)
    54        1320 DIP2(I) = QR(I,J)
    55              CALL INPROD(K,MD,DIP1,DIP2,0,YDJ)
    56        1319 YD(J) = YDJ*BETA
    57              DO 1321 J = KP1,ND
    58              DO 1322 I = K,MD
    59        1322 QR(I,J) = QR(I,J) - QR(I,K)*YD(J)
    60        1321 SUM(J) = SUM(J) - QR(K,J)**2.0
    61        1312 CONTINUE
    62        1170 FORMAT(3X,2I4,3E16.8)
    63        1496 FORMAT(1X,16E8.3)
    64        1318 RETURN
    65              END
END PRT
@PRT BUBAN.SOLVE
?


BUBAN-J-P*BUBAN.SOLVE
     1              SUBROUTINE SOLVE(MD,ND,QR,ALPHA,PIVOT,RS,YD)
     2              INTEGER PIVOT
     3              DIMENSION ALPHA(166),PIVOT(166),YD(166),RS(256),ZS(166
      ),DIP1(256),
     4             $QR(256,166)
     5              DO 1330 J = 1,ND
     6              DO 1331 I = J,MD
     7        1331 DIP1(I) = QR(I,J)
     8              CALL INPROD(J,MD,DIP1,RS,0,CODS)
     9              GAMMA = CODS/(ALPHA(J)*QR(J,J))
    10              DO 1332 I = J,MD
    11        1332 RS(I) = RS(I) + GAMMA*QR(I,J)
    12        1330 CONTINUE
    13              ZS(ND) = RS(ND)/ALPHA(ND)
    14              NM1 = ND - 1
    15              DO 1333 I = 1,NM1
    16              II = NM1 + 1 - I
    17              IIP1 = II + 1
    18              DO 1334 J = IIP1,ND
    19        1334 DIP1(J) = QR(II,J)
    20              CIS = -RS(II)
    21              CALL INPROD(IIP1,ND,DIP1,ZS,CIS,CODS)
    22        1333 ZS(II) = -CODS/ALPHA(II)
    23              DO 1335 I = 1,ND
    24              IP = PIVOT(I)
    25        1335 YD(IP) = ZS(I)
    26              RETURN
    27              END
END PRT
@PRT BUBAN.INPROD
```

```
HUBAN-J-P*BUBAN.INPROD
     1              SUBROUTINE INPROD(MI,NI,AI,BI,CII,COI)
     2              DOUBLE PRECISION DAI,DBI,DCOI
     3              DIMENSION AI(256),BI(256)
     4              DCOI = CII
     5              DO 1300 I = MI,NI
     6              DAI = AI(I)
     7              DBI = BI(I)
     8         1300 DCOI = DCOI + DAI*DBI
     9              COI = DCOI
    10              RETURN
    11              END
END PRT
@FIN
```

BIBLIOGRAPHY

1. Weller, R., "Three Dimensional Photoelasticity Using Scattered Light," J. Appl. Phys., 12, 610-6 (1941).

2. Weller, R., "A New Method for Photoelasticity in Three Dimensions," J. Appl. Phys., 10, 266 (1939).

3. Taylor, C. E., C. E. Bowman, W. P. North, and W. F. Swinson, "Applications of Lasers to Photoelasticity," Experimental Mechanics, Vol. 6, No. 6, 289-296 (June 1966).

4. Dally, J. W. and W. F. Riley, Experimental Stress Analysis, McGraw-Hill, New York, N. Y., 295-307 (1955).

5. Robert, A. and E. Guillemet, "New Scattered Light Methods in Three-Dimensional Photoelasticity," Brit. J. Appl. Phys., Vol. 15, No. 5, 567-78, (May 1964).

6. Drucker, D. C. and R. D. Mindlin, "Stress Analysis by Three-Dimensional Photoelastic Methods," J. Appl. Phys., 11, 724 (1940).

7. Jessop, H. T., "Scattered Light Method of the Exploration of Stresses in Two and Three Dimensional Models," Brit. J. Appl. Phys., Vol. 2, No. 9, 249-60, (September 1951).

8. Mindlin, R. D. and L. E. Goodman, "The Optical Equations of Three Dimensional Photoelasticity," J. Appl. Phys., 20, 89-97, (1949).

9. Aben, H. K., "Optical Phenomena in Photoelastic Models by Rotation of Principal Axis," Experimental Mechanics, Vol. 6, No. 1, 13-22, (January 1966).

10. Srinath, L. S., "Analysis of Scattered Light Methods in Photoelasticity," Experimental Mechanics, Vol. 9, No. 10, 463-468, (October 1969).

11. Cheng, Y. F., "Some New Techniques for Scattered Light Photoelasticity," Experimental Mechanics, Vol. 3, No. 11, 275-278, (November 1963).

12. Frocht, M. M. and L. S. Srinath, "Scattered Light in Photoelasticity-Basic Equipment and Techniques," Proc. Fourth U.S. National Congress Appl. Mech. (1962).

13. Shurcliff, W. A., Polarized Light-Production and Use, Harvard University Press, Cambridge, Mass., (1966).

14. Walker, M. J., "Matrix Calculus and the Stoke's Parameters of Polarized Radiation," Amer. J. Phys., 22, 170-173, (1954).

15. Priebe, J. R., "Operational Form of Mueller Matrices," Opt. Soc. Amer. J., Vol. 59, No. 2, 176-180, (February 1969).

16. Schmeider, R. W., "Stoke's-Algebra Formalism," Opt. Soc. Amer. J., Vol. 59, No. 3, 297-302, (March 1969).

17. Michael, A. J., "Intensity Method for Stress-Optical Measurements," J. Opt. Soc. Amer., 58, 889-894, (1968).

18. Mylonas, C. and G. H. Brown, "Birefringence in Rotating Stress Fields," (Prepared for the National Science Foundation under Grant G-20259, the Advanced Research Projects Agency under contract SD-86, and the Division of Engineering, Brown University).

19. Jones, R. C., "New Calculus for the Treatment of Optical Systems: I, II, III Description and Discussion of the Calculus," J. Opt. Soc. Amer., 31, 488-503, (1941).

20. Jones, R. C., "New Calculus for the Treatment of Optical Systems: IV," J. Opt. Soc. Amer., 32, 486-493, (1942).

21. Berghaus, D. G., "Adapting the Scattered Light Photoelasticity Method for Three Dimensional Stress Analysis in Multilayered Composite," Ph.D. Thesis, Case Western Reserve University, (June 1969).

22. Cheng, Y. F., "Dual-Observation Method for Determining Photoelastic Parameters in Scattered Light," Experimental Mechanics, Vol. 7, No. 3, 140-144, (March 1967).

23. Berghaus, D. G., R. W. Aderholdt, J. P. Buban, and D. R. Womack, "Improvements in Obtaining Scattered Light Photoelastic Data," Submitted to Experimental Mechanics for publication as a technical note. (February 1974).

24. Cheng, Y. F., "Automatic Systems for Scattered Light Photoelasticity," Experimental Mechanics, Vol. 9, No. 9, 407-412, (September 1969).

25. Southwell, R. V., Relaxation Methods in Theoretical Physics, Clarendon Press, Oxford, (1946).

26. Bickeley, W. G., "Numerical Differentiation Formulae for Numerical Differentiation," Math. Gazette, 25, 19-27, (1941).

27. Reinsch, C. H., "Smoothing by Spline Functions," Numerische Mathematik, 10, 177-183, (1967).

28. Berghaus, D. G. and J. P. Cannon, "Obtaining Derivatives from Experimental Data Using Smoothed-spline Functions," Experimental Mechanics, Vol. 13, No. 1, 38-42, (January 1973).

29. Frocht, M. M., Photoelasticity, Vol. I, John Wiley and Sons, New York, New York, (1941).

30. Frocht, M. M. and R. Guernsey, "A Special Investigation to Develop a General Method for Three Dimensional Photoelastic Stress Analysis," NACA Technical Note No. 2822, (December 1952).

31. Berghaus, D. G., "Overdetermined Photoelastic Solutions Using Least Squares," Experimental Mechanics, Vol. 13, No. 3, 97-104, (March 1973).

32. Businger, P. and G. H. Golub, "Linear Least Squares Solution Using Householder Transformations," Numerische Mathematik, 5, 269-277, (1967).

33. Heywood, R. B., Photoelasticity for Designers, Pergamon Press, Oxford, (1969).

34. Love, A. E. H., A Treatise on the Mathematical Theory of Elasticity, Dover Publications, New York, (1944).

35. von Mises, R., "On Saint-Venant's Principle," Bull. Amer. Math. Soc., 51, 555, (1945).

36. Frocht, M. M., Photoelasticity, Vol. II, John Wiley and Sons, New York, (1948).

37. Frocht, M. M., Symposium on Photoelasticity, Macmillian, New York, 277-293, (1963).

38. Desai, C. S. and J. F. Abel, Introduction to the Finite Element Method, van Nostrand, New York, (1972).

39. Kurtz, T. E., Basic Statistics, Prentice-Hall, Englewood Cliffs, N. J., (1963).

40. Sampson, R. C., "A Three-dimensional Photoelastic Method for Analysis of Differential-contraction Stresses," Experimental Mechanics, Vol. 3, No. 10, 225-237, (October 1963).

41. Johnson, R. L., "Model Making and Slicing for Three-dimensional Photoelasticity," Experimental Mechanics, Vol. 9, No. 3, 23N-32N, (March 1969).

42. ...., "Instructions for Making Photoelastic Models," Bulletin IB-P-330R, Photoelastic, Inc., Malvern, Pennsylvania.

43. Holliday, G. H. and W. J. Graff, "Photoelasticity Applied to Analysis of Tubular Connections for Offshore Structures," ASME Publication No. 71-Pet-27, (June 1971).

44. Fung, Y. C., Foundations of Solid Mechanics, Prentice-Hall, Englewood Cliffs, New Jersey, (1965).

45. Robert, A., "New Methods in Photoelasticity," Experimental Mechanics, Vol. 5, No. 10, 224-232, (October 1965).

VITA

John Phillip Buban was born January 25, 1945 in Louisville, Kentucky. He attended California State Polytechnic College, Pomona, California where he received a BSME and a B.S. in Mathematics, June 1966. Subsequently he attended Georgia Institute of Technology. He received his M.S. in Engineering Mechanics June 1968 and his Ph.D. from the School of Engineering Science and Mechanics June 1974.